UNIVERSITY OF SOUTHAMPTON

FACULTY OF MEDICINE

Insight into the physiology of skeletal development – role of BCL-2-associated athanogene-1 (BAG-1)

by

Joanna Greenhough

Thesis for the degree of Doctor of Philosophy

June 2015

Abstract

Endochondral ossification, the process by which majority of the skeleton is formed, relies on the precise development of cartilaginous templates of the future bones that serve as scaffolds for deposition of bone matrix. Disruption of the fine balance coordinating chondrocyte differentiation within the cartilaginous templates and the transition from chondrogenesis to osteogenesis at the vascular front often results in a heterogeneous group of congenital anomalies, referred to as osteochondral dysplasias, which are characterised by dwarfism, skeletal malformations and, in some cases, prenatal death. Moreover, dysregulation of early skeletal development is directly linked to diseases of the adult skeleton such as osteoporosis and osteoarthritis. Improved appreciation of skeletal development, therefore, will not only enhance our understanding of musculoskeletal diseases, but also augment the development of novel strategies for replacement/regeneration of skeletal tissues.

The role of molecular chaperones and their co-chaperones in health and disease has attracted much attention in recent years. The co-chaperone, BCL-2-associated athanogene-1 (BAG-1), is a multifunctional protein, which by its ability to bind multiple partners, predominantly the heat shock chaperone proteins (HSC70/HSP70), can regulate gene transcription and signalling crucial for cell proliferation, differentiation and apoptosis. In prenatal murine development, highest expression of *Bag-1* mRNA is detected in cartilaginous tissues. Both isoforms of BAG-1 (50 kDa and 32 kDa) are expressed ubiquitously in long bones of adult mice by chondrocytes and osteoblast-lineage cells. BAG-1 protects mammalian chondrocytes against apoptosis and plays an important role in the regulation of expression of chondrogenic markers. Interestingly, expression of BAG-1 is increased in human osteoarthritic cartilage, most likely in response to the dysregulation of homeostasis in osteoarthritic chondrocytes. Comprehensive characterisation of the role of BAG-1 and the significance of its interaction with HSC70 in the regulation of skeletal development would, therefore, assist in improved understanding of the molecular regulation of skeletogenesis.

The present study aimed to elucidate the role of *Bag-1* in endochondral ossification, using *Bag-1* null (*Bag-1*$^{-/-}$) and *Bag-1* heterozygous (*Bag-1*$^{+/-}$) mice, in conjunction with *ex vivo* models of chondrocyte and osteoblast development. Micromass cultures of embryonic limb bud cells of *Bag-1*$^{-/-}$ mice were characterised by significantly high number of mineralised cartilage nodules and increased expression of genes crucial for chondrocyte hypertrophy, mineralisation and maintenance of hypertrophic chondrocyte morphology. Bone marrow stromal cells (BMSCs) of skeletally mature *Bag-1*$^{+/-}$ female mice exhibited increased proliferation rate, decreased BMP-2-directed osteogenic differentiation and negligible apoptosis. Moreover, genes crucial for osteogenic differentiation, matrix biosynthesis, mineralisation and maintenance of the mature osteoblast phenotype were expressed at significantly lower levels in cultures of *Bag-1*$^{+/-}$ BMSCs supplemented with BMP-2, while the expression levels of genes with roles in inhibition of BMP-2-directed osteoblast differentiation were significantly upregulated. Since BAG-1, via its interaction with HSC70, can assist in the establishment of functional estrogen receptors (ERs) and modulate cellular responses to estrogen (E2), the significance of BAG-1-regulated modulation of ER function by HSC70 in E2-facilitated, BMP-directed osteogenic differentiation of BMSCs was investigated. Inhibition of the binding of BAG-1 to HSC70 by the small-molecule chemical inhibitor, Thioflavin-S, and a short peptide containing the 8 amino acid binding core of helix 2 of the BAG domain, resulted in significant downregulation of E2/ER-facilitated, BMP-directed osteogenic response of BMSCs of both wild-type and *Bag-1*$^{+/-}$ mice.

Thus, the present study has demonstrated an important role for BAG-1 in skeletal development, specifically in the terminal differentiation of chondrocytes, mineralisation of the hypertrophic cartilage and osteogenic differentiation of BMSCs. Furthermore, downregulation of E2/ER-facilitated, BMP-directed osteogenic differentiation of BMSCs due to disruption of binding between BAG-1 and HSC70 highlighted the significance of BAG-1-mediated protein-protein interactions in osteogenic differentiation of BMSCs.

Acknowledgements

Above all, I would like to recognise the invaluable support of my supervisors, Dr Rahul Tare, Prof Richard Oreffo and Prof Paul Townsend. I would like to thank Biomedical Research Facility staff, especially Mr Andrew Crocker and Mrs Caroline Mercer for their help in maintaining the *Bag-1* mouse colony. I would like to express my gratitude to Dr Stephanie Meakins, Dr Janos Kanczler and Dr Tsiloon Li for their help in performing and analysing the μCT scanning. I would like to thank Dr Franchesca Houghton for providing training in the dissection of mouse fetuses. I would like to thank Dr Manos Papadakis for his help with designing and purchasing BAG domain-derived short peptide and sharing his wide expertise in co-immunoprecipitation technique. I would also like to thank Dr David A Johnston for providing training and allowing access to SEM and Olympus dotSlide virtual slide microscope system. Special thanks go to Miss Julia Wells for proofreading and constructive comments. Importantly, I would like to express my sincere gratitude to all current and previous members of Bone and Joint Research Group, who were always very supportive and helpful, both on professional and personal level. Finally, I would like to acknowledge funding support from the University of Southampton PhD Scholarship and ECTS Career Establishment Award to my supervisor, Dr Rahul Tare, which enabled me to undertake this work.

Last but not least, my warmest thanks go to my family – Kevin, Klara, mum and dad, Liz and Phill, for their patience and endless support. Thank you all for believing in me…

This thesis is dedicated to Klara.

Thank you for the inspiration, motivation and welcomed distractions.

It wouldn’t have happened if it wasn’t for you…

Contents

List of figures

List of tables

List of abbreviations:

Adenosine-5'-diphosphate	ADP
Adenosine-5'-triphosphate	ATP
Alcian blue/Sirius red	A/S
Alkaline phosphatase (tissue non-specific)	ALPL
Ascorbate-2-phosphate	Asc-2-PO_4
Bag-1 heterozygous mice	*Bag-1*$^{+/-}$ mice
Bag-1 knock-out (null) mice	*Bag1*$^{-/-}$ mice
Bag-1 wild type mice	*Bag-1*$^{+/+}$ mice
B-cell lymphoma-2	BCL-2
BCL-2-associated athanogene-1	BAG-1
Bone marrow derived mesenchymal stromal cells	BMSCs
Bone morphogenetic protein	BMP
Bone sialoprotein	BSP
Bovine Serum Albumin	BSA
Complementary DNA	cDNA
Deoxyadenosine triphosphate	dATP
Deoxyribonucleic acid	DNA
Dibutyl phthalate xylene	DPX
Epidermal growth factor receptor	EGFR
Embryonic day 10.5	E10.5
Extracellular matrix	ECM
Fibroblast growth factor	FGF
Fetal calf serum	FCS
Frizzled	Fzd
Growth differentiation factor-5	Gdf-5
Growth hormone	GH
Hsp70/hsc70-associating protein of 46 kDa apparent molecular weight	HAP46
Indian hedgehog	Ihh
Insulin-like growth factor 1	IGF1
Internal ribosome entry sequence	IRES
Kilodalton	kDa
Macrophage colony stimulating factor	M-CSF
Matrix gla protein	MGP

Mesenchymal stem cells	MSCs
Messenger RNA	mRNA
Micro-computed tomography	µCT
Neomycin	Neo
Non-collagenous protein	NCP
Nuclear hormone receptor	NHR
Nuclear localisation sequences	NLS
Nucleoside triphosphate	NTP
Osteocalcin	OCN
Osteopontin	OPN
Osteoprotegerin	OPG
Para-Nitrophenol	pNP
Para-Nitrophenylphosphate	pNPP
Parathyroid hormone	PTH
Parathyroid hormone-related peptide	PTHrP
Phosphate Buffered Saline	PBS
Polymerase chain reaction	PCR
Receptor activator of nuclear factor kappa-B	RANK
Receptor activator of nuclear factor kappa-B ligand	RANKL
Receptor-associating protein of 46 kDa apparent molecular weight	RAP46
Ribonucleic acid	RNA
Runt-related transcription factor 2	RUNX-2
Small Integrin-Binding Ligand, N-linked Glycoprotein	SIBLING
Skeletal stem cells	SSCs
Tartrate-resistant acid phosphatase	TRAP
Terminal deoxynucleotidyl transferase mediated dUTP nick-end labelling	TUNEL
Threshold cycle	C_T
Transforming growth factor β	TGFβ
Triiodothyronine	T3
Tumor necrosis factor	TNF
Tumor necrosis factor (ligand) superfamily, member 11	TNFSF11
Ubiquitin-like domain	ULD
Vitamin D_3 Receptor	VDR
Wingless + Int	Wnt

Declaration of authorship

I, JOANNA GREENHOUGH, declare that this thesis entitled

"INSIGHT INTO THE PHYSIOLOGY OF SKELETAL DEVELOPMENT – ROLE OF BCL-2-ASSOCIATED ATHANOGENE-1 (BAG-1)"

and the work presented in it are my own and has been generated by me as the result of my own original research.

I confirm that:

1. This work was done wholly or mainly while in candidature for a research degree at this University;
2. Where any part of this thesis has previously been submitted for a degree or any other qualification at this University or any other institution, this has been clearly stated;
3. Where I have consulted the published work of others, this is always clearly attributed;
4. Where I have quoted from the work of others, the source is always given. With the exception of such quotations, this thesis is entirely my own work;
5. I have acknowledged all main sources of help;
6. Where the thesis is based on work done by myself jointly with others, I have made clear exactly what was done by others and what I have contributed myself;
7. Parts of this work have been published as:
    - Abstracts
        - "Bone marrow stromal cells of female *Bag-1* heterozygous mice exhibit reduced osteogenic potential"
            - BRS/BORS Conference, 4-5 September 2013, Oxford, UK
            - Faculty of Medicine Research Conference, 12 June 2013, Southampton, UK
            - ECTS conference, 18 - 21 May 2013, Lisbon, Portugal
        - "The significance of BCL-2 associated athanogene-1 (BAG-1)-mediated protein interactions in osteoblast development"
            - ECTS conference, 17-20 May 2014, Prague, Czech Republik

- "The role of Bcl-2-associated athanogene-1 (*Bag-1*) in skeletal development"
    - ECTS conference, 17-20 May 2014, Prague, Czech Republik

Signed: Date: 18/06/2015

Chapter 1

Introduction

1. Introduction

1.1. The skeletal system

Skeletal system comprises of bones, associated cartilages and joints which together form a hard framework for a whole body. Major functions of skeletal system are (Fig. 1-1):

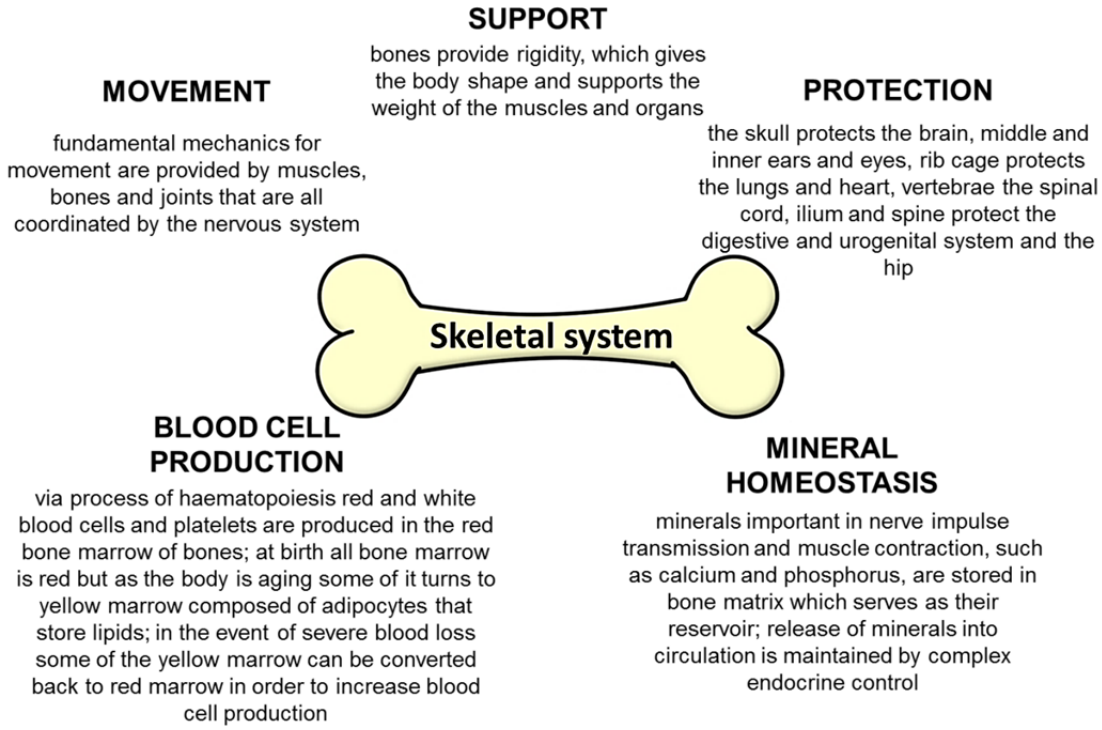

***Figure 1-1**. Major functions of skeletal system.*

1.2. Bone

Bone is a specialized connective tissue that as an organ is remarkably capable of adapting and remodelling while maintaining a functioning skeleton throughout life. It is a hard, mineralised tissue composed of cells and the extracellular matrix. Descriptive anatomy divides bones into two groups, long bones and flat bones.

1.3. Morphology of a long bone

Morphologically, long bone consists of (Fig. 1-2):

- Diaphysis – compact shaft of the bone
- Epiphyses – distal and proximal portions of the bone

- Metaphysis – an intermediate area of the bone. A region of a growing bone where epiphyseal growth plate is located. The growth plate drives its longitudinal growth through the replacement of cartilage by bone
- Articular cartilage – a hyaline cartilage covering the articular surface of the epiphyseal part of a long bone
- Periosteum – a membrane lining outer surface of bones except those capped with cartilage. It divides into two layers: an outer fibrous layer that consists of fibroblasts and collagen fibres with nerves, limphatics and blood vessels penetrating the bone to supply osteocytes and the inner cellular layer (cambium) containing osteoblasts. Cambium is the most prominent in fetal life and early childhood. Periosteum is vital to bone growth, bone fracture repair and nutrition.
- Medullary cavity – medullary cavity or marrow cavity is the hollow centre of the diaphysis that contains the bone marrow. Two types of stem cells can be found in bone marrow: haematopoietic stem cells in haematopoietic compartment (Ogawa et al., 1983) and mesenchymal stem cells (bone marrow stromal cells) in bone marrow stroma (Caplan, 1991).
- Endosteum – a connective tissue membrane lining the marrow cavity. It consists of osteoprogenitor cells

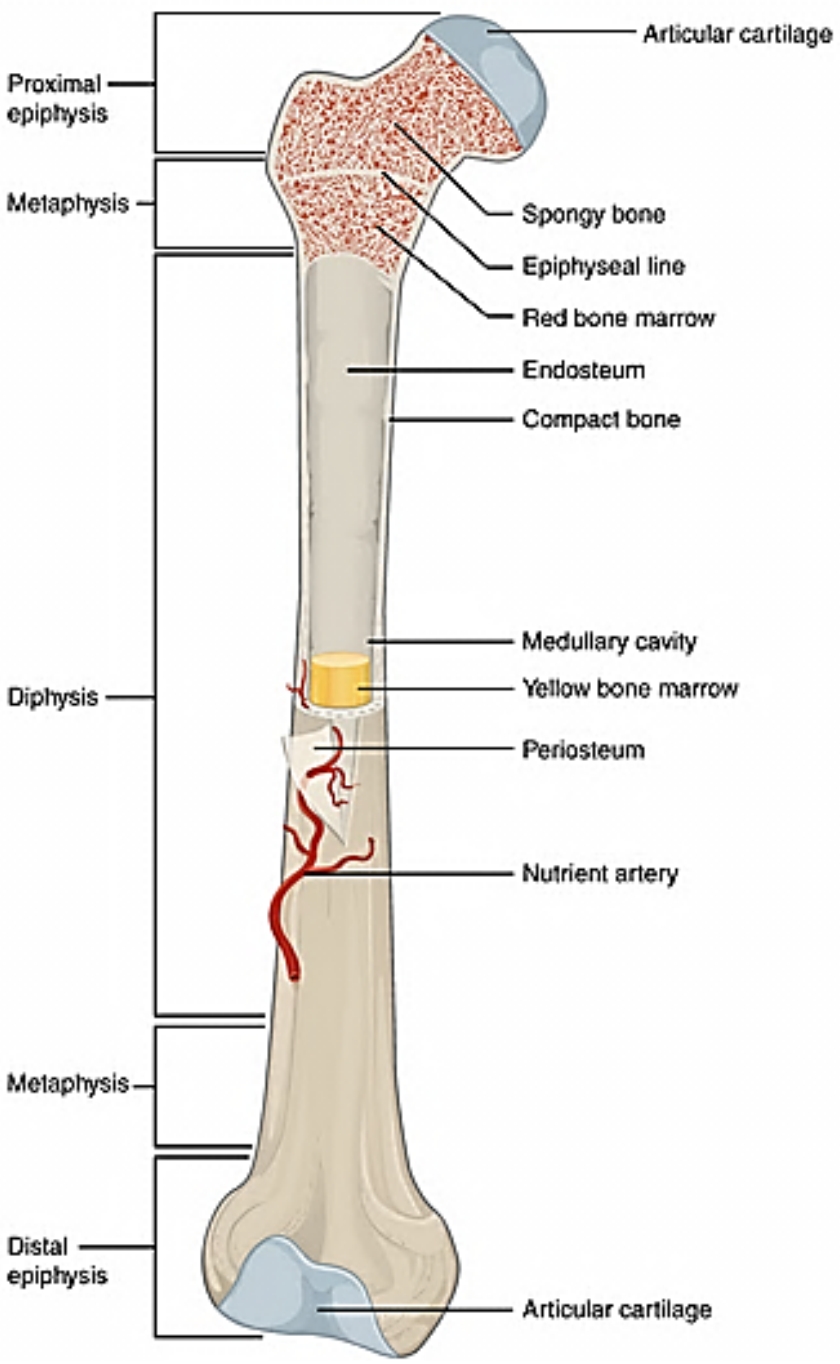

Figure 1-2. *Cross section of a human femur as a representation of a structure of a long bone (http://cnx.org/content/m46281/latest/#fig-ch06_03_01, 11/08/14, OER – Open Educational* Resources*).*

Due to characteristic pattern of locomotion, there are distinctive differences between human and animal long bone anatomy. Animal tibia and fibula are usually fused, which makes the limb more robust. Human femora are angled, the proximal surfaces of tibiae are thicker due to the purpose of greater weight bearing. Human bones are more porous and are thinner in cross section, animal bones are denser in relation to size. When comparing the mineral density of cortical and trabecular bone at femoral neck and head of primates, dogs and rodents, although similar among species, slightly higher values could be observed in rodents due to fewer, but thicker, trabeculae (Bagi et al., 2011). Animal femoral cortical thickness is approximately 50% of the whole diameter compared to ~25% in humans (Watson J, n/d).

1.4. Bone matrix

Bone matrix is composed of an organic matter that is strengthened by inorganic calcium salts. Approximately 65% of the wet weight of the bone is the inorganic component, the organic component contributes on average around 20% of the wet weight with approximately 10% water (Herring, 1977).

1.4.1. Organic bone matrix

Collagens, mostly type I collagen with small amounts of types V and XII ollagen, constitute approximately 90% of the bone organic matrix (Brodsky and Persikov, 2005). The remaining 10% is composed of non-collagenous glycoproteins and bone specific proteoglycans.

1.4.1.1. Type I collagen

Type I collagen is a 300 nm long and 1.5 nm in diameter wide protein that is composed of three coiled subunits: two α1 and one α2 polypeptide chains. Each chain has 1050 amino acids wound around one another in a triple helix (Lodish H, 2000). The structure of this triple helix is based on the abundance of glycine, proline and hydroxyprolie amino acids. These amino acids form the characteristic repeating sequence $(Gly\text{-}X\text{-}Y)_n$ where X and Y can be any other amino acid with about 100 of the X positions being proline and 100 Y positions hydroxyproline (Byers, 1995). Type I collagen molecule is a fundamental component of the bone matrix fibre network. Individual collagen molecules in the matrix are arranged to form an end to end structure with “gap region” between the fibres and neighbouring molecules being offset by approximately one quarter of its length. The first mineral crystals form in the “gap region” of the bone collagen fibres but collagen itself is not an efficient initiator of mineralization (Glimcher, 1989).

1.4.1.2. Non-collagenous proteins

Non-collagenous proteins (NCPs) comprise approximately 10% of the organic bone matrix. Even though most bone NCPs, like type I collagen, are also synthesised in soft tissue, some of NCPs, including osteocalcin, are characterised by restricted patterns of expression in bone and have multiple functions in bone cells, including regulation of collagen fibril mineralisation (Termine et al., 1981) and modulation of cell migration, division, differentiation and maturation.

One of the most abundant bone NCPs is the glycoprotein fibronectin which accumulates extracellularly at sites of osteogenesis. The important role of fibronectin in bone is implied by high expression levels in cultured human bone marrow stromal fibroblasts (Jia et al., 2002). Fibronectin contains an Arg-Gly-Asp amino acid sequence essential for binding cell surface integrin receptors and consecutive osteoblast differentiation (Moursi et al., 1996) and survival (Globus et al., 1998). It has been suggested that fibronectin plays a role in the regulation of the bone mineralisation (Couchourel et al., 1999, Daculsi et al., 1999).

Osteonectin, one of the first NCPs characterised by its bone specific functions, was named “bone connector” for its affinity for mineral and collagen, and was suggested to be a bone specific nucleator of mineralisation (Termine et al., 1981). Osteonectin knock out mice were characterised by low bone turnover resulting in osteopenia (low bone mineral density) with defects in osteoblast and osteoclast activity (Delany et al., 2000). *In vitro*, osteonectin inhibits formation of the phosphate mineral apatite (Boskey, 1989) and blocks crystal growth sites which slows down the growth of hydroxyapatite crystals (Doi et al., 1992) (see section 1.4.2.).

Another abundant NCP in bone is Thrombospondin-2 (Robey et al., 1989). Thrombospondin-2 knock-out mice are characterised by increased thickness of the cortical bone and total density linked to increased formation of endosteum (Hankenson et al., 2000). Increased cortical thickness has been linked to increased number of bone cell precursors, which are normally under negative control of thrombospondin-2 (Hankenson and Bornstein, 2002).

Bone mineralization may be controlled to some extent by small NCP bone gla protein (osteocalcin, OCN) and by related matrix gla protein (MGP). Post translational modifications of these proteins are vitamin K dependent (Price, 1989). OCN is expressed only by the osteoblasts and osteoclasts, MGP can be found in bone, cartilage and arteries. Rats treated with warfarin, a vitamin K antagonist that blocks

gamma carboxylation, exhibit reduced levels of bone OCN (2% of normal levels) and excessive mineralization of growth plates suggesting OCN role in regulating the quantity of the mineral (Price and Williamson, 1981). MGP deficient mice have normal bones but die by the age of 2 months due to spontaneous calcification of arteries and cartilage (Luo et al., 1997). A family of NCPs called SIBLING (Small Integrin-Binding Ligand N-linked Glycoprotein) has been discovered due to the bone specific functions (Fisher and Fedarko, 2003). The SIBLINGs consist of an RGD (Arg-Gly-Asp) cell attachment sequence that has the ability to bind to the integrin receptors on the surface of the cell. SIBLING family consists of 5 members: bone sialoprotein (BSP), osteopontin (OPN), dentin sialophosphoprotein (DSPP), dentin matrix protein (DMP) and matrix extracellular protein (MEPE). OPN expression in bone occurs mainly in osteoblasts, osteocytes and osteoclasts (Merry et al., 1993) but also hypertrophic chondrocytes (McKee et al., 1992). Bones of adult OPN knock-out mice are normal but resist bone resorption induced by factors such as ovariectomy (Yoshitake et al., 1999), PTH treatment (Ihara et al., 2001) and reduced mechanical stress (Ishijima et al., 2001). It has been suggested that OPN plays a role in bone remodelling by anchoring osteoclasts to the bone mineral matrix (Reinholt et al., 1990). It has also been indicated that OPN assists the process of bone resorption by facilitating angiogenesis and accumulation of osteoclasts (Asou et al., 2001). Another member of SIBLING family, bone sialoprotein (BSP), constitutes approximately 8% of all non-collagenous proteins in bone matrix (Fisher et al., 1990). BSP possible function is the facilitation of the formation of the first apatite crystals by acting as a nucleus of this process. BSP is thought to help direct, redirect or inhibit the crystal growth while the apatite forms along the collagen fibres within the extracellular matrix (Robey et al., 1989).

1.4.2. Inorganic mineral salts

The inorganic mineral matrix of bone has two main functions: it gives bones most of their strength and stiffness and acts as iron reservoir (Glimcher, 1992). Associated with the bone mineral crystals are approximately 99% of the body calcium, 85% of the phosphorus, 40 to 60% of the total body sodium and magnesium (Glimcher, 1992). Bone inorganic mineral matrix is composed of carbonated hydroxyapatite [$Ca_{10}(PO_4)_3(OH)_2$], crystals formed from calcium and phosphorus (Legros et al., 1987) and appears as globular and plate structures distributed alongside the collagen fibrils (Bertazzo et al., 2006).

1.5. Bone cells

1.5.1. Osteoprogenitors

Osteoprogenitor cells, immature progenitor cells derived from multipotent mesenchymal stem cells, are located in the inner layer of periosteum, endosteum and the bone marrow (Haynesworth et al., 1992). Osteoprogenitors express runt-related transcription factor 2 (RUNX-2), also known as core-binding factor alpha-1 (CBF-alpha-1), an osteoblast specific transcription factor that is the earliest and, to date most specific marker of the osteogenic lineage (Ducy et al., 1997). Osteoprogenitors that have initiated differentiating into osteoblasts start expressing genetic markers specific for osteogenesis, namely oterix, collagen type I, alkaline phosphatase, osteocalcin, osteonectin and osteopontin.

1.5.2. Osteoblasts

When osteoblasts are actively synthesising bone matrix (osteoid), they have a rounded polyhedral shape and consist of mitochondria, Golgi complex and abundant endoplasmic reticulum. Osteoblasts are polarised, the cell surface of the bone matrix secretion side contains primarily endoplasmic reticulum with the nucleus on the opposite side of the osteoblast. Bone matrix is secreted at the cell surface in contact with older bone matrix. Osteoblast cell processes extend through the osteoid matrix to osteocytes within the mineralised matrix (Fig. 1-3). Active osteoblasts can either get embedded in their matrix and become osteocytes, remain on the surface of the bone acquiring the flatter form of bone-lining cells or migrate from the bone formation site.

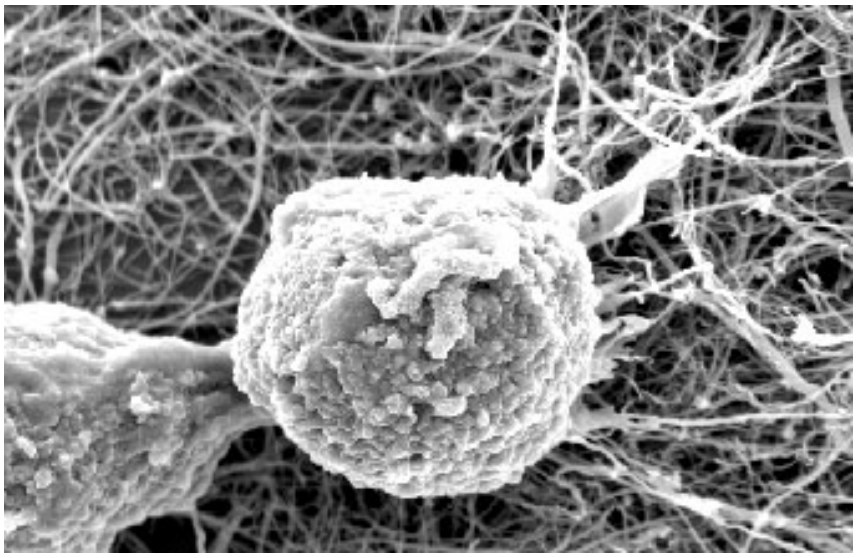

Figure 1-3. *Scanning electron microscopy image of a dividing osteoblast, osteoblast size: 20-30 µm (adapted from http://www.nsti.org/news/item.html?id=52, 02/04/2013).*

1.5.3. Osteocytes

Osteocytes comprise more than 90% of the bone cells in the mature human skeleton (Cooper et al., 1966). Osteoblasts embedded in the bone matrix become osteocytes – osteoblasts are brought into contact with other neighbouring osteoblasts, surround themselves with matrix and become osteocytes. Ellipsoidal in shape, osteocytes project their long branching cytoplasmic processes to come into contact with other cells cytoplasmic processes through canaliculi, channels extending within the mineralised bone matrix (Fig. 1-4). Processes of neighbouring cells communicate by means of gap junctions (Doty, 1981). Osteocytes have a single nucleus and, compared to osteoblasts, reduced Golgi apparatus and rough endoplasmic reticulum.

Osteocytes have been suggested to be the cell type best placed to register abnormal strain (Lanyon, 1993). Osteocytes serve as mechanoreceptors by detecting changes of mechanical forces. The signals detected by the receptor cells are then transferred to the effector cells in the form of osteoblasts and osteoclast which in turn results in formation or resorption of bone according to mechanical load (Turner and Pavalko, 1998).

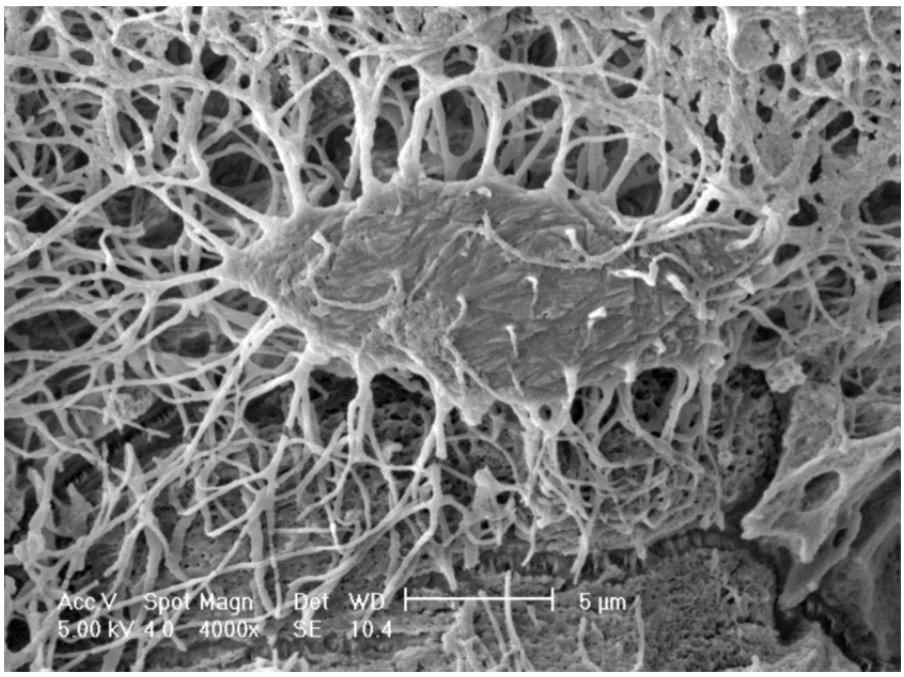

Figure 1-4. *Scanning electron microscopy image of an osteocyte in resin (Pajevic, 2009)*

1.5.4. Bone lining cells

Flattened in shape bone lining cells are situated directly against the bone matrix and cover all endosteal bone surfaces. Their cytoplasmic extensions penetrate the bone matrix and come into contact with the cytoplasmic extensions of osteocytes (Recker, 1992). Withdrawal of bone lining cells is essential for osteoclasts to initiate bone resorption (Zambonin Zallone et al., 1984).

1.5.5. Osteoclasts

Osteoclasts are the only known bone resorbing cells (Fig. 1-5). Multinucleated osteoclasts originate from blood-derived mononuclear precursors cells of the monocyte/macrophage lineage (Boyle et al., 2003). Macrophage colony stimulating factor (M-CSF) and receptor activator of nuclear factor kappa-B ligand (RANKL) are the two cytokines essential for osteoclast formation. M-CSF and RANKL originate mainly from osteoblasts and marrow stromal cells, osteoclastogenesis depends upon the presence of stromal cells and osteoblasts in bone marrow (Teitelbaum and Ross, 2003). M-CSF is required for proliferation, differentiation and survival of osteoclast precursors in addition to osteoclast survival and rearrangements of cytoskeleton crucial for bone resorption. RANKL, a member of the tumor necrosis factor (TNF) superfamily, is essential for osteoclast formation. Osteoprotegerin (OPG) inhibits RANKL action at the RANK receptor by binding it with high affinity (Cohen, 2006). On surfaces of cancellous bone, osteoclasts create characteristic depressions known as Howship lacunae. In compact (cortical) bone osteoclasts create resorption cavities that tunnel through the bone.

Osteoclasts drive the process of bone resorption by secreting hydrogen ions and the enzyme cathepsin K. Hydrogen ions dissolve the mineral component of bone matrix by acidifying the area of the bone surface beneath the osteoclast, cathepsin K digests bone matrix proteins (Boyle et al., 2003). When osteoclasts bind to bone matrix, the bone resorbing surface develops a ruffled border that secretes hydrogen ions and causes exocytosis of cathepsin K and other enzymes.

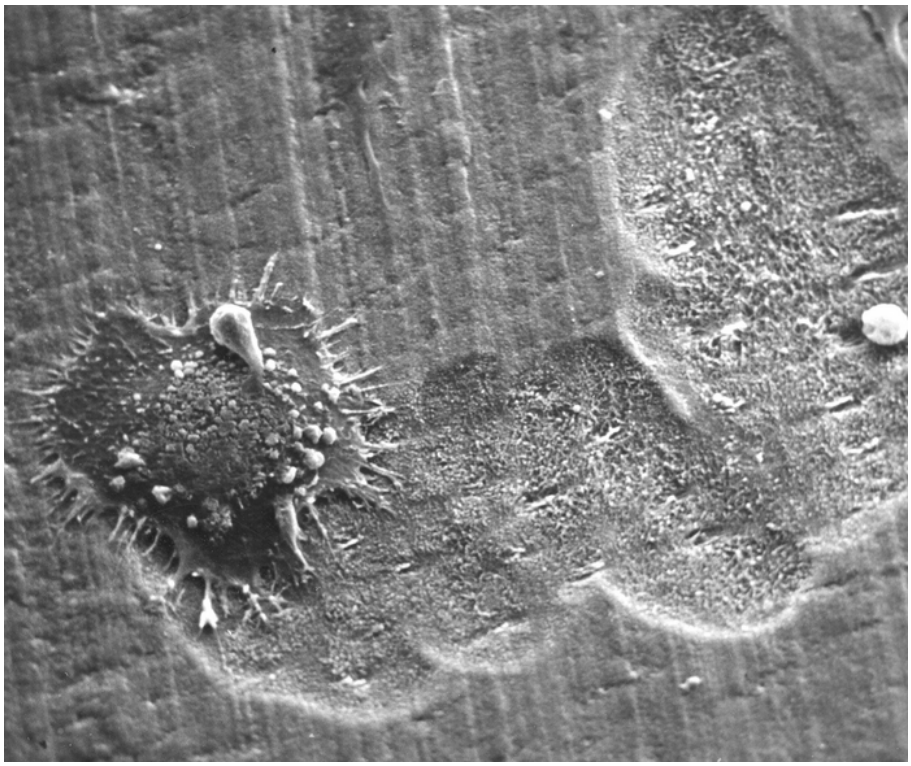

Figure 1-5. *Scanning electron microscopy image of an osteoclast and resorbed bone surface, osteoclast diameter: 150-200 μm (adapted from http://www.ectsoc.org/gallery/images/5lg.jpg, 11/06/15)*

1.6. Types of bone

An adult human skeleton consists of 80% cortical (compact) bone and 20% trabecular (spongy) bone. Different ratios of cortical to trabecular bone characterise different bones in the body – vertebra 25:75, femoral head 50:50, diaphysis 95:5 (Clarke, 2008). Trabecular bone composes of a honeycomb like complex of trabecular rods and plates distributed within the bone marrow space, whereas solid and dense cortical bone surrounds the marrow compartment. Cortical and trabecular bone are composed of osteons. Percent of the cortical bone component in the rat proximal femur is much higher than the human one (72.5% and 12.5%, respectively). Furthermore, cortical bone in rats is distributed evenly across the femoral neck, unlike human bone which is characterised by cionsiderable differences in cortical thickness throughout femoral neck. Rats have far less trabecular bone at the femoral neck (6.8%) than humans (22.7%) (Bagi et al., 1997).

1.6.1. Cortical (compact) bone

Compact bone tissue constitutes the external layer of all bones and most of the diaphysis of long bones. Compact bone (Fig. 1-6) is penetrated by nerves originating in periosteum, blood vessels and lymphatic vessels through Volkmann's canals.

Harvesian canals, centrally located canals that run longitudinally through the bone, are surrounded by concentric lamellae – rings of calcified matrix. Lacunae, spaces containing osteocytes, are situated between the lamellae.

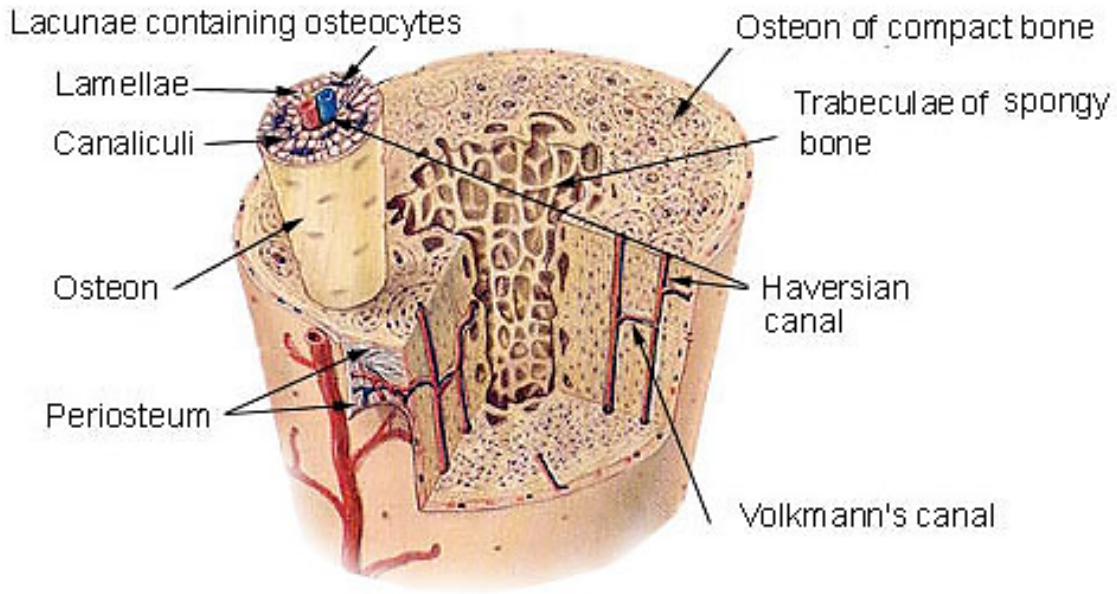

Figure 1-6. *Compact bone and trabecular bone (adapted from http://training.seer.cancer.gov/anatomy/skeletal/tissue.html, 11/06/15).*

Canaliculi, canals filled with extracellular fluid and osteocytes' processes, enable the connection between the lacunae. Osteocytes from adjacent lacunae are connected through gap junctions. Each central canal, surrounded by lamellae with their lacunae, osteocytes and canaliculi, forms a cortical osteon – Harvesian system. Osteons run parallel with the long axis of the diaphysis. Interstitial lamellae with their osteocytes and canaliculi fill areas between the osteons. Lack of osteons (Harvesian systems) in murine skeleton is a major difference between the human and murine skeletal system (Parfitt, 1994).

1.6.2. Trabecular (cancellous) bone

Spongy bone constitutes most of the bone tissue of irregularly shaped, short and flat bones and most of the long bones epiphyses. Trabecular bone consists of lamellae arranged in a network of irregularly shaped thin sheets and spikes of the bone (trabeculae). Lacunae with osteocytes and radiating canaliculi are situated within the trabeculae. The spaces between the trabeculae contain marrow. Trabeculae osteocytes receive nutrients from blood circulating through marrow cavities.

Trabecular and cortical bone are usually formed in a lamellar pattern where collagen fibrils are arranged in alternating orientations. The lamellar pattern is absent in woven bone, where collagen fibrils are disorganised. Lammelar bone is stronger than woven bone which forms the embryonic skeleton and later gets resorbed and replaced by mature bone as the skeleton develops. Woven bone is formed in the growth plates.

1.7. Cartilage

Cartilage can be found throughout the body at various sites. Based on histological classification, cartilaginous tissues can be hyaline, elastic or fibrocartilagenous depending on their molecular composition. Elastic cartilage can be found in the ear and the larynx. Menisci of the knee and the intervertebral discs consist of fibrocartilage. Hyaline cartilage is the most abundant cartilage and is associated with the skeletal system. Many bone anlagen are composed of hyaline cartilage which is also link to growth plate and the articular surface of movable joints. Cartilage is a living material comprised of a small number of cartilage cells chondrocytes embedded in a multicomponent matrix. Water constitutes approximately 70% to 85% of the weight of the whole cartilage tissue.

The cartilage matrix is composed of proteoglycans (around 60% of the total matrix) and collagen (approximately 40% of the total matrix). Cartilage functions, such as cell to cell interactions, tissue strength and architecture rely on their maintenance by matrix molecules. Proteoglycans consist of protein core with attached glycosaminoglycans chondroitin sulphate and keratin sulphate. All hyaline cartilages have high proteoglycan aggrecan content with aggrecan synthesis being a specific marker of the chondrocyte phenotype (Doege et al., 1990). Another major component of the cartilage matrix is type II collagen, another marker specific for chondrocyte phenotype (Dessau et al., 1980). Type X collagen is also found within cartilage, but it is restricted to the matrix of the hypertrophic zone. Chondrocytes of the hypertrophic zone synthesise alkaline phosphatase which is then exported to the extracellular matrix and associated with the matrix vesicles – particles serving as the initial site of calcification in all skeletal tissues (Harrison et al., 1995).

By the time skeletal maturity is reached, articular cartilage localised at each end of the long bone forming a joint with another bone, is the only permanent cartilage remaining. Articular cartilage does not contribute to bone formation. Primary and secondary ossification centres are separated by the growth plate cartilage, which is responsible for the increase in length of the bone. Growth continues until the two ossification centres fuse together causing the disappearance of the growth plate.

1.8. The growth plate

The growth plate is aneural, avascular and comprises of chondrocytes contained within extracellular matrix (Fig. 1-7). The longitudinal growth of long bones takes place in growth plates where chondrocytes produce cartilage that subsequently ossifies. Non ossified growth plate disappears at skeletal maturity in most species with some species, like rat, maintaining inactive growth plate throughout adult life (Horton et al., 2008).

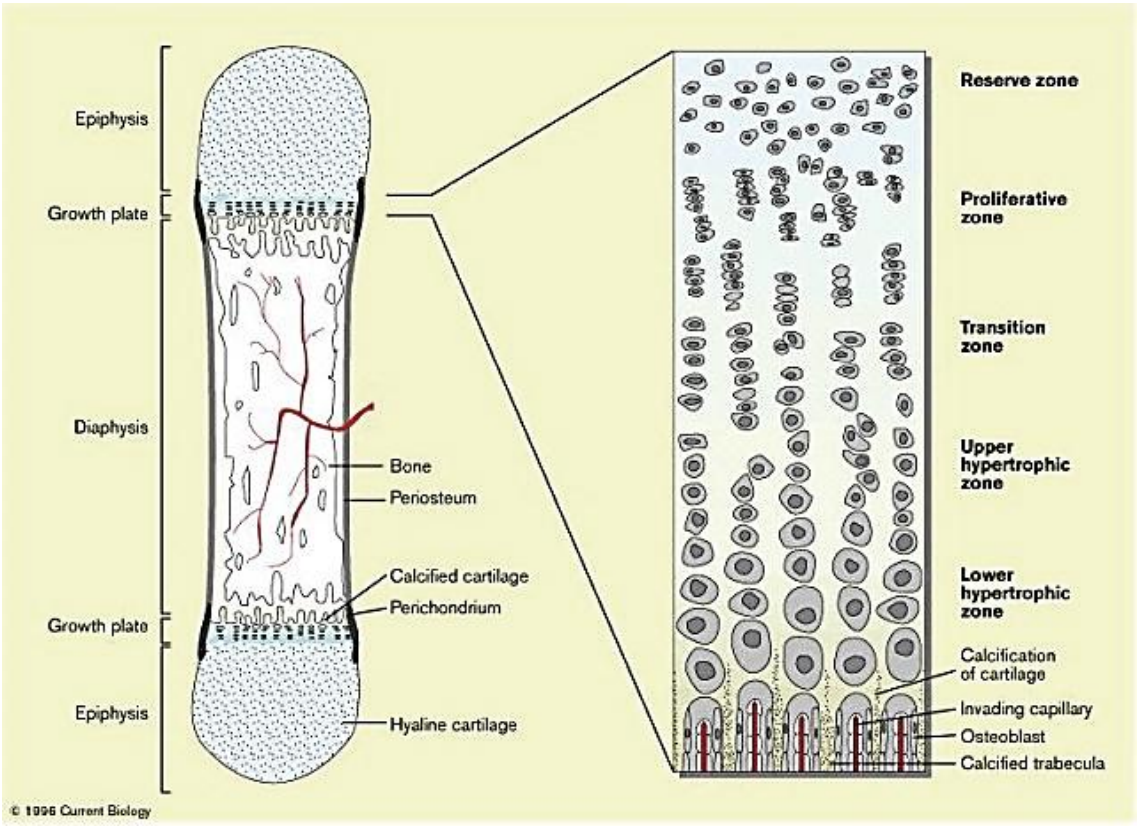

Figure 1-7. *Long bone during fetal development and the growth plate diagram showing the organisation and differentiation of the chondrocytes (Wallis, 1996).*

1.8.1. Reserve (resting) zone

The reserve zone of the growth plate is characterised by irregularly scattered relatively quiescent chondrocytes within the extracellular matrix with high ratio of extracellular matrix to cell volume. The reserve zone is adjacent to the epiphysis and contains stem-like cells that generate clones of proliferative chondrocytes (Abad et al., 2002). Matrix of the reserve zone comprises of proteoglycans and type II collagen that suppresses calcification and functions as a barrier to the progressing front of the secondary ossification centre in the epiphysis (Robertson, 1990).

1.8.2. Proliferative zone

The chondrocytes in the proliferative zone assume a flattened appearance and start to divide. On the side of metaphysis chondrocytes become aligned into columns parallel to the longitudinal bone axis. Mitosis occurs at the base of columns. Cell division results in longitudinal growth of the bone. Synthesis of aggrecan as well as type II collagen and expression of its mRNA increase in proliferative zone (Kosher et al., 1986). Type II collagen fibrils surround the columnar chondrocytes.

1.8.3. Upper hypertrophic zone (maturing zone)

The chondrocytes in the upper hypertrophic zone become enlarged with less regular arrangement of the columns. The cells are metabolically active, deposition of matrix increases in the upper hypertrophic zone in comparison to the proliferative zone. Most abundant elements of the matrix are type II collagen, type X collagen and aggrecan.

1.8.4. Lower hypertrophic zone

Lower hypertrophic zone consists of columns of terminal chondrocytes and the calcifying matrix between them. Calcified matrix acts as scaffolding for the deposition of the bone. The hypertrophic zone is characterised by high levels of alkaline phosphatase that assist in the calcification of the matrix. Hypertrophic chondrocytes show active collagen metabolism and synthesise collagen type II and collagen type X (Kirsch and von der Mark, 1992). Death of terminal hypertrophic chondrocytes is essential for the transition of calcified cartilage to bone and subsequent vascular invasion (Farnum and Wilsman, 1989), osteoclast and osteoblast differentiation and osteoid synthesis and mineralisation (Hatori et al., 1995). Degradation of collagen in the hypertrophic zone decreases content of collagen type II, process linked to a loss of collagen network integrity, while collagen type X level increases (Alini et al., 1992). It has been suggested that collagen turnover is an essential factor of chondrocyte hypertrophy (van Donkelaar and Wilson, 2012).

1.9. Bone development

Two distinct processes during fetal development of the mammalian skeletal system govern the formation of bone tissue and consequently bone development: intramembranous ossification and endochondral ossification.

1.9.1. Bone formation

1.9.1.1. Intramembranous ossification

Intramembranous ossification involves mesenchymal stem cells (MSCs) differentiating directly into bone-forming osteoblasts without involving a cartilage template (Karsenty, 2003). Most flat bones, bones of the skull and some facial bones, such as mandibles and maxillae, are created by intramembranous ossification, which is also essential for natural bone fracture healing. Ossification initiates in the primary ossification centre, where mesesnchymal stem cells (MSCS) within the mesenchymal condensations differentiate into osteoprogenitor cells and subsequently into osteoblasts. Osteoblasts secrete bone matrix (osteoid), some of them become entrapped within the matrix and become osteocytes. These aggregates of developing bone are called spicules which eventually fuse together and form trabecular (spongy) bone. As growth continues trabeculae merge and form woven bone. Differentiating mesenchymal stem cells form periosteum around the trabeculae. Woven bone is eventually replaced by lamelar bone.

1.9.1.2. Endochondral ossification

Most bones in the body, including long bones, develop through a process known as endochondral ossification, also essential for postnatal bone lengthening. This process occurs through condensation of an initial cartilage model, and subsequent replacement with bone tissue (Kronenberg, 2003) (Fig. 1-8). Endochondral ossification occurs throughout fetal development. Condensed MSCs differentiate into both cartilage forming chondrocytes that secrete the components of cartilage extracellular matrix (ECM), and perichondral cells that surround the cartilage template. Expansion of the cartilage model is driven by chondrocyte proliferation. Prior to ossification of the cartilage model, chondrocytes located in the centre differentiate into prehypertrophic, then hypertrophic and finally terminal hypertrophic chondrocytes. These functional changes are reflected in chondrocyte morphology and arrangement in distinct growth plate zones. Cell volume increases noticeably in hypertrophic chondrocytes. Following chondrocyte hypertrophy, blood vessels, osteoclasts and osteoblast precursors invade the region, initiating formation of a primary ossification centre. Removal of ECM and deposition of bone on cartilage templates enables the expansion of the primary ossification centre towards the ends of the bone, where a secondary ossification centre appears around the time of birth. Primary and secondary ossification centres are separated by the growth plate, which is responsible for the increase in length of the bone. Growth continues until the two ossification centres fuse together causing the

disappearance of the growth plate. By the time skeletal maturity is reached (within the onset of puberty in humans), articular cartilage localised at each end of the long bone is the only permanent cartilage remaining. Interestingly, bone longitudinal growth in mice continues after sexual maturity – in most mouse strains peak bone mass is reached at 4-6 months of age while sexual maturity occurs at 6-8 weeks of age.

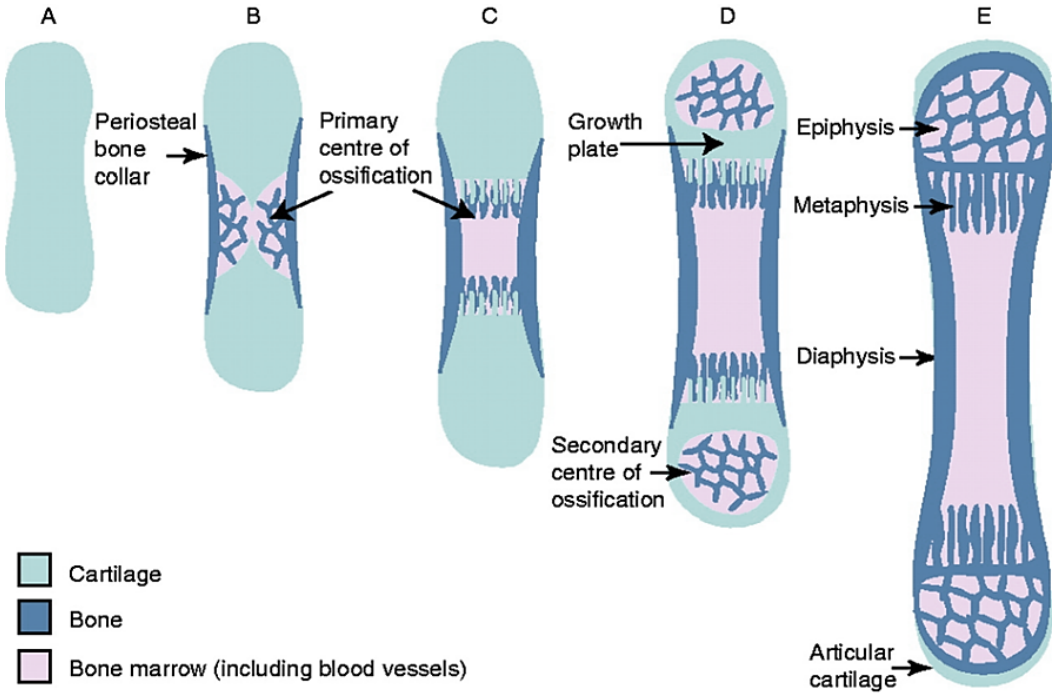

Figure 1-8. *Overview of endochondral bone development (adapted from Mackie et al., 2011). (A) Cartilage anlagen, (B) Formation of the primary centre of ossification, (C) Expansion of the primary centre of ossification towards the ends of the cartilage anlagen, (D) Formation of the secondary centres of ossification (around time of birth), (E) Complete replacement of the growth plate cartilage by bone (skeletal maturity – onset of sexual maturity in humans; peak bone mass – 4-6 months of age in mice).*

1.9.2. Bone resorption

Osteoclasts attach to the mineralised surfaces of the bone that are not covered by bone lining cells. Elimination of bone lining cells is essential for osteoclasts to start bone resorption (Zambonin Zallone et al., 1984). When osteoclasts bind to bone matrix, the bone resorbing surface develops a ruffled border that secretes hydrogen ions (creates an area of lower pH) and causes exocytosis of cathepsin K, acid phosphatase and other enzymes that target bone matrix. As the osteoclasts tunnel thorough the mineralised bone, liberated ground substances such as calcium, magnesium and phosphate are released into extracellular matrix. Osteoclasts are characterised by high expression of tartrate-resistant acid phosphatase (TRAP). Bone matrix phosphoproteins, such as osteopontin and bone sialoprotein, that bind to osteoclasts

when phosphorylated, are efficient *in vitro* TRAP substrates (Ek-Rylander et al., 1994). Once partially phosphorylated, osteopontin and bone sialoprotein lose their capability of bonding to osteoclasts. The regulatory role of TRAP in the process of bone resorption is based on its function of osteopontin and bone sialoprotein dephosphorylation which allows osteoclast migration and further bone resorption. Cathepsin K is a cysteine protease expressed predominantly in osteoclasts and is involved in the degradation of type I collagen and other non-collagenous proteins (Bossard et al., 1999).

1.9.3. Bone remodelling

Bone undergoes remodelling throughout life, including fetal development. Remodelling is a dynamic physiological process based on balanced osteoblast bone formation and osteoclast bone resorption resulting in new bone tissue replacing the old bone (Frost, 1990) (Fig. 1-9). An adult human skeleton undergoes remodelling at a rate of about 10% per year. Turnover of trabecular bone in mice is ~0.7% per day (for distal femur), each remodelling episode takes about 2 weeks (Weinstein et al., 1998). Interestingly, the same process in humans is about 0.1% per day (measured in iliac crest (Parfitt, 2002) with each remodelling event lasting between 6 and 9 months (Parfitt et al., 1997). Quicker bone turnover in mice is in keeping with the higher metabolic rate that characterises small animals.

Bone remodelling plays a role in replacement or reshaping of fractured bone but also micro damages occurring during normal activity and enables bone's adaptation to respond to mechanical load and strain. The remodelling cycle comprises of resorption, reversal and formation phases. Migration of partially differentiated mononuclear preosteoclasts to the bone surface is the first step of the resorption phase. Preosteoclasts form multinucleated osteoclasts which consequently resorb the bone tissue. When the resorption is completed, osteoclasts undergo apoptosis and lift off. Following resorption, unclassified macrophage-like cells appear on the bone surface, preparing it for the new bone formation by osteoblasts and provide signals for osteoblasts differentiation and migration (reversal phase). Osteoblast precursors then proliferate and differentiate into mature osteoblasts. The formation phase proceeds with osteoblasts secreting new bone matrix until resorption pit is filled in. Osteoblasts trapped in their matrix become osteocytes. After completion of the formation phase, the surface is covered with bone lining cells. Resting period lasts until a new remodelling cycle commences.

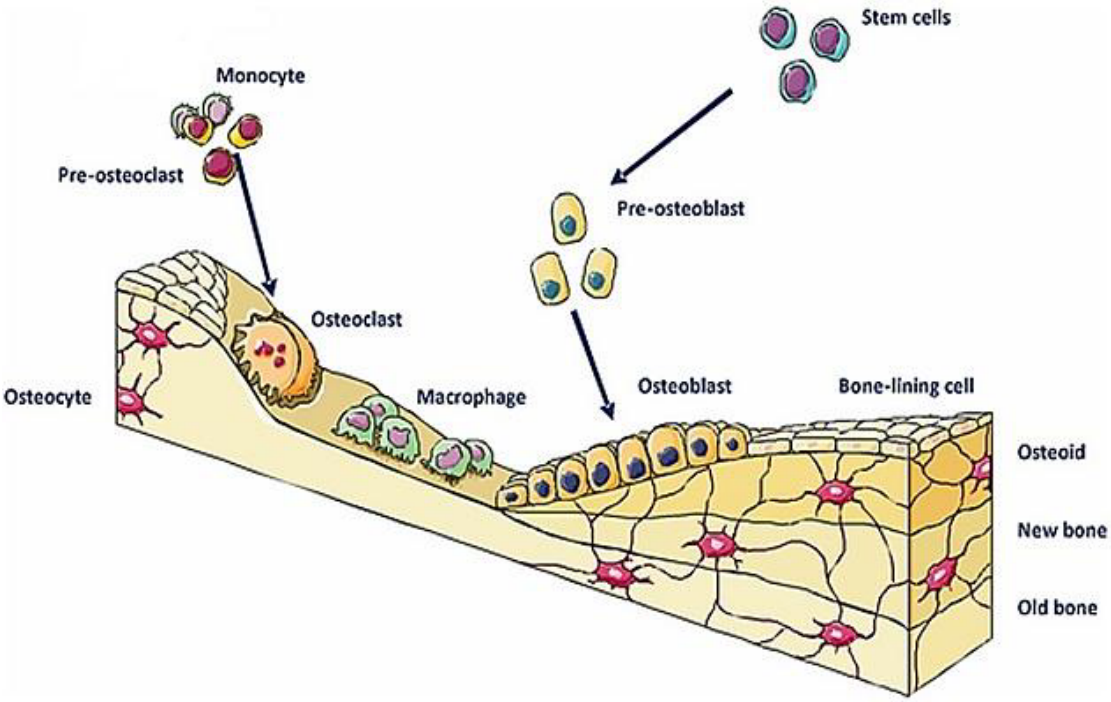

Figure 1-9. *The bone remodelling process (adapted from Stepien, 2011).*

1.10. Regulation of endochondral ossification

Coordinated processes of proliferation, ECM secretion and hypertrophy of growth plate chondrocytes regulate the shape and growth of endochondral bones. These processes are controlled by a complex network of both extracellular factors, such as hormones, and chondrocyte endocrine regulation.

1.10.1. Hormones

Growth hormone (GH), produced in the pituitary gland, is known to be important in bone growth (Nilsson et al., 2005). The main role of GH is to stimulate proliferation of growth plate chondrocytes (Hunziker et al., 1994). Although this effect is mostly dependent on the stimulation of the secretion of insulin-like growth factor 1 (IGF1) by GH, it may also be IGF1-independent (Nilsson et al., 2005). Another important regulator of bone development is thyroid hormone (Shao et al., 2006). Thyroid hormone induces cartilage maturation *in vitro* (Fell and Mellanby, 1955). Triiodothyronine (T3) has been shown to induce both hypertrophy and death of hypertrophic chondrocytes (Ahmed et al., 2007).

1.10.2. Indian hedgehog and parathyroid hormone-related peptide

Prehypertrophic and hypertrophic chondrocytes synthesise and secrete Indian hedgehog (Ihh), a secreted signalling factor that stimulates chondrocyte proliferation and inhibits their hypertrophy (Bitgood and McMahon, 1995, Koyama et al., 1996, St-Jacques et al., 1999). The inhibitory effect of Ihh is linked to the Gli family of transcription factors (Gli-2) – dependent stimulation of expression of parathyroid hormone-related peptide (PTHrP) (Vortkamp et al., 1996, Kronenberg, 2006, Joeng and Long, 2009). In mouse fetuses PTHrP is synthesised by perichondrial cells and chondrocytes at the ends of the growing bones (Lee et al., 1995). PTHrP then moves away from the production site and binds to PTH/PTHrP receptors on adjacent chondrocytes (Lee et al., 1996). Chondrocytes of the proliferative zone express substantially lower levels of PTH/PTHrP receptors compared to non-proliferating chondrocytes. By acting on chondrocytes expressing PTH/PTHrP receptors, PTHrP delays chondrocyte differentiation into prehypertrophic and then hypertrophic chondrocytes and promotes proliferation. Moving away from the source of PTHrP enables chondrocytes to stop proliferating and synthesize Ihh. Ihh then stimulates the synthesis of PTHrP at the end of the growth plate. PTHrP prevents hypertrophy by maintaining chondrocytes in the proliferation stage (Lee et al., 1996), thus PTHrP limits the number of cells expressing Ihh. By participating in this negative feedback loop PTHrP regulates not only the rate of chondrocyte differentiation but also its own expression (Fig. 1-10).

Ihh can act independently of PTHrP enabling neighbouring perichondral cells to become osteoblasts and stimulate chondrocyte proliferation (Long et al., 2001, Long et al., 2004). Ihh also promotes the transformation of round proliferating chondrocytes into flat columnar ones (Kobayashi et al., 2005).

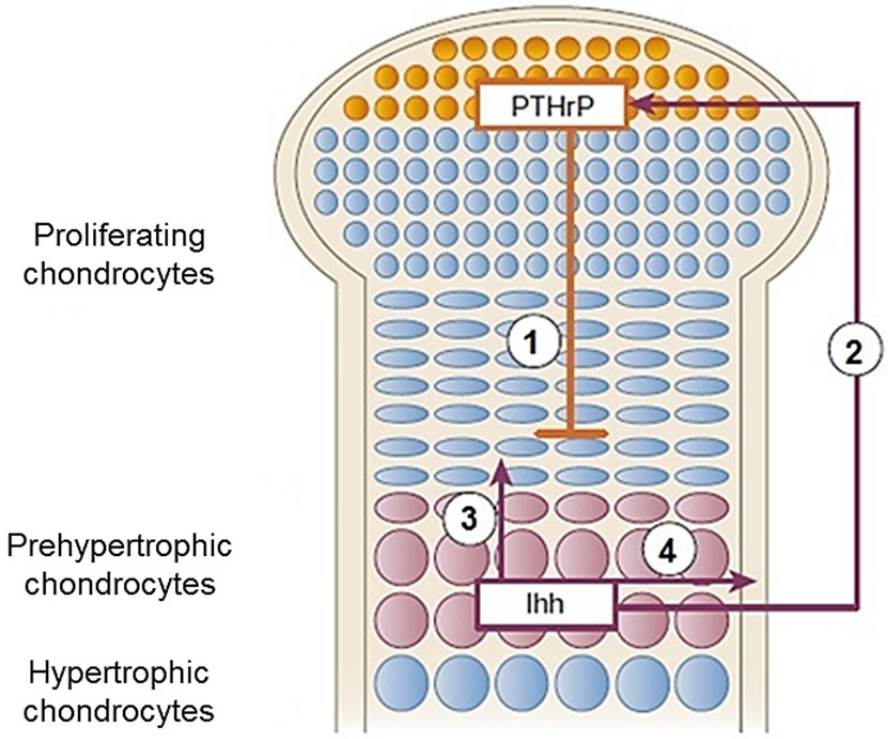

Figure 1-10. *PTHrP-Ihh negative feedback loop (adapted from Kronenberg, 2003). PTHrP is synthesised by perichondrial cells and chondrocytes at the ends of long bones (1). PTHrP promotes chondrocyte proliferation by delaying their differentiation. When the source of PTHrP production is distant enough, production of Ihh starts. Chondrocytes that stopped proliferating (prehypertrophic) synthesize Ihh that in turn stimulates the synthesis of PTHrP at the ends of bones (2). Ihh, independently of PTHrP, stimulates proliferation of adjacent chondrocytes (3), leads perichondral cells to differentiate into osteoblasts of the bone collar (4) and promotes the differentiation of proliferating chondrocytes into flat columnar ones.*

1.10.3. Bone morphogenetic proteins

Bone morphogenetic proteins (BMPs), members of the transforming growth factor β (TGFβ) superfamily of paracrine factors, were originally named due to their capability to induce ectopic bone formation (Wozney et al., 1988). They are now divided into subgroups that comprise not only osteoinductive BMPs and BMP-like proteins present in *Drosophilla* but also growth and differentiation factors (GDFs) and cartilage-derived morphogenetic proteins (Ducy and Karsenty, 2000). Members of BMP family are characterised by a wide spectrum of biological functions that have an effect on a variety of cells, such as monocytes, neuronal, epithelial and mesenchymal cells. BMPs are capable of controlling cell differentiation, proliferation and apoptosis along with regulating biological processes, including mesodermal patterning, neurogenesis, left-right asymmetry and the development of numerous organs, such as lung, gut, kidney, teeth, testis and limbs (Wozney et al., 1988, Balemans and Van Hul, 2002).

BMPs play an important role in formation of mesenchymal condensations and the development of the joints in early limb development. Noggin, a BMP antagonist, prevents the formation of mesenchymal condensations (Pizette and Niswander, 2000), while Noggin knock-out mice are characterised by enlarged cartilage primordial (Brunet et al., 1998). Critical in joint formation GDF5 (Baur et al., 2000), stimulates cartilage development and restricts the expression of molecular markers of joint formation to the appropriate site only to follow this action with induction of apoptosis at the level of the forming joint. Cavitation driven by the process of apoptosis is crucial for joint formation. Mice lacking BMP antagonist Noggin are characterised by substantial failure to form joints as excess BMP activity results in excess cartilage and failure to initiate joint formation (Brunet et al., 1998). BMP-2, BMP-4 and BMP-7, when overexpressed, act as apoptotic signals for the undifferentiated limb mesoderm, which promotes intense growth in radius of the differentiating cartilage and disturbs the development of joints (Macias et al., 1997, Duprez et al., 1996). BMPs are equally important in later stages of cartilage development. Most BMPs (BMP-2, BMP-3, BMP-4, BMP-5, BMP-7) are expressed in the perichondrium, BMP-2 and BMP-6 are also found in hypertrophic chondrocytes, BMP-7 is expressed in proliferating chondrocytes.

It has been shown that BMPs support chondrocyte proliferation (Minina et al., 2001). BMP signalling upregulates the expression of Ihh and delays the differentiation of hypertrophic chondrocytes (Minina et al., 2002). Minina suggested a model of the regulation of the chondrogenesis by the Ihh/PTHrP and BMP signalling pathways. Ihh promotes proliferation of the neighbouring chondrocytes and positively regulates Bmp expression in the proliferating chondrocytes and perichondrium. Ihh also stimulates the expression of PTHrP which, in turn, downregulates hypertrophic differentiation. Signalling of Ihh and BMP together regulates chondrocyte proliferation and enables the cells to move away from the source of PTHrP which leads to activation of Ihh expression. Ihh expression might be directly or indirectly controlled by BMP which upregulates Ihh expression in cells that are not under the influence of PTHrP (Minina et al., 2001).

1.10.4. Wingless + Integrated family molecules

Wingless + Int (Wnt) family (family of highly conserved secreted signalling molecules regulating cell interactions during embryogenesis) are implicated in the regulation of endochondral bone formation. There are 19 known members of Wnt family in vertebrates. By acting via receptors Frizzled (Fzd) and co-receptors Lrp5 and Lrp6, Wnts are involved in signalling pathway leading to the gene expression and regulation

of cell adhesion (Yates et al., 2005). Wnt family members can activate both canonical (β-catenin mediated) and non-canonical (calcium-dependent kinase C-mediated) signalling pathways. The latter pathway can lead to suppression of canonical signalling through β-catenin degradation (Yates et al., 2005). In the canonical pathway Wnt activates the receptor which leads to stabilisation and accumulation of β-catenin in cytosol. β-catenin is then shifted to the nucleus where it regulates gene transcription. Non-canonical calcium pathway that involves release of intracellular calcium and activates protein kinase C may antagonise the canonical pathway by supporting β-catenin degradation (Topol et al., 2003). Differentiation of chondrocytes from mesenchymal progenitors in the developing limb buds during embryogenesis requires non-canonical Wnt signalling with canonical β-catenin pathway inhibiting the process. Both pathways are required for normal chondrocyte proliferation and differentiation in later stages of embryonic development (Hartmann, 2002). Inactivation of β-catenin in mouse embryonic chondrocytes leads to decreased chondrocyte proliferation and hypertrophic differentiation (Hill et al., 2005). Wnt-5, acting through the calcium pathway, negatively regulates the formation of proliferating chondrocytes and maturation of prehypertrophic chondrocytes, Wnt-4 triggers a β-catenin pathway, a positive regulator of chondrogenesis and accelerates maturation of the periosteum (Hartmann and Tabin, 2000). Wnt-5b promotes formation of the proliferative zone and inhibits chondrocyte hypertrophy (Yang et al., 2003). Wnt expression has also been shown in postnatal endochondral bone formation, where it proved to follow the pattern of Ihh expression with low expression levels in resting zone, high in the prehypertrophic zone and lower levels in hypertrophic zone (Andrade et al., 2007). It has also been suggested that some Wnts (i.e. Wnt-3, Wnt-7) that play an important role in early stages of limb formation, are not essential for postnatal chondrocyte differentiation (Andrade et al., 2007).

1.10.5. Fibroblast growth factors

Fibroblast growth factors (FGFs) regulate proliferation and differentiation of growth plate chondrocytes. Expression of many of the twenty two FGF genes and four FGF receptors is characteristic for every stage of endochondral ossification (Ornitz and Marie, 2002). Condensing mesenchyme of the earliest stages of long bone formation expresses FGF receptor 2 (FGFR2) and many FGFs. When chondrocytes form, they express FGF receptors: proliferating chondrocytes express FGF receptor 3 (FGF3), prehypertrophic and hypertrophic chondrocytes alongside perichondrium – FGF receptor 1 (FGF1). FGF receptor 2 (FGFR2) is expressed in the perchondrium, periosteum and primary spongiosa. Activation of FGFR3 results in inhibition of

chondrocyte proliferation and stimulation of hypertrophic differentiation (Minina et al., 2002). It has been suggested that FGF18, expressed in the perichondrium, acts on FGFR3 to decrease chondrocyte proliferation and on FGFR1 to prevent hypertrophic chondrocytes from undergoing terminal differentiation (Kronenberg, 2003). FGF18 is also thought to act on FGFR1 and FGFR2 to delay the development of the osteoblasts. It has been shown that in regulating Ihh expression, process of hypertrophic differentiation and chondrocyte proliferation, FGF and BMP pathways act antagonistically (Minina et al., 2002). Furthermore, FGF signalling is thought to act upstream of the Ihh/PTHrP system in controlling the hypertrophic differentiation as it proves to regulate the onset of hypertrophic differentiation by directly controlling the expression of Ihh. Columns of proliferative chondrocytes get shortened by the direct effect of FGF signalling (reduction of chondrocyte proliferation) and indirectly through FGF suppressing Ihh expression.

1.10.6. Transcription factors

A range of factors, including IGF1 and different members of the TGFβ superfamily (i.e. BMPs) stimulate expression of genes encoding cartilage specific components of ECM such as collagen type II, IX, XI and aggrecan. Expression and secretion of these and other components of ECM is dependent on transcription factor SOX-9 (Bi et al., 1999, Lefebvre and Smits, 2005, Tew et al., 2008). SOX-9 binds and induces *Col2a1* enhancer element of the gene encoding collagen type II, resulting in *Col2a1* expression within proliferative chondrocytes (Lefebvre et al., 1997). Expression of both *Col2a1* and *Sox-9* decreases in hypertrophic chondrocytes (Castagnola et al., 1988, Ng et al., 1997). At this stage, synthesis of collagen type X is induced, which leads to a change in chondrocyte phenotype from proliferative to hypertrophic. Collagen type X synthesis is limited to chondrocytes within the hypertrophic zone of the growth plate (Gerstenfeld and Landis, 1991). RUNX-2 is a transcriptional activator of *Col10a1* (gene encoding collagen type X) (Zheng et al., 2003). *Runx-2* expression is observed from the early stages of hypertrophy, right through to terminal differentiation. RUNX-2 has been found to promote full hypertrophic differentiation (Lefebvre and Smits, 2005). Mice missing *Runx-2* have no osteoblasts (Komori et al., 1997). RUNX-2 also stimulates expression of Ihh by activating its promoter (Yoshida et al., 2004), Ihh can feed back to inhibit *Runx-2* expression through the Protein kinase A (PKA) pathway (Iwamoto et al., 2003). By inhibiting *Runx-2* expression, PTHrP can delay chondrocyte hypertrophy (Guo et al., 2006). RUNX-2 plays an important role in balancing chondrocyte proliferation and hypertrophy by contributing to the previously mentioned Ihh/PTHrP negative feedback loop. Through direct interaction, SOX-9 can suppress activity of RUNX-2 and has been

shown to be dominant over RUNX-2 function in mesenchymal precursors of chondrogenic lineage in endochondral bone formation (Zhou et al., 2006).

1.10.7. Light and dark chondrocytes

There are two co-existing morphologically distinct types of chondrocytes in the proliferative and hypertrophic zones of the growth plate: light and dark chondrocytes (Hwang, 1978). Light chondrocytes are round or oval cells characterised by sparse endoplasmic reticulum, inconspicuous Golgi region and a few cytoplasmic processes that extend into the surrounding matrix. Irregularly shaped dark chondrocytes have numerous endoplasmic processes and are characterised by well-developed endoplasmic reticulum and a prominent Golgi zone present within the cytoplasm.

1.10.8. Chondrocytes and cell death

It is debatable how the hypertrophic chondrocytes die. The process of chondrocyte death has been described as apoptosis (Adams and Shapiro, 2002). Apoptosis is a programmed, physiological cell death characterised by morphological features such as intense condensation of chromatin and fragmentation of cytoplasm and nucleus into apoptotic bodies consisting of cytoplasm with tightly packed organelles enclosed within an intact plasma membrane. Apoptotic bodies are subsequently phagocytosed and degraded. Death of hypertrophic chondrocytes has been described as apoptosis due to the method of DNA strand breaks detection (terminal deoxynucleotidyl transferase dUTP nick end labelling, TUNEL) or other molecular features associated with apoptosis rather than morphological characteristics of the cell (Adams and Shapiro, 2002). The final and conclusive identification of apoptosis proves to be morphological (Kerr et al., 1972). It has been observed that dying hypertrophic chondrocytes lack typical features of apoptosis such as condensation of chromatin, cell shrinkage and fragmentation of nucleus (Roach and Clarke, 1999, Roach and Clarke, 2000). Light and dark chondrocytes are two morphologically distinct post proliferative populations of growth plate chondrocytes. They demonstrate different patterns of gene expression but are also proven to undergo two different non-apoptotic cell death processes (Ahmed et al., 2007). Light chondrocytes disintegrate by dismantling the content of their cytoplasm within the intact plasma membrane, whereas dark chondrocytes break off packets of cytoplasmic contents and plasma membrane.

1.11. BCL-2-associated athanogene-1 (BAG-1)

The process of endochondral ossification involves deposition of bone matrix by osteoblasts on a cartilage template which acts as a scaffold for future bones. Precise formation of this cartilage model during embryogenesis is therefore critical to the correct development of endochondral bones and the adult skeleton. Skeletal growth aberrations, such as chondrosarcomas, dwarfism and chondrodysplasias are commonly caused by disruption of the complex interactions involved in chondrocyte development. Aberrant skeletal development is also strongly linked to osteoporosis and osteoarthritis. Although the process of bone formation has been widely characterised, molecular links between numerous factors controlling endochondral ossification have yet to be completely elucidated. A number of studies have indicated that **BCL-2-associated athanogene-1 (BAG-1)** plays an important role in the physiology of the skeletal system (Crocoll et al., 2002, Kinkel et al., 2004, Tare et al., 2008b). Research into links between BAG-1 and the process of endochondral ossification will hopefully enhance our understanding of musculoskeletal diseases and influence skeletal tissue regeneration and replacement strategies.

B-cell lymphoma 2 (BCL-2), an anti-apoptotic protein, plays an important role in sustaining a stable chondrocyte phenotype. In growth plate it is expressed mainly within late proliferative and prehypertrophic chondrocytes and is downregulated in hypertrophic chondrocytes (Amling et al., 1997). Inhibition of *Bcl-2* expression results in downregulation of *Sox-9*, *Aggrecan* and *Col2a1* (Kinkel and Horton, 2003, Feng et al., 1999).

Originally discovered as a protein that is able to bind and enhance the anti-apoptotic activity of BCL-2 and hence termed “BCL-2-associated athanogen-1” (BAG-1) (Takayama et al., 1995), BAG-1 has been identified in mouse growth plates and articular chondrocytes (Kinkel et al., 2004).

BAG-1 was also independently discovered as an interaction partner of members of the nuclear hormone receptor family. It was named RAP46 (receptor-associating protein of 46 kDa apparent molecular weight) (Zeiner and Gehring, 1995). It was later renamed HAP46 (hsp70/hsc70-associating protein) when the same researchers discovered that HSP70 heat shock proteins were its most conspicuous interaction partners (Zeiner et al., 1997). BAG-1 exists as multiple isoforms and interacts with a number of different cellular targets (Townsend et al., 2003b) such as BCL-2, HSP70 heat shock protein and serine/threonine protein kinase (RAF-1 kinase), nuclear hormone receptors, DNA and components of the ubiquitin and proteasome pathway. BAG-1 controls cell

signalling, proliferation, differentiation, apoptosis and transcription pathways via its binding partners (Takayama and Reed, 2001).

1.11.1. Structure of BAG-1

1.11.1.1. *Bag-1* gene

Proteins of the BAG family are encoded by six genes in mammalian cells: *Bag-1* (encoding all different protein isoforms), *Bag-2*, *Bag-3* (BIS, CAIR-1), *Bag-4* (SODD), *Bag-5* and *Bag-6* (BAT3, SCYTHE) (Takayama et al., 1995).

Bag-1 gene is located on human chromosome 9 in region p12 (9p12) and region 9pter→9q34 of mouse chromosome (Takayama et al., 1996). Human *Bag-1* gene contains 7 exons and is 10 kb in size. BAG-1 isoforms are generated through different translation initiation sites in single mRNA (Packham et al., 1997).

1.11.1.2. BAG-1 protein

After the discovery of HAP46 (274 amino acid residues), which is synthesised from an AUG codon, cloning of cDNAs suggested the existence of a larger isoform. This isoform originates from an upstream CUG start codon and contains 345 amino acids (Packham et al., 1997). Its molecular weight proved to be approximately 50 kDa which consequently led to naming this isoform p50, HAP50 or BAG-1L (L for long). BAG-1L isoform has been detected in both human and murine cells (Packham et al., 1997, Takayama et al., 1998, Yang et al., 1998). To keep nomenclature consistent, human HAP46 was then renamed BAG-1M (M for medium). There are also shorter human isoforms, namely 230 amino acid residue, approximately 36 kDa BAG-1S (S for small), and 207 residue, approximately 29 kDa BAG-1S (Takayama et al., 1998, Yang et al., 1998), both originating from two internal downstream AUG codons. The smaller BAG-1S isoform, however, is not always detected and levels of its expression are low (Yang et al., 1998). All BAG-1 isoforms are generated by alternative translation initiation where three translation initiation sites (CUG for BAG-1L, AUG for BAG-1M, AUG for BAG-1S) are located within the first exon of the gene (Fig. 1-11).

BAG-1S isoform is the most abundant isoform with its translation being at least partially dependent on internal ribosome entry sequence (IRES) mediation. This kind of translation is independent of cap structures and relies on mRNA complex structural elements (Coldwell et al., 2001). Proteins are generated mainly by cap dependent translation where mature mRNA is accessed by ribosomes at the 5'cap structure. Ribosomes then perform scanning of mRNA and initiate translation upon detection of a

translation initiation codon, usually an AUG codon. If BAG-1S isoform was to be translated via cap dependent structure, ribosome would have to disregard eight CUG and two AUG codons. IRES dependent translation is an alternative mechanism that enables translation independent of cap structures. Cells that have been subjected to heat shock or undergoing apoptosis maintain IRES dependent translation while being unable to undergo cap dependent translation.

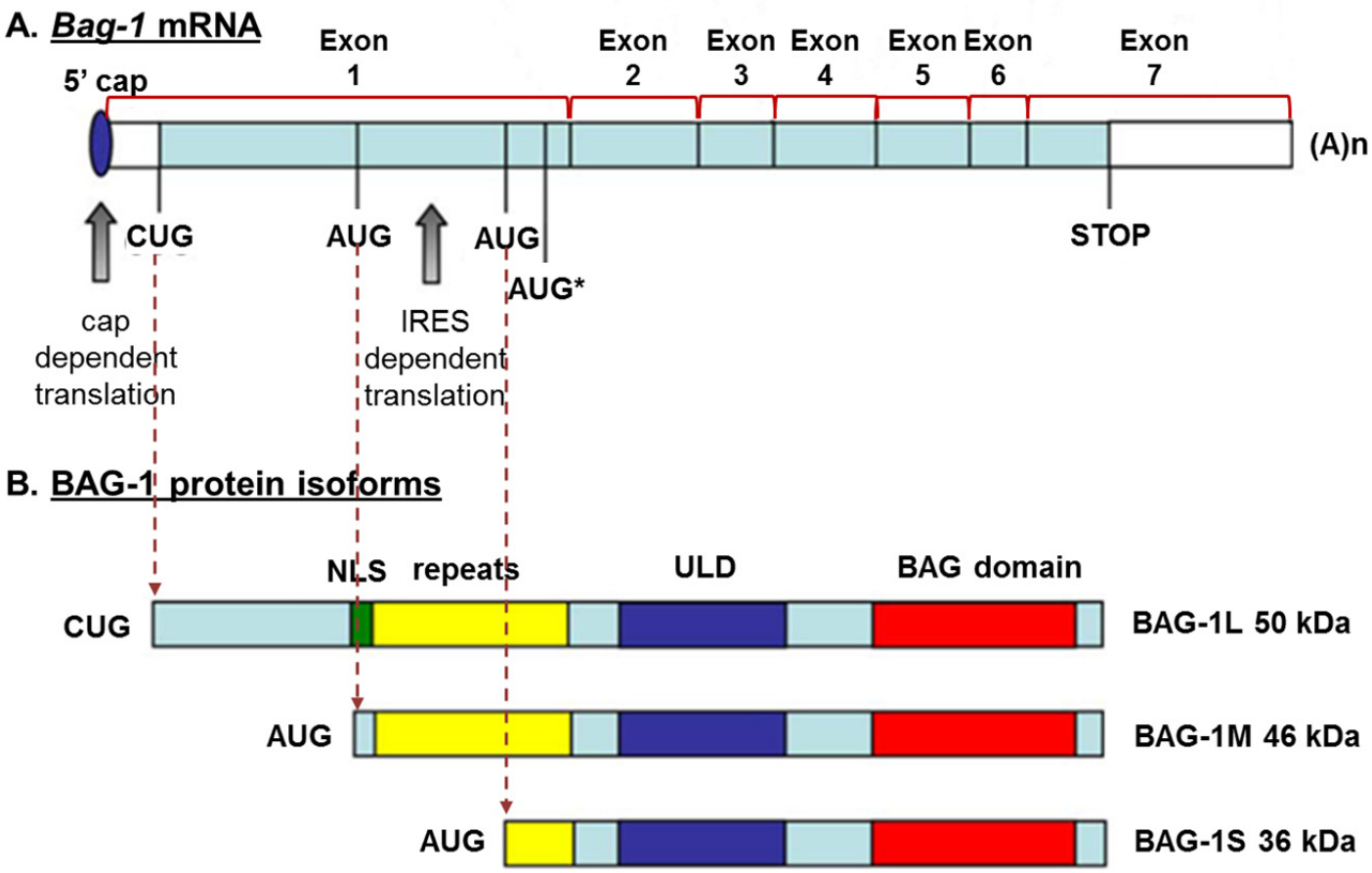

Figure 1-11. *Structure of human Bag-1 mRNA (A) and BAG-1 protein isoforms with their domains (B) (adapted from Townsend et al., 2005). The alternate translation initiation sites are all located within the first exon (CUG for BAG-1L, AUG for BAG-1M, AUG for BAG-1S). Shown are the structures of human BAG-1 isoforms with their size in kDa.*

*NLS – nuclear localization sequence; ULD – ubiquitin-like domain; * - translation initiation site for a smaller Hap29/BAG-1S isoform*

There is no corresponding isoform to human BAG-1M in rodents since the first AUG codon is not conserved (Fig. 1-12). Comparatively, murine mRNA has a GUG codon where human mRNA has an AUG codon. Murine BAG-1S, 32 kDa isoform produced from the internal AUG start codon, originally discovered as 219 amino acid residue protein in mice (Takayama et al., 1995), corresponds to human BAG-1S. Human and murine BAG-1S proteins are highly homologous.

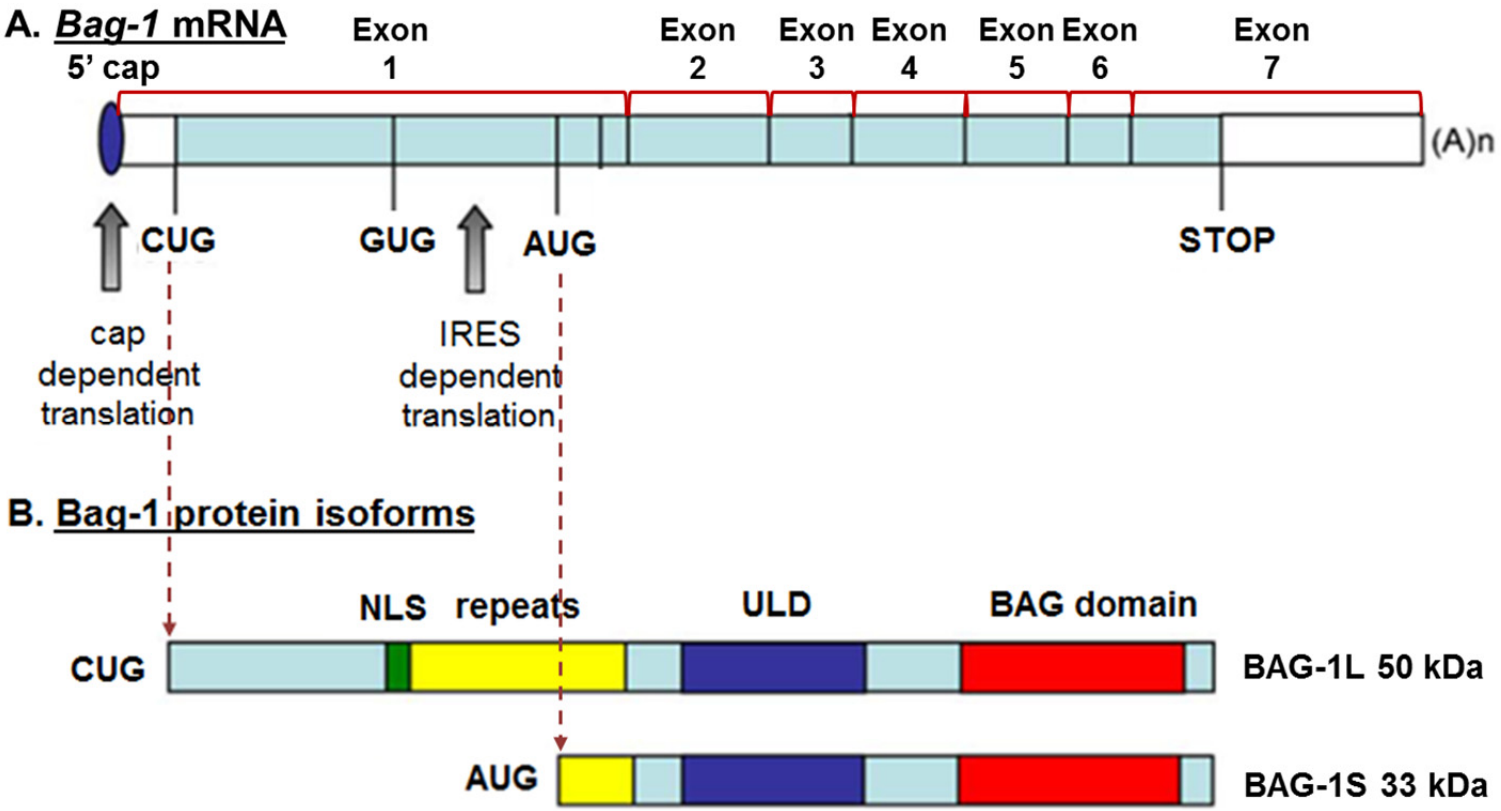

Figure 1-12. *Structure of mouse Bag-1 mRNA (A) and BAG-1 protein isoforms with their domains (B). (adapted from Townsend et al., 2005). The alternate translation initiation sites are all located within the first exon (CUG for BAG-1L, AUG for BAG-1S).*

NLS – nuclear localization sequence; ULD – ubiquitin-like domain.

Cells can express various BAG-1 isoforms. These isoforms differ not only in functionality but also localisation in the cell (Hohfeld, 1998, Townsend et al., 2003a). BAG-1L is a nuclear protein containing the N-terminal nuclear localisation sequence (NLS), whereas BAG-1S is typically found in the cytoplasm (Packham et al., 1997). BAG-1M can be detected in both the cytoplasm and the nucleus as cellular stress such as heat shock can cause relocation of cytoplasmic BAG-1M to the nucleus (Townsend et al., 2003a).

1.11.1.3. BAG-1 protein domains

BAG-1 isoforms are characterised by the presence of various protein domains (Briknarova et al., 2001, Sondermann et al., 2001). All BAG-1 isoforms contain a 70 amino acid residue domain ("BAG domain"). Two amphipathic α-helices responsible for interaction with the HSC70 and HSP70 chaperones represent the main core of the BAG domain (Fig. 1-13). The third helix of this domain may be responsible for maintaining the structure and interactions between proteins (Townsend et al., 2003b). Many BAG-1 functions are thought to be dependent on this region of protein binding to chaperones.

Figure 1-13. *The BAG domain/HSC70 interaction (Sondermann et al., 2001). The structure of BAG-1 BAG domain (red) and the ATPase domain of HSC70 (green) H1, H2, H3 – helices of BAG domain.*

Another domain incorporated in all BAG-1 isoforms is ubiquitin-like domain (ULD) (Takayama et al., 1995). Ubiquitin is an omnipresent protein that binds to protein substrates tagging them for degradation by proteasomes (Hershko and Ciechanover, 1998). All BAG-1 proteins include a ULD domain, which suggests that BAG-1 proteins are a part of the ubiquitin regulating system.

BAG-1 also contains nuclear localisation sequences (NLS). Nuclear localisation sequences are short stretches of amino acids that facilitate the transport of nuclear proteins through the nuclear pore (Kalderon et al., 1984). NLS is localised within the

amino terminal domain of nuclear BAG-1L (Packham et al., 1997). Part of the NLS sequence is detectable at the amino terminus of BAG-1M but it is not considered functional.

1.12. Biological functions of BAG-1

1.12.1. BAG-1 and apoptosis

BAG-1 can suppress apoptosis caused by a range of different factors, such as kinase inhibitors, heat shock, dexamethasone or radiation (Bardelli et al., 1996, Zeiner et al., 1999, Kullmann et al., 1998, Yang et al., 2000). BAG-1 was first discovered as a BCL-2 binding protein, localised mainly to the outer membrane of mitochondria, and was most likely involved in mitochondrial pore complex formation (Reed, 1998, Green and Reed, 1998). The release of cytochrome c and other pro-apoptotic factors from mitochondria activates caspases (apoptotic enzyme mediators). A major role of BAG-1 is to prevent the release of these factors. In gene knock out mouse models, deletion of both *Bag-1* alleles (homozygosity) results in significant cell apoptosis in the embryonic liver, defective haematopoiesis and neuronal differentiation which lead to death between embryonic days 12.5 and 13.5 (Gotz et al., 2005).

1.12.2. BAG-1 and heat shock proteins

Not only does BAG-1 target the BCL-2 regulated mitochondrial point of apoptosis, BAG-1 also functions at other levels of the apoptosis cascade (Takayama and Reed, 2001, Townsend et al., 2003a). HSC70 (expressed constitutively in cells) and HSP70 (induced by cell stress), along with mitochondrial mHSP70 and HSPA5 (immunoglobulin heavy chain-binding protein, BiP/GRP78) are the four major mammalian 70 kDa heat shock proteins, a family of widely characterised molecular chaperones (Schlesinger, 1990, Mayer et al., 2001). Formation of an apoptosome is a recognised feature of apoptosis. Released cytochrome c together with apoptotic protease activating factor 1 (Apaf-1) and dATP/ATP form an apoptosome complex which then cleaves procaspase-9, activates caspase-9 and consequently induces apoptosis through caspase-3 activation. Heat shock proteins are important controllers of apoptosome formation and activation (Hohfeld, 1998). HSP70 inhibits the process of apoptosis by blocking the recruitment of procaspase-9 to the apoptosome complex.

Under stress conditions, intracellular proteins can potentially be so severely damaged that it can lead to cell death. Cells can protect their most important proteins via chaperones such as HSC70 and HSP70, which bind unfolded proteins, prevent their

aggregation and assist their reformation. HSP70 also prevents partially synthesised peptide sequences of incomplete proteins from aggregating and becoming non-functional. HSC70 proteins comprise of three major domains: a) N-terminal ATPase domain that binds adenosine 5'-triphosphate (ATP) and hydrolyses it to adenosine 5'-diphosphate (ADP), b) substrate binging domain with an affinity for hydrophobic amino acid residues and c) C-terminal domain that functions as a binding pocket for the substrate binding domain. Binding and release of substrates by heat shock proteins depends on their adenosine triphosphatase (ATPase) activity. HSC70 binds adenosine 5'-triphosphate (ATP) with high affinity and then slowly hydrolyses the coenzyme to adenosine 5'-diphosphate (ADP) (Fig. 1-14). ADP-bound HSP70 has higher affinity to substrate than the ATP-bound form. HSC70 not interacting with substrate (peptide) is usually in an ATP bound state. When HSC70 substrate binding domain recognises and interacts with hydrophobic amino acid residues of a protein, ATPase activity of HSP70 is stimulated which leads to an increase of normally slow rate of ATP hydrolysis. Following the hydrolysis of ATP to ADP, the binding pocket of HSP70 shuts and binds the trapped peptide chain. When the protein bound to HSC70 is ready to be released, nucleotide exchange factors such as BAG-1 stimulate ADP release and binding of fresh ATP. BAG-1 and HSC70 interact via the ATPase domain of the HSC70 (Sondermann et al., 2001, Briknarova et al., 2001). After binding to the HSC70/ADP, BAG-1 domain promotes nucleotide release from the HSC70. Given that ATP is present at much higher concentrations than ADP and BAG-1 in the cell, ATP will bind and displace BAG-1 protein. This will in turn accelerate the exchange of nucleotide (Sondermann et al., 2001), open the binding pocket and release the protein. BAG-1/HSC70/peptide complexes have been observed between BAG-1M, HSC70 and c-Jun (Zeiner et al., 1997). The possible involvement of HSP70/HSC70 in BCL-2/BAG-1 complex formation has also been suggested (Takayama et al., 1997).

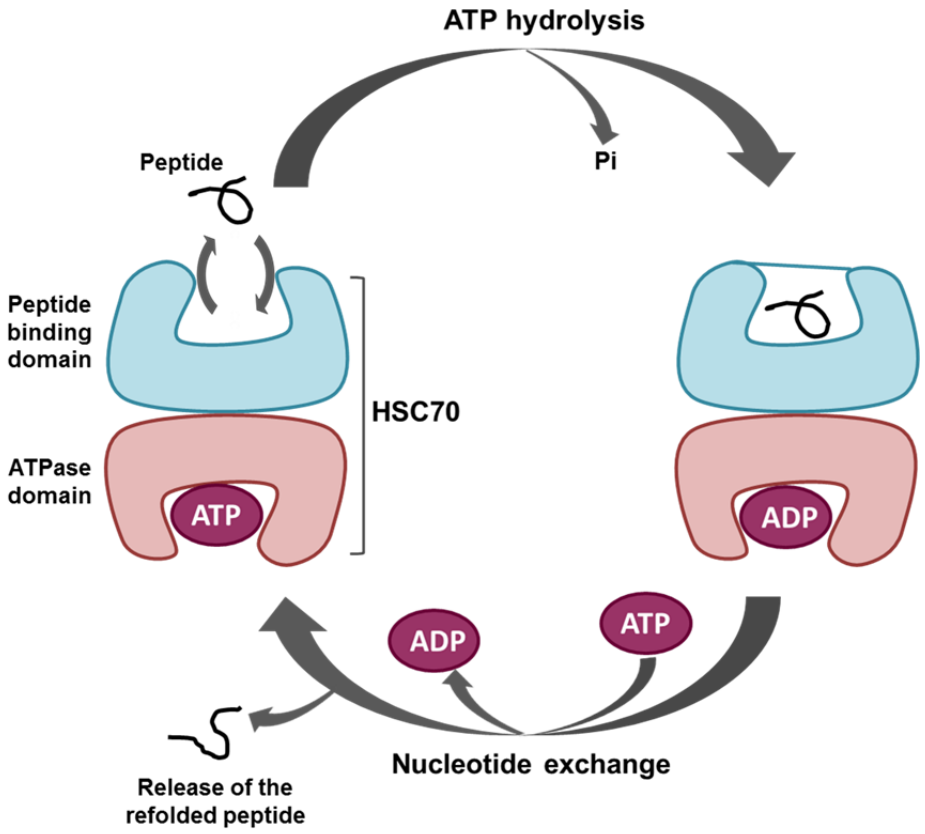

Figure 1-14. *The HSP70/HSC70 cycle (adapted from Townsend et. al., 2003b). HSC70 not interacting with a peptide is in an ATP bound state; following the hydrolysis of ATP to ADP, the binding pocket of HSC70 shuts and binds the trapped peptide chain. Nucleotide exchange allows release of partially refolded substrate.*

1.12.3. BAG-1, signal transduction and cell cycle

Signal transduction is a key factor in cell proliferation and survival. BAG-1 has been shown to regulate the function of many signalling molecules, including the RAF-1 kinase (Wang et al., 1996). RAF-1 is an essential factor of the transmission of growth control signals from the cell surface to cell nucleus. RAF-1 activates mitogen activated protein (MAP) kinases (extracellular signal-regulated kinase 1/2, MEK1/2 and ERK1/2) by phosphorylation. This in turn activates a cascade of phosphorylation events which result in the activation of transcription factors. RAF-1 is usually activated by a signalling molecule RAS. It has been shown that BAG-1 provides another mechanism of RAF-1 activation which is independent of RAS (Wang and Reed, 1998). The binding sites for RAF-1 on BAG-1 overlap with those for HSC70 and both molecules bind competitively to BAG-1 (Song et al., 2001). In addition to regulating signalling molecules, BAG-1 influences the cell cycle by interacting with nuclear hormone receptors (NHR) (Cato and Mink, 2001), growth factors (Lin et al., 2001) or DNA via NLS domain (Zeiner et al., 1999, Niyaz et al., 2001). BAG-1 can also influence functions of protein 53 (p53), a

mediator of DNA damage-induced and stress-induced apoptosis and cell cycle regulator (King et al., 2001).

1.12.4. BAG-1 and Endoplasmic Reticulum Stress

Endoplasmic reticulum (ER), an organelle responsible for synthesis and folding of lysosomal, membrane and secretory proteins and calcium storage, is involved in eukaryotic cell stress response (Hammond and Helenius, 1995). Functions of ER subjected to stress conditions such as oxidative stress are compromised – this state of the organelle is called "ER stress" (Kaufman, 1999). To deal with the ER stress, cells implement a number of strategies, e.g. elimination of misfolded proteins and inhibition of protein accumulation in the ER (Rao et al., 2004). Severe impairment of ER functions leads to apoptosis which protects the organism via the damaged cell elimination; one of the apoptotic pathways involved in this response in the transcriptional activation of growth arrest and DNA damage-inducible gene 153 *(Gadd153)* gene expression (Gotoh et al., 2004).

Chondrocytes can be affected by a number of stress inducing factors, such as mechanical stress, osmotic stress and oxidative stress and are sensitive to deficiency of oxygen and nutrients. It has been shown that ER stress in chondrocytes leads to inhibition of chondrocyte growth and induction of its apoptosis (Yang et al., 2005).

BAG-1 has been shown to play an important role in radiation, hypoxia or cytotoxic drug treatment induced cell stress (Townsend et al., 2003a). The mechanism through which BAG-1 is thought to play a role in controlling cell stress include interaction with HSP70 and Raf-1 kinase (Song et al., 2001), regulation of folding and degradation of protein (Agarraberes and Dice, 2001) and binding to GADD34 (Hung et al., 2003). Yang and co-workers have shown that BAG-1 is important in chondrocyte phenotype regulation and its viability (Yang et al., 2007). They demonstrated downregulation of *Bag-1*/BAG-1 in chondrocytes during ER stress, chondrocyte cell growth arrest and apoptosis in response to knocked down *Bag-1* expression and delayed ER stress induced apoptosis in chondrocytes overexpressing *Bag-1*. The authors also suggest that BAG-1 modulates the expression of chondrocyte matrix proteins under stress conditions – chondrocytes overexpressing *Bag-1* under ER stress maintained collagen II expression longer than the wild type cells.

1.13. BAG-1 and skeletal development

1.13.1. Fetal limb development

Bag-1 expression has been linked with digit formation during mouse limb development (Crocoll et al., 2002). *Bag-1* has been shown to be ubiquitously expressed throughout limb bud mesenchyme at embryonic days (E) 10.5 and 11.5. At day 12.5 of gestation *Bag-1* expression is restricted to the interdigital region and by day 14.5, when digit formation almost reaches its completion, *Bag-1* expression is not detected in cartilaginous structures and is downregulated in the interdigital region (Crocoll et al., 2002). Mesenchymal condensations that appear between E10.5 and E12.5 model future skeletal elements (Karsenty, 1999). Based on these observations it has been suggested that BAG-1 plays an important role in mesenchymal cell condensations, which are crucial for chondrogenic differentiation.

1.13.2. Postnatal bone

BAG-1 has been shown to be expressed in murine growth plate, articular chondrocytes (Kinkel et al., 2004, Tare et al., 2008b), perichondrium, osteoblasts, bone marrow and osteocytes (Tare et al., 2008b). At three weeks of age, when the process of endochondral ossification is still active, BAG-1 expression in the growth plate is localised mostly in the chondrocytes of reserve and upper hypertrophic zones. At the age of ten weeks, when the skeleton is still immature, BAG-1 was shown to be expressed by most of the prehypertrophic and hypertrophic chondrocytes, but was undetectable in proliferative chondrocytes. By the time mice reached 6 months of age, there was no established pattern of BAG-1 expression.

Tare at al. have shown that BAG-1 functions as an anti-apoptotic defence against heat-shock in chondrocytic cells (Tare et al., 2008b). Overexpression of BAG-1L and BAG-1S isoforms protected ATDC5 cells against heat-shock-induced apoptosis.

1.13.3. Osteoarthritis (OA)

Osteoarthritis is a progressive disease that involves degradation of joints, including articular cartilage and subchondral bone. Changes in composition of extracellular matrix (ECM) and chondrocyte gene expression appear before the manifestation of visible structural damage (Hamerman, 1989). It has been shown that BAG-1 is upregulated in OA cartilage and is distributed across the depth of the cartilage in advanced disease, compared to its restriction to the surface zone in minimally involved OA (Nugent et al., 2009). It has been suggested, that chondrocytes upregulate BAG-1

expression in an attempt to antagonise apoptotic signals, a characteristic of OA. BAG-1 is also thought to stimulate proliferative signals via binding to and activating the raf-1 MAP-kinase proliferation pathway (Wang et al., 1996).

1.13.4. Gene transcription

BAG-1 proteins are thought to affect gene transcription both positively and negatively (Cato and Mink, 2001). They have been shown to bind with DNA *in vitro* via the NLS domain. To determine whether they play a role in regulating the transcription of genes crucial for chondrocyte differentiation and endochondral ossification, Tare and co-workers overexpressed gene encoding BAG-1L isoform in ATDC5 cells (Tare et al., 2008b). Monolayer cultures of the ATDC5 murine cell line had been previously demonstrated to be a reliable model for studying the molecular mechanisms linked with chondrocyte differentiation during endochondral bone formation (Akiyama et al., 1996, Enomoto et al., 2000). BAG-1L has been shown to suppress *Col2a1* gene expression and to enhance transcription of *Runx-2* and Alkaline Phosphatase (*Alp*) (Tare et al., 2008b). Both *Runx-2* and *Alp* are markers of early osteogenesis, with RUNX-2 also positively regulating chondrocyte maturation in hypertrophic chondrocytes (Enomoto et al., 2000). The *Bag-1* gene promoter has been found to be enhanced by SOX-9 protein in ATDC5 cell cultures (Tare et al., 2008b). SOX-9 binds to and activates *Col2a1* gene enhancer (Lefebvre et al., 1997). Tare and co-workers observed that even though BAG-1 downregulated *Col2a1* expression, *Sox-9* overexpression resulted in increased *Bag-1* expression. Tare and co-workers suggested that in the presence of low *Bag-1* expression in proliferating chondrocytes, robust *Sox-9* and *Bcl-2* expression would maintain *Col2a1* expression. High BAG-1 protein synthesis, *Sox-9* downregulation (Ng et al., 1997) and *Bcl-2* (Amling et al., 1997) expression characterise the onset of hypertrophy. It has therefore been suggested that BAG-1 plays an important role in the onset of hypertrophic differentiation leading to mineralisation of cartilage by inducing the expression of *Runx-2* and *Alp,* and suppressing *Col2a1* expression (Tare et al., 2008b). BAG-1L also has the ability to enhance Hsp transcription under non stress conditions (Niyaz et al., 2001). It has been shown that HSPs are expressed in terminally differentiated chondrocytes of the growth plate and promote their hypertrophy and calcification (Otsuka et al., 1996). Based on these observations, it has been suggested that expression of BAG-1, together with HSP by growth plate chondrocytes, supports the process of endochondral ossification by facilitating chondrocyte hypertrophy and cartilage mineralisation (Tare et al., 2008b).

1.13.5. Knock-out mice

To characterise human skeletal development, gene knock-out murine models have been used. Deletion of both *Bag-1* alleles (homozygosity) results in significant cell apoptosis in the embryonic liver, defective haematopoiesis and neuronal differentiation which lead to death between E (embryonic day) 12.5 and E13.5 (Gotz et al., 2005). Deletion of only one *Bag-1* allele (heterozygosity) is not lethal in embryonic mice and could provide an important model for investigating the effects of *Bag-1* haploinsufficiency on murine skeletal development (Gotz et al., 2004).

The method of generating *Bag1*$^{+/-}$ strain will be discussed in section 3.1.

Chapter 2

Hypothesis,
aim and objectives

2.1. Hypothesis:

The work is based on the hypothesis that *Bag-1* plays an important role in the regulation of skeletal development

2.2. Aim:

To address the hypothesis, the project aims to delineate the effects of deletion of *Bag-1* on skeletal development using gene knock-out mouse models and *ex vivo* models of chondrocyte and osteoblast differentiation.

2.3. Objectives:

The following objectives were formulated to achieve the aim of the project:

I. To characterise the role of *Bag-1* in embryonic skeletal development by:

a) Examination of the expression of BAG-1 in prenatal wild-type mice,
b) Histological assessment of *Bag-1*$^{+/+}$, *Bag-1*$^{+/-}$ and *Bag-1*$^{+/-}$ mice between E10.5 and E13.5 of gestation,
c) Analysis of BAG-1L and BAG-1S expression in limb buds of *Bag-1*$^{+/+}$, *Bag-1*$^{+/-}$ and *Bag-1*$^{-/-}$ littermates between E10.5 and E13.5,
d) Analysis of the expression of SOX-9 in mouse fetal limb buds of *Bag-1*$^{+/+}$, *Bag-1*$^{+/-}$ and *Bag-1*$^{-/-}$ littermates between E10.5 and E13.5,
e) Analysis of the expression of collagen type II in mouse fetal limb buds of *Bag-1*$^{+/+}$, *Bag-1*$^{+/-}$ and *Bag-1*$^{-/-}$ littermates between E10.5 and E13.5,
f) Elucidation of the role of *Bag-1* in chondrocyte hypertrophy and cartilage mineralisation using micromass cultures of limb bud mesenchymal cells of E11.5 *Bag-1*$^{+/+}$, *Bag-1*$^{+/-}$ and *Bag-1*$^{-/-}$ littermates.

II. To characterise the role of *Bag-1* in osteoblast development by:

a) Isolation of BMSCs from long bones of skeletally mature *Bag-1*$^{+/+}$ and *Bag-1*$^{+/-}$ mice and establishment of monolayer cultures of BMSCs with and without BMP-2,
b) Analysis of the expression of BAG-1L and BAG-1S proteins in BMSC cultures of wild-type (*Bag-1*$^{+/+}$) and *Bag-1* heterozygous/haploinsufficient (*Bag-1*$^{+/-}$) mice,
c) Examination of the differences in cell number and proliferation between BMSC cultures *Bag-1*$^{+/+}$ and *Bag-1*$^{+/-}$ mice,
d) Assessment of the osteogenic potential of BMSCs of *Bag-1*$^{+/+}$ and *Bag-1*$^{+/-}$ mice,

e) Analysis of the cell apoptosis in BMSC cultures of wild-type and *Bag-1* heterozygous mice,
f) Examination of the differences in the expression of focused panel of genes related to skeletal development between BMSC cultures of *Bag-1*$^{+/+}$ and *Bag-1*$^{+/-}$ mice,
g) Analysis of the bone architecture of *Bag-1*$^{+/+}$ and *Bag-1*$^{+/-}$ mice (micro computed tomography, µCT).

III. To characterise the role of BAG-1-mediated protein-protein interactions in E2-facilitated, BMP-2-directed osteogenic differentiation of murine BMSCs by:
a) Analysis of the expression of estrogen receptors, *ERα* and *ERβ*, by murine BMSCs,
b) Investigation of the effect of E2 on BMP-2-directed osteogenic differentiation of murine BMSCs,
c) Demonstration of the binding between endogenous BAG-1 and HSC70 in murine BMSCs by co-immunoprecipitation,
d) Analysis of the effect of inhibition of the interaction between BAG-1 and HSC70 by Thioflavin-S on E2-facilitated BMP-directed osteogenic differentiation of *Bag-1*$^{+/+}$ and *Bag-1*$^{+/-}$ BMSCs,
e) Examination of the effect of inhibition of binding of BAG-1 to HSC70 by the BAG domain-derived short peptide on E2-facilitated, BMP-directed osteogenic differentiation of *Bag-1*$^{+/+}$ and *Bag-1*$^{+/-}$ BMSCs.

Chapter 3

Materials and methods

Most chemicals and reagents were purchased from Sigma – Aldricht (Gillingham, Dorset, UK). Tissue culture reagents were obtained from Invitrogen. For complete list of reagents and antibodies refer to the Appendix.

Equipment used in the experiments is listed in Appendix 5.

3.1. *Bag-1* knock-out, haploinsufficient and heterozygous mice

The murine *Bag1*$^{-/-}$ strain was generated by Gotz et. al from C57BL/6 mice as previously described (Gotz et al., 2004). In brief, the first two coding exons of *Bag-1* were deleted in order to disrupt the expression of BAG-1L (50 kD) and BAG-1S (32 kDa) isoforms which are generated by alternative use of the start codons. Exon 1 and 2 of *Bag-1* null allele were replaced by neomycin-selectable marker to generate a null allele (Fig. 3-1). Intercrossing of heterozygous mice did not produce live offspring of *Bag1*$^{-/-}$ genotype.

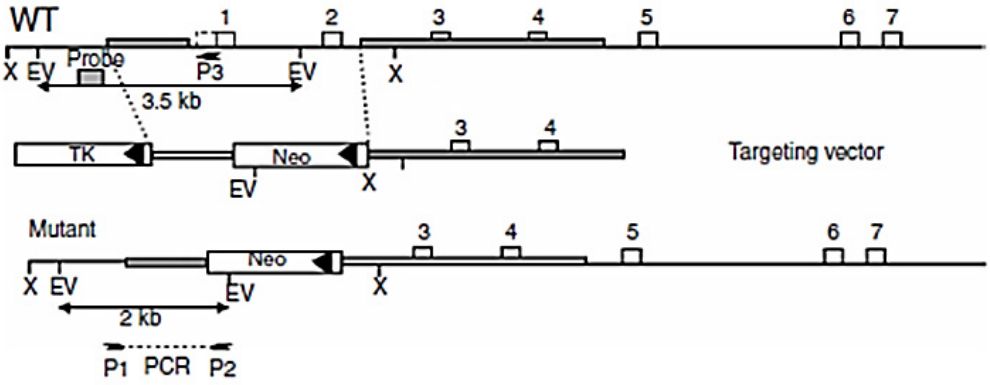

Figure 3-1. *Targeted disruption of Bag-1 gene. Representation of Bag-1*$^{+/+}$ *allele, targeting vector and a mutant allele. The neomycin-selectable marker replaced exons 1 and 2 to generate a full allele. Shown are the primer pairs used to diagnose the targeted allele (P1, P2, P3) and the region recognised by the hybridization probe for Southern analysis. X – XbaI, EV – EcoRV.*

Bag$^{+/-}$ mice were kindly provided by Prof Stefan Wiese, Ruhr University Bochum and bred in the BRF facility at the University of Southampton. All animals used, both adult and embryos, came from the intercrossing of heterozygous mice (Fig. 3-2). The mice were housed in appropriate environments maintained at 21°C ± 2°C and 55% ± 10% humidity with 15-20 room air changes per hour and 12-h/12-h light/dark cycles, had free access to water and were fed *ad libitum*. All experimental procedures performed on animals were carried out under Home Office license in accordance with the Animals Act (1986).

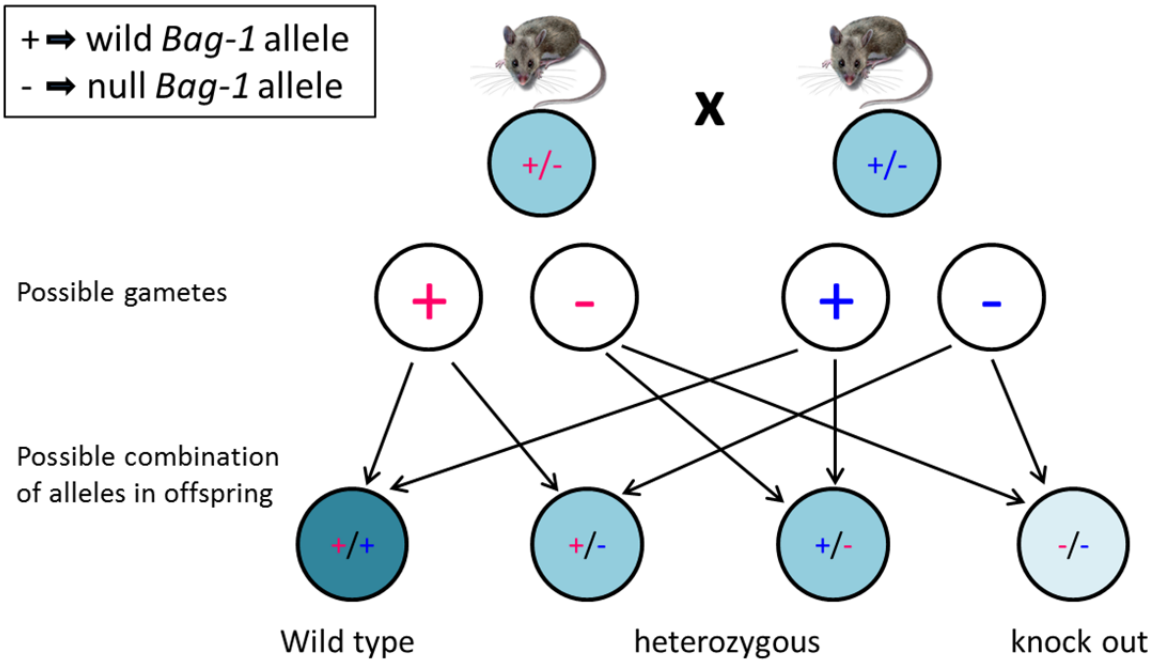

Figure 3-2. *Genetic diagram of intercrossing of Bag-1 heterozygous mice and possible combinations of alleles in offspring.*

3.2. Dissection of mouse fetuses

Pregnant females of *Bag-1*$^{-/-}$ strain mice were sacrificed by 5% CO_2 in a closed atmosphere at the following gestational ages: 10.5, 11.5, 12.5 and 13.5. Pregnancies were detected by checking the female mouse for a vaginal plug every morning at the same time. Uteri were dissected in order to separate the fetuses from the placentas. Fetuses were dissected out, tail snips were taken for analysis of genotype (for method refer to section 3.3) and the fetuses were fixed in ice cold 95% ethanol at 4°C overnight. Following fixation fetuses were imaged with Canon PowerShot G10 Camera. For Western Blot analysis fetal limb buds were collected and processed in RIPA buffer.

3.3. Isolation of genomic DNA and genotyping *Bag-1* littermates using PCR strategy

Genomic DNA was isolated from ear puncture samples from 5-week-old mice or tail snips of fetuses from different stages of embryonic developments. Samples were incubated overnight in DNA isolation buffer (see Appendix 2) containing Proteinase K (Promega). After the incubation samples were spun down and PCR reactions were performed using Veriti® Thermal Cycler (Applied Biosciences) (see Appendix 6). Samples were being used at the volume of 30 µl and consisted of 2 µl of DNA and 28

µl of Master Mix (see Appendix 2) containing 20 µM forward and reverse primer. In order to detect the null type allele two *Bag-1* primers were used: Bag-1 (F) (5' GAGTCTCCCGATCCCTTTTCC 3') located upstream of exon 1 and the Bag-1 (R) (5' ACTTCTAGTCAACTCCCTGGCTGCT 3'), which is located within exon 1 (Fig. 3-3). The absence of bands on agarose gel electrophoresis after PCR distinguishes the *Bag*$^{-/-}$ mice from heterozygous and wild type littermates which both produce bands corresponding to 576 bp PCR products. Detection of the wild type allele was performed by using the Bag-1 (F) primer and Neo (R) primer (5' GATTCGCAGCGCATCGCCTT 3') located within the Neomycin cassette. PCR performed using this primer pair resulted in an observation of no band on agarose gel electrophoresis for wild type littermates and the presence of bands corresponding to 600 bp PCR product for heterozygous and null mice. Electrophoresis was performed on 1% agarose gel containing 0.007% Gel Red at 100 V for 30 minutes. Controls were included in all electrophoresis runs: negative controls had water added to PCR Master Mix instead of DNA, previously tested samples that produced bands corresponding to both 576 bp and 600 bp product were used as positive control. Gels were imaged in InGenius Gel Imaging System (SynGene).

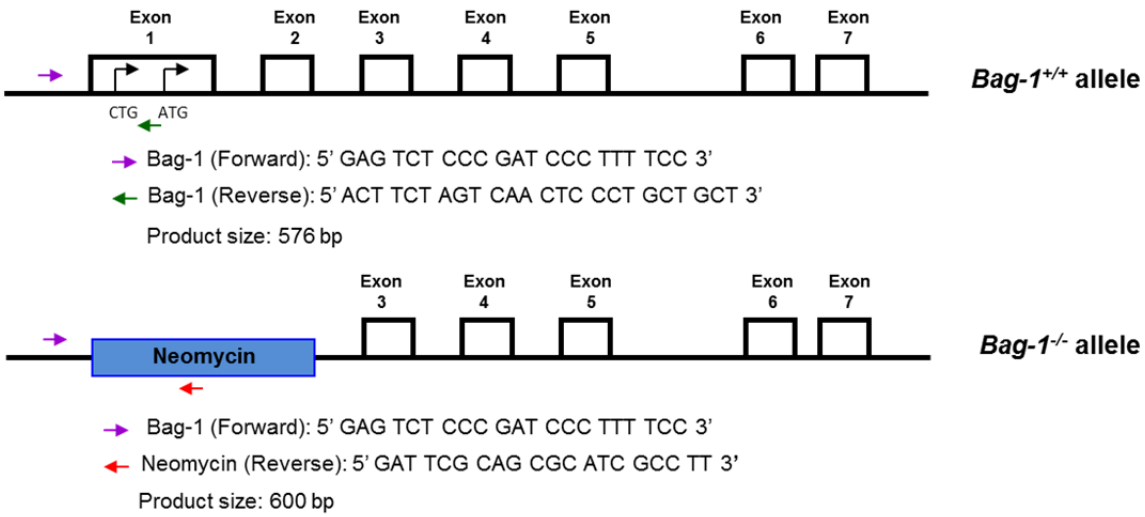

Figure 3-3. *Genotyping Bag-1 littermates using PCR strategy. The Bag-1(F) and Bag-1(R) primers amplify the appropriate Bag-1 sequence only in Bag-1*$^{+/-}$ *and Bag-1*$^{+/+}$ *mice. No band is observed with these primers in Bag-1*$^{-/-}$ *mice. The Bag-1(F) and Neo(R) primers amplify the appropriate sequence only in Bag-1*$^{+/-}$ *and Bag-1*$^{-/-}$ *mice. No band is observed with these primers in Bag-1*$^{+/+}$*.*

3.4. Sample processing and paraffin embedding

Mouse fetuses dissected at different stages of embryonic development were fixed overnight in 95% ethanol at 4°C, processed by dehydration through graded alcohols (50%, 90%, 100%,100%) and histoclear and embedded in paraffin wax. Sagittal sections were cut on the microtome at 5 µm thickness and used for histological analysis

3.5. Staining procedures

3.5.1. Alizarin red

Alizarin red staining identifies calcium deposited by cells in culture or in tissue sections. Monolayers of BMSCs or micromass cultures were fixed with 4% paraformaldehyde. Following a PBS wash, Alizarin red solution (40mM, pH 4.1-4.3) was added to wells and incubated for 20 minutes on the shaker. Wells were then washed number of times with fresh water to remove excess stain. Calcium deposits (orange/red colour) were imaged using Zeiss Axiovert 200 inverted microscope.

3.6. Bone marrow derived stromal cell (BMSC) culture

14-week-old mice were euthanized by 5% CO_2 in a closed atmosphere and hind limbs were dissected. Bones were cleaned of all muscle and connective tissue. Proximal and distal epiphyses were cut off and bone marrow contained within the diaphysis was flushed out with α-modified essential medium (α-MEM) using 3cc syringe with 21 and 25 gauge needle. The animals used in the experiment were divided into four groups: *Bag*$^{+/-}$ female (n=3), *Bag*$^{+/-}$ male (n=3), *Bag*$^{+/+}$ female (n=3), and *Bag*$^{+/+}$ male (n=3). Marrow harvested from animals within these four groups was pooled, dispersed by flushing with the syringe in order to yield a homogeneous cell suspension, filtered through a 70 mm filter and pelleted by centrifugation. Cells were counted and seeded across wells of 6, 24 and 96 well plates at a density of 5 x 10^5 cells/cm^2. After six days of culture under basal conditions in α-MEM supplemented with 1% penicillin/streptomycin, 10% FCS and 50 µM β-mercaptoethanol, non-adherent red blood cells were removed by a wash in 1x PBS and adherent cells cultured for further 22 days in osteogenic medium i.e. α-MEM supplemented with 1% penicillin/streptomycin , 10% FCS, 50 µM β-mercaptoethanol, Asc-2-PO_4 (100 µM) and rhBMP-2 (100 ng/ml) and basal medium. Cultures were harvested on day 1 and 14 for analysis of DNA concentration and day 28 for protein expression analysis by Western

blot, gene expression analysis by qPCR, osteocalcin concentration, ALPL specific activity, DNA concentration and mineralisation.

3.7. Biochemical analyses

3.7.1. Alkaline phosphatase (tissue non-specific) assay (ALPL assay)

Cultures of mouse BMSCs in wells of a 24 well plate maintained in basal and osteogenic medium were fixed in 95% ethanol on day 1, 14 and 28 of culture. Cell lysates in 0.05% TRITON®-X100 were processed for colorimetric turnover of para-Nitrophenylphosphate (pNPP) to para-Nitrophenol (pNP) and inorganic phosphate under alkaline conditions, measured at 410 nm. As ALPL catalyzes dephosphorylation process, the assay allows for the measurement of ALPL activity in samples. In brief, cells were washed in PBS and fixed in 95% ethanol for 10 minutes. After one wash in PBS and air drying, 0.05% TRITON®-X100 was added to the wells and cells were scraped off the plate surface with the cell scraper. Plates with cells were placed at -20°C for 30 minutes and then thawed in 37°C for the next 30 minutes. The process of freezing and thawing was repeated three times and cells were detached from the surface of the wells after each thawing. Five concentrations of 4-nitrophenol, ranging from 0 to 200 nmol/ml, were added in triplicates to wells of a 96 well plate. Test samples were added in triplicate to wells of the same plate, followed by addition of Substrate Buffer (see Appendix 2). After incubation at 37°C for 45 minutes, the reaction was stopped by the addition of 100 µl NaOH to each well and the absorbance was measured at 410 nm on an ELX-800 Universal Microplate Reader using Bio-Tek KC4 KinetiCalc for Windows software (Bio-Tek, USA). A standard curve of absorbance was used to establish the concentrations of ALPL in experimental samples based on absorbance measured at 410 nm (Fig. 3-4).

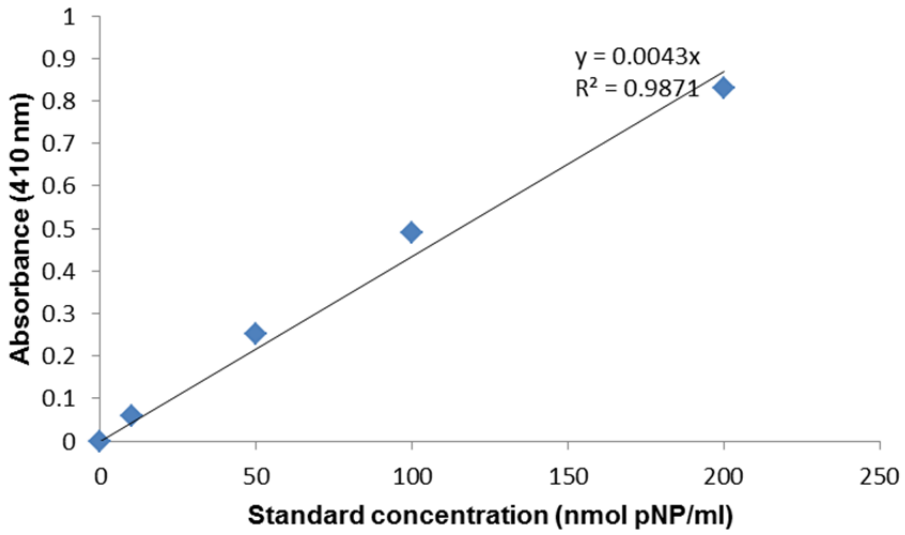

Figure 3-4. *Standard plot for estimation of alkaline phosphatase concentration. R^2 – correlation coefficient, y – value of absorbance, x – concentration.*

3.7.2. PicoGreen DNA quantification assay

Samples were prepared as described in section 3.7.1. and assayed using PicoGreen® double-stranded DNA quantification reagent for calculation of DNA content (ng/ml). In brief, seven concentrations of DNA standards, ranging from 0 ng/ml to 1,000 ng/ml, were added in triplicate to wells of a 96 well plate, followed by addition of 1 x TE buffer (see Appendix 2) and PicoGreen® double-stranded DNA quantification reagent (1:200 in 1 x TE Buffer). Plates were incubated for 5 minutes at room temperature in the dark and fluorescence was measured on a FLX-800 Microplate Fluorescence Reader using Bio-Tek KC4 KinetiCalc for Windows software (Bio-Tek, USA). A standard curve of fluorescence was used to establish the concentrations of DNA in samples (Fig. 3-5).

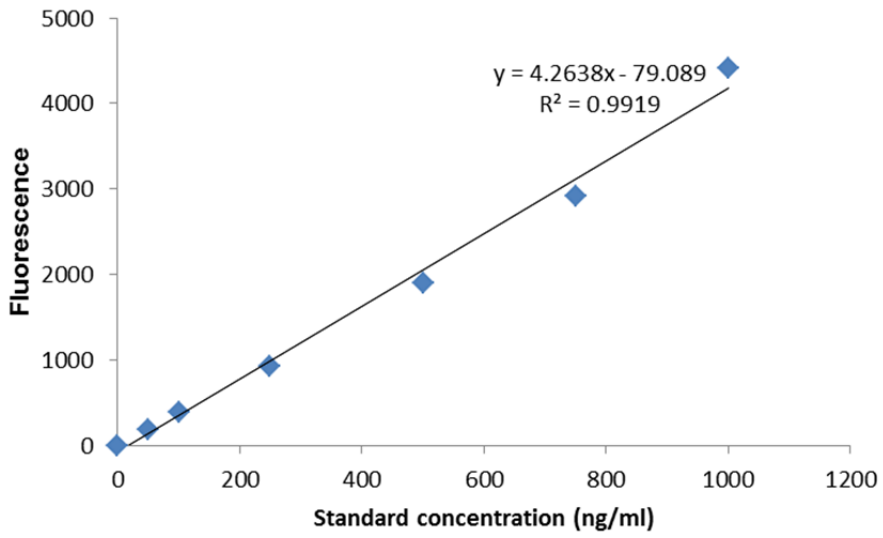

Figure 3-5. *Standard plot for estimation of DNA concentration. R^2 – correlation coefficient, y – value of fluorescence, x – concentration.*

DNA content was calculated and expressed as ng/ml. Assays were run in triplicate, values were expressed as mean ± standard deviation (SD). Statistical analysis was performed using GraphPad Prism software (GraphPad Software Inc., San Diego, CA, USA). Differences in DNA content between groups were analysed using one way ANOVA with a post-Tukey test according to experimental design and were considered to be significantly different if $P \leqslant 0.05$ (probability of occurrence by random chance alone was less than 5%). Results of cell proliferation profiles were compared between days 1 and 14 of culture, and days 14 and 28 of culture.

ALP specific activity was calculated and expressed as nmol pNP/ng DNA/hr. Time of incubation was incorporated into the calculation of ALP specific activity. Assays were run in triplicate, values were expressed as mean ± standard deviation (SD). Statistical analysis was performed using GraphPad Prism software (GraphPad Software Inc., San Diego, CA, USA). Differences in ALP specific activity between groups were analysed using one way ANOVA with a post-Tukey test according to experimental design and were considered to be significantly different if $P \leqslant 0.05$ (probability of occurrence by random chance alone was less than 5%).

3.8. Analysis of osteocalcin concentration

Concentration of osteocalcin (OCN) in cultured MSCs extract was measured using Mouse Osteocalcin EIA Kit (Bioquote, UK) according to manufacturer's protocol. In brief, 25 µl of six concentrations of mouse osteocalcin standards, ranging from 1.56

ng/ml to 50 ng/ml, controls, blank and cultured MSCs extracts where added in duplicates to wells of a 96 well plate followed by 100 µl of osteocalcin antiserum. After incubation at 4°C for 20 hours, wells were washed three times with Phosphate-Saline wash buffer and 100 µl of Streptavidin-Horseradish Peroxidase was added to each well. Following 30 minute incubation at room temperature, wells were washed three times with wash buffer and 100 µl of substrate mix (equal volumes of Peroxidase Substrate TMB and Hydrogen Peroxidase solution) was added to each well. After 15 minute incubation in the dark at room temperature, 100 µl of Stop Solution was added to each well. Absorbance was measured at 450 nm. A standard curve of absorbance was used to establish the osteocalcin concentrations in tested samples (Fig. 3-6). Osteocalcin concentration was calculated and expressed as OCN content (ng OCN/ng DNA). Statistical analysis was performed using GraphPad Prism software (GraphPad Software Inc., San Diego, CA, USA). Differences in osteocalcin protein expression between groups were analysed using one way analysis of variance (ANOVA) with a post-Tukey test according to experimental design and were considered to be significantly different if $p \leqslant 0.05$ (probability of occurrence by random chance alone was less than 5%).

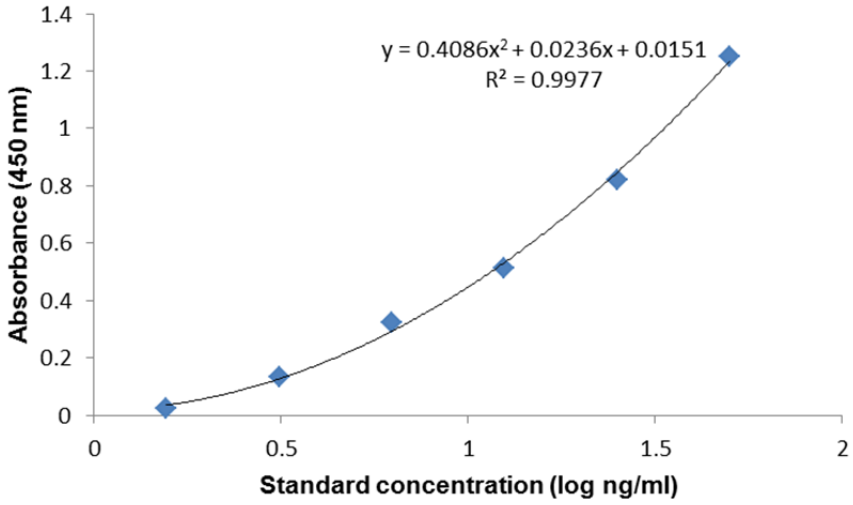

Figure 3-6. *Standard plot for estimation of osteocalcin concentration. R^2 – correlation coefficient, y – value of absorbance, x – concentration*

3.9. Gene expression analysis

3.9.1. Isolation of RNA

Total RNA was extracted from the mouse BMCs on day 28 of culture using RLT Buffer (QIAGEN, UK) according to manufacturer's protocol. In brief, each well of a 6 well plate

was washed with PBS and cells were lysed in 350 µl RLT lysis buffer. Equal volume of 70% ethanol was added to each lysate and mixed by pipetting up and down 10 times. Resulting samples were transferred to RNeasy spin columns in collection tubes and centrifuged for 15 minutes at 10,000 rpm. The flow-through was discarded and 700 µl RW1 buffer was added to each column. After centrifugation for 15 seconds at 10,000 rpm, flow-through was discarded. 500 µl RPE buffer was added and columns were centrifuged for 15 seconds at 10,000 rpm. Flow-through was discarded and the process repeated with a 2 minute centrifugation. Columns were then placed in new collection tubes and centrifuged at full speed (13,000 rpm) for 1 minute. Following addition of 30 µl RNase-free water onto each column membrane, columns were centrifuged in fresh collection tubes for 1 minute at 10000 rpm. The process was repeated using water with eluted DNA in order to achieve higher concentration of RNA. Collection tubes containing RNA were stored at -80°C.

3.9.2. Quantification of RNA

Quantification of extracted RNA was performed using NanoDrop® ND-1000 spectrophotometer (Thermo Fischer Scientific). RNA concentration was established by ultraviolet spectrophotometry at 260 nm. RNA purity was determined based on the absorbance ratios of 260/280 nm.

3.9.3. cDNA synthesis

Samples were reverse transcribed into cDNA using SuperScript VILO cDNA synthesis Kit (Invitrogen, UK) according to manufacturer's protocol. RNA samples were diluted using ultra-pure water to a volume of 14 µl containing 150 ng RNA. Following addition of 4 µl 5x VILO™ reaction mix and 1 µl 10x SuperScript ® enzyme mix to each sample, cDNA synthesis was performed by incubation at 25°C for 10 minutes, 42°C for 60 minutes and 85°C for 5 minutes. The resulting cDNA samples were diluted with ultra-pure water and stored at -20°C.

3.9.4. Real-Time quantitative PCR

Real-time PCR was performed using Applied Biosystems reagents and 7500 Real Time PCR detecting system (Life Technologies, Applied Biosystems, UK). Samples were being used at the volume of 25 µl and consisted of 1 µl of cDNA, 2.5 µl of forward and 2.5 µl reverse primer (5 µM) and 50% of SYBRGreen Master Mix. Reactions were performed in duplicate, primer sequences were validated by melting curve analysis. Conditions applied to the PCR runs were as follows: 50°C for 2 min, 95°C for 10 min, 45 cycles at 95°C for 15 s and 60°C for 1 min. Expression of genes was then analysed.

3.9.5. Analysis of data

Threshold cycle (C_T) values for all genes of interest were established by the software using the same threshold setting (Applied Biosystems 7500 Software). The comparative C_T method ($\Delta\Delta C_T$ method) was used for analysis of the relative transcript levels of the genes of interest. ΔC_T value for each gene was calculated by subtracting the C_T value of housekeeping gene (*β-Actin*) from the C_T value of each gene of interest. $\Delta\Delta C_T$ was calculated by subtracting the lowest ΔC_T value in the group from the ΔC_T value of each sample. Formula $2^{-\Delta\Delta C_T}$ was applied to determine the amount of target relative to the one with lowest ΔC_T value (calibration target) and normalised to endogenous reference. The standard deviation of ΔC_T was calculated using the equation $s' = \sqrt{s_1^2 + s_2^2}$, where s_1 is a standard deviation of ΔC_T values of the gene of interest and s_2 is the standard deviation of ΔC_T values of β-Actin. In order to eliminate potential bias due to averaging of data transformed through the formula $2^{-\Delta\Delta C_T}$, statistical analysis was performed at the level of ΔC_T. The value of one was assigned to the group with the highest relative transcript level. The range of fold relative transcript levels of the genes defined as $2^{-\Delta\Delta C_T}$ with $2^{-(\Delta\Delta C_T + s')}$ and $2^{-(\Delta\Delta C_T - s')}$.

β-Actin, one of the most abundant proteins in eukaryotic cells, was used as an endogenous internal control due to it being constitutively expressed and involved in basic cell maintenance functions. To normalise gene expression, Actins have been widely used as housekeeping/internal control (Sturzenbaum and Kille, 2001) with β-Actin used most commonly due to its expression levels being more stable than other internal controls (Biederman et al., 2004).

3.9.6. Statistical analysis

Results of gene expression levels in male and female samples were analysed separately. Fold relative transcript levels were expressed as mean ± SD. Statistical analysis was performed using GraphPad Prism software (GraphPad Software Inc., San Diego, CA, USA). Differences in relative gene expression between groups were analysed using one way analysis of variance (ANOVA) with a post-Tukey test according to experimental design and were considered to be significantly different if $p \leq 0.05$.

3.10. Western blot

3.10.1. Protein extraction

3.10.1.1. Cells

Samples for Western blot were isolated from mouse BMCs cultures by trypsinising cells cultured in 2 wells of a 6-well plate, centrifugation of cell suspensions for 5 minutes at 12,000 rpm, double wash in PBS and incubation of the cell pellet in RIPA buffer (see Appendix 2) for 20 minutes at 4°C. After the incubation cell suspension was pelleted down and supernatant collected.

3.10.1.2. Mouse limb buds

Samples of fetal limb buds were collected by very delicate homogenisation, incubation for 20 minutes at 4°C in 50 – 70 µl RIPA buffer (see Appendix 2) followed by centrifugation for 20 minutes at 10^{o}C and collection of supernatant.

3.10.2. Estimation of protein concentration

Protein concentrations were determined using BCA Protein Assay Kit (Thermo Scientific Pierce). Six concentrations of Bovine Serum Albumin (BSA) protein standard, ranging from 0 µg/ml to 2,000 µg/ml (in triplicate) and protein samples (in duplicate) were added to wells of a 96 well plate, followed by addition of Working Reagent. After incubation at 37°C for 30 minutes, absorbance was measured at 595 nm on Bio-Tek KC4 microplate fluorescent reader (Bio-Tek, USA). A standard curve of absorbance was used to establish the concentrations of protein samples based on sample absorbance measured at 595 nm (Fig. 3-7). Samples were prepared using Blue Loading Buffer Pack (New England Biolabs). Fresh 3x Redusing Blue Loading Buffer was prepared by adding 1/10 volume 30x Reducing Agent to 1 volume of 3x Blue Loading Buffer. Samples were prepared by adding ½ volume of 3x Reducing Blue Loading Buffer and heated to 95°C for 5 minutes.

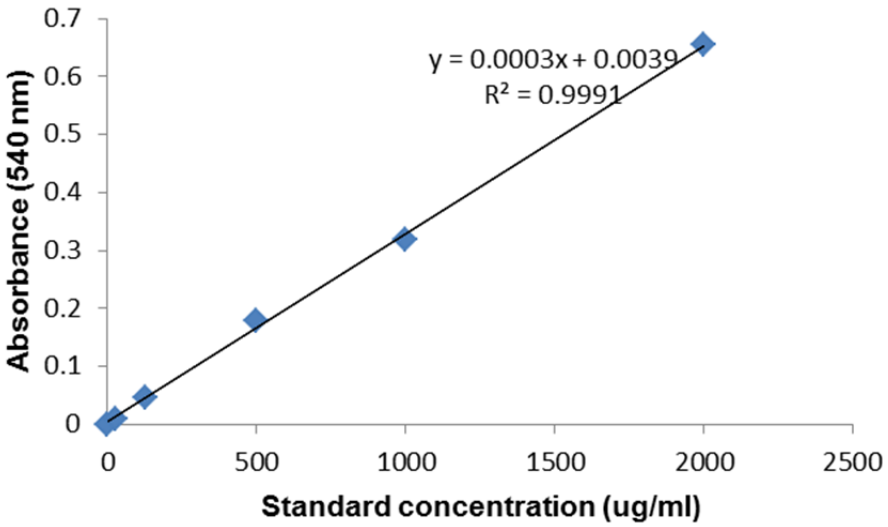

Figure 3-7. *Standard plot for estimation of BSA concentration. R^2 – correlation coefficient, y – value of absorbance, x – concentration*

3.10.3. Gel electrophoresis

Gel electrophoresis was performed using Bio-Rad equipment. 10% resolving gels and stacking gels were prepared with ProtoGel reagents (National Diagmnostics, see Appendix 2). 15 wells in the stacking gel were prepared and samples loaded at concentrations ranging between 6 µg and 20 µg protein in each well with loading volumes of 15 µl. Spectra Multicolor Broad Range Protein Ladder (10-260 kDa) (Thermo Scientific) was used at 15 µl volume per well. Electrophoresis was run at 150V for one hour in 1x Running Buffer (see Appendix 2).

3.10.4. Transfer

Samples and markers were electroblotted on PVDF membrane (Immobilon-P, Merck Millipore). Protein transfer was run at 100 V for one hour in Transfer Buffer (see Appendix 2).

3.10.5. Immunoblotting and signal detection

Membranes were blocked in 5% milk in PBST (0.05% Tween in PBS) for one hour in room temperature and then incubated overnight at 4^{o}C with α-rodent BAG-1 polyclonal primary antibody (C-16), rabbit α-SOX-9 primary antibody, rabbit α-collagen type II primary antibody or monoclonal α-βActin-Peroxidase antibody diluted in 5% milk in PBST. Membranes were then washed three times in PBST and incubated with secondary antibody (Goat polyclonal Secondary Antibody to Rabbit IgG - H&L (HRP) (Abcam) diluted in 5% milk in PBST for one hour at room temperature. After incubation

the membranes were washed three times in PBST and the signal was detected by using Immobilon Western Chemiluminescent HRP Substrate (Merck Millipore) and imaging in VersaDoc Imaging System (BioRad). Monoclonal α-βActin-Peroxidase antibody was used as a loading control. Prior to washing the membrane two times in PBS and two times in PBST, the membrane was stripped in stripping buffer (see Appendix 2). Membranes were then blocked in 5% milk in PBST for one hour (or overnight), washed three times in PBST and incubated with relevant secondary antibody dilution for one hour before signal detection. For digital acquisition of chemiluminescent signals by the CCD camera, the blot was placed on the imaging surface, imaged and the data were analysed using Quantity One® 1-D analysis software. Value of one was assigned to the group with the highest band density.

3.10.6. Statistical analysis

Statistical analysis was performed using GraphPad Prism software (GraphPad Software Inc., San Diego, CA, USA). Differences in band density between groups were analysed using unpaired t-test (two-tailed P value) or one way ANOVA with a post-Tukey test according to experimental design and were considered to be significantly different if $P \leq 0.05$ (probability of occurrence by random chance alone was less than 5%).

Chapter 4

Characterisation of the role of *Bag-1* in embryonic skeletal development

4. Characterisation of the role of *Bag-1* in embryonic skeletal development

4.1. Introduction

Endochondral ossification, the process of the formation of majority of the bones that make up the skeleton, involves deposition of bone matrix by osteoblasts on intermediary cartilage templates, which serve as scaffolds on which bones are built. For the proper growth of endochondral bones and ultimately, the adult skeleton, it is crucial that precise cartilage primordia are formed during early skeletal development. Disruption of this developmental programme can lead to congenital skeletal anomalies namely, the skeletal dysplasias, and contribute to the pathogenesis of diseases of the adult skeleton, such as osteoporosis and osteoarthritis.

The process of bone formation during embryonic development, whether via intramembranous or endochondral ossification, is initiated by the migration of the mesenchymal progenitor cells to the site of skeletogenesis, which is always associated with the epithelium. Interaction of mesenchymal progenitor cells with the products of epithelial cells leads to the condensation of the progenitor cells and further differentiation into chondrocytes or osteoblasts (Hall and Miyake, 1992) (Fig. 4-1).

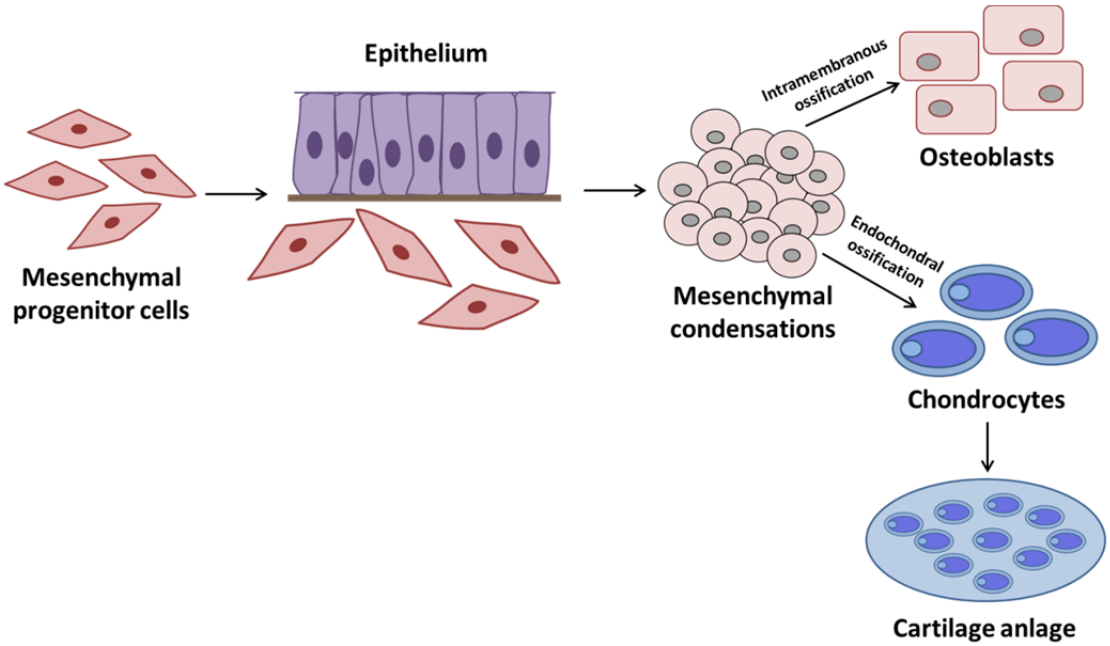

Figure 4-1. *Development of skeletal elements (Adapted from Hall and Miyake, 2000)*

In mouse prenatal limb development, mesenchymal condensations occur around E10.5 of gestation. Cells of the mesenchymal condensations undergo chondrogenesis and chondrocytes differentiate to hypertrophy within cartilaginous nodules between E12.5 and E14.5 (Fig. 4-2). This is followed by mineralisation of the extracellular matrix in

preparation for vascular invasion of the cartilage anlagen by E15.5 (Horton, 1993, Karsenty, 1999).

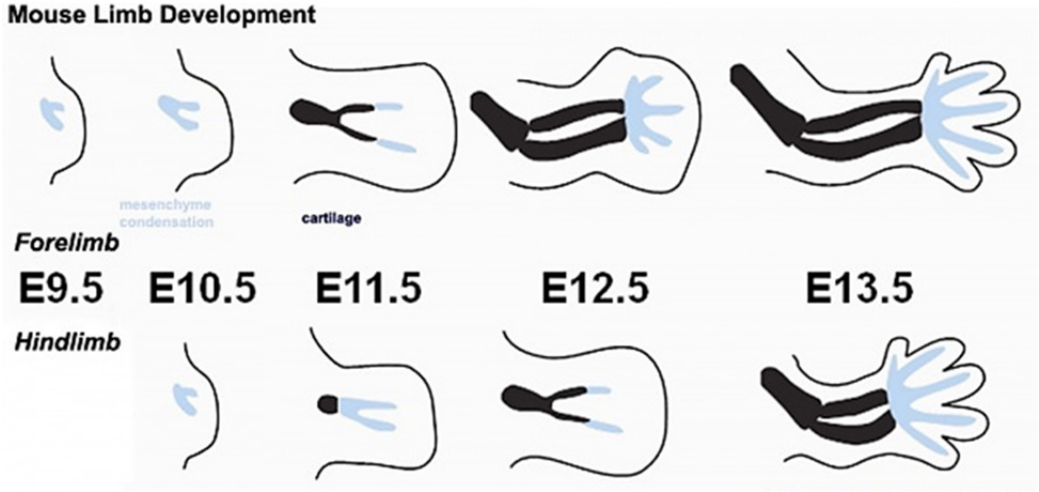

Figure 4-2. *Fore- and hind limb bud development in mice (adapted from Taher et al., 2011). Light grey – mesenchymal condensations, black – cartilage.*

Studies by Crocoll and co-workers have identified stage-specific expression pattern of *Bag-1* mRNA in several organs of the developing mouse embryo, with cartilaginous tissues showing highest expression (Crocoll et al., 2000). *Bag-1* is ubiquitously expressed in the mesenchyme of murine developing limb buds as early as E10.5. Although robust *Bag-1* expression is maintained at E11.5, expression decreases thereafter and is restricted to the interdigital mesenchyme at E12.5, tissue surrounding future digits at E13.5 and the peridigital tissue at E14.5 (Crocoll et al., 2002).

Development of endochondral bones is orchestrated by the equilibrium between chondrocyte proliferation and hypertrophy, which is coordinated by a complex network of genes and hormones. When chondrocytes begin the process of hypertrophy, they withdraw from the cell cycle, enlarge and as prehypertrophic chondrocytes initiate the expression of Indian Hedgehog (Ihh) and Parathyroid Hormone-Related Protein Receptor (PTHrP-R). Hypertrophic chondrocytes increase the expression of tissue non-specific Alkaline phosphatase (Alpl) and transcription factors, such as Runx-2 and Osterix, which play an important role in chondrocyte differentiation and mineralisation of cartilage (Inada et al., 1999, Yoshida et al., 2004, Nakashima et al., 2002).

With progression of hypertrophy, cells continue to enlarge and produce mineralised matrix along with further upregulation of Runx-2 and type X collagen expression. Furthermore, Adseverin (Scinderin), a member of Gelsolin superfamily of actin-binding proteins that control actin assembly in a calcium-dependent manner (Yin, 1987), is dramatically upregulated during chondrocyte maturation and its expression *in vivo* is

restricted to the prehypertrophic and hypertrophic cartilage of the embryonic growth plate (Nurminsky et al., 2007). Adseverin regulates chondrocyte differentiation: over-expression of Adseverin in non-hypertrophic chondrocytes causes a decrease in cell proliferation and promotes differentiation, which is linked to the upregulation of Ihh and collagen type X (Nurminsky et al., 2007).

Deletion of both *Bag-1* alleles is embryonic lethal in mice and *Bag-1*$^{-/-}$ mice die between E12.5 and E13.5 due to appreciable cell apoptosis in the embryonic liver and defects in haematopoiesis and neuronal cell differentiation (Gotz et al., 2005). To date, no studies have been conducted to compare the expression of the BAG-1 protein isoforms and chondrogenic markers in limb buds of wild-type (*Bag-1*$^{+/+}$), *Bag-1* heterozygous (*Bag-1*$^{+/-}$) and *Bag-1* null (*Bag-1*$^{-/-}$) mice between E10.5 and E13.5. Moreover, due to the early embryonic lethality in *Bag-1* null mice, the effect of total deletion of *Bag-1* on the important stages of endochondral ossification, such as chondrocyte hypertrophy, mineralisation of the hypertrophic cartilage and osteoblast development, remains uncharacterised. Micromass cultures of embryonic limb bud mesenchymal cells have been widely applied as an effective *in vitro* system for the study of chondrocyte hypertrophy and mineralisation of cartilaginous matrix (Ahrens et al., 1977). Application of the micromass culture technique could therefore allow *ex vivo* investigation of potential differences between *Bag-1*$^{+/+}$, *Bag-1*$^{+/-}$ and *Bag-1*$^{-/-}$ chondrocyte differentiation beyond E13.5 of gestation.

4.2. Objectives

To characterise the role of *Bag-1* in embryonic skeletal development, the objectives of the present study were:

a) Examination of the expression of BAG-1 in prenatal wild-type mice,
b) Histological assessment of *Bag-1*$^{+/+}$, *Bag-1*$^{+/-}$ and *Bag-1*$^{+/-}$ mice between E10.5 and E13.5 of gestation,
c) Analysis of BAG-1L and BAG-1S expression in limb buds of *Bag-1*$^{+/+}$, *Bag-1*$^{+/-}$ and *Bag-1*$^{-/-}$ littermates between E10.5 and E13.5,
d) Analysis of the expression of SOX-9 in mouse fetal limb buds of *Bag-1*$^{+/+}$, *Bag-1*$^{+/-}$ and *Bag-1*$^{-/-}$ littermates between E10.5 and E13.5,
e) Analysis of the expression of collagen type II in mouse fetal limb buds of *Bag-1*$^{+/+}$, *Bag-1*$^{+/-}$ and *Bag-1*$^{-/-}$ littermates between E10.5 and E13.5,
f) Elucidation of the role of *Bag-1* in chondrocyte hypertrophy and cartilage mineralisation using micromass cultures of limb bud mesenchymal cells of E11.5 *Bag-1*$^{+/+}$, *Bag-1*$^{+/-}$ and *Bag-1*$^{-/-}$ littermates.

4.3. Materials and methods

4.3.1. Dissection of fetuses

Refer to section 3.2

4.3.2. Genotyping of *Bag-1*$^{+/+}$, *Bag-1*$^{+/-}$ and *Bag-1*$^{+/-}$ mice using PCR strategy

Refer to section 3.3

4.3.3. Processing and paraffin embedding of mouse fetuses

Refer to section 3.4

4.3.4. Immunohistochemistry

4.3.4.1. Chromogenic (AEC) detection

Mouse fetuses were dissected (refer to section 3.2), genotyped (refer to section 3.3), processed, embedded in wax and 7 µm sections were cut on the microtome (refer to section 3.4). Sections were permeabilized with 0.5% TritonX-100 for 5 minutes. Following quenching of endogenous peroxidase activity with 3% H_2O_2 and blocking non-specific antibody binding with 1% bovine serum albumin (BSA) in phosphate-buffered saline (PBS), sections were incubated overnight at 4°C with rabbit α-rodent BAG-1 polyclonal antibody (C-16), dilutions of 1:50, 1:100, 1:250, 1:500 in 1% BSA in PBS. The next step involved incubation with the goat anti-rabbit IgG-biotinylated secondary antibody (1:50 in 1% BSA in PBS) for one hour. Visualisation of the immune complex involved the avidin-biotin method linked to peroxidase and 3-amino-9-ethylcarbazole (AEC), resulting in a reddish brown reaction product. Negative controls (omission of primary antibody) were included in all immunohistochemistry procedures. Sections were mounted in Hydramount (National Diagnostics). Stained sections were viewed and imaged using Olympus DotSlide microscope and OlyVia software.

4.3.4.2. Detection using fluorescently tagged secondary antibody

Mouse fetuses were dissected (refer to section 3.2), genotyped (refer to section 3.3), processed and embedded (refer to section 3.4). Sections were permeabilized with 0.5% TritonX-100 for 5 minutes. Following blocking non-specific antibody binding with 1% bovine serum albumin (BSA) in phosphate-buffered saline (PBS), sections were incubated overnight at 4°C with rabbit α-rodent BAG-1 primary antibody (C-16) (1:50 dilution in 1% BSA in PBS). Negative controls (omission of primary antibody) were included in all immunohistochemistry procedures. Sections were then washed three times for 5 minutes in PBS containing 0.5% Tween and incubated for one hour at room

temperature with goat anti-rabbit AlexaFluor 488 IgG (1:50 dilution in 1% BSA in PBS). Following mounting in Fluoromount (Sigma), images were taken on Zeiss Axiovert 200 inverted microscope with the use of AxioVision imaging software.

4.3.5. Micromass cultures of embryonic limb bud mesenchymal cells

Fetuses from 4 dams were dissected (refer to section 3.2) at E11.5, genotyped (refer to section 3.3) and limb buds of *Bag-1*$^{+/+}$, *Bag-1*$^{+/-}$ and *Bag-1*$^{+/-}$ fetuses were collected separately in 100 µl 1 x glucose/PBS (25 ml 10 x glucose in 250 ml PBS; 10 x glucose stock preparation: 2.5 g glucose in 250 ml H_2O). Limb buds were dissociated by digestion with 100 µl 0.01% trypsin/EDTA in 1 x glucose/PBS (2 µl of 10x trypsin/0.5% trypsin added to 100 µl 1 x glucose/PBS) at 37°C, followed by addition of equal volume (100 µl) of 10% FCS/DMEM in order to stop the enzymatic reaction. Cells were then seeded across 6-well tissue culture plates and culture expanded in monolayer cultures in 10% FCS/DMEM to generate sufficient number of cells for the micromass cultures. After dissociation of the cells from tissue culture plastic with trypsin/EDTA, cells of the same genotype were combined and cell numbers were determined. For each genotype, cells were plated in 24-well tissue culture plates as 10 µl drops containing 2.5 x 10^5 cells/drop and incubated for 2 hours at 37°C to allow the cells to adhere to the tissue culture plastic and form 3-D micromasses. 1ml of 10% FCS/DMEM was then gently added to each well without disturbing the micromasses. After 24 hours, the medium was changed to fresh 10% FCS/DMEM. After further 24 hours, medium was replaced with fresh 10% FCS/DMEM (basal medium) or treatment medium, i.e. basal medium containing 0.25 mM ascorbic acid and 1 mM β-glycerophosphate. Micromasses were cultured for 21 days, number of mineralised nodules were counted in day 21 cultures and the micromass cultures were harvested for the analysis of hypertrophic gene expression and histological staining. Expression of *β-Actin*, *Col10a1*, *Tissue-nonspecific Alkaline Phosphatase (Alpl)*, *Runx-2, Indian Hedgehog* (*Ihh)* and *Adseverin* genes was analysed. Primer sequences for these genes are detailed in Appendix 4. All primers were designed based on previously published primer sequences (Tare et al., 2008b, Tare et al., 2011).

4.3.6. Staining procedures

4.3.6.1. Alcian blue/Sirius red

Sections were dewaxed in Citroclear (twice) and hydrated in decreasing alcohol concentrations (100%, 90% 50%). Following nuclear counterstaining with Weigert's haematoxylin, sections were stained in 0.5% Alcian Blue 8GX for proteoglycan-rich cartilage matrix and 1% Sirius red F3B for collagenous matrix (Lison, 1954). Stained

sections were then mounted in dibutyl phthalate xylene (DPX, Fisher). Stained sections were viewed and imaged using Olympus DotSlide microscope and OlyVia software.

4.3.6.2. Alkaline phosphatase

Micromass cultures were fixed with 95% ethanol. Following wash with PBS, cultures were left to air dry. Staining solution contained 9.6 ml H_2O, 400 µl Naphtol AS-MX Phosphate Alkaline Solution and 0.0024g Fast Violet Salt, and was added to wells (incubation for 40 minutes in the dark at 37°C). Reaction was then stopped by rinsing the wells with H_2O. Stained cultures were imaged using Zeiss Axiovert 200 inverted microscope.

4.3.7. Western blot analysis of fetal limb bud lysates

For the detailed description of western blot procedure refer to section 3.10.

Samples were prepared by very delicate maceration of fetal limb buds. Samples were incubated for 20 minutes at 4°C in 50 – 70 µl RIPA buffer (see Appendix 1) followed by centrifugation for 20 minutes at 10°C and collection of the supernatant.

Samples for electrophoresis were loaded at concentrations ranging between 6 µg protein (e.g. in case of E10.5 limb buds) and 20 µg protein (e.g. in case of E13.5 limb buds) in each well, with loading volumes of 15 µl. Spectra Multicolor Broad Range Protein Ladder (10-260 kDa) (Thermo Scientific) was used at 15 µl volume per well. Electrophoresis was performed at 150V for one hour in 1x running buffer (see Appendix 1).

4.3.8. Statistical analysis

Statistical analysis was performed using GraphPad Prism software (GraphPad Software Inc., San Diego, CA, USA). Differences between groups were analysed using one way ANOVA with a post-Tukey test according to experimental design and were considered to be significantly different if $P \leq 0.05$ (probability of occurrence by random chance alone was less than 5%).

4.4. Results

4.4.1. α-BAG-1 antibody titration

In order to establish the optimum concentration of α-BAG-1 polyclonal antibody (C16) for immunostaining, four different dilutions of α-BAG-1 antibody, i.e. 1:50, 1:100, 1:250 and 1:500 were applied to sections of E12.5 wild-type fetus, followed by the chromogenic detection of the immune complex (Fig. 4-3).

Robust staining was observed in sections immunostained with the α-BAG-1antibody applied at a dilution of 1:50 (Fig. 4-3A). Intensity of the immunostaining decreased with the dilution of primary antibody (Fig. 4-3B – 4-3D). No staining was observed in the negative control, (primary antibody omission) (Fig. 4-3E).

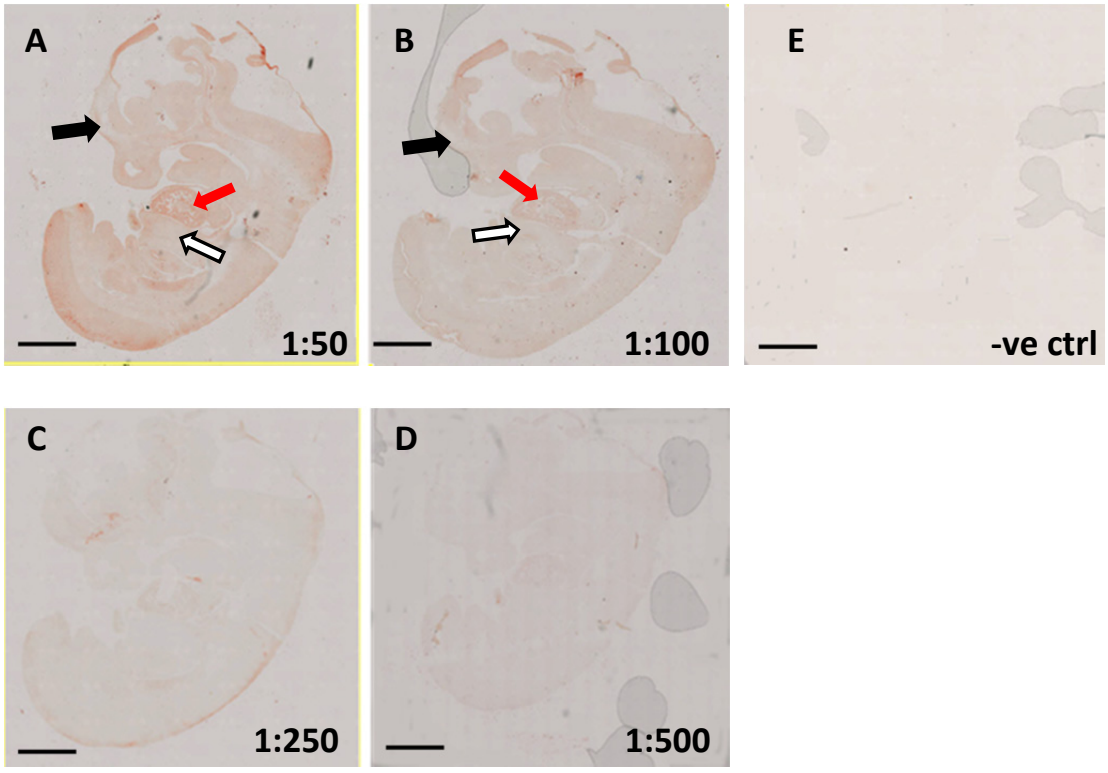

Figure 4-3. *Titration of α-BAG-1 polyclonal antibody (C16) – 1:50 (A), 1:100 (B), 1:250 (C) and 1:500 (D) concentrations of α-BAG-1 antibody applied to sections of prenatal E12.5 wild-type mouse, E – negative control (omission of primary antibody), scale bar: 1 mm;* ➡ *heart,* ⇨ *liver,* ➡ *forebrain.*

4.4.2. Comparison of immunostaining using chromogenic (AEC) detection versus immunofluorescence

Histological sections of E16.5 wild-type mouse were immunostained with the α-BAG-1 polyclonal antibody (C16), followed by either the goat anti-rabbit IgG-biotinylated secondary antibody or the fluorescently tagged goat anti-rabbit AlexaFluor 488 IgG secondary antibody. Detection of the antigen was performed via the visualisation of the immune complex involving the avidin-biotin method linked to peroxidase and 3-amino-9-ethylcarbazole (AEC) or the use of the fluorescent tag, respectively (Fig. 4-4).

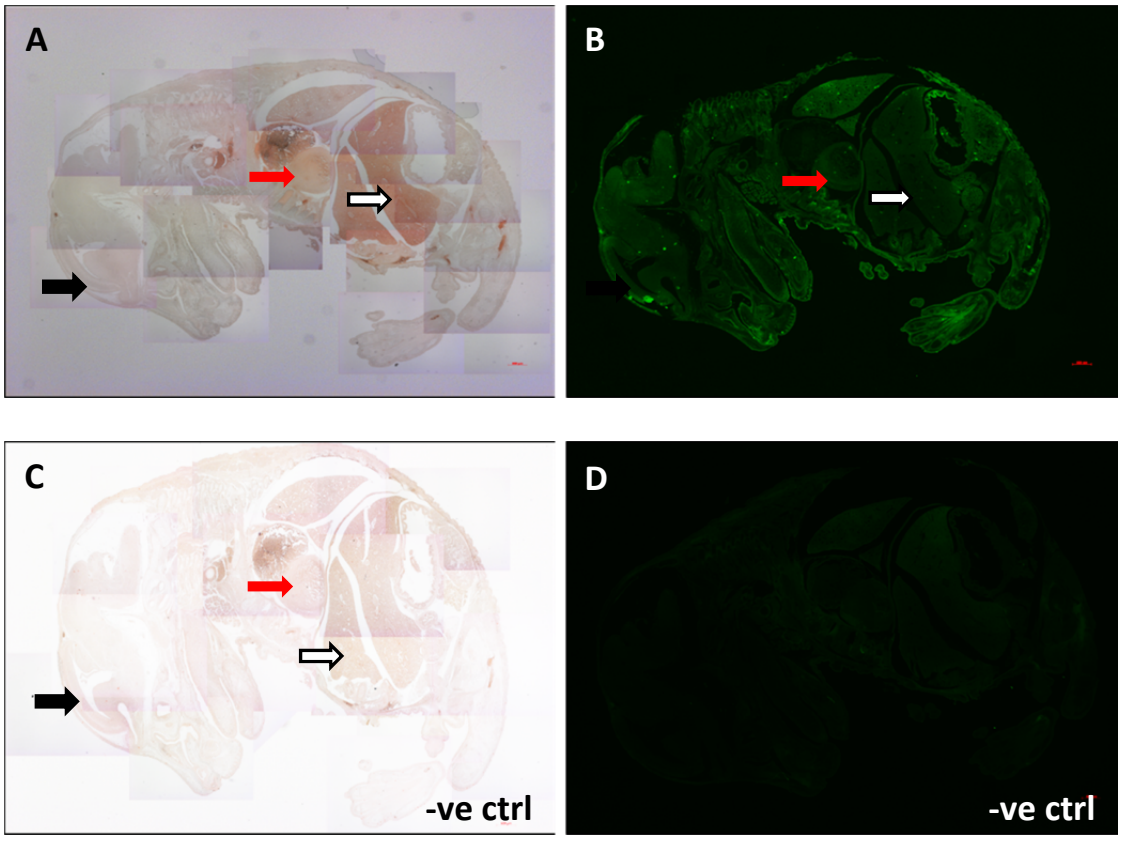

Figure 4-4. *Comparison of chromogenic - AEC (A, C) and fluorescent - goat anti-rabbit AlexaFluor 488 IgG (B, D) reporters applied for α-BAG-1 immunostaining of prenatal E16.5 mouse histological sections, C and D - negative control (omission of primary antibody);➡heart, ⇨liver, ➡forebrain.*

Staining could be observed clearly and consistently in sections stained using the fluorescently tagged secondary antibody (Fig. 4-4B) in comparison to sections stained using the AEC protocol (Fig. 4-4A). Moreover, no staining was observed in the negative control, where the primary antibody was omitted from the immunostaining protocol and only the fluorescently tagged secondary antibody was applied to the section (Fig. 4-4D). Some nonspecific background staining was observed in the sections processed

following the AEC protocol, likely as a result of nonspecific binding of the biotin-binding protein streptavidin to endogenous tissue targets (Fig 4-4C).

4.4.3. Examination of site-specific expression of BAG-1 in prenatal wild-type mice

4.4.3.1. Skeletal tissue

Histological sections of prenatal wild-type mice were immunostained with the α-BAG-1 polyclonal antibody (C16), which was raised against a peptide mapping the C-terminus of BAG-1 of mouse origin. The α-BAG-1 antibody was applied at a dilution of 1:50 for immunostaining the sections (Fig. 4-5) and no immunofluorescence was observed when the primary antibody was omitted from the immunostaining protocol (Fig 4-5D – 4-5F, 4-6C, 4-7H) The antibody was able to detect both isoforms, BAG-1L and BAG-1S, in murine tissues. Staining for BAG-1 was observed in cells of the future intervertebral discs (marked by blue boxes), however expression of BAG-1 was found to be largely absent from the cartilage primordia of the future vertebral column (marked by red boxes) in the E14.5 fetus (Fig. 4-5G – 4-5L).

Staining for BAG-1 in the cells of the future intervertebral discs was observed in the cytoplasm (Fig. 4-5H, 4-5I), as well as the nuclei (Fig. 4-5K, 4-5L), indicative of the presence of BAG-1S and BAG-1L isoforms, respectively.

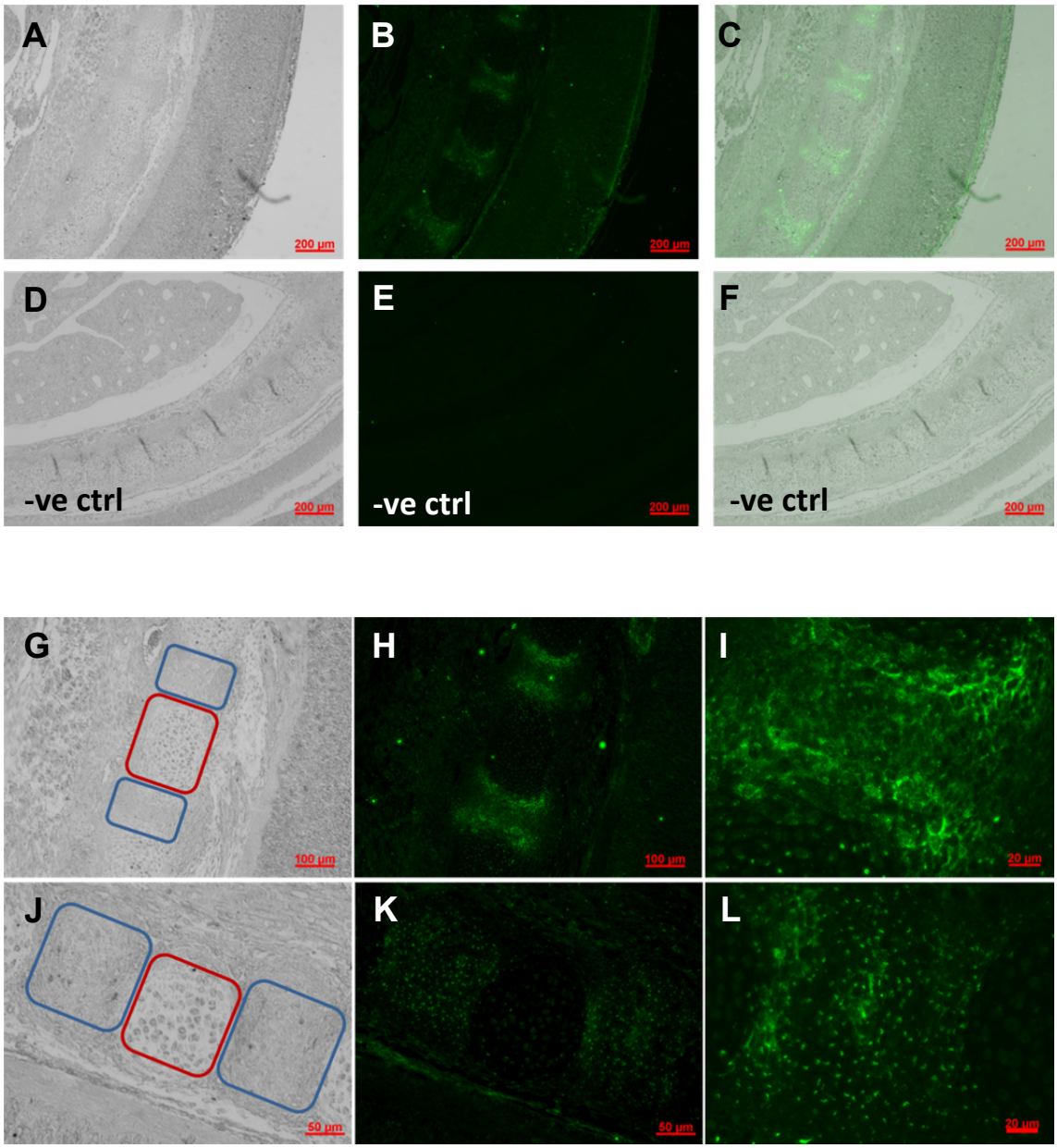

Fig 4-5. *Immunolocalisation of BAG-1 in cells of future intervertebral discs and vertebral column of prenatal E14.5 Bag-1$^{+/+}$ mouse. The anti-BAG-1 polyclonal antibody raised against a peptide mapping the C-terminus of BAG-1 of mouse origin and able to detect both BAG-1 isoforms, was applied for immunostaining histological sections of prenatal E14.5 Bag-1$^{+/+}$. A, D, G, J - digital phase images; B, E, H, K – respective corresponding fluorescence; I, L – magnification of H and K, respectively; D, E, F – negative control (omission of primary antibody); blue boxes – future interverterbral discs, red box – cartilage primordia of the future vertebral column; scale bar: A-F – 200 µm, G, H – 100 µm, J, K– 50 µm, I, L – 20 µm.*

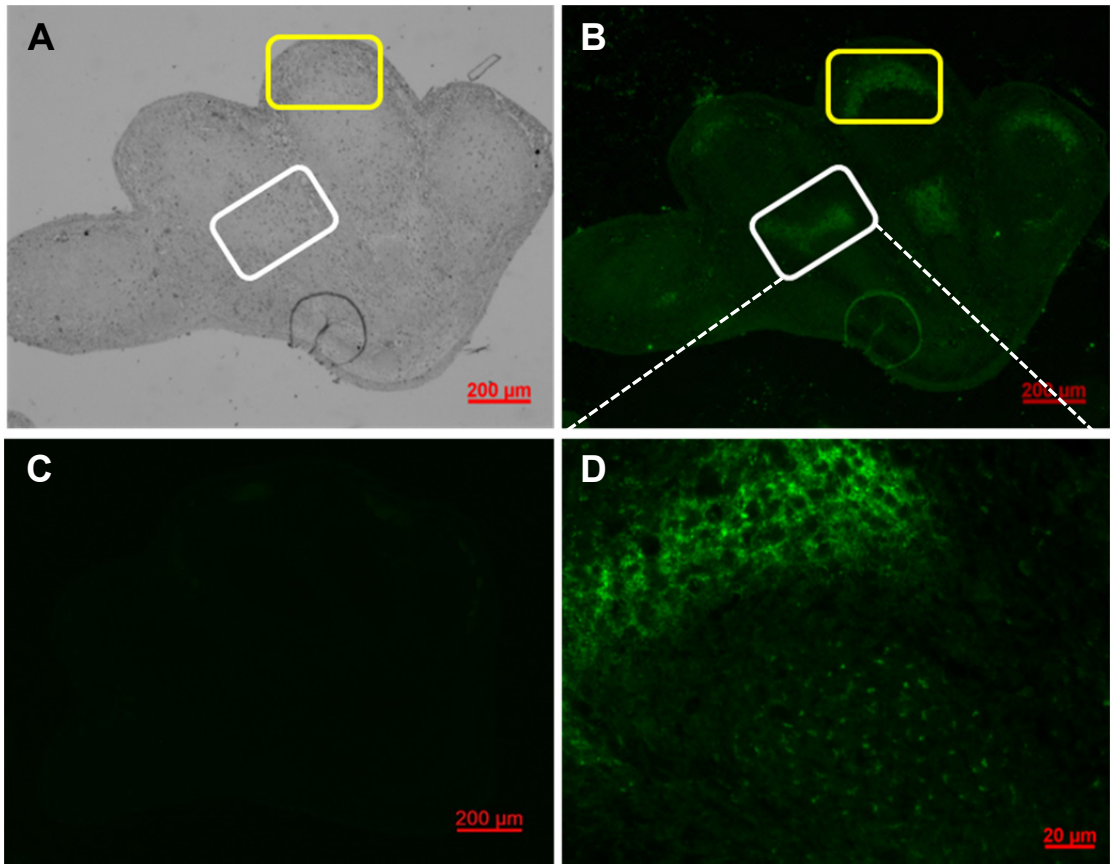

Figure 4-6. *Immunolocalisation of BAG-1 in cells of the forelimb of prenatal E14.5 Bag-1$^{+/+}$ mouse. The anti-BAG-1 polyclonal antibody raised against a peptide mapping the C-terminus of BAG-1 of mouse origin and able to detect both BAG-1 isoforms, was applied for immunostaining histological sections of prenatal E14.5 Bag-1$^{+/+}$. A - digital phase image; B,– respective corresponding fluorescence; C – negative control (omission of primary antibody), D – magnification of the prospective metacarpal-phalangeal region marked with white box.*

Predominantly cytoplasmic immunolocalisation of BAG-1S was detected at the prospective metacarpal-phalangeal (Fig. 4-6A and 4-6B marked with white boxes, Fig. 4.6D) and inter-phalangeal sites (Fig. 4-6A, 4-6B; marked by yellow boxes) in the incipient joints of the forelimb of the E14.5 fetus.

In hindlimb of the E16.5 fetus (Fig. 4-7), staining for BAG-1 in the femur (Fig.4-7C – 4-7H) and tibia was detected prominently in the mineralized hypertrophic cartilage at the vascular front.

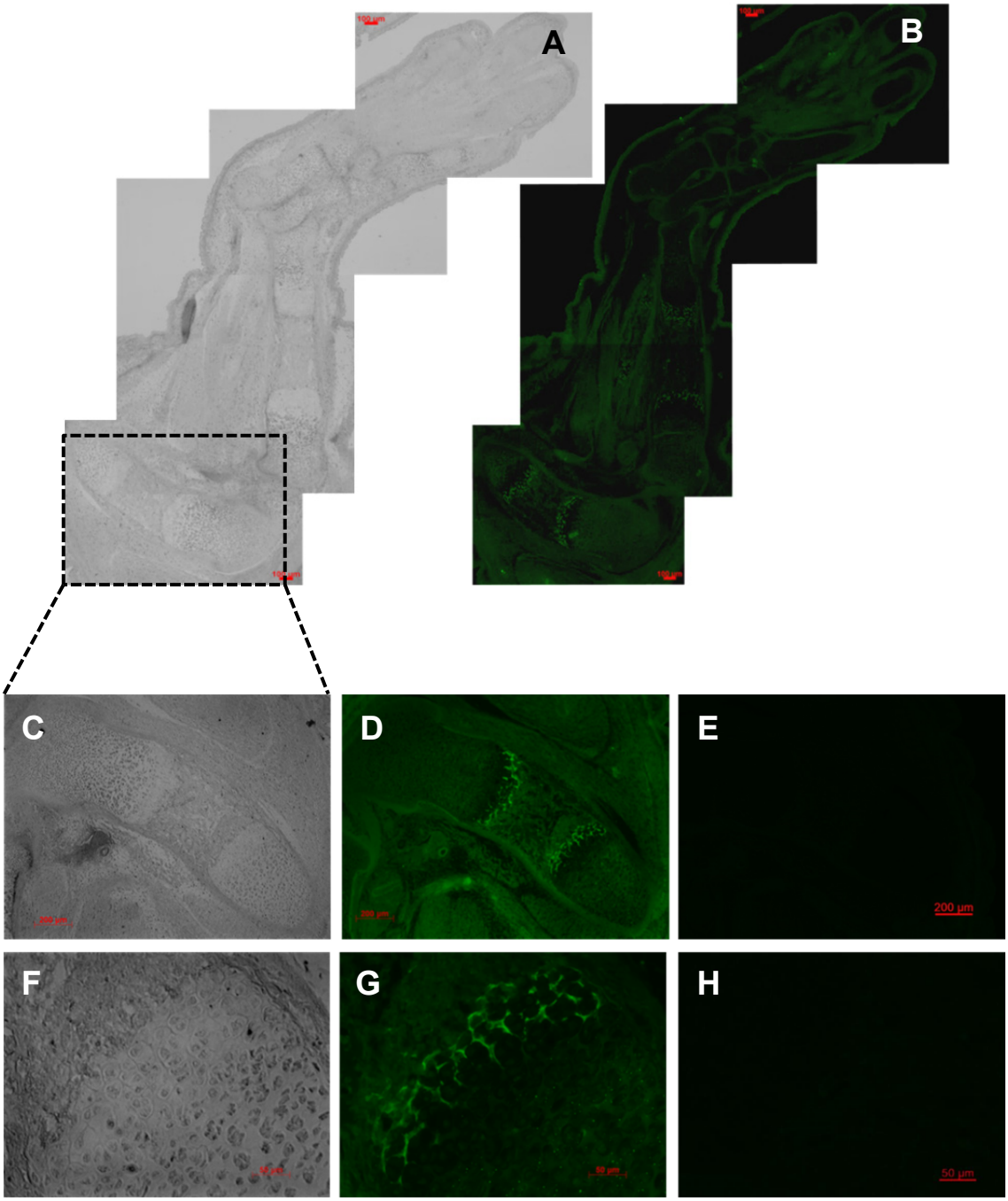

Figure 4-7. *Immunolocalisation of BAG-1 in cells of the hind limb of prenatal E16.5 Bag-1$^{+/+}$ mouse. The anti-BAG-1 polyclonal antibody raised against a peptide mapping the C-terminus of BAG-1 of mouse origin and able to detect both BAG-1 isoforms, was applied for immunostaining histological sections of prenatal E16.5 Bag-1$^{+/+}$. A, C, F - digital phase images; B, D, G – respective corresponding fluorescence; E, H – negative control (omission of primary antibody); scale bar: A, B – 100 µm, C-E – 200 µm, F-H– 50 µm.*

4.4.3.2. Non-skeletal tissues

BAG-1 was immunolocalised to non skeletal tissues such as the heart, specifically in the atrial walls and ventricle, as well as the septum primum (Fig. 4-8A, 4-8B), and dorsal root ganglia (Fig. 4-8D, 4-8E) at E11.5, and vibrissae papillae (Fig. 4-8G, 4-8H) at E16.5.

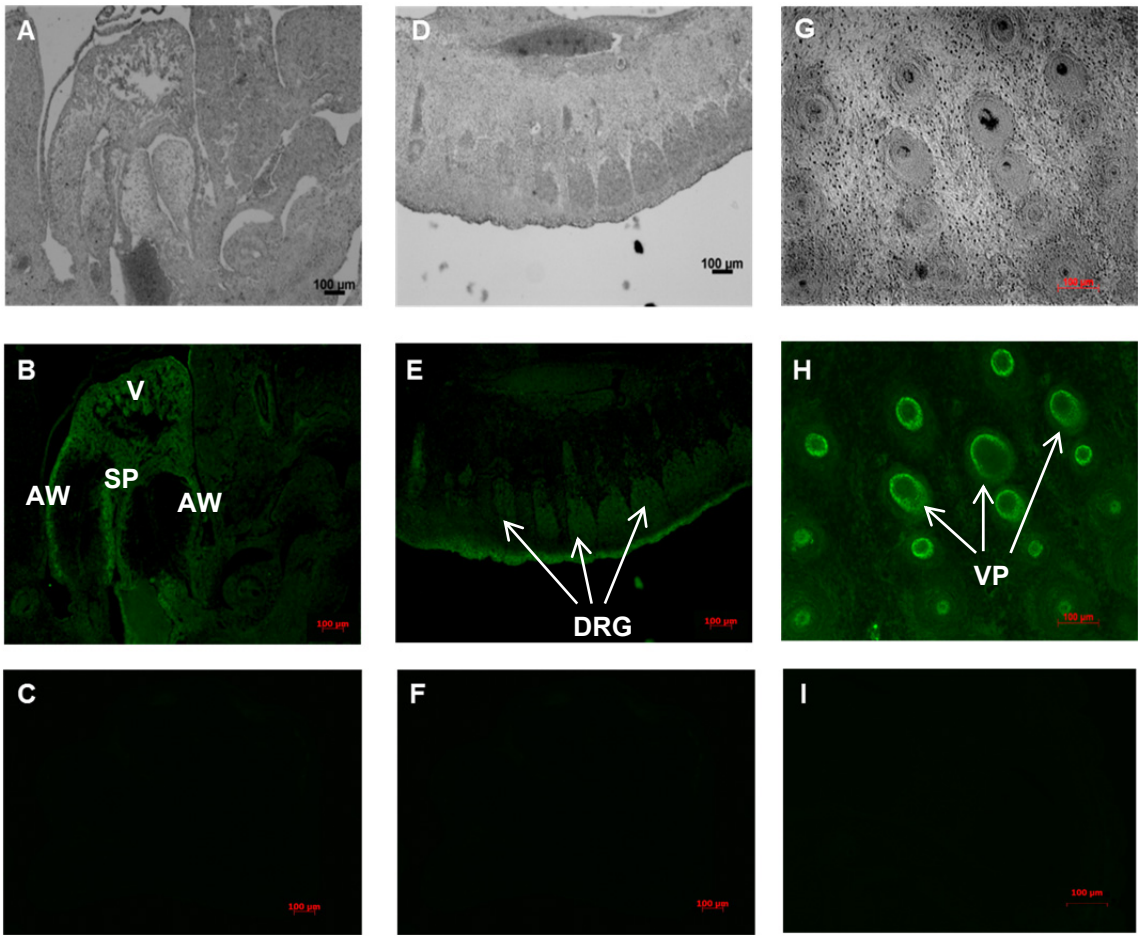

Figure 4-8. *Immunolocalisation of BAG-1 in cells of the non-skeletal tissue of prenatal E11.5 (A, B, C, D, E, F) and E16.5 (G, H, I) Bag-1$^{+/+}$ mouse. A, D, G - digital phase images; B, E, H – respective corresponding fluorescence; C, F, I – negative control (omission of primary antibody); V – ventricle, AW – atrial walls, SP – septum primum, DRG – dorsal root ganglia, VP* – vibrissae papillae; scale bar: 100 µm.

4.4.4. Genotyping *Bag-1*$^{+/+}$, *Bag-1*$^{+/-}$ and *Bag-1*$^{+/-}$ littermates

Genomic DNA samples isolated from the tail pieces of the fetuses were utilized for genotyping, performed using a PCR strategy. All three genotypes were present in the litters harvested at E10.5, E11.5, E12.5 and E13.5 of gestation; as a representative example, the results of genotyping E10.5 fetuses are shown (Fig. 4-9A). The first row of bands represents products (576 bp) of the PCR performed using *Bag-1* (F) and *Bag-1* (R) primers, while the second row of bands represents products (600 bp) of the PCR performed using *Bag-1* (F) and *Neo* (R) primers. The wild-type *Bag-1* allele was detected using the *Bag-1* (F) primer, located upstream of exon 1, and the *Bag-1* (R) primer, located within exon 1 of the *Bag-1* gene. PCR using this primer pair identified *Bag-1*$^{-/-}$ mice (nos. 1, 4, 6, characterised by absence of bands) from *Bag-1*$^{+/+}$ and *Bag*$^{+/-}$ littermates (bands corresponding to 576 bp PCR products observed for both genotypes). The null allele was detected using the *Bag-1* (F) primer and *Neo* (R) primer, located in the Neomycin-resistance gene. PCR using this primer pair distinguished the *Bag-1*$^{+/+}$ mouse (no. 7, characterised by the absence of a band) from the *Bag-1*$^{+/-}$ littermates (nos. 2, 3, 5, characterised by presence of bands corresponding to 600 bp PCR products). Thus, the three genotypes were present in the litter harvested at E10.5: one wild-type (*Bag-1*$^{+/+}$), three heterozygous (*Bag-1*$^{+/-}$) and three null (*Bag-1*$^{-/-}$) mice.

Western blot analysis mirrored the results of the PCR analysis (Fig. 4-9B). Bands specific for BAG-1L (50 kDa) and BAG-1S (32 kDa) were not observed in samples from mice 1 and 6 indicating a lack of expression of BAG-1 isoforms in the *Bag-1*$^{-/-}$ mice. Densitometric quantification of the bands was performed using the Quantity One® 1-D software to measure the expression levels of the BAG-1L and BAG-1S proteins. Data was normalised to β-Actin (loading control) and plotted in the form of bar graphs (Fig. 4-9C), which showed lower average levels of BAG-1L and BAG-1S proteins in *Bag-1*$^{+/-}$ mice (n = 3), relative to the levels of BAG-1L and BAG-1S proteins (that were assigned a value of 1) in the *Bag-1*$^{+/+}$ littermate (n = 1).

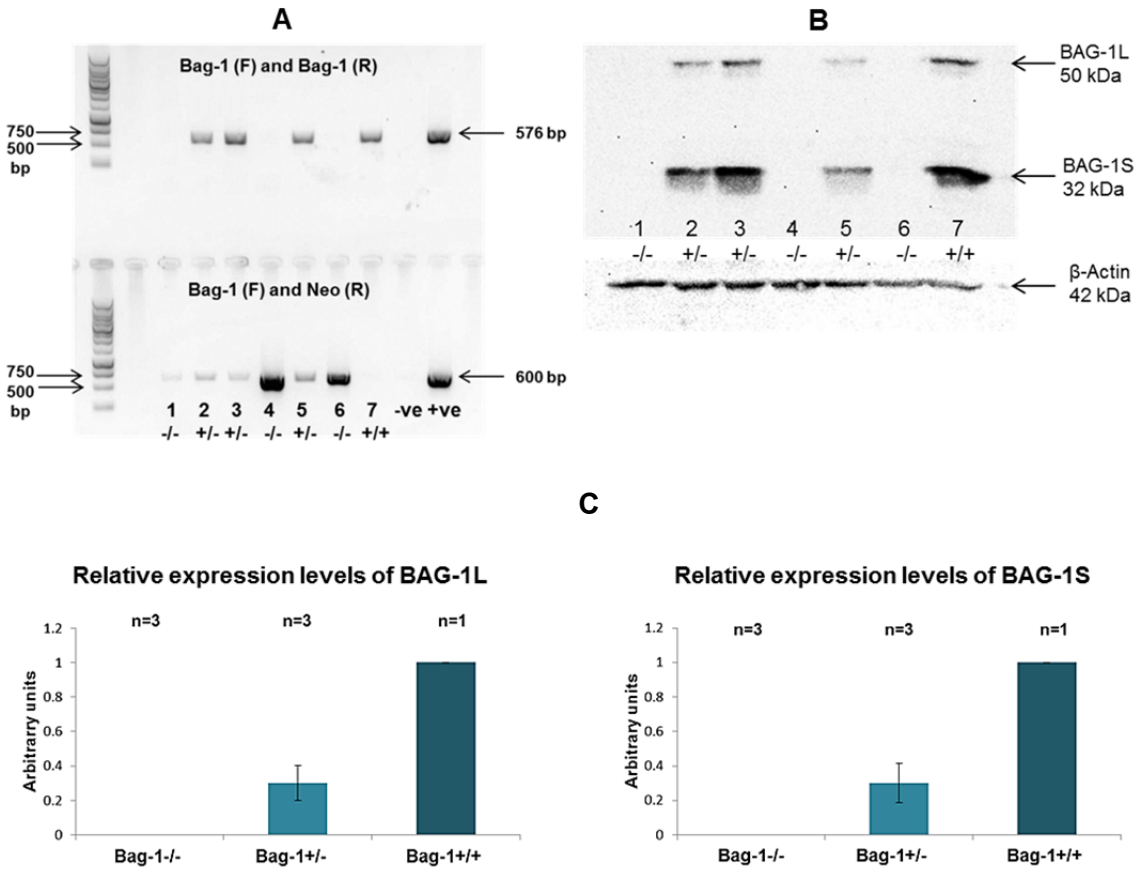

Figure 4-9. *Image of agarose gel with bands following electrophoresis of the PCR products amplified from genomic DNA of E10.5 fetuses (A) and representative immunoblot of limb bud protein lysates of E10.5 littermates probed with the anti-BAG-1 antibody (C16) (B), densitometric quantification of the bands performed to measure the expression of the BAG-1L and BAG-1S proteins, data was normalised to β-Actin (loading control) and plotted in the form of bar graphs (C).*

4.4.5. Phenotypic analyses of *Bag-1*$^{+/+}$, *Bag-1*$^{+/-}$ and *Bag-1*$^{+/-}$ mice between E10.5 and E13.5 of gestation

Female *Bag-1*$^{+/-}$ mice at different stages of gestation were sacrificed and fetuses were collected between E10.5 and E13.5. Following determination of the genotypes, fetuses were analysed for phenotypic differences. Representative images of *Bag-1*$^{+/+}$, *Bag-1*$^{+/-}$ and *Bag-1* $^{-/-}$ fetuses at E10.5, E11.5, E12.5 and E13.5 of development are shown (Fig. 4-10). At E10.5, no marked phenotypic differences were observed between littermates of the three genotypes. The *Bag-1*$^{-/-}$ fetuses exhibited significantly reduced thickness of the forebrain compared to *Bag-1*$^{+/+}$ and *Bag-1*$^{+/-}$ fetuses at E11.5. In comparison to the *Bag-1*$^{+/+}$ and *Bag-1*$^{+/-}$ fetuses, marked brain hypertrophy, reduced forebrain thickness, underdeveloped lower jaw and snout with exterior signs of cleft palate/lack of palate closure (Fig. 4-11D) were detected in the *Bag-1*$^{-/-}$ fetuses at E12.5 of development. At all the studied gestation time points, one out of thirty five *Bag-1*$^{-/-}$ fetuses exhibited signs of brain hypertrophy, all of them had visible reduction of forebrain thickness. By

E13.5, compared to the *Bag-1*$^{+/+}$ and *Bag-1*$^{+/-}$ littermates, the *Bag-1*$^{-/-}$ fetuses appeared significantly under developed, most likely as a consequence of being absorbed at this stage of gestation.

Histological analysis of whole body sagittal sections of E12.5 fetuses stained with Alcian blue and Sirius red (Fig. 4-11A – 4-11C) revealed that fetal livers of *Bag-1*$^{-/-}$ and *Bag-1*$^{+/-}$ mice were smaller than those of *Bag-1*$^{+/+}$ mice (open black arrows), the forebrains of *Bag-1*$^{-/-}$ mice were significantly reduced in thickness in comparison to wild type and heterozygous littermates (closed black arrows) and fetal hearts of *Bag-1*$^{-/-}$ and *Bag-1*$^{+/-}$ mice were larger than those of *Bag-1*$^{+/+}$ mice (red arrows).

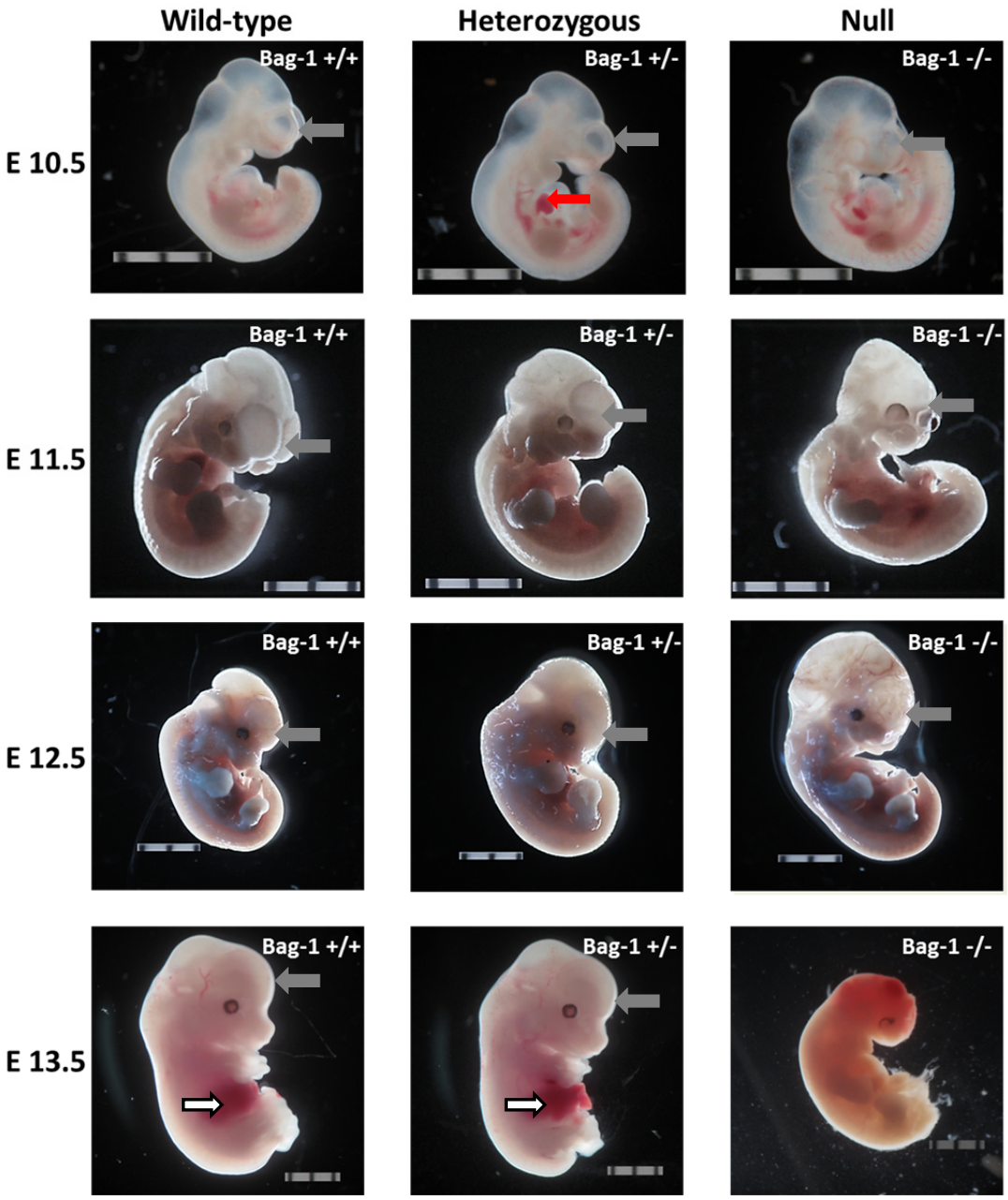

Figure 4-10. *Representative images of Bag-1$^{+/+}$, Bag-1$^{+/-}$ and Bag-1 $^{-/-}$ fetuses at E10.5, E11.5, E12.5 and E13.5 of development. At E10.5, no marked phenotypic differences were observed between littermates of the three genotypes. At E11.5 Bag-1$^{-/-}$ fetus exhibited significantly reduced thickness of the forebrain compared to Bag-1$^{+/+}$ and Bag-1$^{+/-}$ fetuses. At E12.5 of development, in comparison to the Bag-1$^{+/+}$ and Bag-1$^{+/-}$ fetuses, marked brain hypertrophy and an underdeveloped lower jaw were detected in the Bag-1$^{-/-}$ fetus. By E13.5, compared to the Bag-1$^{+/+}$ and Bag-1$^{+/-}$ littermates, the Bag-1$^{-/-}$ fetus appeared significantly underdeveloped, most likely as a consequence of being absorbed at this stage of gestation.* ➡ *forebrain,* ➡ *heart,* ⇨ *liver. Scale bar: 2 mm.*

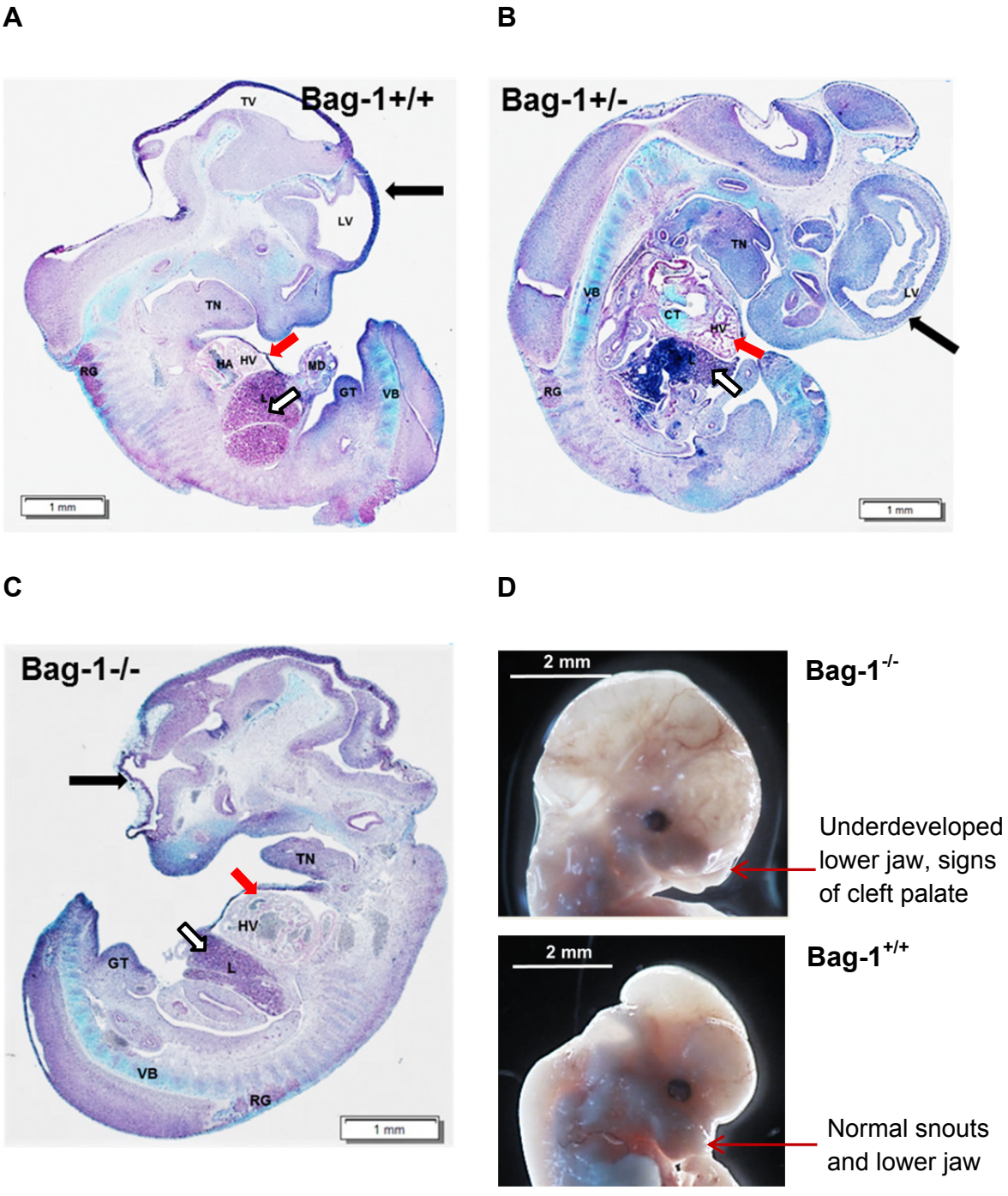

Figure 4-11. *A, B, C - Sagittal sections of E12.5 embryos stained with Alcian blue/Sirius red to visualise proteoglycan-rich cartilage matrix and collagenous matrix respectively. (A) Bag-1$^{+/+}$, (B) Bag-1$^{+/-}$, (C) Bag-1$^{-/-}$(**LV**-lateral ventricle, **TV**-third ventricle**, HV**-heart ventricle, **CT**-endocardial cushion tissue, **HA**-heart atrium, **L**-liver, **GT**-genital tubercle, **MD**-part of midgut loop passing into the physiological umbilical hernia, **TN**-tongue muscle and lower jaw, **RG**-dorsal (posterior) root ganglian**, VB**-cartilage. primordium of vertebra body). Closed black arrow indicates forebrain, open black arrow indicates liver, red arrow indicates heart.Scale bar: 1mm; D – images representing craniofacial development of Bag-1$^{+/+}$ and Bag-1$^{-/-}$ E12.5 mouse fetuses, thin black arrows indicate differences in the development of the jaw; scale bar: A-C – 1 mm, D – 2 mm.*

4.4.6. Expression of BAG-1 isoforms, SOX-9 and collagen type II in mouse fetal limb buds at different gestation time points

Female *Bag-1*$^{+/-}$ mice were sacrificed at different stages of gestation and fetuses were collected between E10.5 and E13.5. Genomic DNA samples isolated from the tail pieces of the fetuses were utilized for genotyping. Mouse fetal limb buds were carefully dissected (Fig. 4-12), homogenised in RIPA buffer and protein lysates were immunoblotted for the analyses of expression of BAG-1L and BAG-1S isoforms, SOX-9 and type II collagen expression in *Bag-1*$^{+/+}$, *Bag-1*$^{+/-}$ and *Bag-1*$^{-/-}$ littermates at different stages of gestation (E10.5 to E13.5). Densitometric quantification of the bands was performed using the Quantity One® 1-D software to measure the expression levels of the BAG-1L, BAG-1S, SOX-9 and type II collagen proteins. Data were normalised to β-Actin (loading control) and plotted in the form of bar graphs.

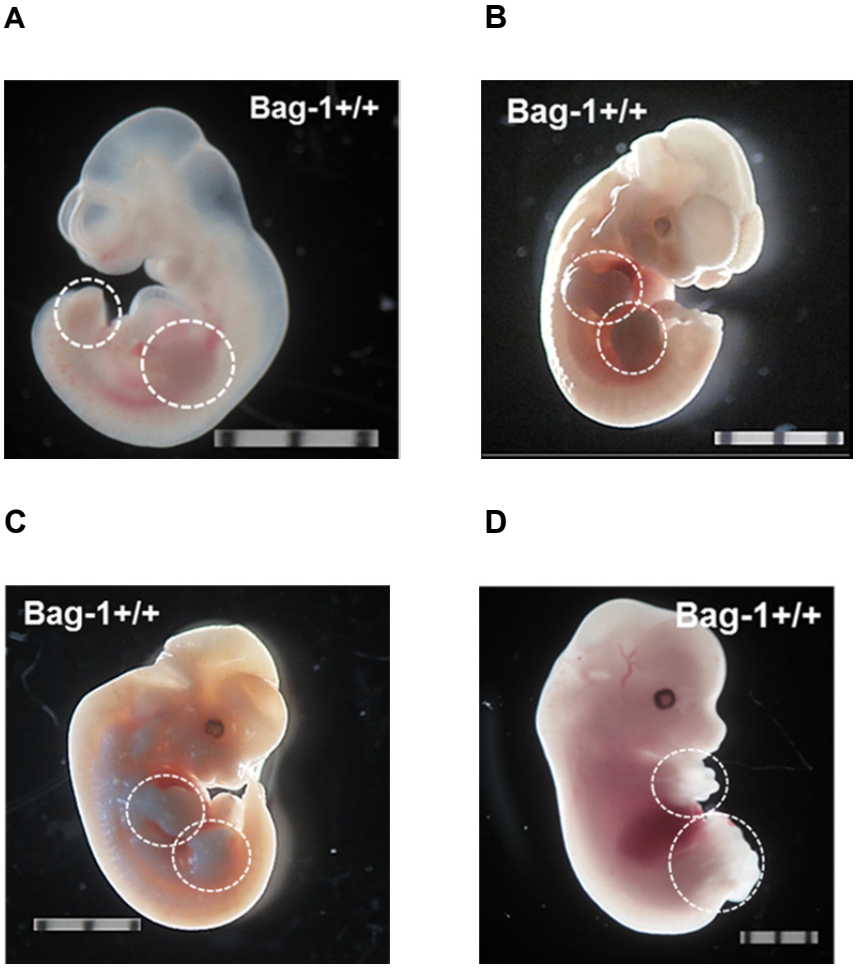

Figure 4-12. *Representative images of mouse Bag-1 wild type fetuses with highlighted (encircled) limb buds at E10.5 (A), E11.5 (B), E12.5 (C), E13.5 (D). Scale bar: 2 mm.*

The results of genotyping demonstrated that all three genotypes were present in the litters harvested at E10.5, E11.5, E12.5 and E13.5 (Fig. 4-13A, 4-14A, 4-15A, 4-16A).

Representative immunoblots of limb bud protein lysates of E10.5, E11.5, E12.5 and E13.5 littermates probed with the anti-BAG-1 antibody (C16) exhibited bands corresponding to BAG-1L (50 kDa) and BAG-1S (32 kDa) proteins for *Bag-1*$^{+/+}$ and *Bag-1*$^{+/-}$ mice, while no bands were detected for *Bag-1*$^{-/-}$ mice confirming the results of genotyping (Fig. 4-13B, 4-14B, 4-15B, 4-16B).

Expression of BAG-1L and BAG-1 S proteins in prenatal *Bag-1*$^{+/+}$ and *Bag-1*$^{+/-}$ mouse limb buds was quantified by densitometric analysis of the corresponding bands. Limb buds of *Bag-1*$^{+/-}$ mice expressed lower levels of BAG-1L and BAG-1S proteins compared to the *Bag-1*$^{+/+}$ littermates at the four time points of gestation examined in the study (Fig. 4-13C, 4-14C, 4-15C, 4-16C).

Expression of SOX-9 (band corresponding to 65 kDa, Fig. 4-13D, 4-14D, 4-15D, 4-16D) and type II collagen/COL II (band corresponding to 100 kDa, Fig. 4-13F, 4-14F, 4-15F, 4-16F) was observed in all limb bud samples of prenatal *Bag-1*$^{+/+}$, *Bag-1*$^{+/-}$ and *Bag-1*$^{-/-}$ mice.

Expression of SOX-9 and COL II proteins in prenatal *Bag-1*$^{+/+}$, *Bag-1*$^{+/-}$ and *Bag-1*$^{-/-}$ mouse limb buds was quantified by densitometric analysis of the corresponding bands. Levels of expression of both SOX-9 (Fig. 4-13E, 4-14E, 4-15E, 4-16E) and COL II (Fig. 4-13G, 4-14G, 4-15G, 4-16G) were similar in *Bag-1*$^{+/+}$, *Bag-1*$^{+/-}$ and *Bag-1*$^{-/-}$ littermates at the four time points of gestation examined in the study.

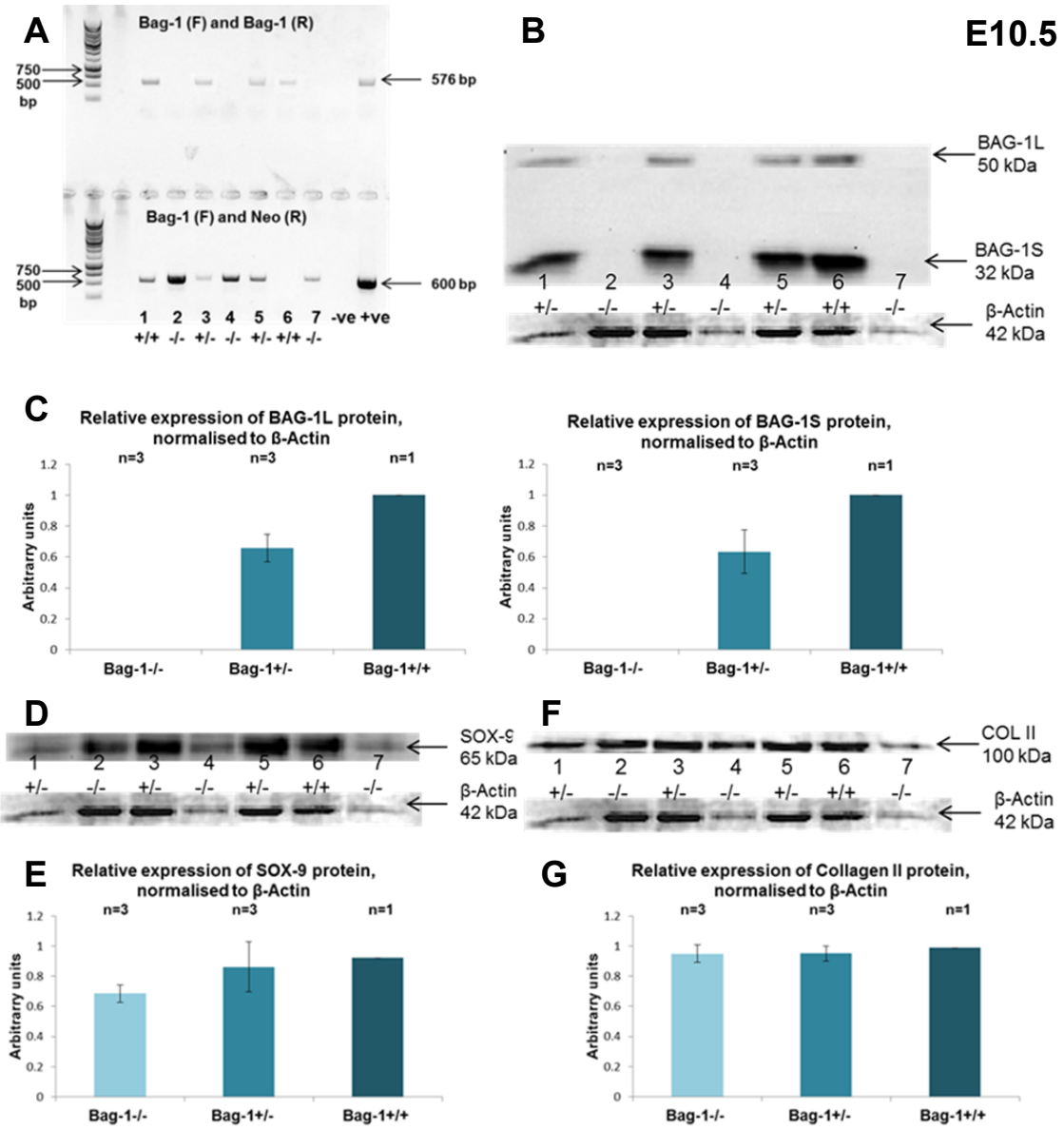

Figure 4-13. *Results of genotyping E10.5 fetuses following agarose gel electrophoresis of PCR products (A). The first row of bands represents products (576 bp) of PCR performed using Bag-1 (F) and Bag-1 (R) primers, while the second row of bands represents products (600 bp) of PCR performed using Bag-1 (F) and Neo (R) primers. Bands corresponding to 50 kDa BAG-1L, 32 kDa BAG-1S and 42 kDa β-Actin (loading control) following immunoblotting of protein lysates of E10.5 fetal limb buds (B). Expression of the BAG-1L and BAG-1S proteins was quantified by densitometric analysis of the corresponding bands and data was normalised to β-Actin. Bar graphs show levels of BAG-1L and BAG-1S proteins in Bag-1$^{+/-}$ and Bag-1$^{-/-}$ littermates relative to the levels of BAG-1 proteins in the Bag-1$^{+/+}$ littermate that were assigned a value of 1(C). Bands corresponding to 65 kDa SOX-9 and 42 kDa β-Actin (loading control) (D) and bands corresponding to 100 kDa type II collagen (COL II) and 42 kDa β-Actin (loading control) (F) following immunoblotting of protein lysates of E10.5 fetal limb buds. Quantification of SOX-9 (E) and COL II (G) expression by densitometric analysis of the corresponding bands, normalised to β-Actin.*

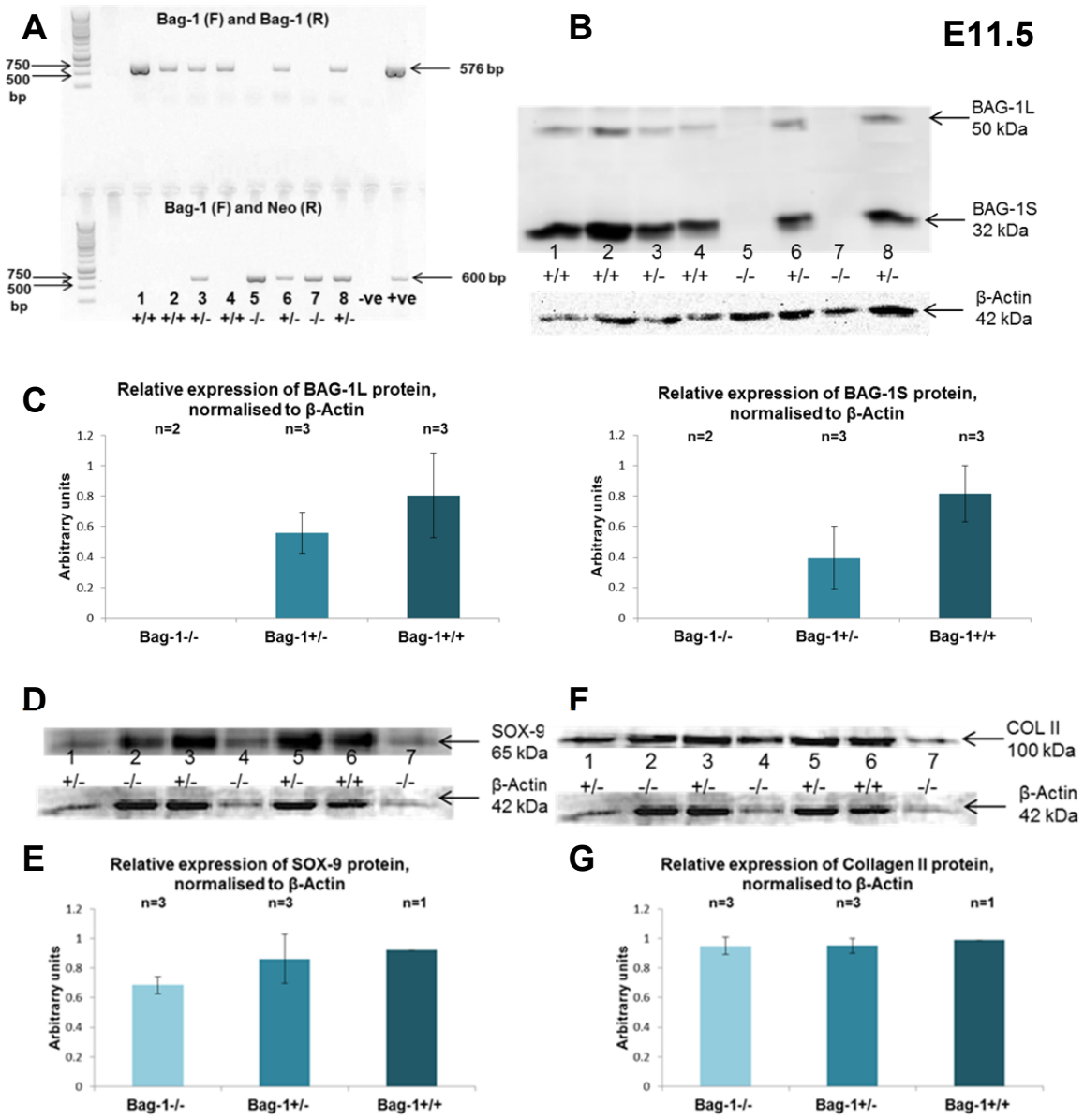

Figure 4-14. *Results of genotyping E11.5 fetuses following agarose gel electrophoresis of PCR products (A). The first row of bands represents products (576 bp) of PCR performed using Bag-1 (F) and Bag-1 (R) primers, while the second row of bands represents products (600 bp) of PCR performed using Bag-1 (F) and Neo (R) primers. Bands corresponding to 50 kDa BAG-1L, 32 kDa BAG-1S and 42 kDa β-Actin (loading control) following immunoblotting of protein lysates of E11.5 fetal limb buds (B). Expression of the BAG-1L and BAG-1S proteins was quantified by densitometric analysis of the corresponding bands and data was normalised to β-Actin. Bar graphs show levels of BAG-1L and BAG-1S proteins in Bag-1$^{+/-}$ and Bag-1$^{-/-}$ littermates relative to the levels of BAG-1 proteins in the Bag-1$^{+/+}$ littermate that were assigned a value of 1(C). Bands corresponding to 65 kDa SOX-9 and 42 kDa β-Actin (loading control) (D) and bands corresponding to 100 kDa type II collagen (COL II) and 42 kDa β-Actin (loading control) (F) following immunoblotting of protein lysates of E11.5 fetal limb buds. Quantification of SOX-9 (E) and COL II (G) expression by densitometric analysis of the corresponding bands, normalised to β-Actin.*

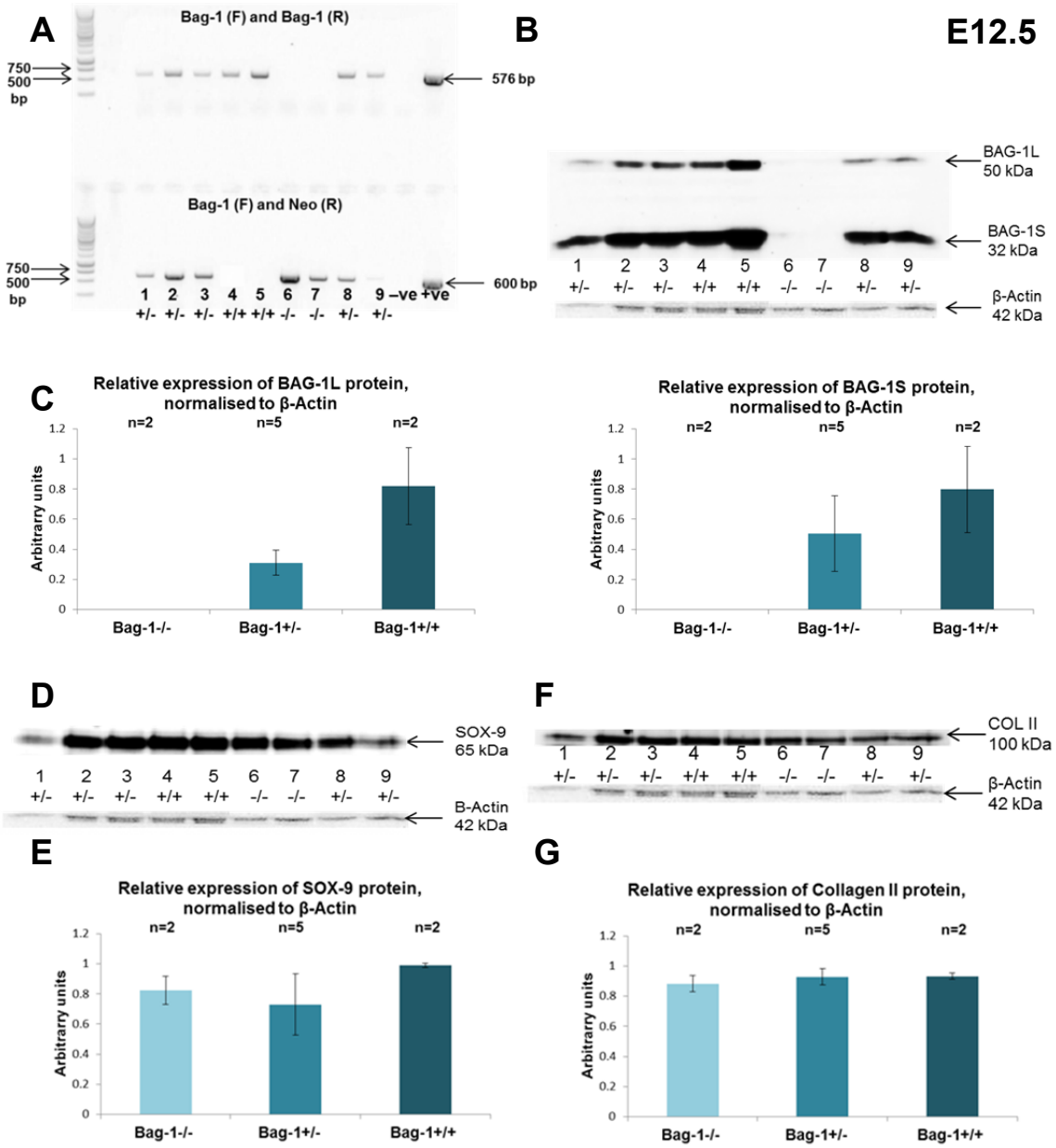

Figure 4-15. *Results of genotyping E12.5 fetuses following agarose gel electrophoresis of PCR products (A). The first row of bands represents products (576 bp) of PCR performed using Bag-1 (F) and Bag-1 (R) primers, while the second row of bands represents products (600 bp) of PCR performed using Bag-1 (F) and Neo (R) primers. Bands corresponding to 50 kDa BAG-1L, 32 kDa BAG-1S and 42 kDa β-Actin (loading control) following immunoblotting of protein lysates of E11.5 fetal limb buds (B). Expression of the BAG-1L and BAG-1S proteins was quantified by densitometric analysis of the corresponding bands and data was normalised to β-Actin. Bar graphs show levels of BAG-1L and BAG-1S proteins in Bag-1$^{+/-}$ and Bag-1$^{-/-}$ littermates relative to the levels of BAG-1 proteins in the Bag-1$^{+/+}$ littermate that were assigned a value of 1(C). Bands corresponding to 65 kDa SOX-9 and 42 kDa β-Actin (loading control) (D) and bands corresponding to 100 kDa type II collagen (COL II) and 42 kDa β-Actin (loading control) (F) following immunoblotting of protein lysates of E12.5 fetal limb buds. Quantification of SOX-9 (E) and COL II (G) expression by densitometric analysis of the corresponding bands, normalised to β-Actin.*

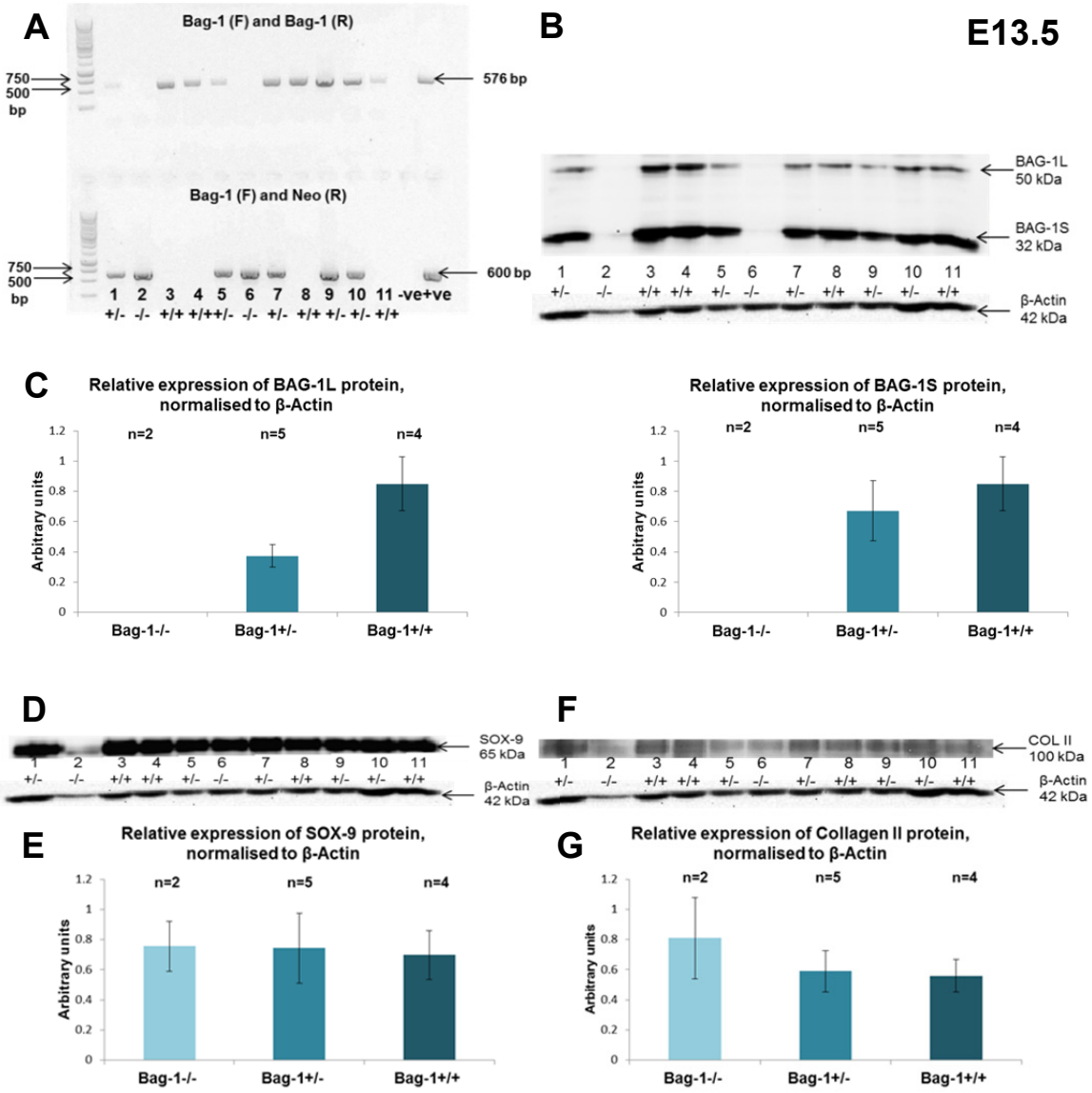

Figure 4-16. *Results of genotyping E13.5 fetuses following agarose gel electrophoresis of PCR products (A). The first row of bands represents products (576 bp) of PCR performed using Bag-1 (F) and Bag-1 (R) primers, while the second row of bands represents products (600 bp) of PCR performed using Bag-1 (F) and Neo (R) primers. Bands corresponding to 50 kDa BAG-1L, 32 kDa BAG-1S and 42 kDa β-Actin (loading control) following immunoblotting of protein lysates of E13.5 fetal limb buds (B). Expression of the BAG-1L and BAG-1S proteins was quantified by densitometric analysis of the corresponding bands and data was normalised to β-Actin. Bar graphs show levels of BAG-1L and BAG-1S proteins in Bag-1$^{+/-}$ and Bag-1$^{-/-}$ littermates relative to the levels of BAG-1 proteins in the Bag-1$^{+/+}$ littermate that were assigned a value of 1(C). Bands corresponding to 65 kDa SOX-9 and 42 kDa β-Actin (loading control) (D) and bands corresponding to 100 kDa type II collagen (COL II) and 42 kDa β-Actin (loading control) (F) following immunoblotting of protein lysates of E13.5 fetal limb buds. Quantification of SOX-9 (E) and COL II (G) expression by densitometric analysis of the corresponding bands, normalised to β-Actin.*

4.4.7. Analysis of the expression of BAG-1 isoforms in mouse fetal limb buds at different gestation time points

Litters at different stages of gestation were collected, the fetal limb buds were dissected and processed for western blot analysis of BAG-1 expression. Three litters for E10.5, three litters for E11.5, three litters for E12.5 and two litters for E13.5 were used in order to achieve n⩾3 fetuses for each genotype. Densitometric quantification of bands corresponding to BAG-1L and BAG-1S was performed using Quantity One® 1-D software. Results were normalised to β-Actin (loading control) and levels of BAG-1 proteins in *Bag-1*$^{+/-}$ and *Bag-1*$^{-/-}$ mice were plotted relative to the levels of BAG-1L and BAG-1S proteins in *Bag-1*$^{+/+}$ (i.e. the group showing highest expression of BAG-1 proteins). Results from separate litters for each time point were analysed together in order to achieve n⩾3 fetuses per genotype and statistical analysis was performed using one way ANOVA with a post-Tukey test.

Differences in the expression of BAG-1 L isoform between *Bag-1*$^{+/-}$ and *Bag-1*$^{+/+}$ fetuses were statistically significant at the four time points of gestation examined in the study (Fig. 4-17A, 4-17D $P<0.001$, 4-17B $P\leq0.05$, 4-17C $P<0.01$). Differences in expression of BAG-1S isoform between *Bag-1*$^{+/-}$ and *Bag-1*$^{+/+}$ littermates were statistically significant at E10.5 ($P<0.001$) and E11.5 ($P<0.01$), while no statistically significant differences in the levels of BAG-1S were observed at E12.5 and E13.5.

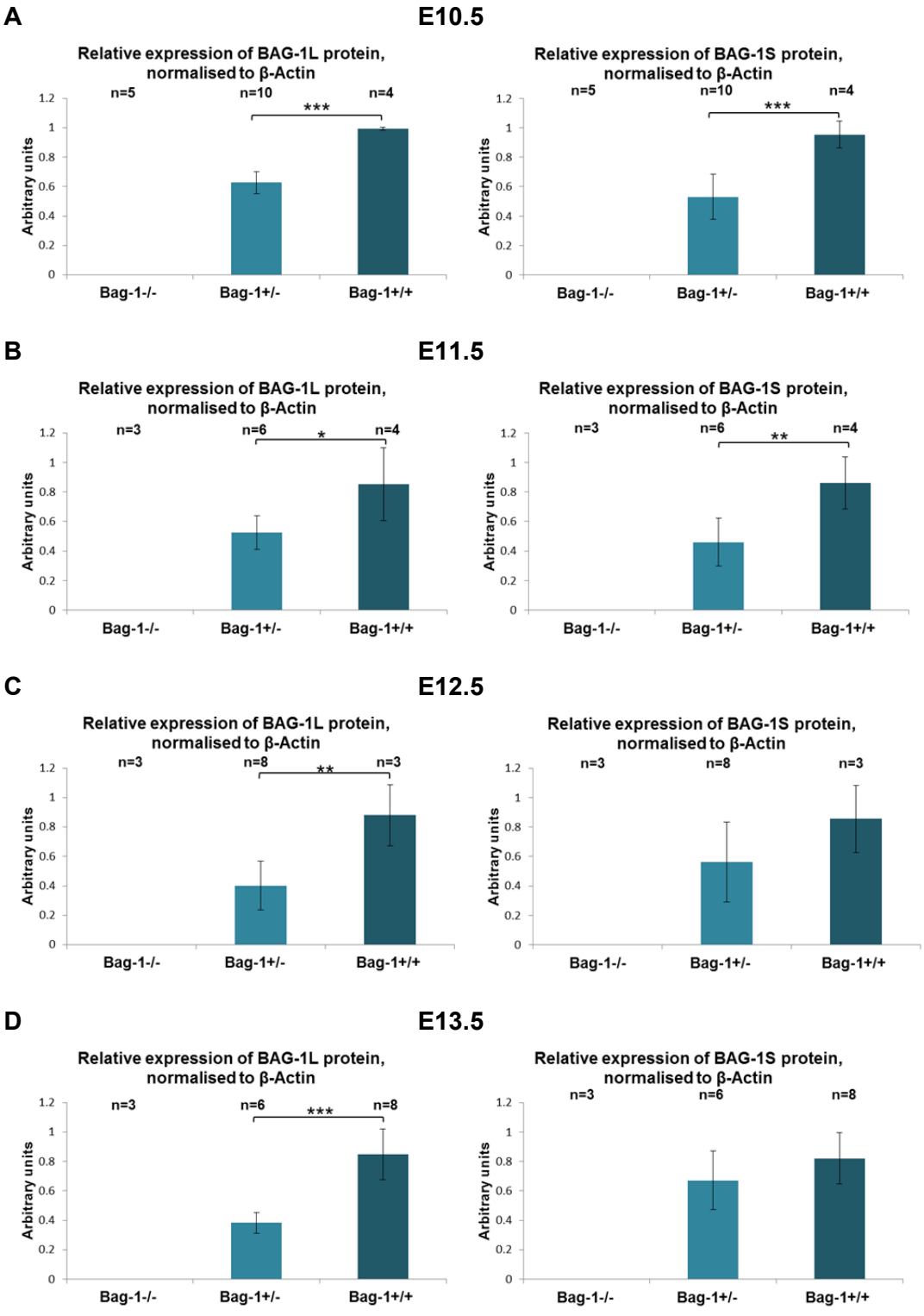

Figure 4-17. *Quantification and statistical analysis of western blot results of BAG-1L and BAG-1S expression in fetal limb buds at E10.5 (A), E11.5 (B), E12.5 (C), E13.5 (D) stage of gestation. Quantified band densities were considered to be significantly different between groups if P≤0.05. *** P<0.001, **P<0.01, *P≤0.05.*

4.4.8. Analysis of the expression of SOX-9 and type II collagen in mouse fetal limb buds at different gestation time points

Litters at different stages of gestation were collected, the fetal limb buds were dissected and processed for Western Blot analyses of SOX-9 and type II collagen expression. Three litters for E10.5, three litters for E11.5, three litters for E12.5 and two litters for E13.5 were used in order to achieve n⩾3 fetuses for each genotype. Densitometric quantification of bands corresponding to SOX-9 and type II collagen was performed using Quantity One® 1-D software. Results were normalised to β-Actin (loading control) and levels of SOX-9 and type II collagen were plotted relative to the levels of SOX-9 and type II collagen, respectively, in the group showing highest expression. Results from separate litters for each time point were analysed together in order to achieve n⩾3 fetuses per genotype and statistical analysis was performed using one way ANOVA with a post-Tukey test.

There were no statistically significant differences in expression of SOX-9 (Fig. 4-18) and type II collagen (Fig. 4-19) between *Bag-1*$^{+/+}$, *Bag-1*$^{+/-}$ and *Bag-1*$^{-/-}$ littermates at E10.5, E11.5, E12.5 and E13.5.

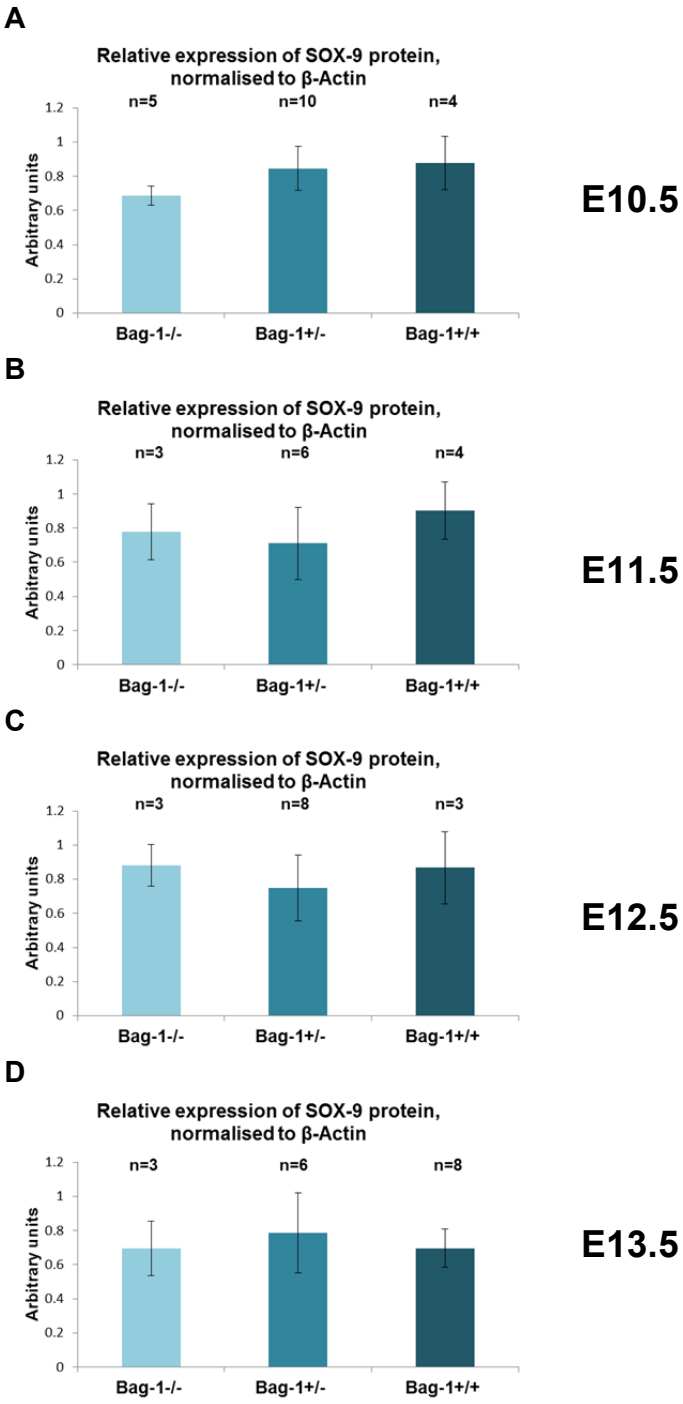

Figure 4-18. *Quantification and statistical analysis of western blot results of SOX-9 expression in fetal limb buds at E10.5 (A), E11.5 (B), E12.5 (C), E13.5 (D) stage of gestation. Quantified band densities were determined to be statistically non-significant between groups.*

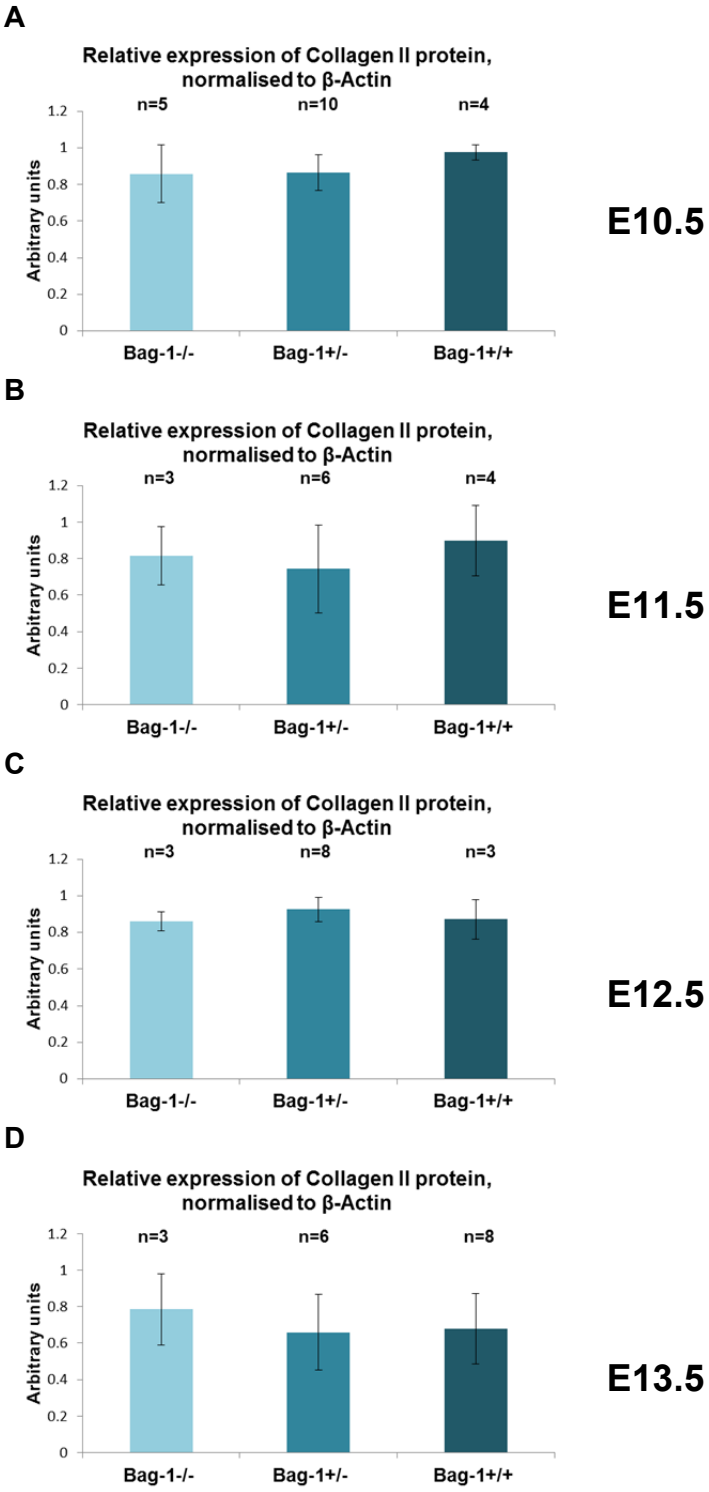

Figure 4-19. *Quantification and statistical analysis of western blot results of type II collagen expression in fetal limbs at E10.5 (A), E11.5 (B), E12.5 (C), E13.5 (D) stage of gestation. Quantified band densities were determined to be statistically non-significant between groups.*

4.4.9. Role of *Bag-1* in chondrocyte hypertrophy and cartilage mineralisation

Following culture for 21 days in basal (Bas) and treatment (Tr) media, the numbers of cartilage nodules were determined in micromass cultures of limb bud mesenchymal cells of E11.5 *Bag-1*$^{+/+}$, *Bag-1*$^{+/-}$ and *Bag-1*$^{-/-}$ mice.

In the basal medium, no differences were observed in the number of cartilage nodules in day-21 micromass cultures of limb bud mesenchymal cells of *Bag-1*$^{+/+}$, *Bag-1*$^{-/-}$ and *Bag-1*$^{-/-}$ mice. In the treatment medium, no differences were observed in the number of cartilage nodules between micromass cultures of limb bud mesenchymal cells of *Bag-1*$^{+/+}$ and *Bag-1*$^{+/-}$ mice, while micromass cultures of *Bag-1*$^{-/-}$ limb bud mesenchymal cells were characterised by significantly higher number of mineralised cartilage nodules in comparison to corresponding day-21 micromass cultures of *Bag-1*$^{+/+}$ and *Bag-1*$^{+/-}$ limb bud mesenchymal cells (Fig. 4-20).

Furthermore, genes crucial for chondrocyte hypertrophy, mineralisation and maintenance of hypertrophic chondrocyte morphology, namely *Col10a1*, *Alpl*, *Runx-2*, *Ihh* and *Adseverin*, were significantly upregulated in day-21 micromass cultures of limb bud mesenchymal cells of *Bag-1*$^{-/-}$ mice in the treatment medium, compared to cultures of *Bag-1*$^{+/+}$ and *Bag-1*$^{+/-}$ cells in similar conditions (Fig. 4-21). Additionally, in the treatment medium, no differences in the expression of these genes were observed between micromass cultures of limb bud mesenchymal cells of *Bag-1*$^{+/+}$ and *Bag-1*$^{+/-}$ mice. In basal culture conditions, there were no differences in the expression of these genes between micromass cultures of limb bud mesenchymal cells of *Bag-1*$^{+/+}$, *Bag-1*$^{-/-}$ and *Bag-1*$^{-/-}$ mice.

Day-21 micromass cultures in the treatment medium were stained with Alcian blue to demonstrate the synthesis of proteoglycans by the cartilage nodules (Fig. 4-22). Extensive staining for Alkaline phosphatase in the cartilage nodules and surrounding matrix, coupled with intense Alizarin red staining of the cartilage nodules in day 21-micromass cultures of *Bag-1*$^{-/-}$ cells were indicative of pronounced chondrocyte hypertrophy and robust mineralization of the hypertrophic cartilage (Fig. 4-22).

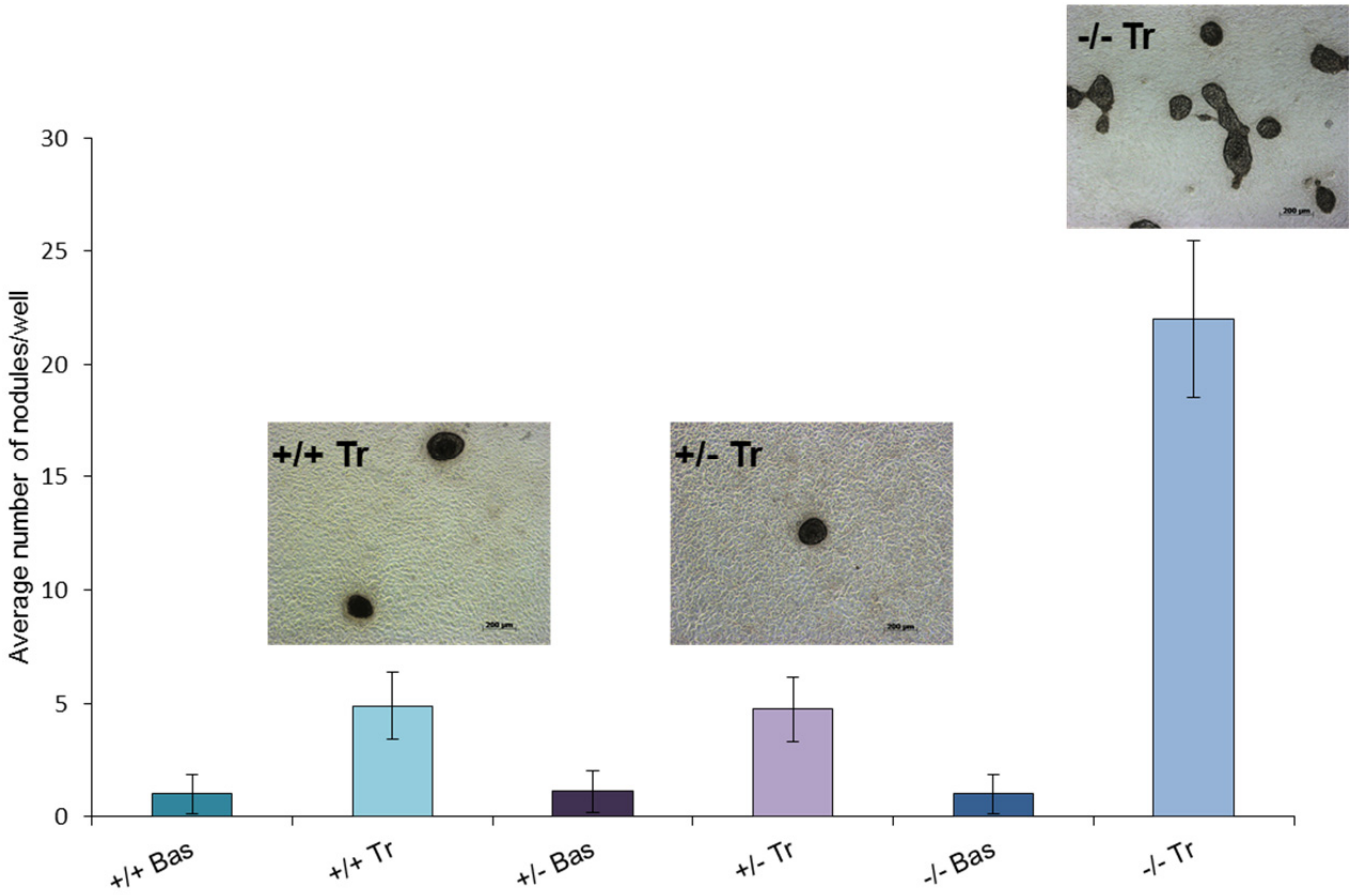

Figure 4-20. *Average number of cartilage nodules/well in day-21 micromass cultures of limb bud mesenchymal cells of E11.5 Bag-1$^{+/+}$, Bag-1$^{+/-}$ and Bag-1$^{-/-}$ mice in basal (Bas) and treatment (Tr) media, n = cells from 7 mice per group.*

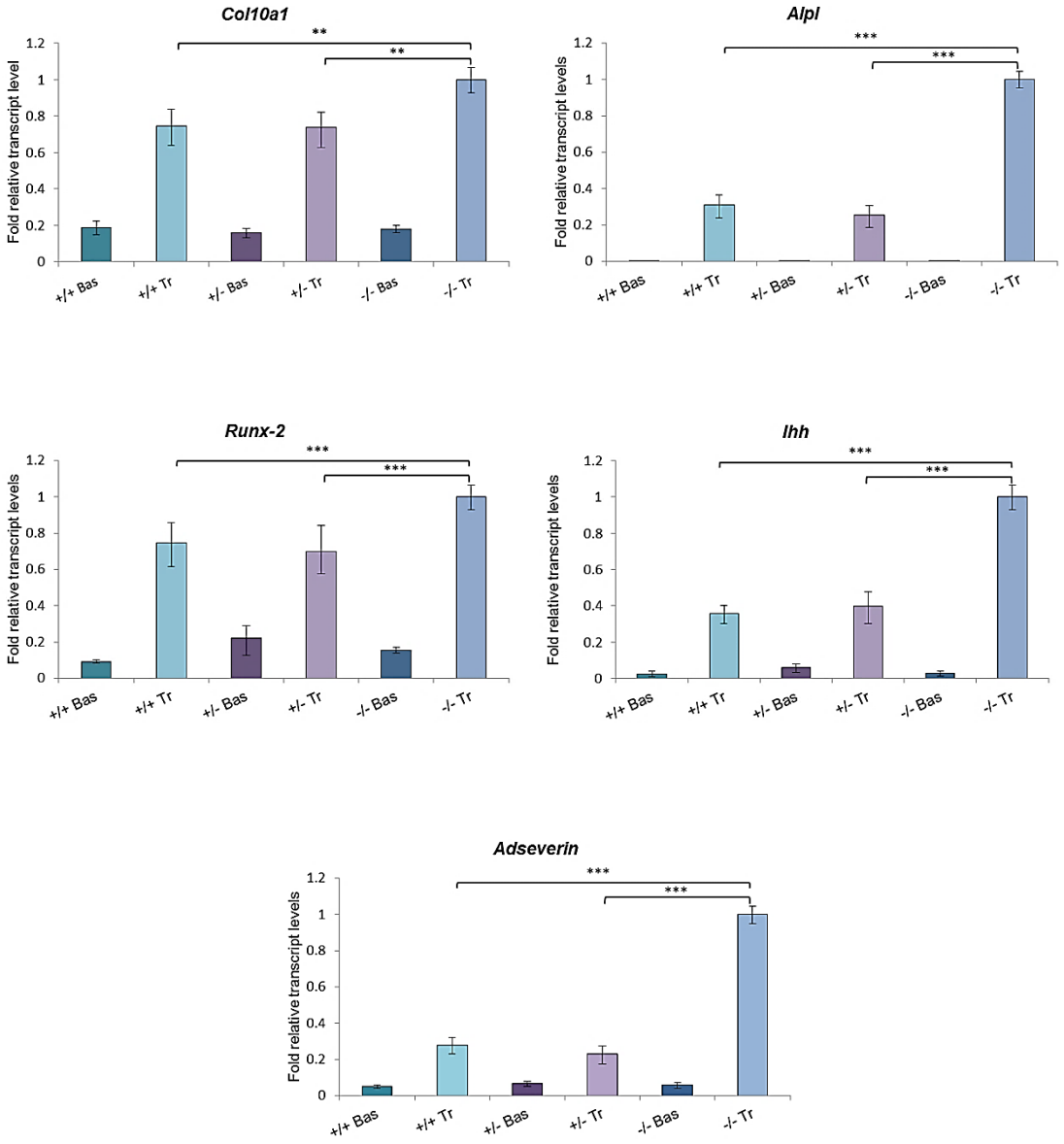

Figure 4-21. *Expression of Col10a1, Alpl, Runx-2, Ihh and Adseverin (markers of chondrocyte hypertrophy and mineralisation) in day-21 micromass cultures. Bar graphs illustrate fold changes ($2^{-\Delta\Delta C_T}$) in relative mRNA transcript levels normalised to the endogenous reference (β-Actin). The range of gene expression is indicated by $2^{-(\Delta\Delta C_T + SD)}$ and $2^{-(\Delta\Delta C_T - SD)}$, where SD is the standard deviation of the $\Delta\Delta C_T/\Delta C_T$ value. Statistical analysis is performed at the level of ΔC_T in order to exclude potential bias due to averaging of data transformed through the $2^{-\Delta\Delta C_T}$ equation; n = cells from 7 mice per group; ***P<0.001, **P<0.01.*

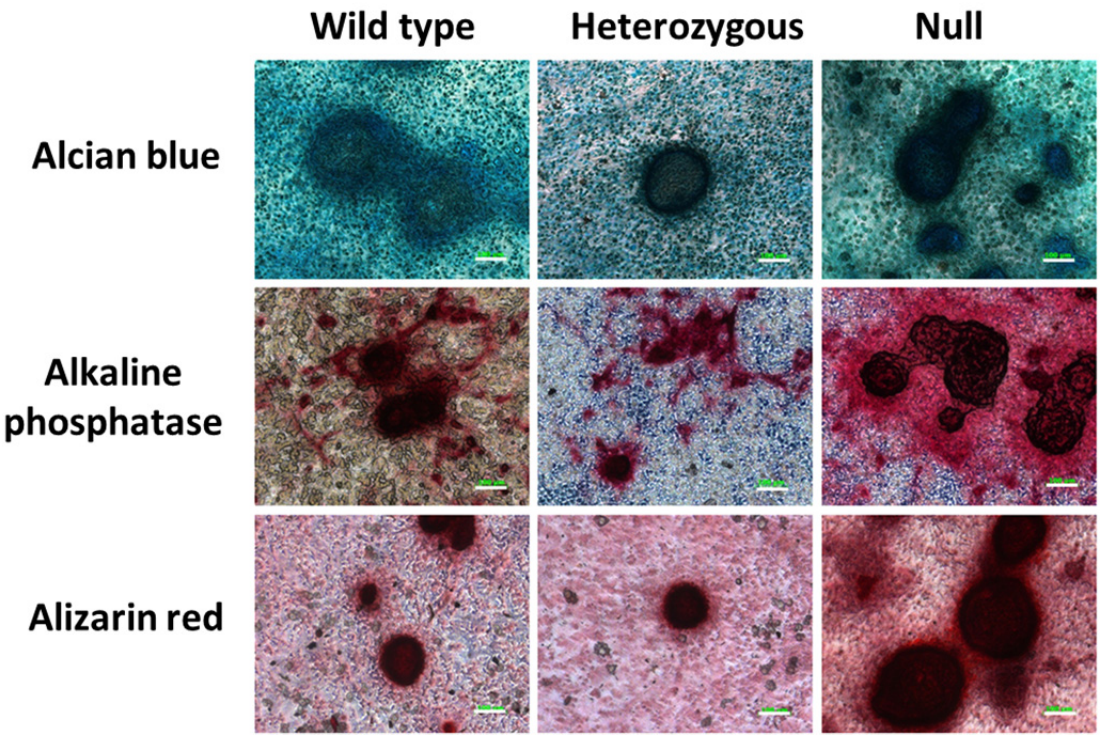

Figure 4-22. *Alcian blue* (*detection of the synthesis of proteoglycans by the cartilage nodules), Alkaline phosphatase (marker of chondrocyte hypertrophy) and Alizarin red (marker of mineralization of the hypertrophic cartilage) stained cartilage nodules in day-21 micromass cultures in treatment media. n = cells from 7 mice per group, Scale bars: 100 µm.*

4.5. Summary of results

a) Staining for BAG-1 in the cells of the future intervertebral discs was observed in the cytoplasm (BAG-1S) and the nuclei (BAG-1L); predominantly cytoplasmic staining for BAG-1S was observed in the cells at the prospective metacarpal-phalangeal and inter-phalangeal sites in the incipient joints of the forelimb of the E14.5 fetus; staining for BAG-1 in hind limb of the E16.5 fetus was prominently seen in the mineralized hypertrophic cartilage at the vascular front.

b) At E12.5 fetal livers of *Bag-1*$^{-/-}$ and *Bag-1*$^{+/-}$ mice were smaller than those of *Bag-1*$^{+/+}$ mice, the forebrains of *Bag-1*$^{-/-}$ mice were significantly reduced in thickness in comparison to wild type and heterozygous littermates and fetal hearts of *Bag-1*$^{-/-}$ and *Bag-1*$^{+/-}$ mice were larger than those of *Bag-1*$^{+/+}$ mice.

c) There were no statistically significant differences in the expression of SOX-9 and type II collagen in the limb buds of *Bag-1*$^{+/+}$, *Bag-1*$^{+/-}$ and *Bag-1*$^{-/-}$ littermates at E10.5, E11.5, E12.5 and E13.5 in the limb bud lysates.

d) In comparison to micromass cultures of limb bud cells of *Bag-1*$^{+/+}$and *Bag-1*$^{+/-}$ mice, micromass cultures of limb bud cells of *Bag-1*$^{-/-}$ mice were characterised

by higher number of mineralised cartilage nodules, significant upregulation of expression of hypertrophic genes, which was indicative of enhanced terminal differentiation of chondrocytes, and intense ALPL and Alizarin red staining, suggestive of increased mineralization of the hypertrophic cartilage.

4.6. Discussion

The present study aimed to characterise the role of the multifunctional *Bag-1* gene in embryonic skeletal development using the *Bag-1* knock-out mouse model. *Bag-1* knock-out mice were genetrated by Gotz and co-workers (Gotz et al., 2005), who reported that *Bag-1*$^{-/-}$ fetuses died between E12.5 and E13.5 of gestation due to appreciable cell apoptosis in the embryonic liver, defects in neuronal cell differentiation and haematopoiesis. These observations were elucidated by the results of our study, which demonstrated that fetal livers of *Bag-1*$^{-/-}$ mice were smaller than those of *Bag-1*$^{+/+}$ and *Bag-1*$^{+/-}$ mice and the forebrains of *Bag-1*$^{-/-}$ mice were significantly reduced in thickness in comparison to *Bag-1*$^{+/+}$ and *Bag-1*$^{+/-}$ littermates.

Additionally, underdeveloped lower jaws and hypertrophic hearts were consistently observed in *Bag-1*$^{-/-}$ fetuses. It has been shown that cardiac-specific overexpression of Epidermal Growth Factor Receptor 2 (ErbB2) leads to cardiac hypertrophy in the heart (Sysa-Shah et al., 2012). Furthermore, Epidermal Growth Factor Receptor (EGFR) signalling is necessary for normal craniofacial development; *Egfr*$^{-/-}$ mice are born with, amongst other features, shorter/underdeveloped lower jaws, misshapen snouts and high incidence of cleft palate (Miettinen et al., 1999). EGFR is a member of the epidermal growth factor receptor family (EGFR/ErbB1/HER1, ErbB2/HER2, ErbB3/HER3, and ErbB4/HER4) of transmembrane tyrosine kinases that are activated by dimerization following binding to specific ligands, such as epidermal growth factor (EGF) or transforming growth factor-α (TGF-α) (Carpenter and Cohen, 1990, Yarden and Sliwkowski, 2001). EGFR family members play an important role in cell proliferation, regulation and migration. Furthermore, cleft palate, an inadequate fusion of the palatal shelves, is associated in humans with polymorphism of *Tgfa* gene that encodes TGF-α, which is an EGFR ligand produced by epithelia (Chenevix-Trench et al., 1992).

BAG-1 has been shown to interact with membrane form of heparin binding EGF-like growth factor (HB-EGF), a member of the EGF family and a direct activating ligand for EGFR (Lin et al., 2001). As HB-EGF interaction site on BAG-1 is distinct from the HSC70/HSP70 interaction site, it has been suggested that HB-EGF and BAG-1 interact directly in a HSP70-independent manner (Lin et al., 2001). It is therefore likely that BAG-1 plays a role in the EGFR signalling and is involved in craniofacial development. Thus, the significance of the interaction between BAG-1 and HB-EGF in regulating craniofacial development via downstream EGFR signalling would benefit from further investigation.

Western blot analysis of BAG-1 isoform expression in mouse fetuses across the four gestation time points demonstrated no expression of BAG-1L and BAG-1S in *Bag-1*$^{-/-}$ littermates (as expected), while the two isoforms of BAG-1 were expressed in *Bag-1*$^{+/+}$ and *Bag-1*$^{+/-}$ littermates. This observation stands in opposition to that by Crocoll and co-workers (Crocoll et al., 2000), who claimed to have detected the 46 kDa BAG-1M protein alongside the 32 kDa BAG-1S isoform in mouse fetal lysates, with the 46 kDa protein being the most prominent BAG-1 isoform throughout mouse development. All BAG-1 isoforms are generated by alternative translation initiation and the three translation initiation sites (non-canonical codon CUG for BAG-1L, AUG codon for BAG-1M, AUG codon for BAG-1S) are located within the first exon of the *Bag-1* transcript. There is no corresponding isoform to human BAG-1M in rodents since the first AUG codon is not conserved - murine mRNA has a GUG codon where human mRNA has AUG codon (Gehring, 2006).

Moreover, BAG-1S has been recognised as the major BAG-1 isoform in rodents (Townsend et al., 2003b, Yang et al., 2007). Translation of the BAG-1S isoform is partially dependent on internal ribosome entry sequence (IRES) mediation, which enables BAG-1S translation to be maintained independent of cap structures (Coldwell et al., 2001). We suggest that compensatory mechanisms in the form of IRES-mediated translation are involved in maintaining the expression of the BAG-1S isoform in heterozygous mice at E12.5 and E13.5.

During normal murine development, expression of *Bag-1* mRNA was detected in several organs, with highest expression observed in cartilaginous tissues of the developing mouse embryo (Crocoll et al., 2000). In addition to the sites of *Bag-1* expression demonstrated previously, we were able to demonstrate expression of BAG-1L and BAG-1S in cells of the developing intervertebral discs – fibrocartilaginous joints functioning as shock absorbers between the adjacent vertebrae. Expression of BAG-1S was also observed in the mesenchymal tissue at the nascent metacarpal-phalangeal and inter-phalangeal sites in the incipient joints of the developing limbs. Although robust expression of BAG-1 is detected in cells of the nascent joints, its exact role at these sites is not known.

It has been shown that a distinct cohort of skeletal progenitor cells, which are characterized by *Gdf5* (growth/differentiation factor-5) expression, reside at the nascent joint sites and, in response to the actions of chondrogenic and anti-chondrogenic factors, are devoted to limb joint formation, including bulk of the articular cartilage, synovial lining, intra-joint ligaments, inner capsule and superficial layer of the articular

cartilage (Koyama et al., 2008). GDF-5 also has an important role in the maintenance of the intervertebral discs and their ability to function as shock absorbers, since deficiency of *Gdf5* in cells of the intervertebral discs results in decreased proteoglycan content and collagen expression (Li et al., 2004). It is likely that BAG-1, in conjunction with other factors with defined roles in joint formation, has a regulatory role in the process of limb joint formation by the *Gdf5*-expressing progenitor cells or BAG-1 may assist GDF-5 in maintenance of normal intervertebral disc structure.

Interestingly, during normal endochondral development of fetal long bones, we observed the expression of BAG-1 in the mineralised hypertrophic cartilage at the vascular front. Since *Bag-1*$^{-/-}$ mice die between E12.5 and E13.5, the present study employed micromass cultures of E11.5 limb bud mesenchymal cells to elucidate the function of BAG-1 in chondrocyte hypertrophy and cartilage mineralisation. The micromass culture technique, an *in vitro* method for examining chondrogenic differentiation, enables characterisation of the differentiation processes occurring during the development of the cartilage anlagen *in vivo* (Lengner et al., 2004). Treating the micromass cultures of embryonic limb bud mesenchymal cells with medium containing 0.25 mM ascorbic acid and 1 mM β-glycerophosphate facilitates the establishment of an *ex vivo* model, specifically elaborating the late stages of chondrogenic differentiation, i.e. chondrocyte hypertrophy and cartilage mineralisation (Ahrens et al., 1977).

In the absence of *Bag-1*, formation of mineralised cartilage nodules was significantly enhanced in micromass cultures of limb bud mesenchymal cells. Moreover, increased expression of hypertrophic genes, in combination with intense ALPL and Alizarin red staining of the cartilage nodules and surrounding matrix, indicated marked upregulation of chondrocyte hypertrophy and matrix mineralisation in the cartilage nodules generated by limb bud mesenchymal cells lacking *Bag-1*. This suggests that BAG-1 has an important function in chondrocyte development and, by regulating terminal differentiation of chondrocytes and hypertrophic cartilage mineralisation, the co-chaperone protein plays a critical role in the transition from chondrogenesis to osteogenesis at the vascular front during the process of endochondral ossification. One of the avenues to further investigate is the role of BAG-1 in chondrocyte hypertrophy and cartilage mineralisation. This would entail determining whether BAG-1 functions as a physiological regulator of p38 MAPK signalling, which has been demonstrated to have an important role in promoting hypertrophic chondrocyte differentiation and cartilage mineralisation (Stanton et al., 2004).

Gene knock-out mouse models have enabled for the expansion of our understanding of skeletal development; gene targeting technology is therefore the preferred method of studying gene function *in vivo* (Capecchi, 1989). However, as the targeted genes are often characterised by non-redundant systemic roles, gene knock-out strategies can lead to possible embryonic lethality of knock-out mice, thereby precluding analyses of the role of the gene of interest in different stages of development. In the case of the *Bag-1* knock-out mouse model, *Bag-1*$^{-/-}$ mice die between E12.5 and E13.5 of gestation. Early embryonic lethality of *Bag-1* null mice made it challenging to study the role of the gene in skeletal development/endochondral ossification *in vivo* beyond E12.5/13.5 of gestation. Constitutive knock-out models can also have limitations such as complex phenotypes or various compensatory mechanisms. In order to bypass the limitations of the constitutive knock-out model, generation of tissue-specific conditional knock-out mouse models, where the target gene is specifically inactivated in the tissue of interest, can be harnessed. Use of *Bag-1* conditional knock-out mice in which the *Bag-1* gene is deleted specifically from chondrocytes using *Col2a1*– Cre recombinase may prevent early embryonic lethality and allow improved analysis of the role of *Bag-1* in skeletal development.

Chapter 5

Characterisation of the role of *Bag-1* in postnatal skeletal development

5. Characterisation of the role of *Bag-1* in postnatal skeletal development

5.1. Introduction

The co-chaperone protein BAG-1 is ubiquitously expressed in postnatal bone, including growth plate and articular chondrocytes, and cells of the osteoblast-lineage, i.e. bone marrow stromal cells, osteoblasts and osteocytes (Kinkel et al., 2004, Tare et al., 2008b). BAG-1 is a multifunctional protein that binds multiple partners and plays an important role in cell proliferation, differentiation and apoptosis by regulating gene transcription and cell signalling (Townsend et al., 2003b). BAG-1 has been shown to protect mammalian chondrocytes against apoptosis induced by ER stress and heat shock and plays an important role in the regulation of chondrogenic gene expression (Yang et al., 2007, Tare et al., 2008b). In contrast, no studies, to date, have investigated the role of *Bag-1* in bone marrow stromal cell (BMSC) proliferation, differentiation and apoptosis.

In order to effectively relate skeletal studies to the understanding of human physiology, in addition to *in vitro* experimentation, studies should also be performed *in vivo,* ideally in mammals, to demonstrate functionality. Characterisation of human development by means of mouse biology study is largely permitted due to the degree of conservation between mouse and human genomes (Waterston et al., 2002). The choice of mice as an experimental model is dictated by the similarity of their skeleton and physiology to humans. Moreover, the development of the mouse skeleton has been well described; gene manipulation techniques and analysis of genetically modified animals have been standardised and established for the mouse species. It is therefore not surprising that gene knock-out mice have been a major driving force in defining skeletogenesis, as knock-out mice provide models for studying the role of genes and determining their functionality in skeletal development.

Significant apoptosis in the embryonic liver and brain, along with defective haematopoiesis and neuronal cell differentiation have been identified as the major causes of death in *Bag-1* null mice between E12.5 and E13.5 of gestation. Around E14.5 – E15.5, the calcified hypertrophic cartilage is invaded by blood vessels that bring in the osteoblasts for deposition of bone matrix (Horton, 1993, Karsenty, 1999). Given the early embryonic lethality in *Bag-1*$^{-/-}$ mice, it is not possible to assess their bone development. However, mice heterozygous for the *Bag-1* gene i.e. containing one functional *Bag-1* allele are not embryonic lethal and survive into adulthood. This has allowed the study to investigate the role of *Bag-1* haploinsufficiency in osteoblast development.

Osteoblasts are derived from the discrete population of bone marrow stromal stem cells, commonly referred to as mesenchymal stem cells (MSCs) or skeletal stem cells (SSCs) (Caplan, 1991, Bianco and Robey, 2004). These multipotent cells are capable of giving rise to osteoblasts, chondrocytes, adipocytes, smooth muscle cells, astrocytes and myelosuportive stroma (Fig. 5-1) (Tare et al., 2008a).

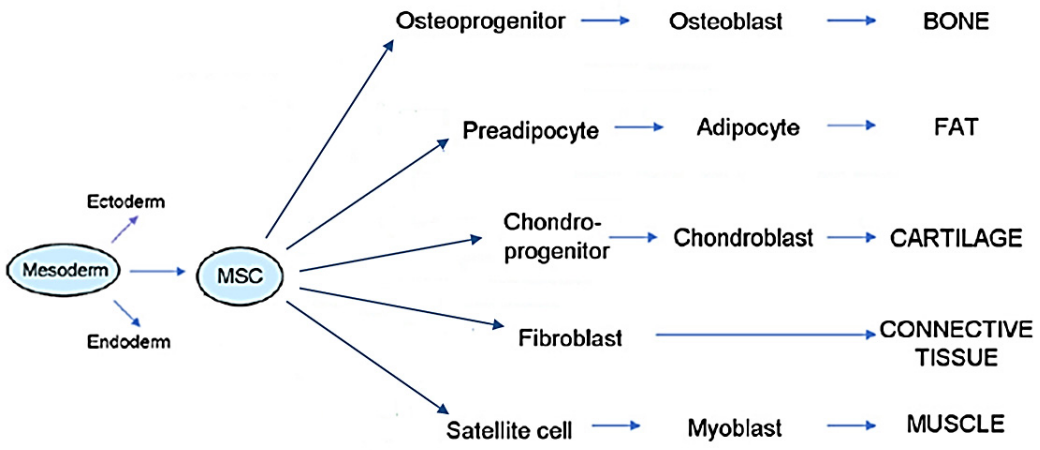

Figure 5-1. *Generation of stromal lineage cells from the bone marrow stromal stem cells (mesenchymal stem cells, skeletal stem cells), adapted from Tare et al., 2008a.*

Upon stimulation by osteogenic growth factors, glucocorticoids and hormones, such as BMPs, Dexamethasone and Calcitrol ($1,25(OH)_2D_3$), the SSC population of BMSCs undergo osteogenic differentiation. The developmental stages of osteoblastogenesis are characterised by the expression of distinct phenotypic markers (Fig. 5-2), namely early osteprogenitor markers such as Runx-2 and Osterix (Komori et al., 1997, Nakashima et al., 2002), early osteoblast marker, ALPL, which also plays an important role in matrix mineralisation (Lian and Stein, 1992) and the non-collagenous bone matrix protein Osteocalcin that acts as a phenotypic marker of terminally differentiated osteoblasts (Hauschka et al., 1989).

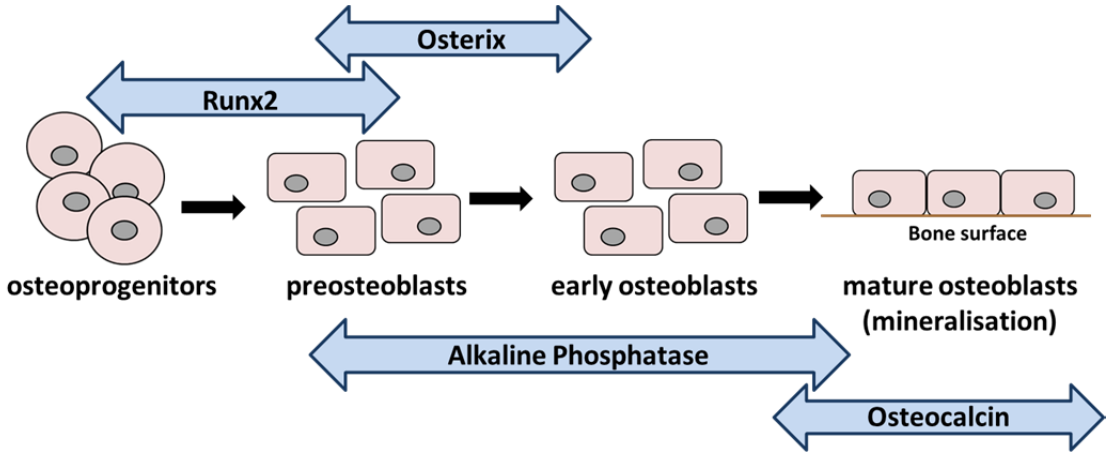

Figure 5-2. *Osteogenesis and markers of osteogenic differentiation.*

Bone morphogenetic proteins (BMPs), members of the transforming growth factor β (TGFβ) superfamily of paracrine factors, were originally named due to their ability to induce ectopic bone formation (Wozney et al., 1988). Members of the BMP family e.g. BMP-2, BMP-4 and BMP-7 are characterised by robust osteoinductive properties and have been shown to induce differentiation of osteoblast lineage cells (Asahina et al., 1996, Katagiri et al., 1990, Yamaguchi et al., 1996). BMPs bind to type I and type II serine/threonine kinase cell surface receptors and form heteromeric complexes composed of dimers of type I and type II receptors. Formation of heterotetracomplexes, where two type II kinase receptors transphosphorylate two type I receptors, activates type I receptor kinase which phosphorylates intracellular receptor substrates, SMADs. This group of intracellular mediators includes the BMP SMADs, namely SMAD1, SMAD5 and SMAD8 (Shi and Massague, 2003). Phosphorylated SMADs 1, 5 and 8 associate with the common mediator SMAD4, these complexes translocate to the nucleus, where they regulate transcription of target genes in cell-state specific manner via partnering with transcription factors, such as *Runx-2*, transcription activators and repressors (Ross and Hill, 2008).

Current methods for the osteoinduction of BMSCs also include cell culture in the presence of dexamethasone and calcitrol ($1,25(OH)_2D_3$ – the active form of vitamin D_3). Glucocorticoids such as dexamethasone are potent inducers of osteogenic differentiation of human and rat stromal cells, but have negligible effect on ALP activity of mouse osteoprogenitor cells (Lian et al., 1997, Bellows et al., 1998). Moreover, glucocorticoids have questionable clinical relevance as they are potent inducers of osteoporosis *in vivo* (Diefenderfer et al, 2003). $1,25(OH)_2D_3$ binds to the vitamin D receptor (VDR), which in turn heterodimerises with retinoid X receptor and binds to the vitamin D response element (VDRE) in the promoter region of genes that are under

vitamin D regulation (Kliewer et al., 1992). The transcriptional regulation of *Osteocalcin* gene expression in osteoblasts by 1,25$(OH)_2$ D_3 has been widely described, e.g. vitamin D induces *Osteocalcin* transcription by activating VDR receptor to bind to VDRE located in both rat and human gene promoters (Demay et al., 1990, Kerner et al., 1989). Interestingly, 1,25$(OH)_2$ D_3 does not induce mouse *Osteocalcin* expression due to the inability of VDR to bind and transactivate the mouse promoter (Clemens et al., 1997). Furthermore, 1,25$(OH)_2$ D_3 treatment of murine cells has been shown to abolish the binding of RUNX-2 to the critical cis-acting enhancer element present in the *Osteocalcin* gene promoter (Zhang et al., 1997).

The *Osteocalcin* gene is regulated by a number of growth factors, cytokines, and hormones, i.e. BMP-2 and BMP-4 (Yamaguchi et al., 1996), parathyroid hormone (Jiang et al., 2004) and FGF (Xiao et al., 2002) that have an inductive effect on *Osteocalcin* expression. Since *Osteocalcin* is an important marker of osteoblast development, BMP-2 was used in the current study for stimulating comprehensive osteogenic differentiation of murine BMSCs.

5.2. Objectives

To characterise the role of *Bag-1* in postnatal skeletal development, the objectives of the present study were:

a) Isolation of BMSCs from long bones of skeletally mature *Bag-1*$^{+/+}$ and *Bag-1*$^{+/-}$ mice, and establish monolayer cultures of BMSCs with and without BMP-2,
b) Analysis of the expression of BAG-1L and BAG-1S proteins in BMSC cultures of wild-type (*Bag-1*$^{+/+}$) and *Bag-1* heterozygous/haploinsufficient (*Bag-1*$^{+/-}$) mice,
c) Examination of the differences in cell number and proliferation between BMSC cultures *Bag-1*$^{+/+}$ and *Bag-1*$^{+/-}$ mice,
d) Assessment of the osteogenic potential of BMSCs of *Bag-1*$^{+/+}$ and *Bag-1*$^{+/-}$ mice,
e) Analysis of the cell apoptosis in BMSC cultures of wild-type and *Bag-1* heterozygous mice,
f) Examination of the differences in the expression of focused panel of genes related to skeletal development between BMSC cultures of *Bag-1*$^{+/+}$ and *Bag-1*$^{+/-}$ mice,
g) Analysis of the bone architecture of *Bag-1*$^{+/+}$ and *Bag-1*$^{+/-}$ mice (micro computed tomography, µCT).

5.3. Materials and methods

5.3.1. Bone marrow derived stromal cells (BMSCs) cultures

BMSCs were isolated and cultured for 28 days is basal and osteogenic media (refer to section 3.6). Cultures were harvested on day 1 and 14 for analysis of DNA concentration (refer to section 3.7.2) and day 28 for Western blot, gene expression analysis by qPCR (refer to section 3.9), osteocalcin concentration by ELISA (refer to section 3.8), tissue non-specific alkaline phosphatase specific activity (ALPL) (refer to section 3.7.1), DNA concentration (refer to section 3.7.2) and the staining of mineralisation by Alizarin red (refer to section 3.5.1) (Figure 5-3). Expression of *β-Actin*, *Runx-2*, *Alpl*, *Osterix* and *Osteocalcin* genes was analysed. Primer sequences for these genes can be found in Appendix 4. *β-Actin*, *Runx-2*, *Alpl*, *Osterix* and *Osteocalcin* primers were designed based on previously published primer sequences (Tare et al., 2008b).

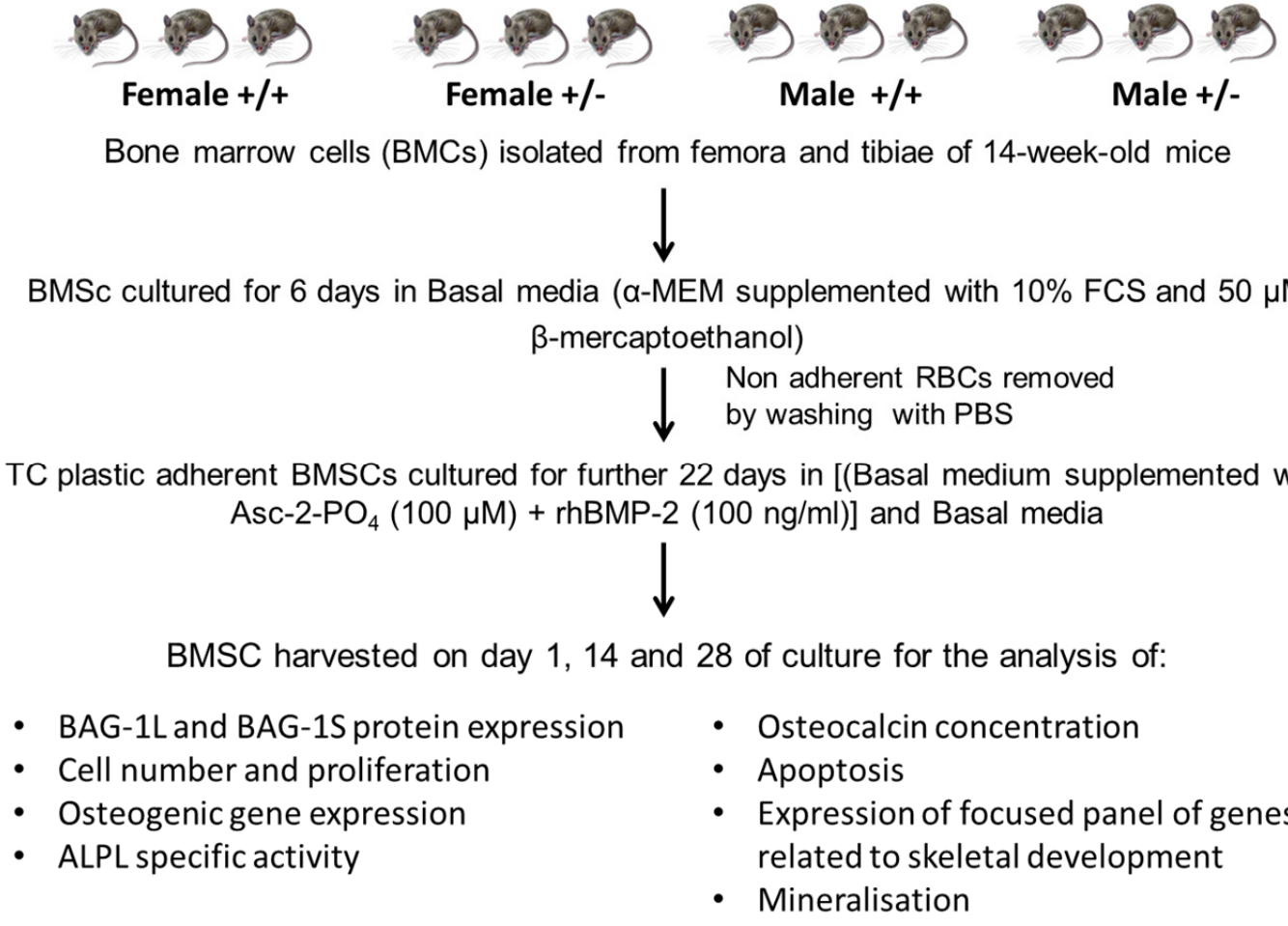

Figure 5-3. *Bone marrow stromal cells (BMSCs) experimental design.*

5.3.2. Detection of apoptosis

For detection of apoptosis, cultures of mouse BMSCs were used (4 groups: *Bag-1*$^{+/+}$ female, *Bag-1*$^{+/-}$ female, *Bag-1*$^{+/+}$ male, *Bag-1*$^{+/-}$ male). Terminal deoxynucleotidyl transferase-mediated dUTP nick-end labeling (TUNEL) staining was performed by using the Apoptosis Detection System (Fluorescein) from Promega, according to the manufacturer's instructions. In brief, cells cultured in 48 well plates were fixed in 4% paraformaldehyde for 25 minutes at 4°C. Following two washes in PBS for 5 minutes each, cells were permeabilized with 0.2% TritonX-100 and equilibrated at room temperature for 5 minutes with Equilibration buffer (see Appendix 2). Cultures were then labelled with rTdT incubation buffer (see Appendix 2) and incubated for 60 minutes at 37°C. Reaction was stopped by addition of 2x SSC (see Appendix 2). Cultures were then washed three times in PBS (5 minutes each). Nuclei were labelled with Propidium Iodide (2.5 µg/ml), positive controls for detection of DNA fragmentation were prepared by treating human BMSCs with DNase I (Promega). Images were taken on a fluorescence microscope with the use of AxioVision imaging software (Zeiss). For quantification, cells positive for TUNEL staining were counted in five different viewing areas and the percentage of apoptotic cells was calculated against all nucleated cells (staining positive for Propidium Iodide).

5.3.3. Western blot

For the detailed description of Western blot procedure used, refer to section 3.10.

Samples were isolated from mouse BMCs cultures by trypsinising cells cultured in 2 wells of a 6-well plate, centrifugation of cell suspensions for 5 minutes at 12000 rpm, double wash in PBS and incubation of the cell pellet in RIPA buffer (see Appendix 2) for 20 minutes at 4°C. After the incubation cell suspension was span down and supernatant collected.

For electrophoresis samples were loaded at concentrations of 12 µg protein in each well with loading volumes of 15 µl. Spectra Multicolor Broad Range Protein Ladder (10-260 kDa) (Thermo Scientific) was used at 15 µl volume per well. Electrophoresis was run at 150 V for one hour in 1x Running Buffer (see Appendix 2).

5.3.4. PCR Array

Mouse Osteogenesis PCR Array (RT^{2}Profiler PCR Array, Qiagen) was used according to the manufacturer's protocol to profile the expression of 84 genes related to osteogenic differentiation in BMSCs of *Bag-1*$^{+/+}$ and *Bag*$^{+/-}$ female mice. In brief, total

RNA was extracted from the BMSCs of *Bag-1*$^{+/+}$ and *Bag*$^{+/-}$ female mice cultured in osteogenic conditions on day 28 of culture using RLT Buffer (refer to section 3.9.1).

Quantification of extracted RNA was performed using NanoDrop® ND-1000 spectrophotometer (refer to section 3.9.2). Samples were then reverse transcribed into cDNA using RT^{2}PreAMP cDNA Synthesis Kit (Qiagen) according to manufacturer's protocol. Firstly, RNA samples were diluted using ultra-pure water to a volume of 8 µl containing 80 ng RNA, added to 2 µl of Buffer GE and incubated at 42°C for 5 minutes in order to eliminate genomic DNA. 10 µl of reverse transcription mix (5 µl 5x Buffer BC3, 1 µl Control P2, 1 µl cDNA Syntesis Enzyme Mix, 1 µl RNase Inhibitor, 1 µl RNase free water) were then added to 10 µl of each RNA sample, mixed gently and incubated at 42°C for 30 minutes. Reaction was then immediately stopped by incubation at 95°C for 5 minutes, these cDNA synthesis reaction were then kept on ice.

Preamplification mix was prepared (12.5 µl RT^{2}PreAMP PCR Mastermix and 7.5 µl RT^{2}PreAMP Pathway Primer Mix/sample) and added at the volume of 10 µl/sample to the 0.2 ml PCR tubes containing 5 µl of cDNA synthesis reaction. The content of the tubes was then gently mixed and briefly spun. Tubes were then placed in the real – time Veriti® Thermal Cycler (Applied Biosciences), for cycling conditions see Appendix 7. Following the cycling procedure, 2 µl of Side Reaction Reducer were added to each preamplification reaction. After gentle mix samples were incubated at 37°C for 15 minutes followed by heat inactivation at 95°C. 84 µl of nuclease-free water were then added immediately to each sample.

Real-time PCR was performed using the 7500 Real Time PCR detection system (Life Technologies, Applied Biosystems, UK). PCR components mixes were prepared for each sample (1350 µl RT^{2}SYBR Green Mastermix, 102 µl Preamplification reaction, 1248 µl RNase freen water) and dispensed into RT^{2}Profiler PCR Arrays at the volume of 25 µl/well. Conditions applied to the PCR runs were as follows: 50°C for 2 min, 95°C for 10 min, 45 cycles at 95^{o}C for 15 s and 60°C for 1 min. Samples were being used at the volume of 25 µl and consisted of 1 µl of cDNA, 2.5 µl of forward and 2.5 µl reverse primer (5 µM) and 50% of SYBRGreen Master Mix. Reactions were performed in duplicates, primer sequences were validated by melting curve analysis. Conditions applied to the PCR runs were as follows: 95^{o}C for 10 minutes and 40 cycles of 95^{o}C for 15 s and 60^{o}C for 1 min. PCR Arrays were run in triplicates, results were analysed using RT^{2}Profiler PCR Array Data Analysis version 3.5 (Qiagen). Assays of 5 housekeeping genes included in the array (i.e. *β-Actin, β-2-Microglobulin, Glyceraldehyde-3-phosphate dehydrogenase, β-Glucoronidase, α-Heat shock protein*

90) enabled normalisation of data.The significance of differences in gene expression was calculated with p-value set at 0.05 and fold–change at 2. Results were also presented as a volcano plot.

5.3.5. Micro computed tomography (µCT)

Quantitative 3-D analysis of mouse femurs was performed using a SkyScan 1176 scanning system for µCT (Bruker micro-CT, Kontich, Belgium). Samples (n = femora from 3 mice in each group) were placed in polystyrene foam tube which was mounted vertically in the scanner sample chamber and scanned at 18 µm resolution. Parameters of the scan were as follows: X ray voltage: 50 kV, X-ray current: 500 µA, filter: 0.5 mm aluminium, Image pixel size: 18 µm, Rotation step: 0.2º. Using phantoms of known density (Skyscan, Kontich, Belgium), all the voxels that formed the structure were automatically assigned BMD in g/cm3. µCT scans were reconstructed using NRecon software interface (v.1.6.4.6, Bruker micro-CT, Kontich, Belgium).
CT Analyser v.1.13.2.1+ (CTAn, Bruker micro-CT, Kontich, Belgium) was used for quantification of a set of variables describing trabecular and cortical bone. The regions of interest (ROI) were selected based on a growth plate reference slide selected by moving slice-by-slice from the epiphysis through the growth plate and selecting the crossectional level at which bony primary spongiosa crosses the low density cartilage. Trabecular and cortical regions were defined as positions along the long axis of the femur relative to the growth plate reference. Separation of the trabecular from cortical bone was performed freehand. Morphometric parameters were calculated for the ROIs selected for the trabecular and cortical bone respectively and single grey threshold values were applied to these ROIs.

5.3.6. Statistical analysis

Statistical analysis was performed using GraphPad Prism software (GraphPad Software Inc., San Diego, CA, USA). Results were expressed as mean ± SD. For Western Blot and µCT, differences in band density between variables were analysed using unpaired t-test (two-tailed P value) according to experimental design and were considered to be significantly different if $P \leq 0.05$.

Results of gene expression levels in male and female samples were analysed separately. Differences in relative gene expression between groups were analysed using one way analysis of variance (ANOVA) with a post-Tukey test according to experimental design and were considered to be significantly different if $P \leq 0.05$.

5.4. Results

5.4.1. Expression of BAG-1L and BAG-1S proteins in bone marrow stromal cell (BMSC) cultures of wild-type (*Bag-1*$^{+/+}$) and *Bag-1* heterozygous/haploinsufficient (*Bag-1*$^{+/-}$) mice

Protein lysates of cells of day-28 cultures in basal medium were immunoblotted for analysis of expression of BAG-1. Representative immunoblots probed with the anti-BAG-1 antibody (C16) exhibited bands specific for BAG-1L (50 kDa) and BAG-1S (32 kDa) proteins (Fig. 5-4A). Densitometric quantification of the bands was performed using the Quantity One® 1-D software to measure the expression levels of the BAG-1L and BAG-1S proteins. Data was normalised to β-Actin (loading control) and plotted in the form of bar graphs, which demonstrated lower average levels of BAG-1L and BAG-1S proteins in *Bag-1*$^{+/-}$ mice, compared to the average levels of BAG-1L and S proteins in the *Bag-1*$^{+/+}$ mice (Fig. 5-4B). BAG-1S was expressed as a predominant BAG-1 isoform in mouse BMSCs of *Bag-1*$^{+/+}$ and *Bag-1*$^{+/-}$ male and female mice.

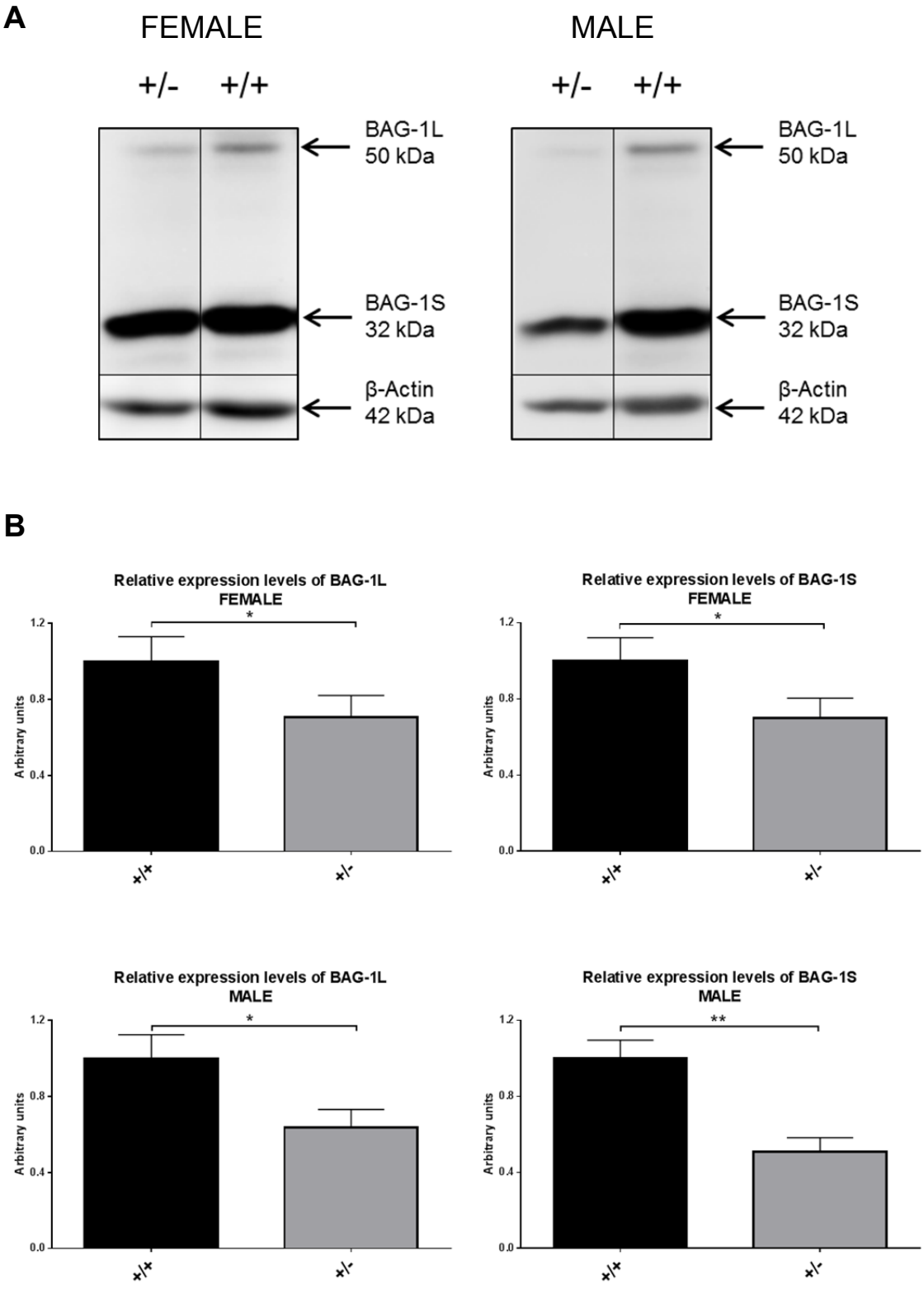

Figure 5-4. *Immunoblot demonstrating expression of BAG-1L and BAG-1S proteins in day-28 cultures (in basal medium) of BMSCs of 14-week-old Bag-1$^{+/+}$ and Bag-1$^{+/-}$ female and male mice (A). Densitometric quantification of the bands was performed to measure the expression of the BAG-1L and BAG-1S proteins, data was normalised to β-Actin (loading control) and plotted in the form of bar graphs (B). Results expressed as mean ± SD, n = cells from 3 mice per group, **P<0.01, *P<0.05*

5.4.2. Examination of the differences in cell number between bone marrow stromal cell (BMSC) cultures of wild-type (*Bag-1*$^{+/+}$) and *Bag-1* heterozygous/haploinsufficient (*Bag-1*$^{+/-}$) mice

Given the direct correlation between cell number and deoxyribonucleic acid (DNA) content, cell numbers in day 28 cultures of BMSCs in basal and osteogenic media were determined by measuring the cellular DNA content using the PicoGreen assay.

In wild-type female mice, no differences in DNA concentration (and therefore cell number) were observed between day 28 BMSC cultures in basal and osteogenic media (Fig. 5-5A). In contrast, in BMSC cultures of *Bag-1* heterozygous female mice, DNA levels and therefore cell concentration of day 28 cultures in osteogenic medium were significantly higher ($P<0.001$) than DNA levels/cell concentration of day 28 cultures in basal medium (Fig. 5-5A). In both *Bag-1*$^{+/+}$ and *Bag-1*$^{+/-}$ male mice, cell numbers, reflected by the DNA concentration of day 28 BMSC cultures, were significantly lower ($P<0.001$) in osteogenic conditions compared to basal conditions (Fig. 5-5B). Moreover, in male mice, DNA levels of day 28 cultures of BMSCs of *Bag-1* heterozygous mice in basal (155.66 ng/ml ± 5.85) and osteogenic (51.76 ng/ml ± 7.21) media were approximately half the DNA content of day 28 cultures of BMSCs of wild-type mice in basal (333.05 ng/ml ± 4.53) and osteogenic (125.49 ng/ml ± 16.31) media, respectively (Fig. 5-5B).

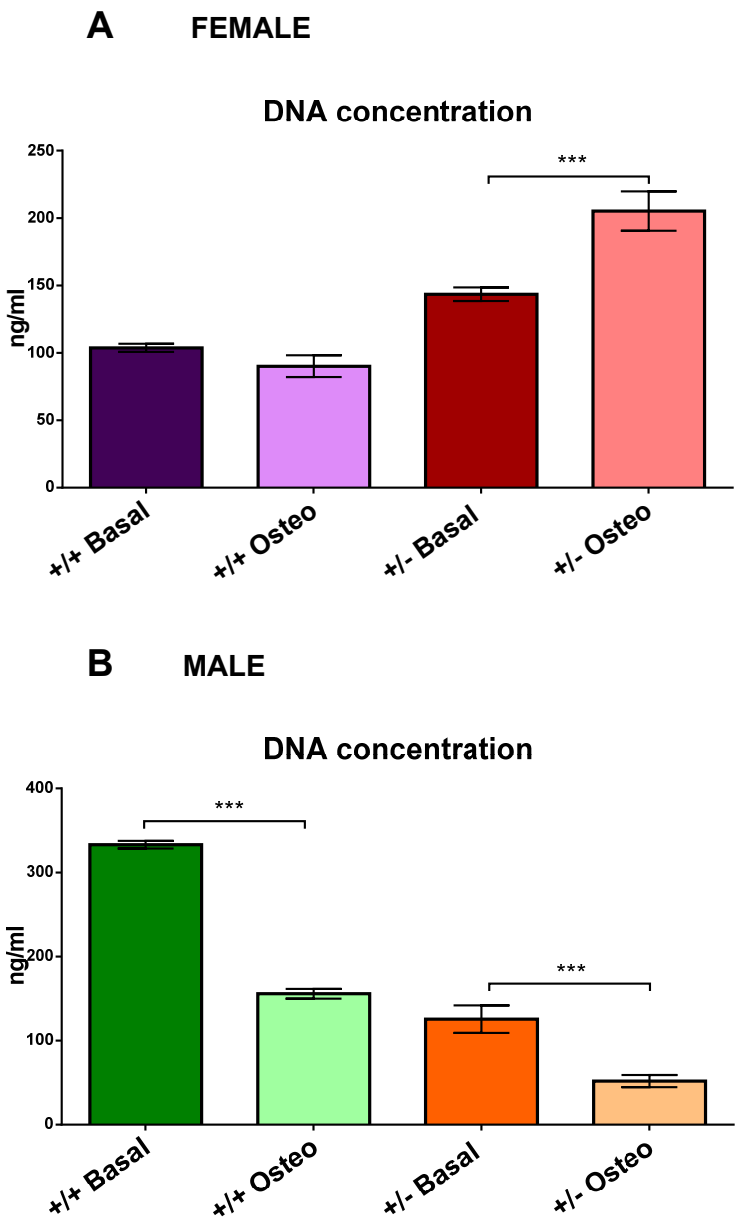

Figure 5-5. *DNA content (ng/ml) of day 28 cultures of BMSCs of 14-week-old female (A) and male (B) Bag-1$^{+/+}$ and Bag-1$^{+/-}$ mice. BMSCs were cultured for 28 days in either basal or osteogenic (osteo) media and the DNA content of cells was measured using the PicoGreen assay. Results expressed as mean ± SD, n = cells from 3 mice per group, *** P<0.001.*

5.4.3. Examination of the differences in cell proliferation between bone marrow stromal cell (BMSC) cultures of wild-type (*Bag-1*$^{+/+}$) and *Bag-1* heterozygous/haploinsufficient (*Bag-1*$^{+/-}$) mice

In order to determine the rate of cell proliferation over the 28-day culture period in osteogenic medium, cells were harvested at days 1, 14 and 28 of culture for measurement of DNA content using the PicoGreen assay.

In osteogenic cultures, BMSCs of wild-type female mice proliferated at a significantly slower rate ($P<0.001$) over the 28-day culture period in comparison to BMSCs of *Bag-1*$^{+/-}$ female mice that exhibited a rapid rate of proliferation over 28 days (Fig. 5-6A). BMSCs of *Bag-1* wild type male mice cultured under osteogenic conditions proliferated at a significantly higher rate ($P<0.001$) than their heterozygous counterparts between days 1 and 14 of culture, while proliferation of BMSCs in the two groups of male mice decreased significantly ($P<0.001$) between days 14 and 28 of culture (Fig. 5-6B). BMSCs of wild type male mice proliferated at a higher rate than the BMSCs of wild type female mice between days 1 and 14 of culture (Fig. 5-6A, 5-6B).

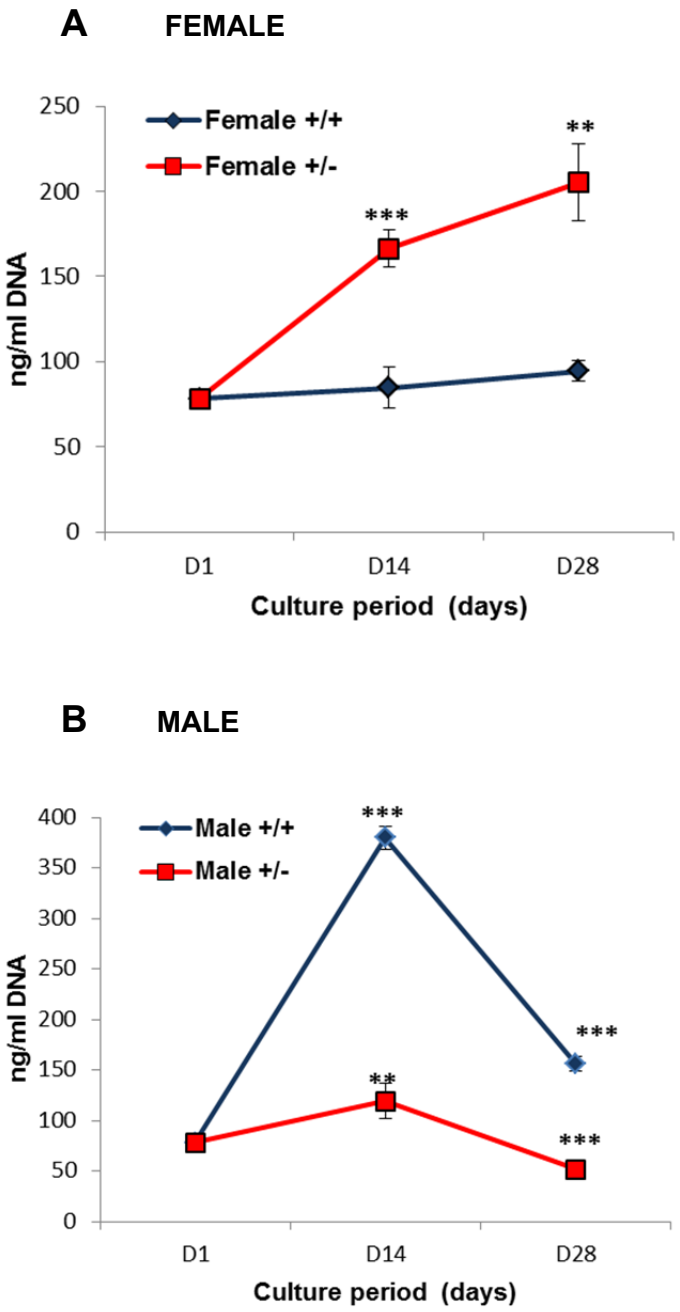

Figure 5-6. *Cell proliferation profiles over the course of 28-day cultures of BMSCs of female (A) and male (B) Bag-1$^{+/+}$ and Bag-1$^{+/-}$ mice. DNA content of cells harvested on days 1, 14 and 28 of culture in osteogenic medium was measured using the PicoGreen assay. For statistical analyses, results were compared between days 1 and 14 of culture, and days 14 and 28 of culture. Results expressed as mean ± SD, *** P<0.001, ** P<0.01; n = cells from 3 mice per group.*

5.4.4. Assessment of osteogenic potential of BMSCs of wild-type and *Bag-1* heterozygous mice

5.4.4.1. Analysis of osteogenic gene expression in BMSC cultures of wild-type and *Bag-1* heterozygous mice

To examine the effect of haploinsufficiency of *Bag-1* on the ability of BMSCs to differentiate in response to BMP-2, 28-day cultures of *Bag-1*$^{+/+}$ and *Bag-1*$^{+/-}$ BMSCs were analysed for expression of the early osteogenic gene *Runx-2* and *Osterix/Osx*.

In female wild-type and *Bag-1* heterozygous mice, no statistically significant differences in *Runx-2* expression were observed between day 28 cultures of BMSCs in basal and osteogenic media (Fig. 5-7A). In female wild type mice, compared to day 28 cultures of BMSCs in basal media, expression of *Osx* by BMSCs was significantly increased ($P<0.001$) following the 28-day culture period in osteogenic media (Fig. 5-7B). While a similar trend was observed for female *Bag-1* heterozygous mice, the increase in *Osx* expression by BMSCs in osteogenic media was not statistically significant compared to expression levels in basal cultures (Fig. 5-7B). Under osteogenic conditions, expression of the early osteoblast gene *Osx* was significantly higher ($P<0.001$) in day 28 cultures of BMSCs of wild type female mice in comparison to day 28 BMSC cultures of *Bag-1* haploinsufficient female mice as indicated by red line and red asterix (Fig. 5-7B).

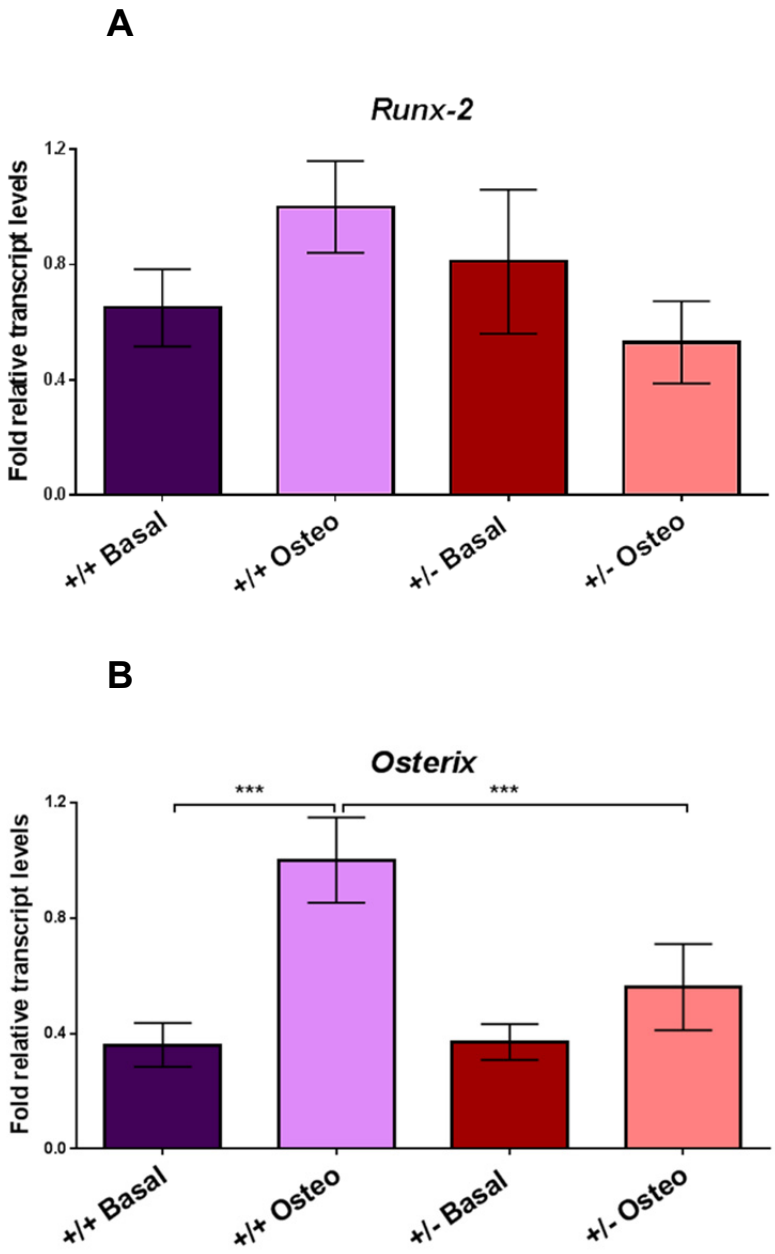

Figure 5-7. *Analysis of Runx-2 (A) and Osterix (B) expression in day 28 cultures of BMSCs by Real-time qPCR. BMSCs were isolated from femora and tibiae of 14-week-old female Bag-1$^{+/+}$ and Bag-1$^{+/-}$ mice and, cultured for 28 days in medium without (basal) and with 100 ng/ml rhBMP-2 (osteogenic). Bar graphs illustrate fold changes in relative mRNA transcript levels normalised to the endogenous reference (β-Actin) and compared to a calibrator (i.e. group exhibiting the highest expression), given by the equation, $2^{-\Delta\Delta C}{}_T$. The range of gene expression is indicated by $2^{-(\Delta\Delta C}{}_T{}^{+ SD)}$ and $2^{-(\Delta\Delta C}{}_T{}^{- SD)}$, where SD is the standard deviation of the $\Delta\Delta C_T/\Delta C_T$ value. Statistical analysis is performed at the level of ΔC_T, in order to exclude potential bias due to averaging of the data transformed through the $2^{-\Delta\Delta C}{}_T$ equation. *** P<0.001; n = cells from 3 mice per group.*

In male wild-type and *Bag-1* heterozygous mice, no statistically significant changes in *Runx-2* expression were observed between day 28 cultures of BMSCs in basal and osteogenic media (Fig. 5-8A). Both male *Bag-1* heterozygous and wild-type BMSC 28-day cultures were characterised by significantly higher levels ($P<0.001$) of *Osx* in osteogenic media compared to basal media (Fig. 5-8B). Unlike female mice, no statistically significant differences were observed between day 28 osteogenic cultures of BMSCs of male *Bag-1* heterozygous and wild-type mice (Fig. 5-8B).

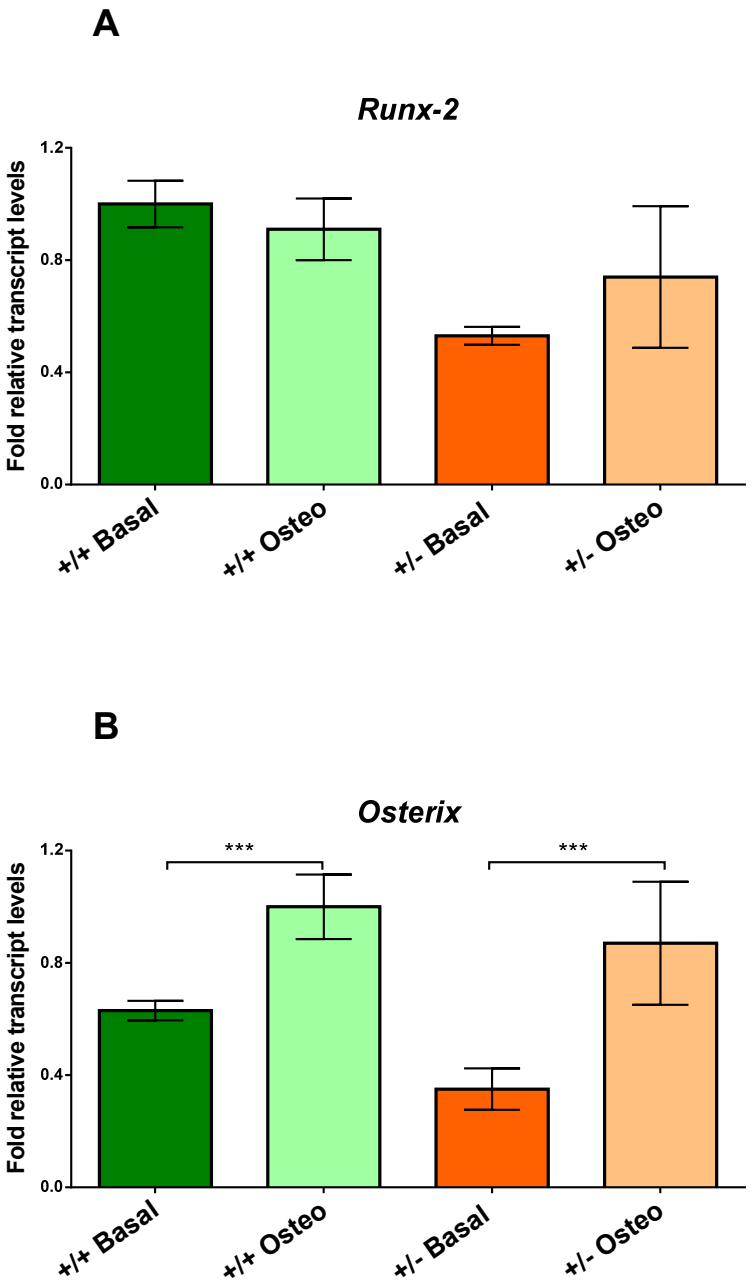

***Figure 5-8**. Analysis of Runx-2 (A) and Osterix (B) expression in day 28 cultures of BMSCs by Real-time qPCR. BMSCs were isolated from femora and tibiae of 14-week-old male Bag-1$^{+/+}$ and Bag-1$^{+/-}$ mice and, cultured for 28 days in medium without (basal) and with 100 ng/ml rhBMP-2 (osteogenic). Bar graphs illustrate fold changes in relative mRNA transcript levels normalised to the endogenous reference (β-Actin) and compared to a calibrator (i.e. group exhibiting the highest expression), given by the equation, $2^{-\Delta\Delta C}{}_T$. The range of gene expression is indicated by $2^{-(\Delta\Delta C}{}_T{}^{+ SD)}$ and $2^{-(\Delta\Delta C}{}_T{}^{- SD)}$, where SD is the standard deviation of the $\Delta\Delta C_T/\Delta C_T$ value. Statistical analysis is performed at the level of ΔC_T, in order to exclude potential bias due to averaging of the data transformed through the $2^{-\Delta\Delta C}{}_T$ equation. *** P<0.001; n = cells from 3 mice per group.*

5.4.4.2. Estimation of alkaline phosphatase (ALPL) enzyme activity and osteocalcin (OCN) concentration in BMSC cultures of wild-type and *Bag-1* heterozygous mice

Specific activity of the ALPL enzyme and concentration of OCN were determined in day 28 BMSC cultures of wild-type and Bag-1 heterozygous mice by spectrophotometric enzymatic assay and ELISA respectively.

In wild-type female mice, the specific activity of ALPL and the concentration of OCN were significantly higher ($P<0.001$) in day 28 BMSC cultures in osteogenic media compared to basal media (Fig. 5-9A, 5-9B). In contrast, in *Bag-1* heterozygous female mice, no significant differences in ALPL enzyme activity and OCN content were observed between day 28 BMSC cultures in basal and osteogenic media (Fig. 5-9A, 5-9B). In osteogenic culture conditions, ALPL specific activity and the concentration of OCN in day 28 cultures of BMSCs of wild-type female mice were significantly higher ($P<0.001$) compared to day 28 cultures of BMSCs of heterozygous female mice as indicated by red line and red asterix (Fig. 5-9A, 5-9B).

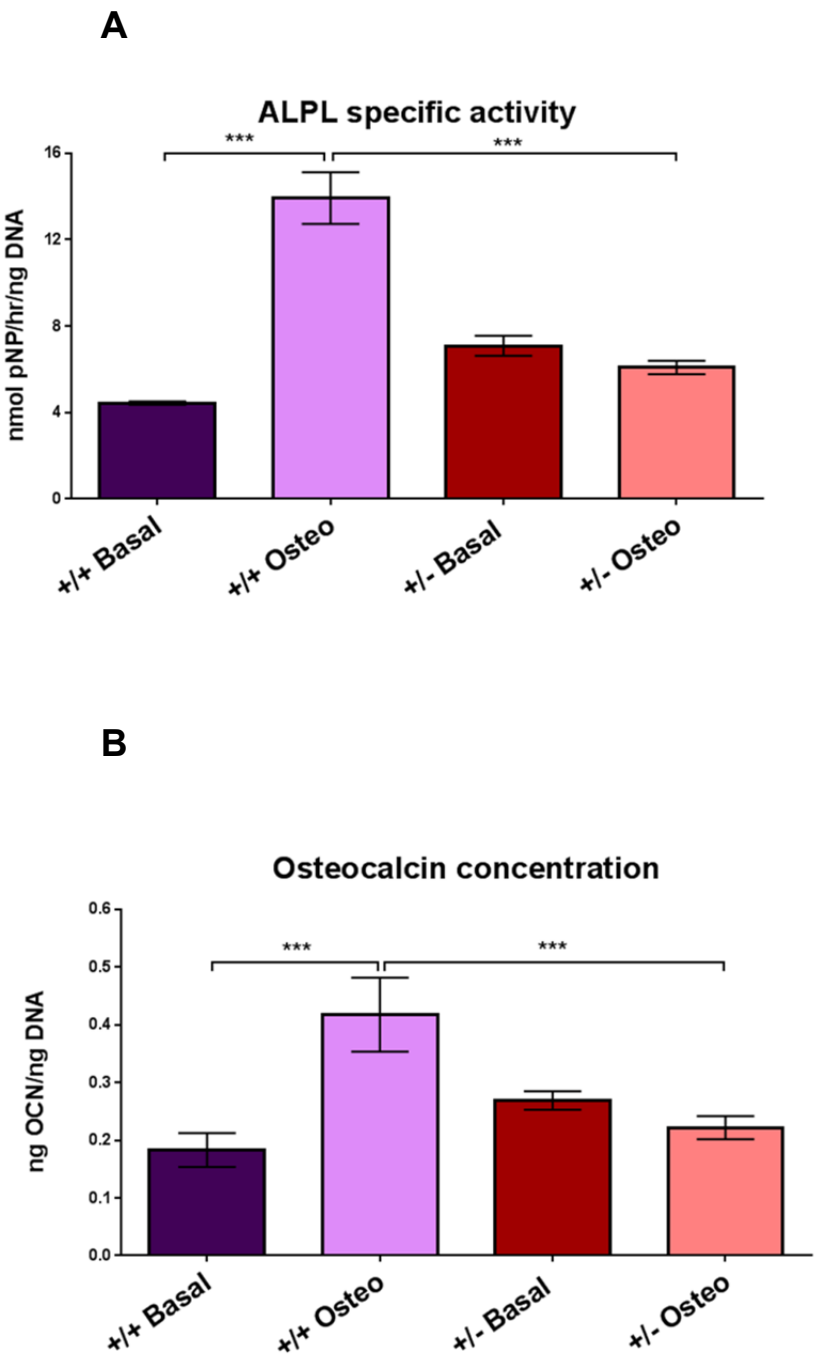

Figure 5-9. *Intracellular ALPL enzyme activity (A) and concentration of OCN (B) measured in day 28 BMSC cultures of female wild-type (+/+) and Bag-1 heterozygous (+/-) mice. BMSCs were cultured in basal and osteogenic (osteo) conditions i.e. media without and supplemented with 100 ng/ml BMP-2 respectively. Enzyme activity was normalised to DNA content of the cells and specific ALP activity was calculated as nanomole of pNP (p-nitrophenol) released per hour per nanogram of DNA. Concentration of OCN was normalised to DNA content of the culture and expressed as nanogram per nanogram of DNA. Results for ALPL specific activity and OCN concentration were expressed as mean ± SD for plotting as bar graphs, n = cells from 3 mice per group, *** P<0.001.*

In day 28 cultures of BMSCs of both wild-type and *Bag-1* heterozygous male mice, ALPL specific activity and OCN concentration were significantly higher ($P<0.001$) in osteogenic conditions compared to basal conditions (Fig. 5-10A, 5-10B). In contrast to female mice, specific activity of ALPL in day 28 osteogenic cultures of BMSCs of wild-type male mice was significantly lower ($P<0.001$) than enzyme activity in day 28 osteogenic cultures of BMSCs of *Bag-1* heterozygous male mice (Fig. 5-10A). Levels of OCN, elevated in response to BMP-2, were comparable between day 28 osteogenic cultures of BMSCs of wild-type and *Bag-1* heterozygous male mice (Fig. 5-10B).

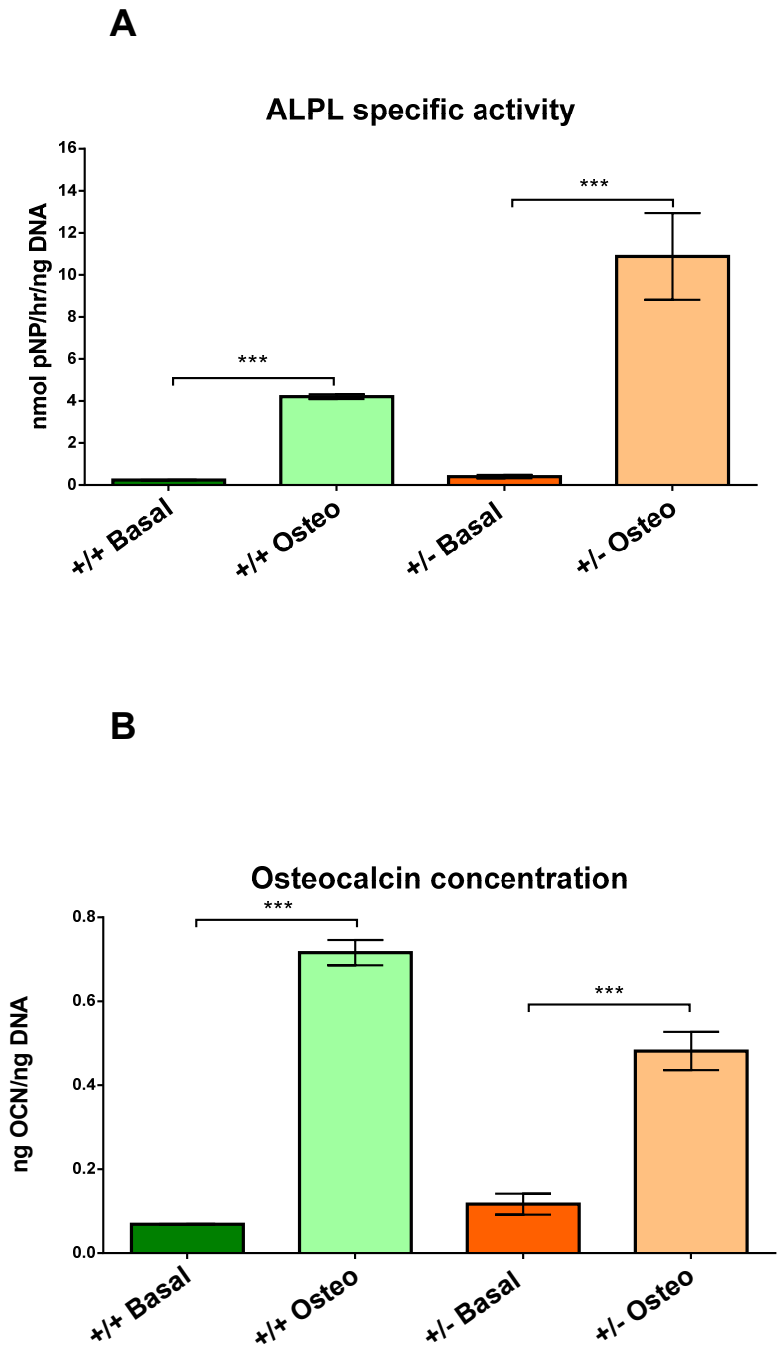

Figure 5-10. *Intracellular ALPL enzyme activity (A) and concentration of OCN (B) measured in day 28 BMSC cultures of male wild-type (+/+) and Bag-1 heterozygous (+/-) mice. BMSCs were cultured in basal and osteogenic (osteo) conditions i.e. media without and supplemented with 100 ng/ml BMP-2 respectively. Enzyme activity was normalised to DNA content of the cells and specific ALP activity was calculated as nanomole of pNP (p-nitrophenol) released per hour per nanogram of DNA. Concentration of OCN was normalised to DNA content of the culture and expressed as nanogram per nanogram of DNA. Results for ALPL specific activity and OCN concentration were expressed as mean ± SD for plotting as bar graphs, n = cells from 3 mice per group, *** P<0.001.*

5.4.5. Analysis of cell apoptosis in BMSC cultures of wild-type and *Bag-1* heterozygous mice

Day 28 cultures of BMSCs of wild-type and *Bag-1* heterozygous mice (both male and female) in basal and osteogenic media were fixed in 4% paraformaldehyde, permeabilised using 0.2% Triton X-100 and the apoptotic cells were detected by TUNEL staining. Additionally, cell nuclei were labelled with Propidium Iodide (PI) to determine the total number of cells in the cultures.

Overall, a very low incidence of apoptosis was observed in the BMSC cultures. To quantify the results of TUNEL staining, PI-stained nucleated cells and TUNEL-positive apoptotic cells were counted in five different fields (2 representative fields shown Fig. 5-11A) and the number of apoptotic cells was determined as a percentage of the total cell number. In both basal and osteogenic cultures of BMSCs, no differences in cell apoptosis were observed between the wild-type and *Bag-1* heterozygous female (Fig. 5-11B) and male (Fig. 5-11C) mice.

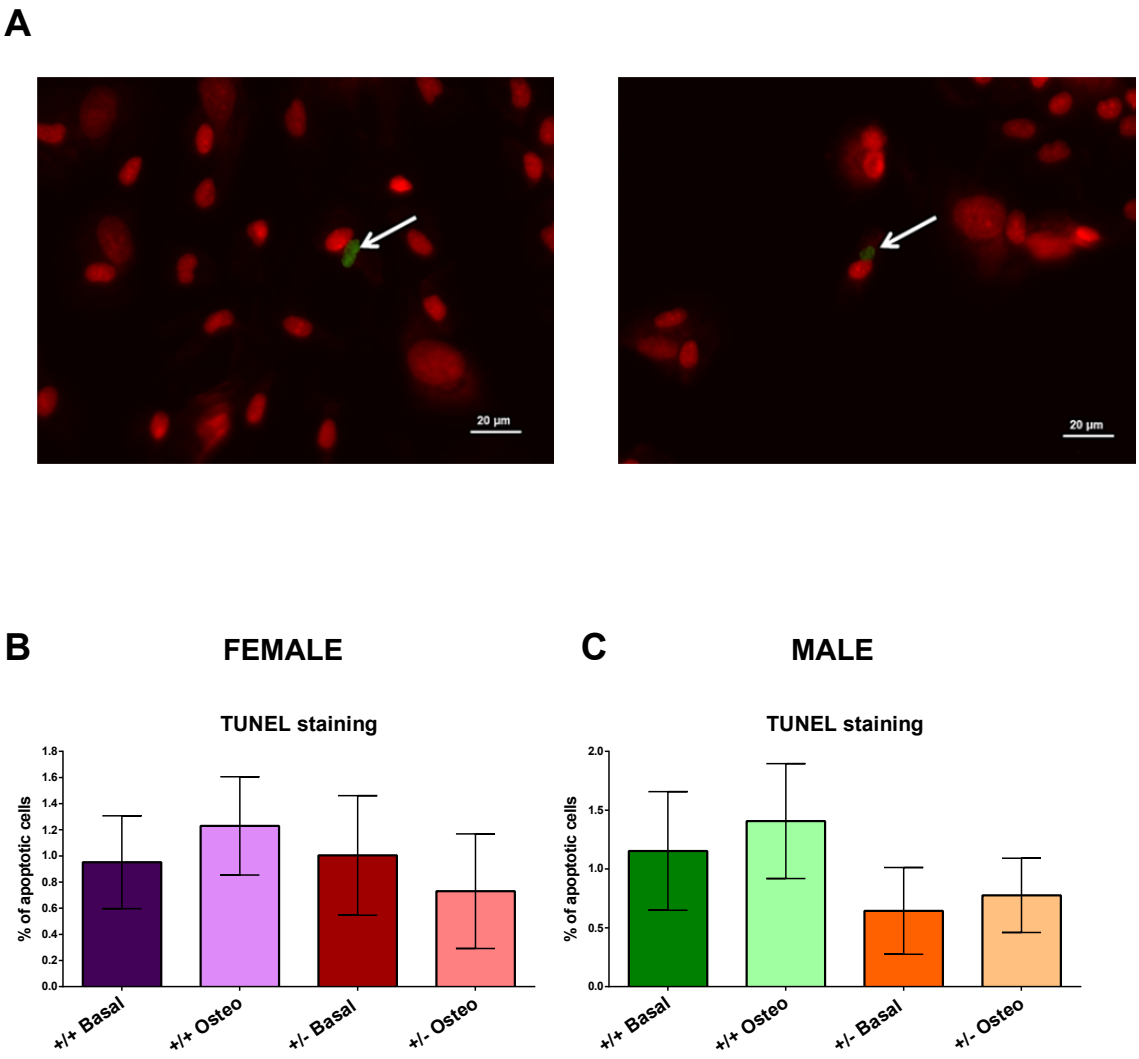

Figure 5-11. *Representative images of day 28 cultures of BMSCs showing PI-stained cell nuclei and TUNEL-positive apoptotic cells indicated by arrows (A). Bar graphs show percentage of TUNEL-positive apoptotic cells in day 28 basal and osteogenic (osteo) cultures of BMSCs isolated from female (B) and male (C) Bag-1$^{+/+}$ and Bag-1$^{+/-}$ mice. Results, expressed as mean ± SD, were determined to be statistically non-significant between groups, n = cells from 3 mice per group, cells TUNEL positive counted in five different viewing areas.*

5.4.6. Examination of differences in the expression of focused panel of genes related to skeletal development between BMSC cultures of *Bag-1*$^{+/+}$ and *Bag-1*$^{+/-}$ mice

The mouse osteogenesis RT² Profiler™ PCR arrays were utilised to analyse differences in the expression of 84 genes (see Appendix 8) crucial for skeletal development between BMSCs of 14-week-old *Bag-1*$^{+/+}$ and *Bag-1*$^{+/-}$ female mice, following culture for 28 days in osteogenic medium (α-MEM supplemented with 10% FCS, 50 μM β-mercaptoethanol, 100 ng/ml rhBMP-2, 100 μM ascorbate-2-phosphate). Out of the 84 genes, 30 genes were differentially expressed between day-28 BMSC cultures of *Bag-1*$^{+/+}$ and *Bag-1*$^{+/-}$ female mice in response to the osteogenic stimuli, primarily BMP-2. The list of genes, which were upregulated and downregulated in day-28 osteogenic cultures of *Bag-1*$^{+/-}$ BMSCs compared to day-28 osteogenic cultures of *Bag-1*$^{+/+}$ BMSCs, along with values of fold regulation and p-values were tabulated (Table 1).

The volcano plot, constructed by plotting the negative log of the p-value on the y-axis and log of the fold change between the two conditions on the x-axis, enabled rapid visual identification of the differentially expressed 30 genes, which were either significantly upregulated (red circles) or downregulated (green circles) in day-28 osteogenic cultures of *Bag-1*$^{+/-}$ BMSCs compared to day-28 osteogenic cultures of *Bag-1*$^{+/+}$ BMSCs (Fig. 5-12).

Genes upregulated in F+/- vs F+/+		
Gene Symbol	Fold Regulation	p-value
Ahsg	11.7483	0.005014
Col14a1	4.4248	0.000427
Col4a1	2.6928	0.000057
Fgf2	3.7754	0.000282
Fn1	2.0112	0.000306
Gdf10	2.1227	0.000829
Mmp8	3.6264	0.000622
Tnfsf11	3.8004	0.000042
Vcam1	2.4633	0.015619

Genes downregulated in F+/- vs F+/+		
Gene Symbol	Fold Regulation	p-value
Alpl	-2.0739	0.003856
Bglap	-14.2169	0.000236
Bmp2	-2.9503	0.000007
Bmp3	-658.5576	0.000016
Bmp4	-3.9187	0.000009
Bmp7	-3.6754	0.000372
Col1a1	-6.9066	0.000088
Col1a2	-5.1735	0.0001
Col5a1	-2.4909	0.000269
Comp	-3.1683	0.000034
Ctsk	-2.4984	0.000031
Fgf1	-4.0543	0.000088
Mmp10	-2.2709	0.000847
Mmp2	-2.0047	0.000014
Pdgfa	-2.5567	0.000011
Phex	-511.9712	0.000002
Serpinh1	-3.5068	0.000003
Sost	-7.3678	0.000031
Sp7	-2.2845	0.000037
Spp1	-2.0299	0.000112
Vegfa	-2.6407	0.000091

Table 1. *Differential expression of genes related to osteoblast development between BMSC cultures of Bag-1$^{+/+}$ and Bag-1$^{+/-}$ mice in osteogenic conditions: list of genes from the mouse osteogenesis PCR array (n = 3 arrays) that are upregulated (red) and downregulated (green) in day-28 osteogenic cultures of BMSCs of female Bag-1$^{+/-}$ mice compared to day-28 osteogenic cultures of BMSCs of female Bag-1$^{+/+}$ mice.*

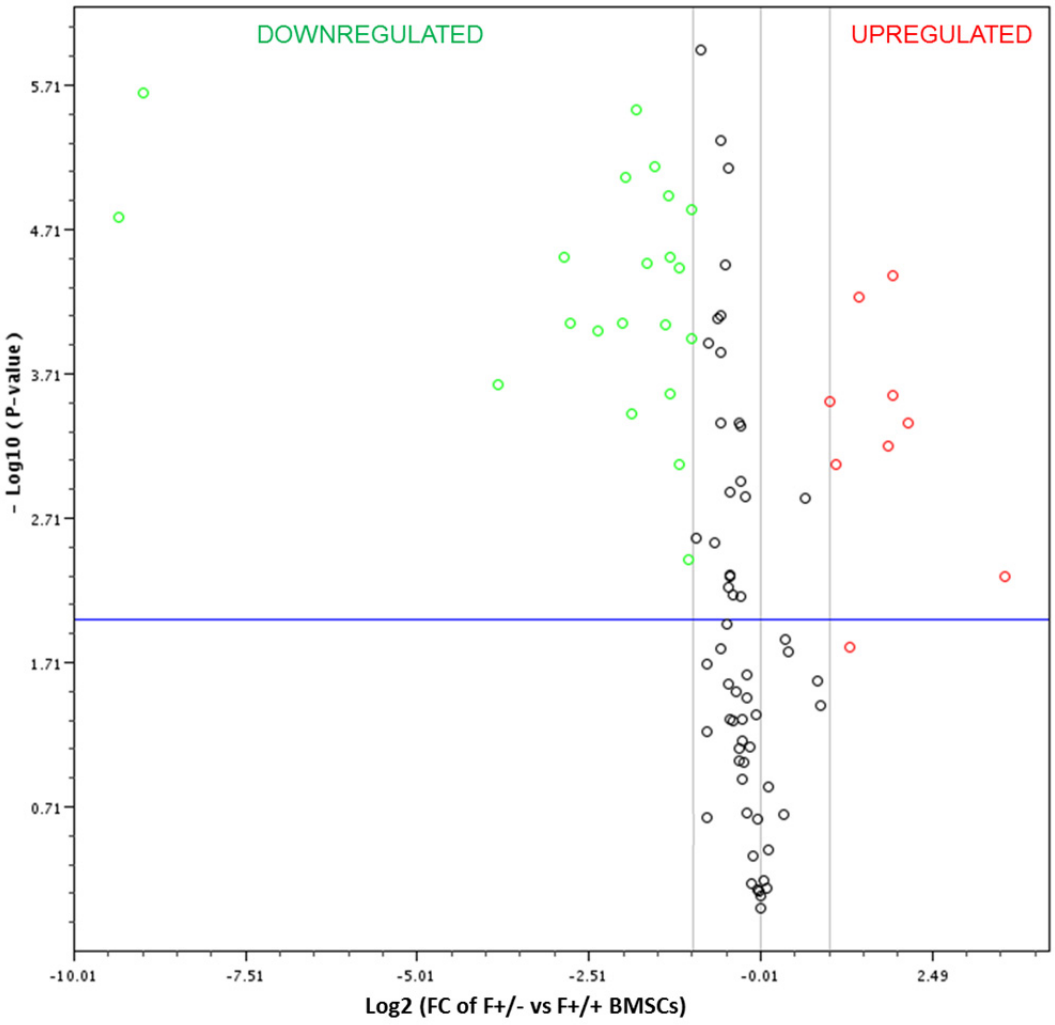

Figure 5-12. *Differential expression of genes related to osteoblast development between BMSC cultures of Bag-1$^{+/+}$ and Bag-1$^{+/-}$ mice in osteogenic conditions: Volcano plot illustrating 30 genes that were differentially expressed between day-28 osteogenic cultures of BMSCs of Bag-1$^{+/+}$ and Bag-1$^{+/-}$ female mice, and changes in expression of which were statistically significant. For the full list of upregulated and downregulated genes refer to Table 1.*

The expression of 9 genes, namely *Ahsg* (fetuin), *Col14a1* (type 14 collagen, undulin), *Col4a1* (type IV collagen), *Fgf-2* (fibroblast growth factor-2), *Fn-1* (fibronectin-1), *Gdf-10* (growth differentiation factor-10, BMP-3B), *Mmp-8* (matrix metalloproteinase-8), *Tnfsf-11* (tumor necrosis factor (ligand) superfamily, member 11, RANKL), *Vcam-1* (vascular cell adhesion molecule 1, CD106), with important roles in mineralisation, collagen fibril organisation, osteogenic differentiation, cell adhesion, remodelling of extracellular matrix molecules during skeletal development and osteoclastogenesis, were significantly upregulated ($P<0.05$) in day-28 osteogenic cultures of *Bag-1*$^{+/-}$ BMSCs compared to day-28 osteogenic cultures of *Bag-1*$^{+/+}$ BMSCs.

Additionally, the expression of 21 genes was significantly downregulated ($P<0.05$) in day-28 osteogenic cultures of *Bag-1*$^{+/-}$ BMSCs, in comparison to day-28 osteogenic cultures of *Bag-1*$^{+/+}$ BMSCs. Genes whose expression levels were downregulated included *Bmp-2*, *Bmp-4*, *Bmp-7*, *Sp7* (osterix), *Pdgfa* and *Vegfa*, with important roles in osteogenic differentiation; *Col1a1* (type I collagen), *Col1a2* (type I collagen, alpha 2), *Col5a1* (type V collagen), *Serpinh-1*, important for collagen biosynthesis and whose products are vital constituents of the extracellular matrix, and, *Spp1* (osteopontin), *Alpl* (tissue non-specific alkaline phosphatase/ALPL), *Sost* (sclerostin), *Bglap* (osteocalcin), *Phex*, which have regulatory roles in bone matrix mineralisation and the maintenance of the mature osteogenic phenotype (Fig. 5-13).

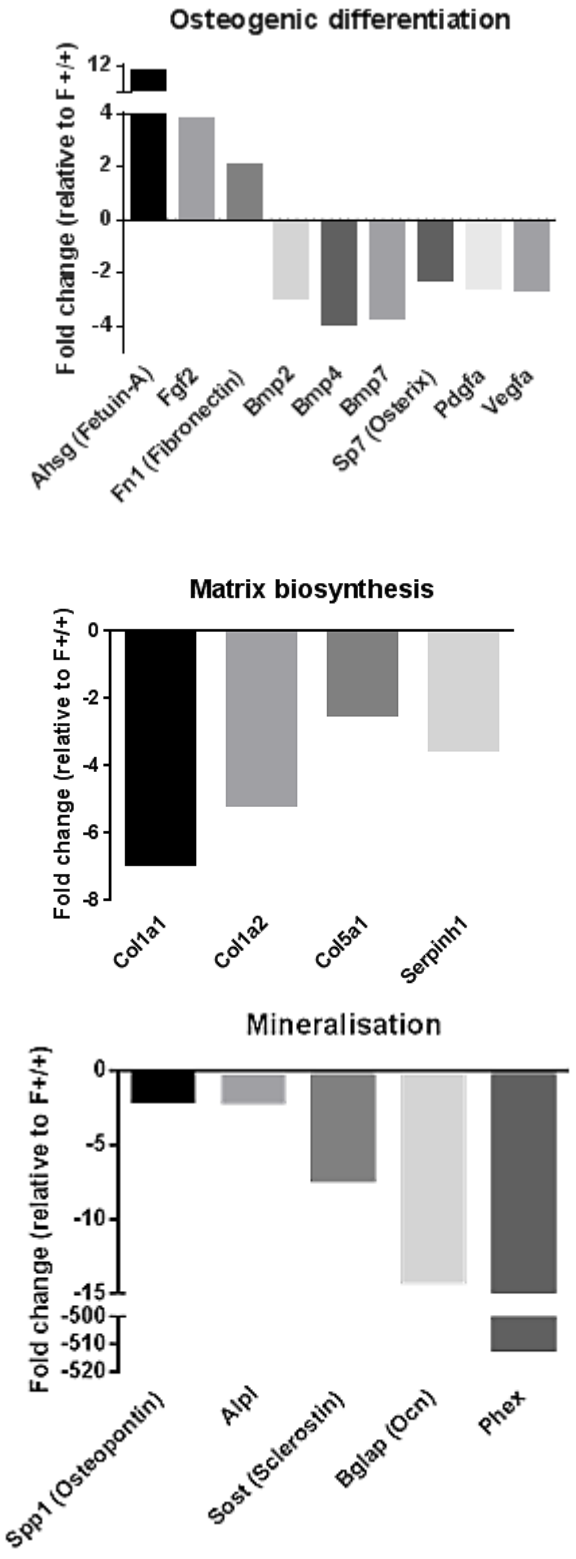

***Figure 5-13**. Differential expression of genes related to osteoblast development between BMSC cultures of Bag-1$^{+/+}$ and Bag-1$^{+/-}$ mice in osteogenic conditions: Bar graphs showing significant downregulation of genes related to osteoblast differentiation, bone matrix synthesis and mineralisation in day-28 osteogenic cultures of BMSCs of female Bag-1$^{+/-}$ mice compared to day-28 osteogenic cultures of BMSCs of Bag-1$^{+/+}$ mice.*

5.4.7. Assessment of mineralised bone nodule formation in osteogenic cultures of BMSCs of *Bag-1*$^{+/+}$ and *Bag-1*$^{+/-}$ female mice

BMSCs of *Bag-1* heterozygous and wild type female mice were cultured for 28 days in basal medium (α-MEM supplemented with 10% FCS and 50μM β-mercaptoethanol), and osteogenic medium (basal medium supplemented with 100ng/ml rhBMP-2, 100μM ascorbate-2-phosphate). Both *Bag-1*$^{+/+}$ and *Bag-1*$^{+/-}$ female BMSCs in osteogenic medium exhibited qualitatively stronger Alizarin red staining compared to cultures in basal medium, where staining was negligible (Fig. 5-14). The number of mineralised nodules in day-28 cultures of *Bag-1*$^{+/+}$ BMSCs in osteogenic media was higher than corresponding day-28 cultures of *Bag-1*$^{+/-}$ BMSCs.

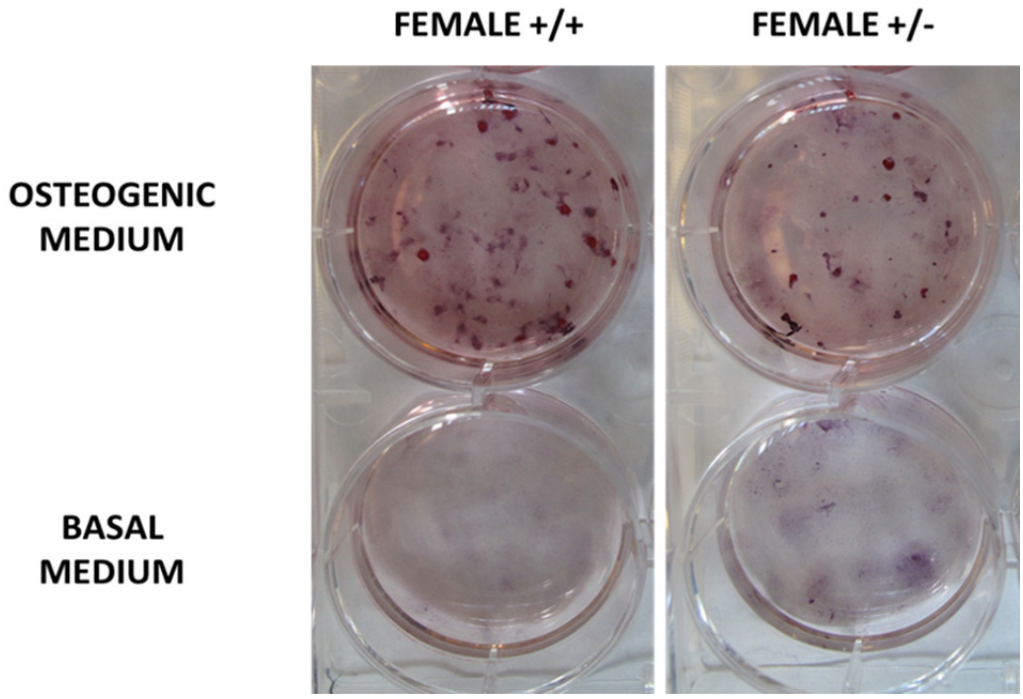

Figure 5-14. *Alizarin red staining of day 28 Bag-1*$^{+/+}$ *and Bag-1*$^{+/-}$ *female BMSCs in basal and osteogenic medium.*

5.4.8. Analyses of bone architecture of *Bag-1*$^{+/+}$ and *Bag-1*$^{+/-}$ mice

There were no phenotypical differences between *Bag-1* wild type and haploinsufficient mice (Fig. 5-15). Long bones i.e. femora and tibiae (Fig. 5-16A) of 14-week-old, skeletally mature *Bag-1*$^{+/+}$ and *Bag-1*$^{+/-}$ female mice did not differ in their length (example of femoral length shown in Fig. 5-16B). The SkyScan 1176 high resolution *in vivo* μCT scanner was used for morphometric analyses of the femoral microarchitecture. Analyses of trabecular bone morphology were performed in the head of femur (Fig. 5-17) and distal femur (Fig. 5-18), in addition to the investigation of tibia cortical bone architecture (Fig. 5-19). No statistically significant differences were

observed between *Bag-1*$^{+/+}$ and *Bag-1*$^{+/-}$ female mice in the indices of trabecular bone morphology, namely bone volume, bone surface/bone volume, trabecular thickness, trabecular number and trabecular separation, and cortical bone morphometry, namely total cross-sectional area, cortical bone area, cortical bone area fraction and cortical thickness.

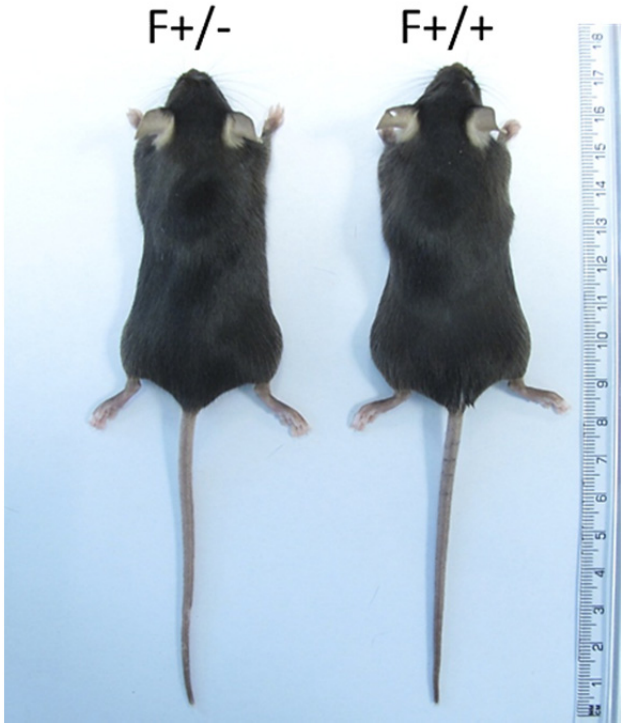

Figure 5-15. *Bag-1*$^{+/-}$ *and Bag-1*$^{+/+}$ *skeletally mature, 14-week-old female mice.*

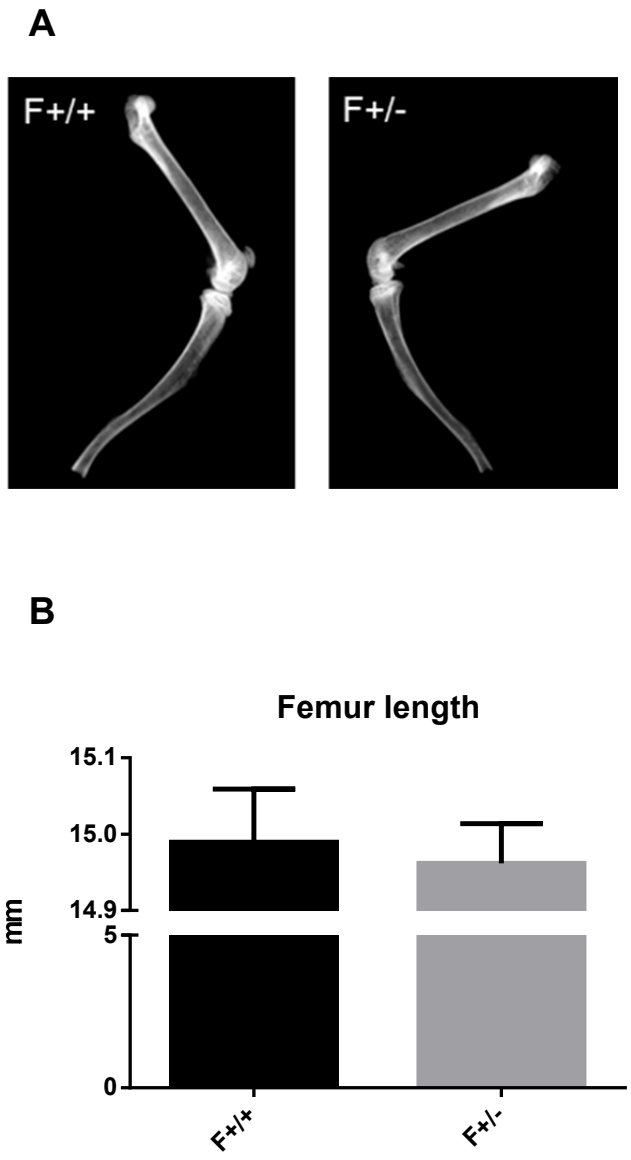

Figure 5-16. *Bone morphology of Bag-1$^{+/+}$ and Bag-1$^{+/-}$ mice: faxitron images of femora and tibiae of 14-week-old, skeletally mature Bag-1$^{+/+}$ and Bag-1$^{+/-}$ female mice (A). Bar graph demonstrating lengths of femurs of 14-week-old Bag-1$^{+/+}$ and Bag-1$^{+/-}$ female mice (B), results are expressed as mean ± SD; n = 3 mice per group.*

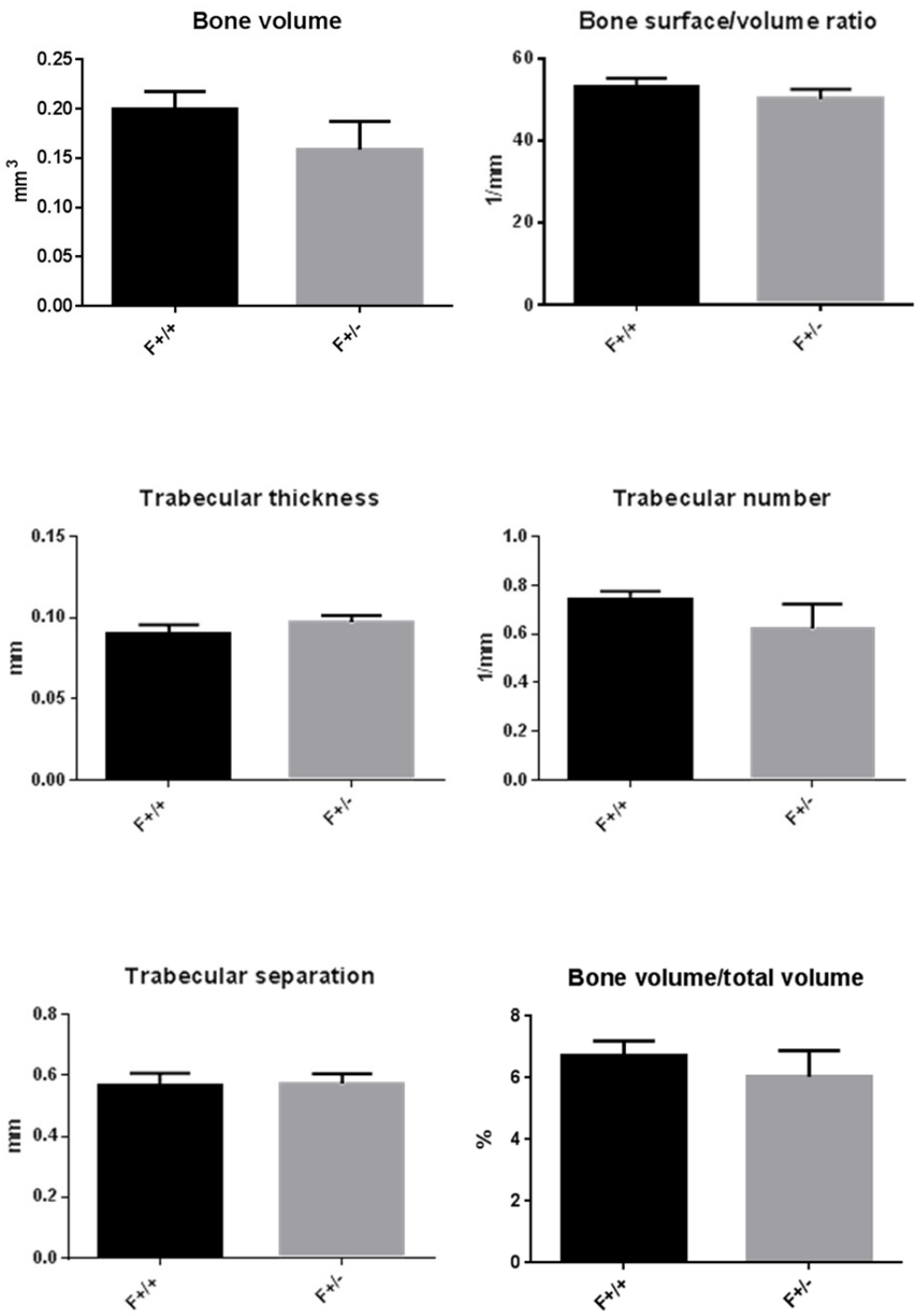

Figure 5-17. *Bone microstructure of Bag-1$^{+/+}$ and Bag-1$^{+/-}$ mice: µCT analyses of trabecular bone morphology performed in the trabecular bone - head of femur. Results are expressed as mean ± SD; n = 3 mice per group.*

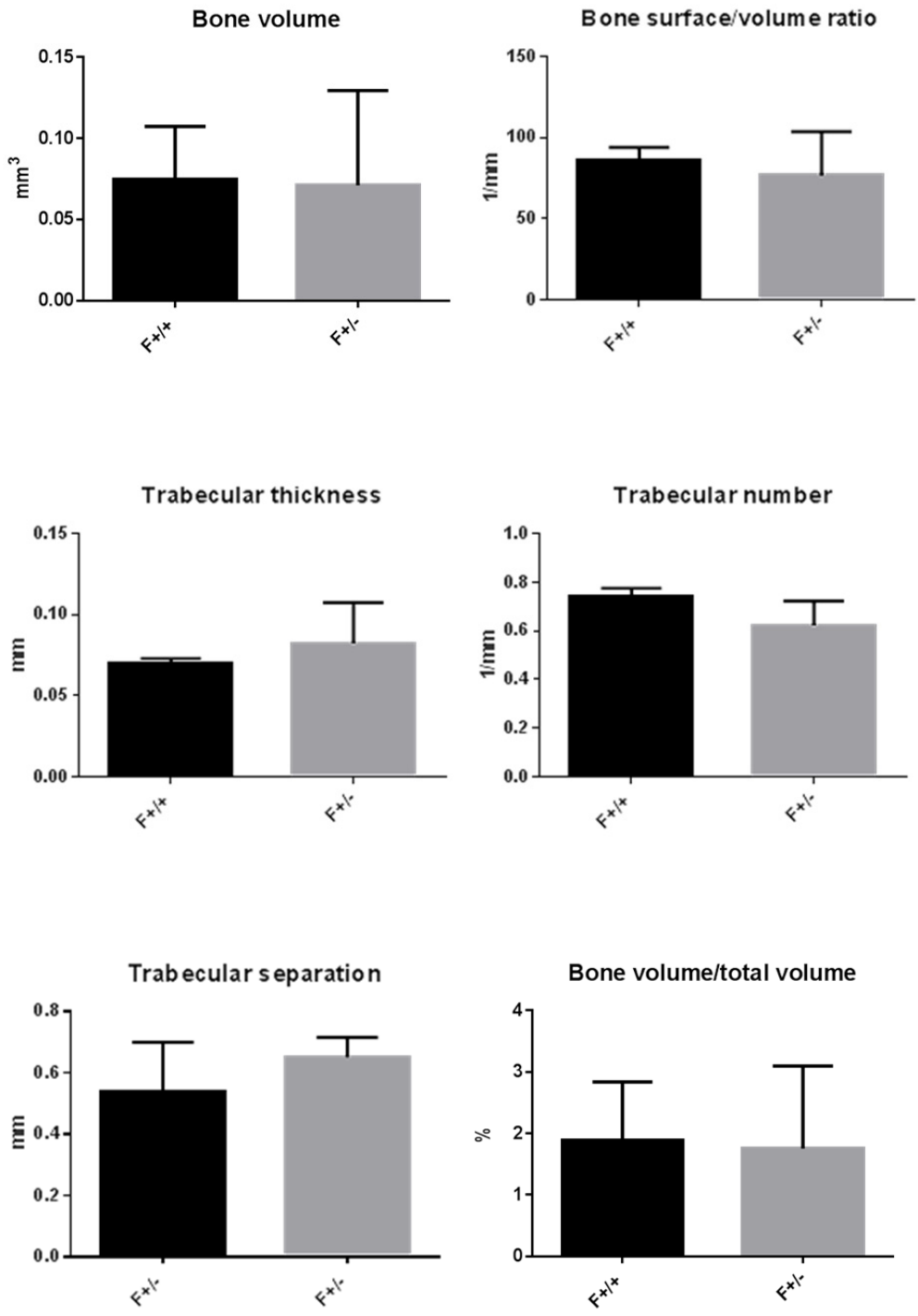

Figure 5-18. *Bone microstructure of Bag-1$^{+/+}$ and Bag-1$^{+/-}$ mice: µCT analyses of trabecular bone morphology performed in the trabecular bone - distal femur. Results are expressed as mean ± SD; n = 3 mice per group.*

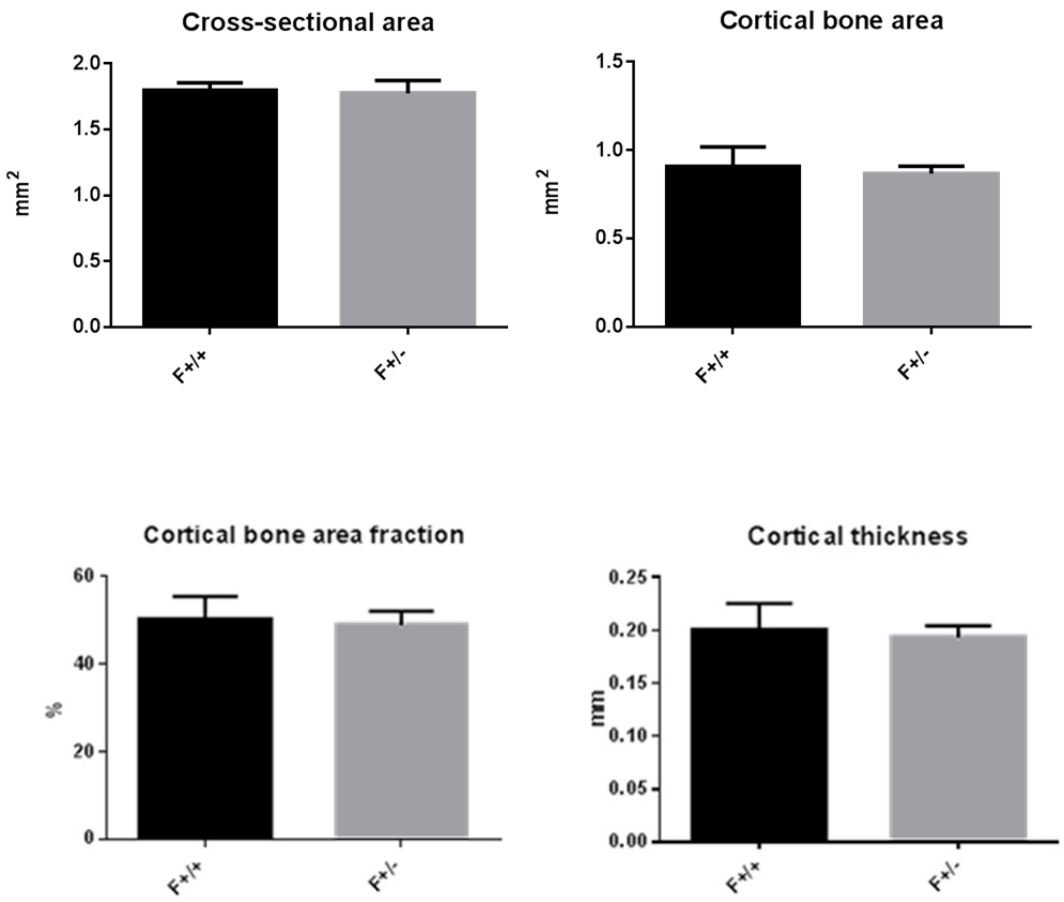

Figure 5-19. *Bone microstructure of Bag-1$^{+/+}$ and Bag-1$^{+/-}$ mice: µCT analyses of trabecular bone morphology performed in cortical bone. Results are expressed as mean ± SD; n = 3 mice per group.*

5.5. Summary of results

a) BAG-1S was the predominant BAG-1 isoform expressed by murine BMSCs.
b) *Bag-1* haploinsufficiency led to lower levels of BAG-1L and BAG-1S expression in BMSCs of both female and male mice.
c) BMSC cultures of *Bag-1*$^{+/-}$ female mice were characterised by significantly higher cell numbers and an increased rate of cell proliferation under osteogenic culture conditions.
d) BMSC cultures of *Bag-1*$^{+/-}$ female mice exhibited reduced osteogenic differentiation potential in response to BMP-2.
e) No differences in cell apoptosis were observed between the different groups of BMSC cultures.
f) *Bag-1* haploinsufficiency did not cause any phenotypical differences or significant alterations in bone length and microarchitecture.

5.6. Discussion

The present study aimed to characterise the role of *Bag-1* in postnatal skeletal development by analysing differences in osteogenic differentiation of BMSCs and the microarchitecture of long bones of *Bag-1*$^{+/+}$ and *Bag-1*$^{+/-}$ mice. BAG-1S was identified as the predominant BAG-1 isoform expressed by murine BMSCs, this finding is in keeping with the observation that BAG-1S is the major BAG-1 isoform in rodents (Townsend et al., 2003b, Yang et al., 2007). Quantification of Western blot results of the expression of BAG-1L and BAG-1S isoforms in mouse BMSCs cultured for 28 days in basal conditions demonstrated that *Bag-1* haploinsufficiency results in lower levels of BAG-1L and BAG-S expression in BMSCs of both *Bag-1*$^{+/-}$ female and *Bag-1*$^{+/-}$ male mice.

Deletion of one *Bag-1* allele did not affect the rate of apoptosis of *Bag-1*$^{+/-}$ BMSCs; this is a surprising outcome as BAG-1 is a pro-survival protein. No differences in the rate of apoptosis suggest a possible compensatory role of other anti-apoptotic factors such as BCL-2 in preventing apoptosis of *Bag-1* haploinsufficient BMSCs. It is also possible that the presence of one functional *Bag-1* allele in *Bag-1*$^{+/-}$ BMSCs is sufficient to prevent cell apoptosis in the BMSC cultures of *Bag-1*$^{+/-}$ mice.

To elucidate the role of BAG-1 in osteoblast development, differences in osteogenic differentiation of BMSCs from *Bag-1*$^{+/+}$ and *Bag-1*$^{+/-}$ skeletally mature mice were examined. BMSCs of *Bag-1*$^{+/-}$ female mice demonstrated significantly lower ($P<0.001$) osteogenic differentiation potential in response to BMP-2, compared to BMSCs of *Bag-1*$^{+/+}$ female mice. Interestingly, *Bag-1* haploinsufficiency did not affect the osteogenic response to BMP-2 of BMSCs of *Bag-1*$^{+/-}$ male mice. The current results indicate an important role for BAG-1 in osteoblast development and the need to understand the role of interacting factors modulating the gender differences in osteoblast development. Estrogen (E2), the primary female sex hormone, binds to the estrogen receptors (ERs), ligand-activated enhancer proteins that are members of the nuclear hormone receptor superfamily, and E2-liganded ER is functionally involved in the process of osteoblast differentiation directed by BMPs (Matsumoto et al., 2013). Further studies could look into investigating the role of gender-specific factors in modulation of BMP-2-directed osteogenic differentiation of BMSCs.

Based on the inverse relationship between cell differentiation and proliferation, it is possible that proliferation of BMSCs of *Bag-1*$^{+/-}$ female mice is enhanced at the expense of differentiation. This, however, is a relatively simplistic explanation; to further examine the causes of decreased BMP-2-directed osteogenic differentiation of BMSCs

of *Bag-1*$^{+/-}$ female mice, we analysed differences in the expression of an array of genes crucial for skeletal development between osteogenic cultures of BMSCs of *Bag-1*$^{+/-}$ and *Bag-1*$^{+/+}$ female mice.

Increased expression of *Ahsg* (fetuin) and *Fgf2* in osteogenic cultures of *Bag-1* heterozygous BMSCs may have contributed, in part, to the lower osteogenic response of the cells to BMP-2 and increased rate of cell proliferation. Fetuin has been shown to act as an inhibitor of osteogenesis in rodent BMSC cultures due to its high affinity for binding BMP2/4/6 and blocking the osteogenic activity of these factors in cell culture assays (Binkert et al., 1999). Similarly, FGF-2 has been shown to inhibit BMP-stimulated osteoblast differentiation and increased levels of FGF-2 have been demonstrated to maintain osteoprogenitor cells in a proliferative state and delay their subsequent differentiation, maturation and mineralisation (Chaudhary et al., 2004, Huang et al., 2010). It has been shown that fibronectin, an extracellular matrix glycoprotein, is synthesised by osteoblasts and accumulated in the extracellular matrix during cell proliferation and early differentiation while its synthesis is dramatically reduced with cell maturation (Winnard et al., 1995). It is therefore possible that upregulation of *Fn1* gene in BMSCs of *Bag-1*$^{+/-}$ female mice in comparison to BMSCs of *Bag-1*$^{+/+}$ female mice reflects the proliferative state of *Bag-1*$^{+/-}$ BMSCs.

The present study demonstrated significant downregulation of *Bmp-2*, *Bmp-4 and Bmp-7 expression*. BMP-2, BMP-4 and BMP-7 have been shown to induce differentiation of osteoblast lineage cells (Asahina et al., 1996, Katagiri et al., 1990, Yamaguchi et al., 1996). Downregulation of the expression of osteoinductive BMPs most likely was a contributing factor in compromised osteogenic differentiation of *Bag-1*$^{+/-}$ BMSCs in comparison to *Bag-1*$^{+/+}$ BMSCs. Surprisingly, a significant downregulation of *Bmp-3* in cultures of *Bag-1*$^{+/-}$ BMSCs was observed. BMP-3 accounts for ~65% of the total content of BMPs in demineralised bone (Wozney, 1993). BMP-3 inhibits osteoblast differentiation by antagonizing osteogenic BMP signalling through binding to a shared receptor and interfering with the osteogenic BMP pathway (Gamer et al., 2005). BMP-3 has also been shown to block the BMP-2 mediated differentiation of osteoprogenitor cells into osteoblasts (Daluiski et al., 2001) and to promote mesenchymal stem cells proliferation (Stewart et al., 2010). As BMP-3 is a recognised inhibitor of bone formation, downregulation of *Bmp-3* expression alongside osteoinductive *Bmp-2*, *Bmp-4 and Bmp-7 expression* in *Bag-1*$^{+/-}$ BMSCs characterised by compromised osteogenesis, was a surprising observation. At this stage rational explanation for this contradictory observation cannot yet be offered.

Furthermore, downregulation of expression of *Col1a1*, *Col1a2*, *Col5a1*, *Serpinh1*, *Alpl*, *Phex* and *Bglap* in osteogenic cultures of BMSCs of *Bag-1*$^{+/-}$ female mice contributed to decreased bone matrix synthesis and mineralisation. Type I collagen is the most abundant collagen in bone matrix, while type V collagen is essential for the formation of normal type I collagen fibrils as it plays critical roles in early fibril initiation, determination of fibril structure and matrix organisation (Wenstrup et al., 2004). The collagen-specific molecular chaperone, serpinh-1/HSP47, is located in the ER and plays an important role in collagen biosynthesis (Dafforn et al., 2001). Matrix mineralisation is regulated by ALPL, an enzyme with recognised promineralisation role (Narisawa et al., 2013), and PHEX, which binds to a group of extracellular matrix proteins including MEPE (matrix extracellular phosphoglycoprotein), inhibits the cleavage of MEPE, prevents release of protease-resistant phosphorylated peptides and therefore releases the inhibitory effects of these peptides on mineralisation (Addison et al., 2010). Osteocalcin, an osteoblast-specific protein, contains γ-carboxyglutamic acid (Gla) residues (Hauschka et al., 1989) that usually characterise proteins with high affinity for mineral ions. Indeed, Boskey and co-workers have implied the role of Osteocalcin in regulating bone mineral maturation (Boskey et al., 1998). These results correlate with our observation that osteogenic cultures of *Bag-1*$^{+/-}$ BMSCs exhibit compromised mineralisation, indicated by lower number of mineralised nodules stained with Alizarin red.

Following the observation of the differences in osteogenic responses of BMSCs of *Bag-1*$^{+/+}$ and *Bag-1*$^{+/-}$ *f*emale mice, 3-D microarchitecture of long bones of skeletally mature, 14-week-old female mice was studied. µCT analysis revealed no significant differences in bone microarchitecture between *Bag-1*$^{+/+}$ and *Bag-1*$^{+/-}$ female mice. Lack of significant detectable differences in bone microstructure of *Bag-1*$^{+/+}$ and *Bag-1*$^{+/-}$ female mice could be due to a number of limitations of the experimental design. As there are no phenotypical differences between *Bag-1*$^{+/+}$ and *Bag-1*$^{+/-}$ mice, effects of *Bag-1* haploinsufficiency on bone development *in vivo* are expected to be subtle. In the current study, samples were scanned at 18 µm voxel resolution, which is not sensitive enough to detect subtle differences in the bone microstructure. In order to distinguish calcium phosphate depositions in bone, scanning at 1 µm voxel resolution is needed; use of nano-CT scanner capable of achieving resolutions of 0.3 µm allows visualisation of structural features linked to bone quality, such as osteocytes and resorption lacunae (Salmon and Sasov, 2007).

In the present study, for each group, µCT analyses were performed on long bones from three mice (i.e. n=3). Power calculations for sample sizes needed to obtain statistically

meaningful results for the variables describing trabecular and cortical bone indicated that minimum sample numbers per group should be 18 (calculation based on 80% power of detection at the 5% level of confidence. Lack of statistically significant differences in bone architecture between *Bag-1*$^{+/+}$ and *Bag-1*$^{+/-}$ female mice could be due to our study being underpowered. Moreover, scans were performed on long bones of skeletally mature, but relatively young mice (14 weeks old). Studies of the effects of maternal diet on offspring skeletal development in rodents have shown that significant alterations to bone structure and bone mineral content were present in elderly animals (47 weeks and 26 weeks old) (Lanham et al., 2008, Romano et al., 2009). It is possible, that potential alterations in bone architecture as a result of *Bag-1* haploinsufficiency would manifest themselves with aging.

It is also important to stress, that compromised osteogenic response of BMSCs of *Bag-1*$^{+/-}$ female mice to the osteogenic stimulus (BMP-2) were observed *in vitro*, while the *in vivo* investigation of the role of *Bag-1* haploinsufficiency in bone development was performed on animals that were not put under any intervention, i.e. no growth factors were administered. Moreover, the *in vitro* environment of BMSC culture is a highly controlled environment that allows precise stimulation of the cells with a chosen factor and concurrent elimination of any other factors present in the organism *in vivo*. *In vitro* research provides environment with fewer variables with amplified responses to these variables and more distinguishable results, which proves to be more suitable for delineating biological mechanisms.

Bag-1 knock-out mice were generated from a C57BL/6 inbred strain of laboratory mouse. The C57BL/6 strain, alongside FVB/N, is commonly used to create transgenic mice due to their ability to superovulate in response to hormones and to produce a large number of high quality embryos. However, it has been shown that BMSCs from C57BL/6 strain of mice are present in marrow at a low frequency and exhibit poor growth *in vitro*. The relative abundance of BMSCs in the bone marrow of commonly used inbred strains of mice can vary as much as 10-fold, with C57BL/6 exhibiting very low initial yield of plastic adherent cells (Phinney et al., 1999). Isolation of low number of BMSCs from long bones of *Bag-1*$^{+/+}$ and *Bag-1*$^{+/-}$ mice limited the number of experiments that could be performed. The heterogenous BMSC population had to be utilised as it was not possible to isolate adequate number of BMSCs for immunoselection of the MSC population. It was also not possible to perform experiments to elucidate the effects of overexpression of *Bag-1* in BMSCs of *Bag-1*$^{+/-}$ female mice (i.e. to rescue the haploinsufficient phenotype) on proliferation and osteogenic differentiation. It would also have been useful to confirm the results by

assessing the protein expression (by immunoblotting) of the important candidate genes identified from the PCR array platform.

In conclusion, this study has demonstrated that although haploinsufficiency of *Bag-1* did not affect bone development and 3-D bone microarchitecture of 14-week old female mice, loss of one functional *Bag-1* allele resulted in profound effects on the ability of BMSCs of 14-week old female mice to differentiate into osteoblasts in response to BMP-2 *in vitro*. *Bag-1* haploinsufficiency did not affect the osteogenic response to BMP-2 of BMSCs of *Bag-1*$^{+/-}$ male mice. In order to better understand the intricacies of osteoblast development, the role of interacting factors modulating the gender differences in osteogenesis should be studied. Estrogen (E2), the primary female sex hormone, binds to the estrogen receptors (ERs) and E2-liganded ER is functionally involved in the process of osteoblast differentiation directed by BMPs (Matsumoto et al., 2013). Further studies could look into investigating the role of gender-specific factors in modulation of BMP-2-directed osteogenic differentiation of BMSCs.

Chapter 6

The role of BAG-1-mediated protein-protein interactions in osteogenesis

6. Characterisation of the role of BAG-1-mediated protein-protein interactions in osteogenesis

6.1. Introduction

The current studies have demonstrated that, unlike bone marrow stromal cells (BMSCs) of *Bag-1*$^{+/-}$ male mice, BMSCs of *Bag-1*$^{+/-}$ female mice do not exhibit robust osteogenic differentiation in response to BMP-2. This highlights the need to understand the role of interacting factors, which are capable of modulating gender differences in BMP-2-directed osteogenic differentiation of BMSCs of *Bag-1*$^{+/-}$ mice. Estrogen (E2), the primary female sex hormone, binds to estrogen receptors (ERs), ligand-activated enhancer proteins that are members of the nuclear hormone receptor (NHR) superfamily. The E2-ER complex is functionally involved in the process of osteoblast differentiation directed by BMPs (Mangelsdorf et al., 1995, Okazaki et al., 2002, Matsumoto et al., 2013). Osteoblast precursor cells express both ERs (α and β) and treatment of osteoprogenitor cells with E2 is known to upregulate expression of BMP type II receptor (*Bmpr2*), leading to increased responsiveness of the osteoprogenitor cells to BMP-2, upregulation of BMP-induced Smad 1/5/8 phosphorylation and enhanced E2-facilitated BMP-directed expression of osteogenic genes, namely *Runx-2*, *Osterix*, *Alpl* and *Osteocalcin* (Matsumoto et al., 2013) (Fig. 6-1).

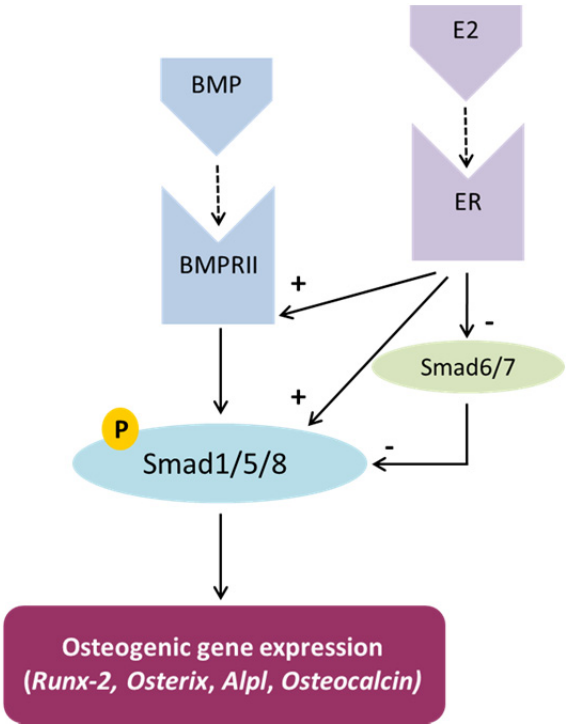

Figure 6-1. *Role of estrogen in BMP-4 directed osteoblast development (adapted from Matsumoto et al., 2013)*

BAG-1 is a multifunctional co-chaperone protein, which interacts with a diverse array of molecular targets, namely the 70-kDa heat shock proteins (HSC70/HSP70), NHRs, RAF-1 kinase and components of the ubiquitylation/proteasome machinery, to regulate gene transcription and molecular signalling crucial for cell proliferation, motility, differentiation and apoptosis (Townsend et al., 2003b). The chaperone proteins, HSC70/HSP70, due to their ability to bind most (if not all) proteins in their non-native states and stabilize the protein conformation, have been shown to play important roles in folding, translocation and degradation of proteins in eukaryotic cells (Hartl, 1996). Expression of HSP70 is induced in cells due to stress, while HSC70, which is constitutively expressed in cells, is an important chaperone protein that mediates the correct assembly of NHRs (Wu et al., 1985, Chappell et al., 1986).

NHRs have been acknowledged as key regulators of cell proliferation, differentiation and apoptosis, and BAG-1 has been shown to regulate the function of a number of NHRs, including the glucocorticoid receptor (Zeiner and Gehring, 1995, Kullmann et al., 1998), androgen receptor (AR) (Froesch et al., 1998), ERs (Cutress et al., 2003), retinoic acid receptor (Liu et al., 1998) and vitamin D_3 receptor (Guzey et al., 2000, Lee et al., 2007). BAG-1 frequently interacts with NHRs via its carboxy terminus, which also mediates the binding of BAG-1 to HSC70/HSP70 (Briknarova et al., 2001, Cato and Mink, 2001). Binding of BAG-1 to HSC70/HSP70 has now been recognised to be vital for most functions of BAG-1, including its effects on NHRs. Mutant BAG-1 proteins containing specific point mutations in the carboxy terminus BAG domain demonstrate diminished capacity to affect AR transactivation due to ablation of HSC70 binding (Briknarova et al., 2001). It is now widely acknowledged that most protein-protein interactions involving the BAG-1 co-chaperone are mediated by the HSC70/HSP70 chaperone proteins (Zeiner et al., 1997).

NHRs undergo a series of transformation steps that are mediated by molecular chaperones and regulated by co-chaperones, which assist the nuclear receptors to achieve correct conformation/assembly and facilitate binding to hormones / ligands. Heat shock proteins can interact with most NHRs resulting in functional active conformations (Cato and Mink, 2001). Consistent with this ability, heat shock proteins are known to be important components of the NHR complexes in cells (Cheung and Smith, 2000). HSC70 comprises of a central peptide-binding domain that interacts with short hydrophobic segments in the polypeptide substrates, a carboxy terminal region that forms a “lid” over the peptide-binding pocket and the ATPase domain, which regulates the binding process through cycles of ATP binding and hydrolysis whereby the misfolded protein substrates are alternatively bound and released to effect protein

folding (Rassow et al., 1997) Substrates interact transiently with the ATP-bound form of HSC70, whereas binding is stabilised when ATP is hydrolysed, thereby allowing the substrates to bind with high affinity to the ADP-bound form of HSC70. Release of ADP and subsequent binding of ATP, referred to as nucleotide exchange, enables the release of the refolded substrate (Bukau and Horwich, 1998).

As part of its co-chaperone activity, BAG-1 stimulates the nucleotide exchange of HSC70 and, therefore, regulates (re)folding and activation of NHRs by HSC70 when transitioning from ligand-bound to ligand-free conformations (Takayama et al., 1997, Luders et al., 2000) (Fig. 1-14). Hence, by acting as a nucleotide exchange factor in the activation cycle, BAG-1 plays a crucial regulatory role in the activation of NHRs before hormone binding. After hormone binding, BAG-1 is also able to influence receptor-mediated transcription of the nuclear hormone-responsive genes e.g. BAG-1 has been shown to interact with and stimulate the activity of both ERα and ERβ, and enhance E2-dependent transcription in breast cancer cells (Cheung and Smith, 2000, Cutress et al., 2003). Thus, BAG-1, via its interaction with/binding to HSC70, can regulate the function of NHRs, such as ERs, and play an important role in modulating cellular responses to hormones such as E2. The functional significance of BAG-1-regulated activation of ERs by HSC70 in E2/ER-facilitated, BMP-2-directed osteogenic differentiation of BMSCs has not been elucidated to date.

Given BAG-1 interacts with most of the molecular targets in cells via HSC70/HSP70, disruption of binding of BAG-1 to the heat shock proteins leads to loss of BAG-1-mediated protein-protein interactions. Compound collections obtained from the National Cancer Institute Developmental Therapeutics Programme (Rockville, MD) for identification of small molecule inhibitors of the BAG-1-HSC70/HSP70 interaction, resulted in the identification of NSC71948, which is structurally similar to Thioflavin-S (Sharp et al., 2009a). Furthermore, short peptides derived from the C-terminal BAG domain, which mediates binding with HSC70/HSP70, have been shown to inhibit the interaction between BAG-1 and HSC70/HSP70 (Sharp et al., 2009b). Inhibition of BAG-1 function through disruption of the binding of BAG-1 to HSC70 by Thioflavin-S and the C-terminal BAG domain-derived short peptides can, therefore, be employed as an effective strategy to elucidate the role of BAG-1-mediated protein-protein interactions in E2/ER-facilitated, BMP-2-directed osteogenic differentiation of BMSCs.

6.2. Objectives

To characterise the role of BAG-1-mediated protein-protein interactions in E2-facilitated, BMP-2-directed osteogenic differentiation of murine BMSCs, the objectives of the present study were:

a) Analysis of the expression of estrogen receptors, *ERα* and *ERβ*, by murine BMSCs,
b) Investigation of the effect of E2 on BMP-2-directed osteogenic differentiation of murine BMSCs,
c) Demonstration of the binding between endogenous BAG-1 and HSC70 in murine BMSCs by co-immunoprecipitation,
d) Analysis of the effect of inhibition of the interaction between BAG-1 and HSC70 by Thioflavin-S on E2-facilitated BMP-directed osteogenic differentiation of *Bag-1*$^{+/+}$ and *Bag-1*$^{+/-}$ BMSCs,
e) Examination of the effect of inhibition of binding of BAG-1 to HSC70 by the BAG domain-derived short peptide on E2-facilitated, BMP-directed osteogenic differentiation of *Bag-1*$^{+/+}$ and *Bag-1*$^{+/-}$ BMSCs.

6.3. Materials and methods

6.3.1. Bone marrow stromal cell (BMSC) and MC3T3-E1 culture

BMSCs of *Bag-1*$^{+/+}$ 14-week-old female mice were isolated (refer to section 3.6) and cultured for 28 days in α-MEM containing 1% penicillin/streptomycin, 10% FCS and 50 μM β-mercaptoethanol. Murine osteoblast-like MC3T3-E1 cells were also cultured for 28 days in D-MEM with 1% penicillin/streptomycin and 10% FCS. Cultures were harvested on day 28 for *ERα* and *ERβ* gene expression. Primer sequences for these genes can be found in Appendix 4. *ERα* and *ERβ* primers were designed using previously published primer sequences (Nakada et al., 2014, Tachibana et al., 2000). Primers were ordered from Sigma.

6.3.2. Bone marrow stromal cell (BMSC) culture in presence of 17-β-estradiol (E2)

E2 (Sigma-Aldrich, UK) was constituted as 20 μg/ml stock solution in 2% solution of ethanol in α-MEM. BMSCs of 14-week-old female *Bag-1*$^{+/+}$ mice were isolated and cultured in basal medium (phenol red free α-MEM with 1% penicillin/streptomycin, 10% charcoal stripped FCS, 50 μM β-mercaptoethanol), osteogenic medium (phenol red-free α-MEM containing 10% charcoal-stripped FCS, 50μM β-mercaptoethanol, 100ng/ml rhBMP-2, 100 μM ascorbate-2-phosphate) and osteogenic medium supplemented with E2 in concentrations of: 10 pM, 100 pM, 10 nM and 100 nM. As phenol red structurally resembles estrogens and has a mild estrogenic activity, phenol red free medium was used (Berthois et al., 1986). Dextran-treated charcoal stripping of FCS selectively removes hormones without non-specific loss of other serum components making it an ideal supplement of cell culture media used in studying processes influenced by steroid hormones. Cultures were harvested on day 28 for analysis of *Alpl* gene expression, utilised as an index of osteogenic differentiation.

Following the selection of the appropriate E2 concentration from the E2 dose response experiment, BMSCs of *Bag-1*$^{+/+}$ and *Bag-1*$^{+/-}$ 14-week-old female mice were isolated and cultured for 28 days in basal medium (phenol red free α-MEM with 1% penicillin/streptomycin, 10% charcoal stripped FCS, 50 μM β-mercaptoethanol), osteogenic medium (phenol red-free α-MEM containing 10% charcoal-stripped FCS, 50 μM β-mercaptoethanol, 100 ng/ml rhBMP-2, 100 μM ascorbate-2-phosphate) and osteogenic medium supplemented with 100 nM E2. Cultures were harvested on day 28 for analysis of *Bmpr2* gene expression. Primer sequences for this gene can be found in

Appendix 3. *Bmpr2* primers were designed based on previously published primer sequences (Yu et al., 2008) and ordered from Sigma.

6.3.3. Co-immunoprecipitation technique

BMSCs of *Bag-1*$^{+/+}$ female mice were isolated and cultured for 28 days in basal medium (α-MEM with 1% penicillin/streptomycin, 10% FCS, 50 μM β-mercaptoethanol). Cells from day 28 monolayer cultures were harvested by trypsinisation (1 x solution of Trypsin, Lonza, UK), followed by centrifugation of the cell suspension for 5 minutes at 12000 rpm and two washes with 1 x PBS. Pelleted cells were resuspended in HMKEN buffer (see appendix 2) by trituration through a 21 gauge needle, lysed on ice for 30 minutes and centrifuged for 30 minutes at 13000 rpm. Protein concentrations were determined using Thermo Scientific™ Pierce™ BCA™ Protein Assay (Thermo Fisher Scientific, UK) (refer to section 3.10.2) – total protein concentration was estimated as 600 μg. One-sixtieth, i.e. 10 μg of the total amount of protein was retained as whole cell lysate.

Protein G-sepharose beads (GE Healthcare, UK) were supplied pre-swollen in 20% ethanol. After the pre-treatment with HMKEN buffer involving 4 washes in HMKEN buffer in order to eliminate ethanol, Protein G-sepharose beads were used to preclear the remaining sample (590 μg) by rotation for 30 minutes in 4°C; leftover beads were subsequently removed by centrifugation. Half of the lysate (295 μg) was incubated with rabbit polyclonal IgG α- BAG-1 antibody (C-16, Santa Cruz, USA; 200 μg/ml stock) at 2 μg (10 μl of antibody)/295 μg of lysate protein to investigate the interaction between BAG-1 and HSC70/HSP70, and the remaining half of the lysate was incubated with rabbit pre-immune control serum at 2.5 μl of pre-immune serum/295 μg of lysate protein, to monitor non-specific interactions (16 h, 4°C). Protein G-Sepharose beads were incubated with the immune complexes (2 h, 4°C) and subsequently removed by centrifugation. Bead pellets were washed three times with HMKEN buffer, resuspended in sample buffer using Blue Loading Buffer (refer to section 3.10.2), heated at 95°C for 5 minutes, resolved in 10% polyacrylamide gels and electroblotted on PVDF membrane (refer to section 3.10.3 and 3.10.5). Immunoblotting was performed as described previously, blots were probed with mouse monoclonal IgG α-HSC70 (B-6, Santa Cruz, USA; 1:200 dilution) and rabbit polyclonal IgG α- BAG-1 antibody (C-16, Santa Cruz, USA; 1:200 dilution).

6.3.4. Bone marrow derived stromal cell (BMSC) culture in presence of Thioflavin-S

Thioflavin S (Sigma-Aldrich, UK) was prepared as a 10 mmol/L stock solution in DMSO. BMSCs of 14-week-old *Bag-1*$^{+/+}$ and *Bag-1*$^{+/-}$ female mice were isolated and cultured for 28 days in basal medium (phenol red free α-MEM with 1% penicillin / streptomycin, 10% charcoal striped FCS, 50 μM β-mercaptoethanol), osteogenic medium (phenol red-free α-MEM containing 10% charcoal-stripped FCS, 50 μM β-mercaptoethanol, 100 ng/ml rhBMP-2, 100 μM ascorbate-2-phosphate), osteogenic medium supplemented with 100 nM E2, and osteogenic medium containing 100 nM E2 and 5 μM Thioflavin-S. Since Thioflavin-S was constituted in DMSO and the effective concentration of DMSO in the culture medium containing 5 μM Thioflavin-S was 0.05%, the osteogenic medium containing 100 nM E2 was also supplemented with 0.05% DMSO. Day-28 BMSC cultures were harvested for the analyses of expression of osteogenic genes: *Runx-2*, *Osterix*, *Alpl* and *Osteocalcin* (refer to section 3.9), estimation of tissue non-specific alkaline phosphatase (ALPL) specific activity (refer to section 3.7.1) and DNA concentration (refer to section 3.7.2).

Study groups:

- Basal – BMSCs cultured in basal medium
- Osteo - BMSCs cultured in osteogenic medium
- Osteo+E2 - BMSCs cultured in osteogenic medium supplemented with 100 nM E2 and 0.05% DMSO
- Osteo+E2+ThS - BMSCs cultured in osteogenic medium containing 100 nM E2 and 5 μM Thioflavin-S in DMSO

6.3.5. Bone marrow stromal cell (BMSC) culture in presence of BAG domain-derived short peptides

A short peptide, H2-Penetratin, containing the 8 amino acid binding core of helix 2 of the BAG-1 domain (Fig. 6-3, sequence highlighted blue) coupled via a peptide bond at its C-terminus to Penetratin (cell-penetrating peptide that is capable of permeating through cell membranes) (Fig. 6-3, sequence highlighted red), was used to inhibit the binding between BAG-1 and HSC70. A mutant peptide, H2mutant-Penetratin, with alanine (A) substitutions, particularly for arginine (R) residues at positions 205 and 206 (underlined), representing the ‘hot-spot’ on the interaction surface between BAG-1 and

HSC70, was also used as a control peptide (Fig. 6-2). Peptides were ordered from ProteoGenix SAS, Schiltigheim, France.

H2-Penetratin: CKLDRRVKATIERQIKIWFQNRRMKWKK

H2mutant-Penetratin: AALDAAVKATIERQIKIWFQNRRMKWKK

Figure 6-2. *Sequences of a short peptide, H2-Penetratin, containing the 8 amino acid binding core of helix 2 and a mutant peptide, H2mutant-Penetratin*

1 mg of H2-Penetratin and 1 mg of H2mutant-Penetratin (ProteoGenix SAS, Schiltigheim, France) were constituted in 1 ml of water. In order to calculate the molar concentrations of each of the peptide, peptide impurities (determined by analytical HPLC) and the net peptide content (NPC) had to be taken into account. The following formula was applied:

$$\text{Molar amount of desired peptide (mol)} = \frac{\text{Gross weight (g) x NPC (\%) x HPLC purity (\%)}}{\text{Molecular weight } \left({}^{\text{g}}/_{\text{mol}}\right) \text{ x } 10000}$$

The gross weight, peptide molecular weight, NPC and HPLC purity values were provided by the manufacturer and were substituted in the above formula to determine the molar concentrations of the stock solutions of H2-Penetratin and H2mutant-Penetratin, calculated as 0.179 µmol/ml (179 µmol/L) and 0.176 µmol/ml (176 µmol/L), respectively.

BMSCs of *Bag-1*$^{+/+}$ and *Bag-1*$^{+/-}$ female mice were isolated and cultured for 28 days in basal medium (phenol red free α-MEM with 1% penicillin/streptomycin, 10% charcoal striped FCS, 50 µM β-mercaptoethanol), osteogenic medium (phenol red-free α-MEM containing 10% charcoal-stripped FCS, 50 µM β-mercaptoethanol, 100 ng/ml rhBMP-2, 100µM ascorbate-2-phosphate) supplemented with 100 nM 17-β-estradiol (E2), and osteogenic medium containing 100 nM E2 in addition to either 10 µM H2-Penetratin or 10 µM H2mutant-Penetratin. Day-28 BMSC cultures were harvested for the analyses of expression of osteogenic genes: *Runx-2*, *Osterix*, *Alpl* and *Osteocalcin,* estimation of tissue nonspecific alkaline phosphatase (ALPL) specific activity, osteocalcin and DNA concentrations.

Study groups:

- Basal – BMSCs cultured in basal medium
- Osteo+E2 - BMSCs cultured in osteogenic medium supplemented with 100 nM 17-β-estradiol

- Osteo+E2+H2 - BMSCs cultured in osteogenic medium containing 100 nM E2 and 10 μM H2-Penetratin
- Osteo+E2+H2 mut - BMSCs cultured in osteogenic medium containing 100 nM E2 and 10 μM H2mutant-Penetratin

6.4. Results

6.4.1. Expression of estrogen receptors by BMSCs

Expression of estrogen receptors (ERs), namely *ERα* and *ERβ*, in murine primary BMSCs was compared to murine osteoblast-like MC3T3-E1 cells which are known to express both receptors. Although murine BMSCs were found to express both ERs, in comparison to MC3T3-E1 cells, expression of ERα was significantly lower (P<0.001) in BMSCs (Fig. 6-3A), while expression of *ERβ* was significantly higher (P<0.001) in BMSCs (Fig. 6-3B).

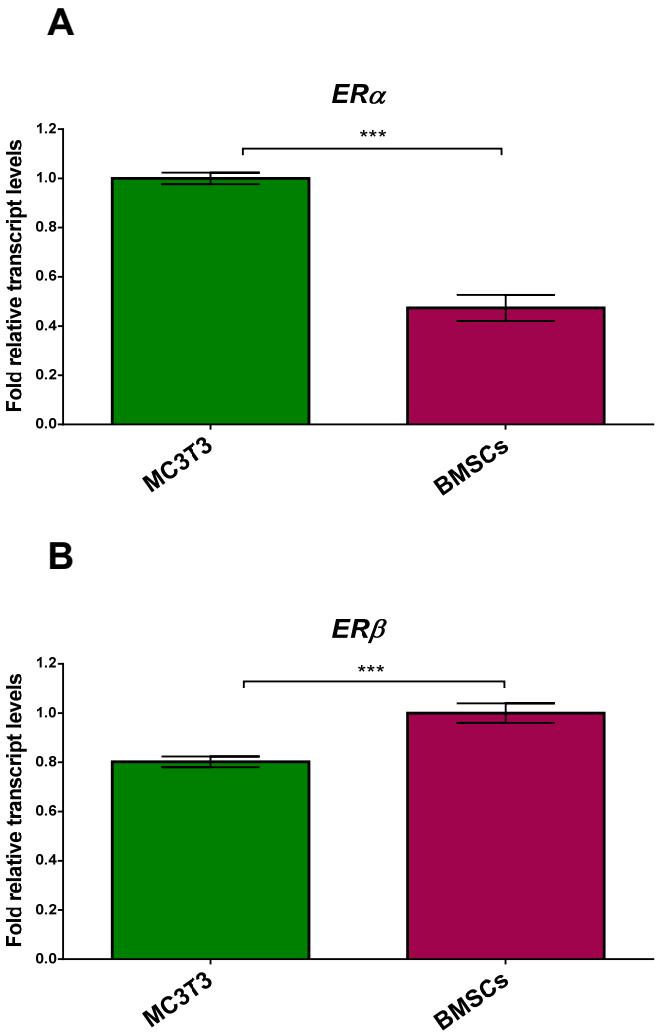

Figure 6-3. *Expression of ERα (A) and ERβ (B) in murine BMSCs compared to murine osteoblast-like MC3T3-E1 cells. Bar graphs illustrate fold changes ($2^{-\Delta\Delta C_T}$) in relative mRNA transcript levels normalised to the endogenous reference (β-Actin). The range of gene expression is indicated by $2^{-(\Delta\Delta C_T + SD)}$ and $2^{-(\Delta\Delta C_T - SD)}$, where SD is the standard deviation of the $\Delta\Delta C_T/\Delta C_T$ value. Statistical analysis was performed at the level of ΔC_T in order to exclude potential bias due to averaging of data transformed through the $2^{-\Delta\Delta C_T}$ equation; n = cells from 3 mice; ***P<0.001.*

6.4.2. Estrogen-facilitated, BMP-directed osteogenic differentiation of BMSCs

Osteogenic culture medium (phenol red-free α-MEM containing 10% charcoal-stripped FCS, 50 μM β-mercaptoethanol, 100 ng/ml rhBMP-2, 100μM ascorbate-2-phosphate) was supplemented with estrogen/17-β-estradiol (E2), in concentrations of 10 pM, 100 pM, 10 nM and 100 nM, to determine which concentration of E2 promoted BMP-2-directed osteogenic differentiation of BMSCs. Following culture for 28 days in basal (phenol red-free α-MEM containing 10% charcoal-stripped FCS, 50 μM β-mercaptoethanol) medium, osteogenic medium and osteogenic medium containing the different concentrations of E2, expression of *Alpl* was determined as an index of osteogenic differentiation of BMSCs.

Expression of *Alpl* was significantly upregulated (P<0.001) in response to BMP-2 in the osteogenic medium compared to basal culture conditions. In comparison to osteogenic culture conditions, a significant increase (P<0.05) in the expression of *Alpl* was observed in BMSC cells cultured for 28 days in osteogenic medium supplemented with 100 nM E2 (Fig. 6-4).

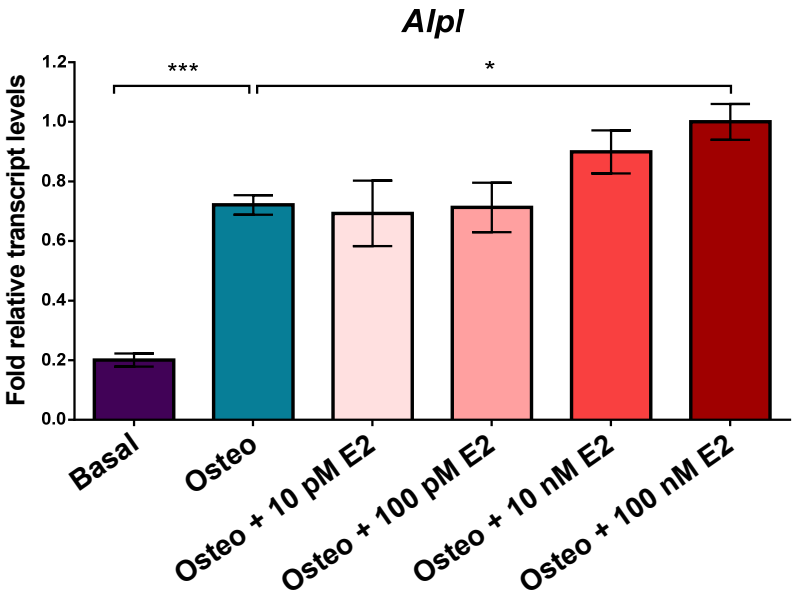

Figure 6-4. *BMP-2-directed osteogenic response of BMSCs in presence of 17-β-estradiol (E2) - Alpl expression in day-28 cultures of BMSCs in basal medium, osteogenic medium and osteogenic medium supplemented with 17-β-estradiol (E2). Bar graph illustrates fold changes ($2^{-\Delta\Delta C_T}$) in relative mRNA transcript levels normalised to the endogenous reference (β-Actin). The range of gene expression is indicated by $2^{-(\Delta\Delta C_T + SD)}$ and $2^{-(\Delta\Delta C_T - SD)}$, where SD is the standard deviation of the $\Delta\Delta C_T/\Delta C_T$ value. Statistical analysis was performed at the level of ΔC_T in order to exclude potential bias due to averaging of data transformed through the $2^{-\Delta\Delta C_T}$ equation; n = cells from 3 mice; *P<0.05.*

Moreover, culture of BMSCs of 14-week-old *Bag-1*$^{+/+}$ and *Bag-1*$^{+/-}$ female mice for 28 days in osteogenic medium containing 100 nM E2 resulted in significant increases ($P<0.05$, $P<0.001$) in the expression of *Bmpr2* (BMP type II receptor), compared to BMSC cultures in osteogenic medium (Fig. 6-5A and 6-5B).

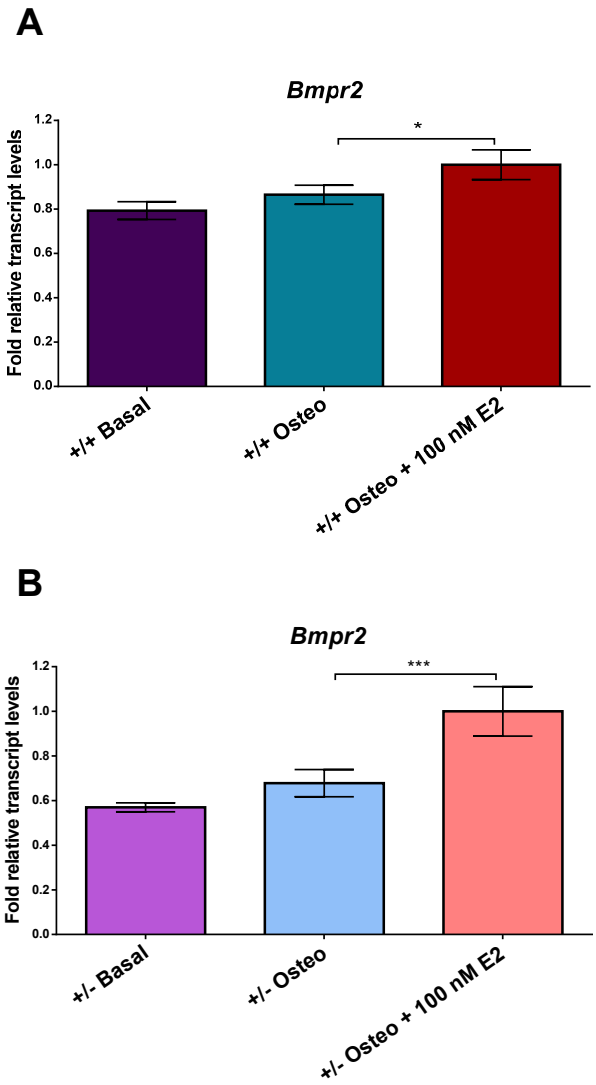

Figure 6-5. *BMP-2-directed osteogenic response of BMSCs in presence of 17-β-estradiol (E2) – Bmpr2 expression in day-28 cultures of BMSCs of Bag-1*$^{+/+}$ *(A) and Bag-1*$^{+/-}$ *(B) female mice in basal medium, osteogenic medium and osteogenic medium supplemented with 17-β-estradiol (E2). Bar graphs illustrate fold changes ($2^{-\Delta\Delta C}{}_T$) in relative mRNA transcript levels normalised to the endogenous reference (β-Actin). The range of gene expression is indicated by $2^{-(\Delta\Delta C}{}_T{}^{+ SD)}$ and $2^{-(\Delta\Delta C}{}_T{}^{- SD)}$, where SD is the standard deviation of the $\Delta\Delta C_T/\Delta C_T$ value. Statistical analysis was performed at the level of ΔC_T in order to exclude potential bias due to averaging of data transformed through the $2^{-\Delta\Delta C}{}_T$ equation; n = cells from 3 mice; *P<0.05, ***P<0.001.*

6.4.3. Interaction between endogenous BAG-1 and HSC70 in BMSCs

BMSCs of *Bag-1*$^{+/+}$ mice were cultured in basal conditions for 28 days and the interaction of BAG-1 and HSC70 determined by co-immunoprecipitation (Fig. 6-6). Whole cell lysate was kept at a proportion of 1/60 of the total amount of protein. Half of the remaining lysate was incubated with rabbit polyclonal IgG α-BAG-1 primary antibody (C-16) to investigate the interaction between BAG-1 and HSC70/HSP70 while the other half of the lysate was incubated with rabbit pre-immune control serum (PIS) to monitor non-specific interactions.

Immunoblot of the whole cell lysate probed with mouse monoclonal IgG α-HSC70 antibody exhibited a band specific for HSC70 protein (70 kDa) and probing with the rabbit polyclonal IgG α-BAG-1 antibody (C-16) yielded bands specific for BAG-1L (50 kDa) and BAG-1S (32 kDa) proteins (Fig. 6-6, Lane1, top and bottom boxes). As shown previously (refer to section 5.3.1.), BAG-1S was expressed as a predominant BAG-1 isoform in mouse BMSCs (Fig. 6-6, Lane1, top and bottom boxes).
Immunoblot of the IP fraction of the lysate probed with mouse monoclonal IgG α-HSC70 antibody exhibited a band specific for HSC70 protein (70 kDa) in the fraction pre-incubated with rabbit polyclonal IgG α-BAG-1 antibody (C-16) (Fig. 6-6, Lane 3 top box). There was no visible band corresponding to HSC70 in the rabbit pre-immune control serum-treated lysate fraction (Fig. 6-6, Lane 2, top box).
Immunoblot of the IP fraction of the lysate probed with rabbit polyclonal IgG α- BAG-1 antibody (C-16) exhibited presence of bands specific for BAG-1L (50 kDa) and BAG-1S (32 kDa) proteins in the fraction pre-incubated with rabbit polyclonal IgG α-BAG-1 antibody (C-16) (Fig. 6-6, Lane 3, bottom box). Furthermore bands corresponding to the heavy (~50 kDa) and light (~25 kDa) chain of Immunoglobulin G (IgG) of the denatured IP antibody (Fig. 6-6, Lane 3, bottom box) were visible.

Immunoblot of the IP fraction of the lysate pre-treated with rabbit pre-immune control serum exhibited strong non-specific bands after probing with the rabbit polyclonal IgG α-BAG-1 primary antibody (C-16), due to the use of goat α-rabbit secondary antibody against rabbit polyclonal IgG α-BAG-1 antibody. The immunoblot exhibited strong bands corresponding to the heavy (~50 kDa) and light (~25 kDa) chain of Immunoglobulin G (IgG) as IgG is the most abundant antibody isotype present in the circulation (Fig. 6-6, Lane 2, bottom box).

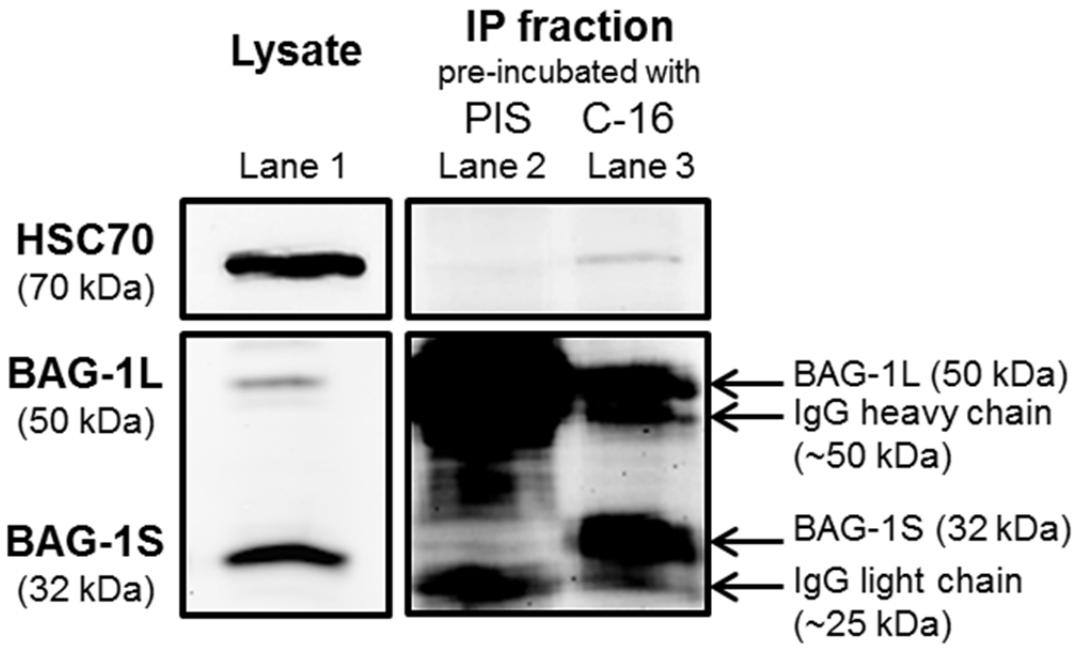

Figure 6-6. *Immunoblot demonstrating the presence of BAG-1/HSC-70 interaction in 14 week-old mouse Bag-1$^{+/+}$ BMSCs cultured for 28 days in basal conditions. Whole cell lysate was kept at a proportion of 1/60 of the total amount of protein. Immunoprecipitations were performed by use of rabbit polyclonal IgG α- BAG-1 primary antibody (C-16) or with control pre-immune rabbit serum (PIS) on IP fraction of lysate. Expressions of HSC70, BAG-1L and BAG-1S were analysed by immunoblotting*.

6.4.4. Effect of inhibition of the interaction between BAG-1 and HSC70 by Thioflavin-S on estrogen-facilitated, BMP-directed osteogenic differentiation of *Bag-1*$^{+/+}$ and *Bag-1*$^{+/-}$ BMSCs

The interaction between the ATPase domain of HSC70 and the C-terminal BAG domain of BAG-1 is disrupted by Thioflavin-S, which functions as a small-molecule chemical inhibitor of BAG-1-HSC70 binding. Thioflavin-S was therefore utilised to investigate the functional significance of BAG-1-mediated protein-protein interactions, specifically BAG-1-regulated activation of ERs by HSC70 in estrogen-facilitated BMP-directed osteogenic differentiation of BMSCs. BMSCs of 14-week-old *Bag-1*$^{+/+}$ and *Bag-1*$^{+/-}$ female mice were cultured for 28 days in basal medium (phenol red-free α-MEM containing 10% charcoal-stripped FCS, 50 μM β-mercaptoethanol), osteogenic medium (phenol red-free α-MEM containing 10% charcoal-stripped FCS, 50 μM β-mercaptoethanol, 100 ng/ml rhBMP-2, 100 μM ascorbate-2-phosphate), osteogenic medium supplemented with 100 nM 17-β-estradiol (E2), and osteogenic medium containing 100 nM E2 and 5 μM Thioflavin-S. Day-28 BMSC cultures were harvested for the analyses of expression of osteogenic genes: *Runx-2*, *Osterix*, *Alpl* and

Osteocalcin, estimation of tissue non-specific alkaline phosphatase (ALPL) specific activity and DNA concentration.

Compared to cultures in basal medium, day-28 cultures of BMSCs of *Bag-1*$^{+/+}$ mice exhibited significant increases (P<0.001) in the expression of osteogenic genes, namely *Runx-2*, *Osterix*, *Alpl* and *Osteocalcin* and specific activity of ALPL in osteogenic and E2-containing osteogenic media (Fig. 6-7, 6-9A). In contrast, as demonstrated previously, BMSCs of *Bag-1*$^{+/-}$ female mice did not exhibit a robust osteogenic response to BMP-2 after culture for 28 days in osteogenic medium (Fig. 6-8, 6-9B). However, expression of osteogenic genes and the specific activity of ALPL were significantly upregulated (P<0.001) in day-28 BMSC cultures of *Bag-1*$^{+/+}$ and *Bag-1*$^{+/-}$ female mice in osteogenic medium supplemented with E2, compared to day-28 cultures of BMSCs in osteogenic and basal media (Fig. 6-7, 6-8, 6-9). In comparison to the robust osteogenic responses by *Bag-1*$^{+/+}$ and *Bag-1*$^{+/-}$ BMSCs as a consequence of culture for 28 days in E2-containing osteogenic medium, osteogenic responses of BMSCs of *Bag-1*$^{+/+}$ and *Bag-1*$^{+/-}$ mice were significantly decreased (P<0.001) following culture for 28 days in E2-containing osteogenic medium supplemented with Thioflavin-S (Fig. 6-7, 6-8, 6-9).

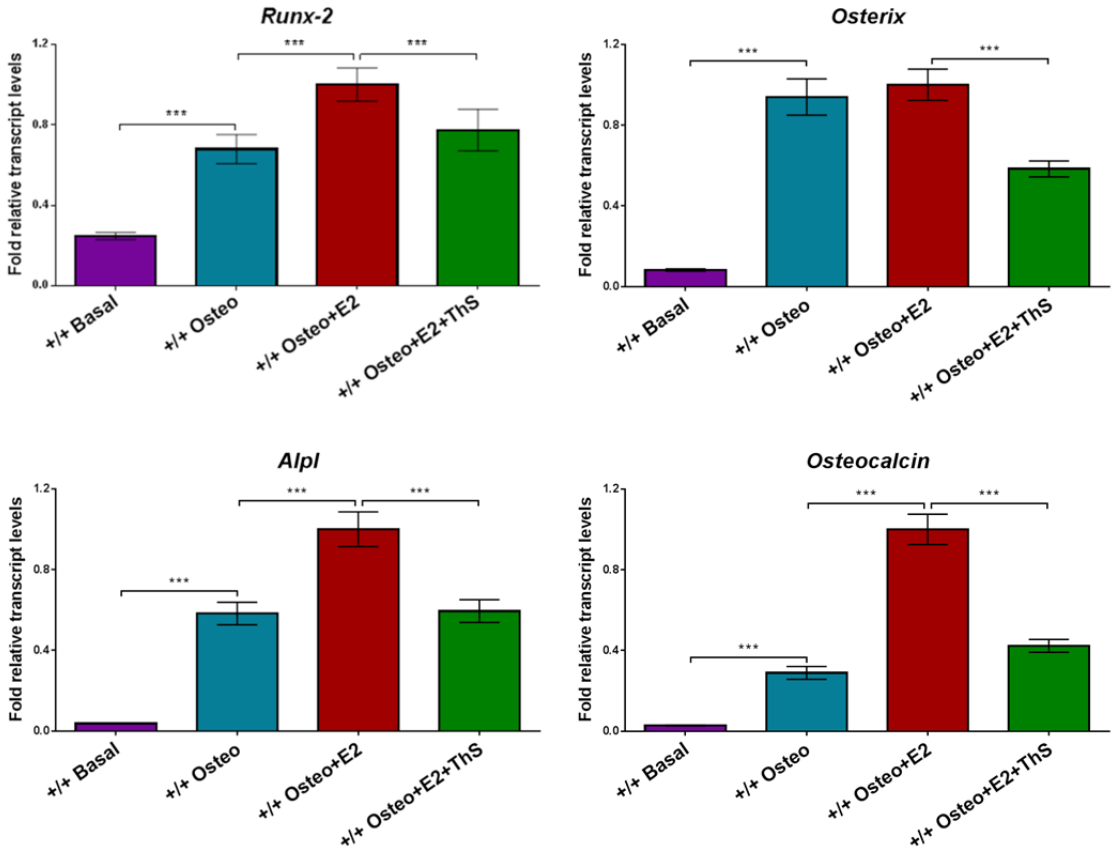

Figure 6-7*. Expression of osteogenic genes in day-28 cultures of BMSCs of female Bag-1$^{+/+}$ mice. Bar graphs illustrate fold changes ($2^{-\Delta\Delta C_T}$) in relative mRNA transcript levels normalised to the endogenous reference (β-Actin). The range of gene expression is indicated by $2^{-(\Delta\Delta C_T + SD)}$ and $2^{-(\Delta\Delta C_T - SD)}$, where SD is the standard deviation of the $\Delta\Delta C_T/\Delta C_T$ value. Statistical analysis was performed at the level of ΔC_T in order to exclude potential bias due to averaging of data transformed through the $2^{-\Delta\Delta C_T}$ equation. Results are expressed as mean ± SD; n = cells from 4 mice per group; *** P<0.001.*

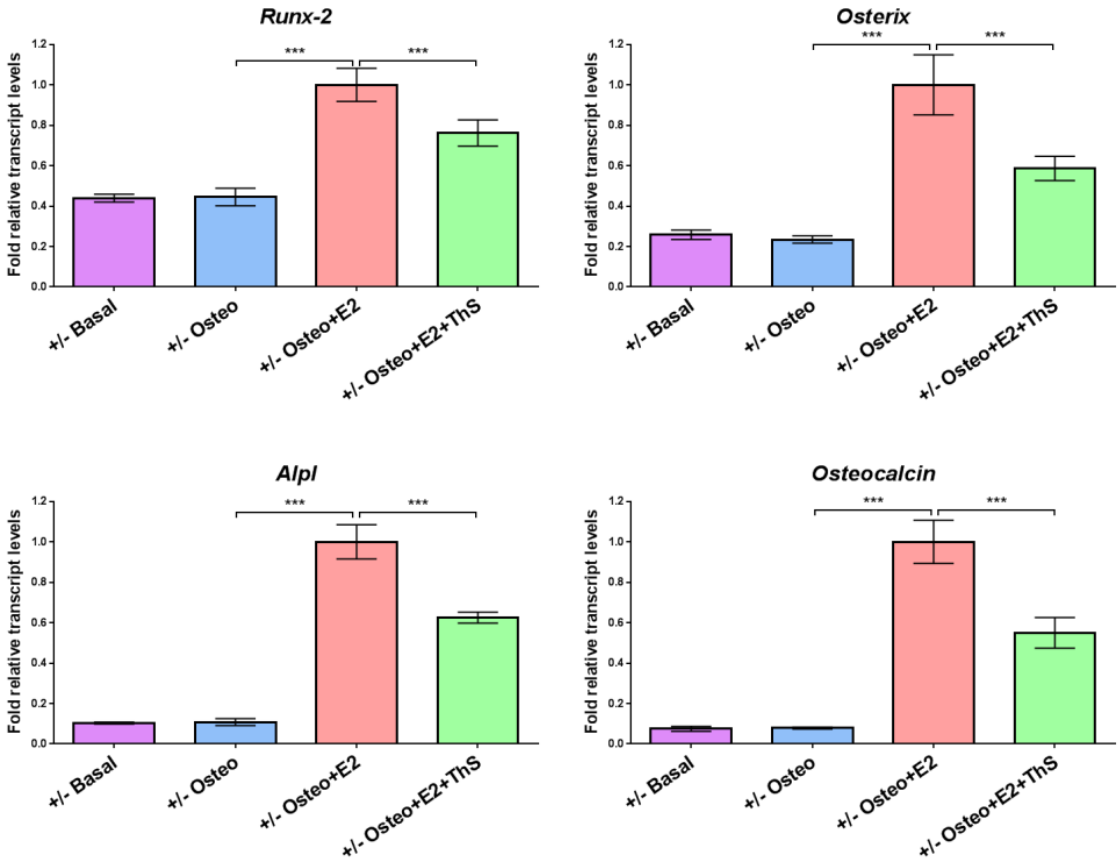

Figure 6-8*. Expression of osteogenic genes in day-28 cultures of BMSCs of female Bag-1$^{+/-}$ mice. Bar graphs illustrate fold changes ($2^{-\Delta\Delta C_T}$) in relative mRNA transcript levels normalised to the endogenous reference (β-Actin). The range of gene expression is indicated by $2^{-(\Delta\Delta C_T + SD)}$ and $2^{-(\Delta\Delta C_T - SD)}$, where SD is the standard deviation of the $\Delta\Delta C_T/\Delta C_T$ value. Statistical analysis was performed at the level of ΔC_T in order to exclude potential bias due to averaging of data transformed through the $2^{-\Delta\Delta C_T}$ equation. Results are expressed as mean ± SD; n = cells from 4 mice per group; *** P<0.001.*

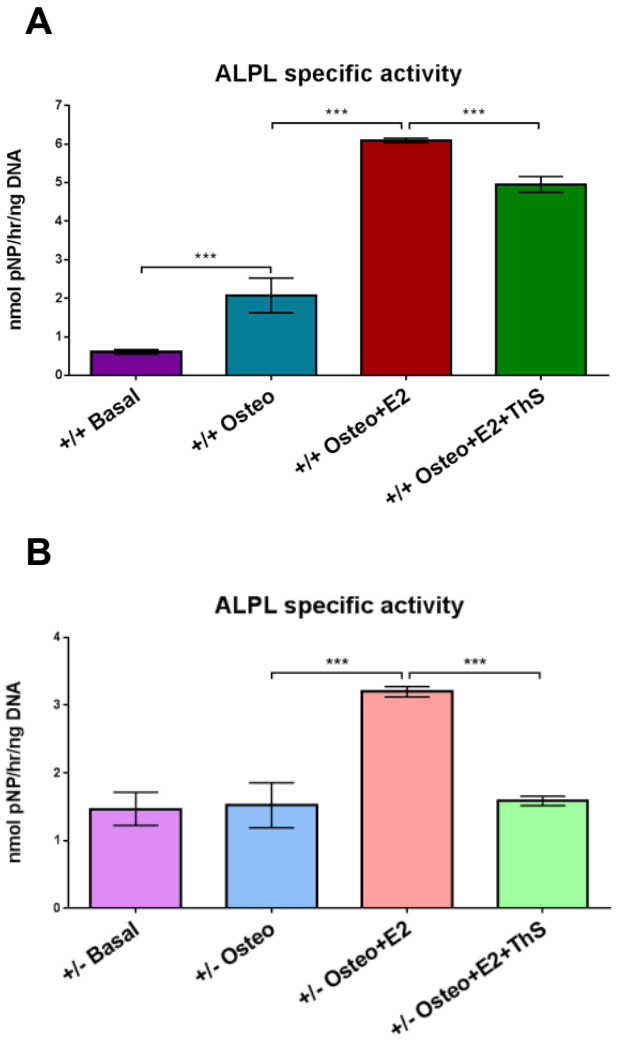

Figure 6-9. *Specific activity of ALPL in day-28 cultures of BMSCs of female Bag-1$^{+/+}$ (A) and Bag-1$^{+/-}$ (B) mice. Results are expressed as mean ± SD; n = cells from 4 mice per group; *** P<0.001.*

No differences in cell number /DNA contcentration between day-28 cultures of BMSCs (of both *Bag-1*$^{+/+}$ and *Bag-1*$^{+/-}$ mice) in osteogenic medium containing E2 and osteogenic medium containing E2 and Thioflavin-S, confirmed that Thioflavin-S was not toxic to cells and did not influence BMSC viability and proliferation (Fig. 6-10)

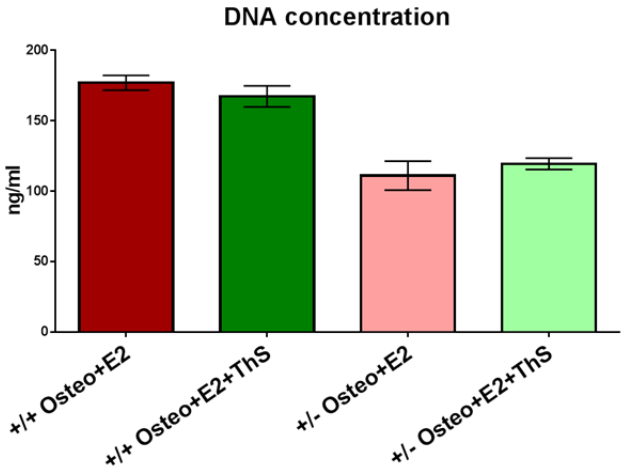

Figure 6-10. *DNA concentration of day-28 cultures of BMSCs of female Bag-1*$^{+/+}$ *(A) and Bag-1*$^{+/-}$ *(B) mice. Results are expressed as mean ± SD; n = cells from 4 mice per group.*

6.4.5. Effect of inhibition of binding of BAG-1 to HSC70 by the BAG domain-derived short peptide on estrogen-facilitated BMP-directed osteogenic differentiation of *Bag-1*$^{+/+}$ and *Bag-1*$^{+/-}$ BMSCs

The interaction between the ATPase domain of HSC70 and the C-terminal BAG domain (composed of three alpha-helices) of BAG-1 is disrupted by a short peptide derived from helix 2 of the BAG domain, which exhibits high specificity for binding to the ATPase domain of HSC70 and prevents the interaction between BAG-1 and HSC70. The BAG domain-derived short peptide was therefore utilised to investigate the functional significance of BAG-1-mediated protein interactions, specifically BAG-1-regulated activation of ERs by HSC70, in estrogen-facilitated BMP-directed osteogenic differentiation of BMSCs.

BMSCs of 14-week-old *Bag-1*$^{+/+}$ and *Bag-1*$^{+/-}$ female mice were cultured for 28 days in basal medium (phenol red-free α-MEM containing 10% charcoal-stripped FCS, 50 μM β-mercaptoethanol), osteogenic medium (phenol red-free α-MEM containing 10% charcoal-stripped FCS, 50 μM β-mercaptoethanol, 100 ng/ml rhBMP-2, 100 μM ascorbate-2-phosphate) supplemented with 100 nM 17-β-estradiol (E2), and osteogenic medium containing 100 nM E2 in addition to either 10 μM H2-Penetratin or 10 μM H2mutant-Penetratin. Day-28 BMSC cultures were harvested for the analyses of expression of osteogenic genes, namely *Runx-2*, *Osterix*, *Alpl* and *Osteocalcin*, estimation of tissue nonspecific alkaline phosphatase (ALPL) specific activity, osteocalcin and DNA concentrations.

In comparison to cultures in basal medium, BMSCs of *Bag-1*$^{+/+}$ and *Bag-1*$^{+/-}$ mice exhibited significant increases ($p<0.001$) in the expression of osteogenic genes, namely *Runx-2*, *Osterix*, *Alpl* and *Osteocalcin* (Fig. 6-11, 6-12), activity of ALPL (Fig. 6-13A, 6-13B) and osteocalcin concentration (Fig. 6-14A, 6-14B) following culture for 28 days in osteogenic medium containing E2. Culture of BMSCs for 28 days in osteogenic medium containing E2 and H2-Penetratin resulted in significant decreases ($P<0.001$) in the estrogen-facilitated BMP-directed osteogenic responses of BMSCs of both *Bag-1*$^{+/+}$ and *Bag-1*$^{+/-}$ mice (Fig. 6-11, 6-12, 6-13, 6-14). In contrast, no differences in expression of osteogenic genes (Fig. 6-13, 6-14), specific activity of ALPL (Fig. 6-13A, 6-13B) and osteocalcin concentration (Fig. 6-14A, 6-14B) were observed between cultures of BMSCs (of both *Bag-1*$^{+/+}$ and *Bag-1*$^{+/-}$ mice) in osteogenic medium containing E2 and osteogenic medium containing E2 along with H2mutant-Penetratin.

Levels of osteogenic genes (Fig. 6-11, 6-12), ALPL specific activity (Fig. 6-13A, 6-13B) and osteocalcin concentration (Fig. 6-14A, 6-14B) were significantly increased ($P<0.001$) in BMSCs (of both *Bag-1*$^{+/+}$ and *Bag-1*$^{+/-}$ mice) in osteogenic medium containing E2 and H2mutant-Penetratin in comparison to osteogenic medium containing E2 and H2-Penetratin.

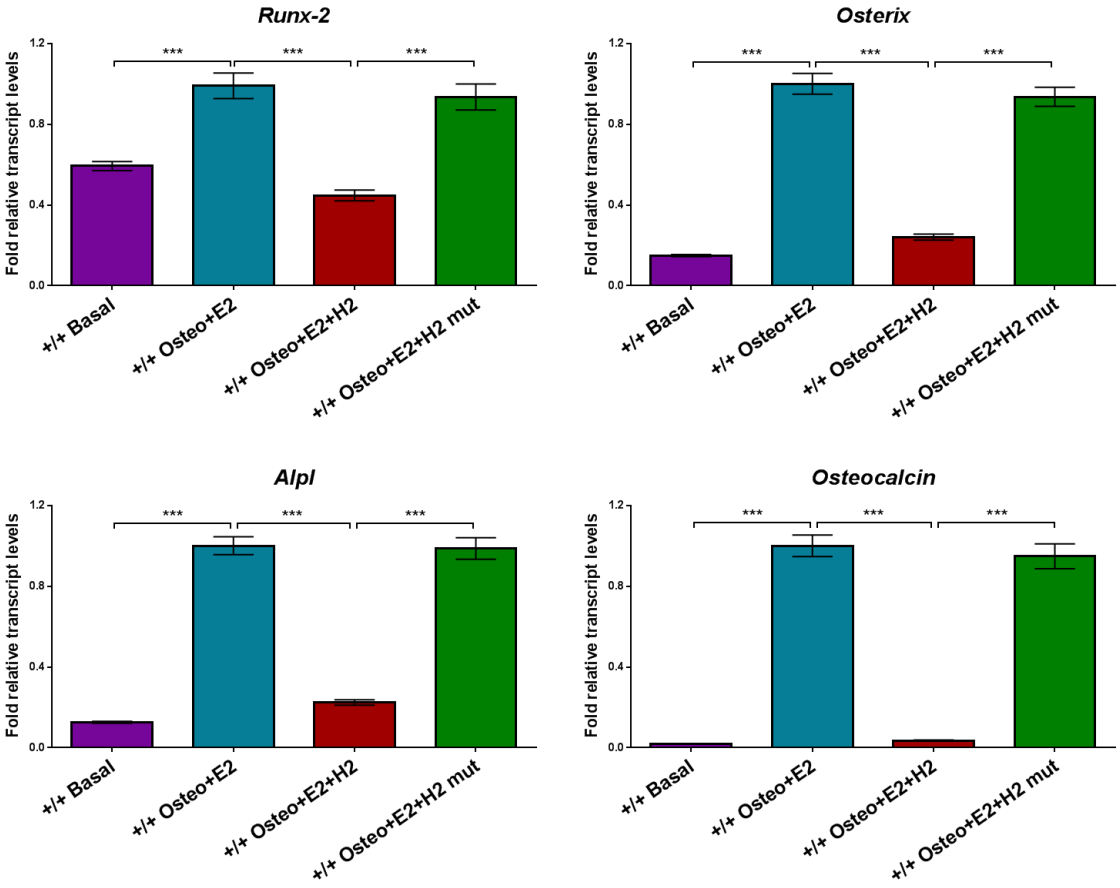

Figure 6-11. *Expression of osteogenic genes in day-28 cultures of BMSCs of female Bag-1$^{+/+}$ mice. Bar graphs illustrate fold changes ($2^{-\Delta\Delta C_T}$) in relative mRNA transcript levels normalised to the endogenous reference (β-Actin). The range of gene expression is indicated by $2^{-(\Delta\Delta C_T + SD)}$ and $2^{-(\Delta\Delta C_T - SD)}$, where SD is the standard deviation of the $\Delta\Delta C_T/\Delta C_T$ value. Statistical analysis is performed at the level of ΔC_T in order to exclude potential bias due to averaging of data transformed through the $2^{-\Delta\Delta C_T}$ equation. Results are expressed as mean ± SD; n = cells from 3 mice per group; *** P<0.001.*

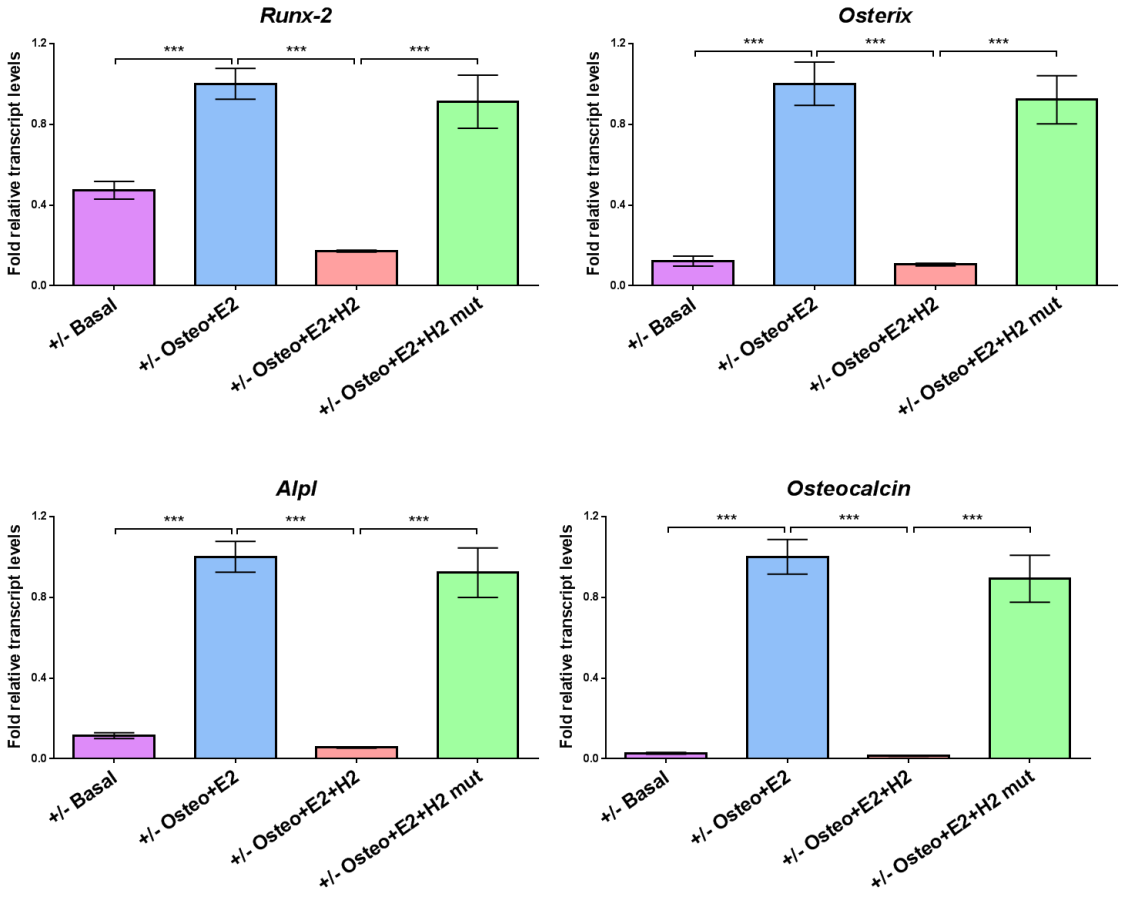

Figure 6-12. *Expression of osteogenic genes in day-28 cultures of BMSCs of female Bag-1$^{+/-}$ mice. Bar graphs illustrate fold changes ($2^{-\Delta\Delta C}{}_T$) in relative mRNA transcript levels normalised to the endogenous reference (β-Actin). The range of gene expression is indicated by $2^{-(\Delta\Delta C}{}_T{}^{+\,SD)}$ and $2^{-(\Delta\Delta C}{}_T{}^{-\,SD)}$, where SD is the standard deviation of the $\Delta\Delta C_T/\Delta C_T$ value. Statistical analysis was performed at the level of ΔC_T in order to exclude potential bias due to averaging of data transformed through the $2^{-\Delta\Delta C}{}_T$ equation. Results are expressed as mean ± SD; n = cells from 3 mice per group; *** P<0.001.*

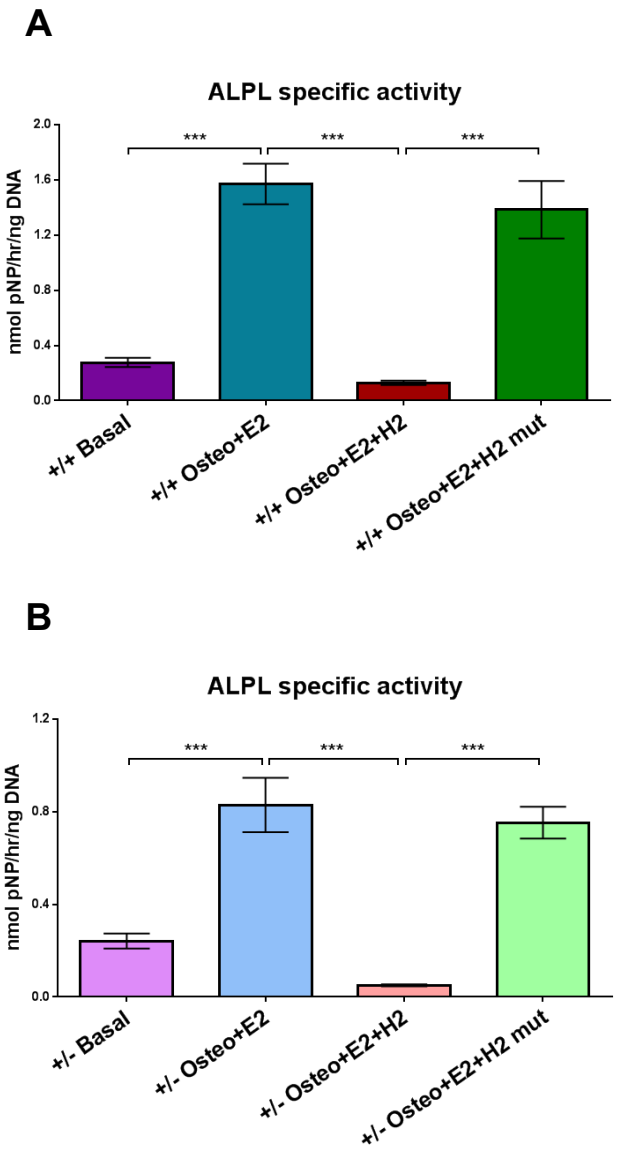

Figure 6-13. *Specific activity of ALPL in day-28 cultures of BMSCs of female Bag-1$^{+/+}$ and Bag-1$^{+/-}$ mice. Results are expressed as mean ± SD; n = cells from 3 mice per group; *** P<0.001.*

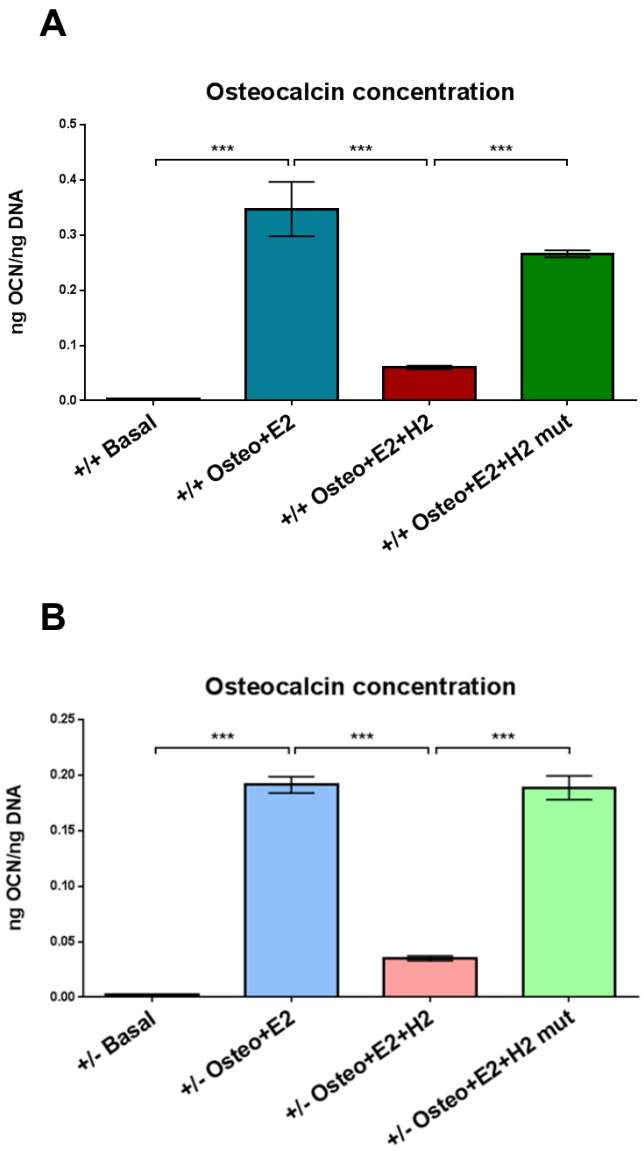

Figure 6-14. *Osteocalcin concentration in day-28 cultures of BMSCs of female Bag-1$^{+/+}$ and Bag-1$^{+/-}$ mice. Results are expressed as mean ± SD; n = cells from 3 mice per group; *** P<0.001.*

BMSC viability and proliferation were not affected by the peptides as demonstrated by no differences in cell number / DNA concentration between day-28 cultures of BMSCs (of both *Bag-1*$^{+/+}$ and *Bag-1*$^{+/-}$ mice) in osteogenic medium containing E2, and osteogenic medium containing E2 and the short peptides (Fig. 6-15).

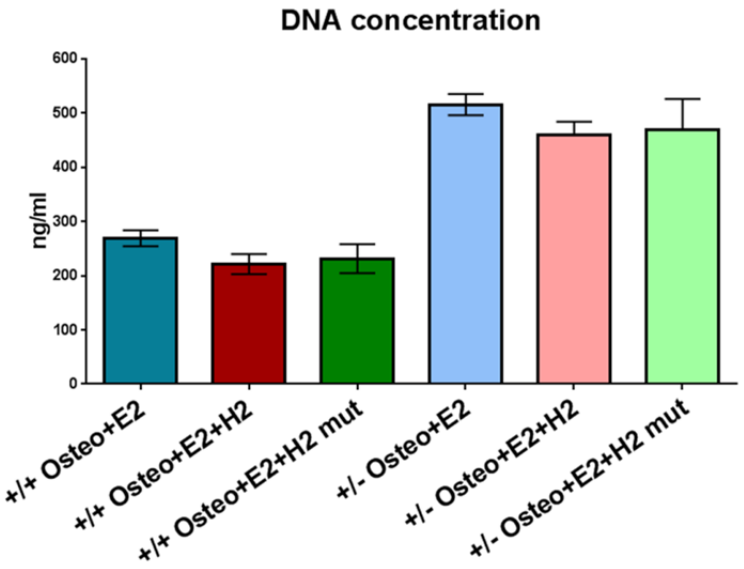

Figure 6-15. *DNA concentration in day-28 cultures of BMSCs of female Bag-1*$^{+/+}$ *and Bag-1*$^{+/-}$ *mice. Results are expressed as mean ± SD; n = cells from 3 mice per group.*

6.5. Summary of results

a) Murine BMSCs express estrogen receptors, namely *ER*α and *ER*β.
b) BMSCs of *Bag-1*$^{+/+}$ and *Bag-1*$^{+/-}$ mice, treated with E2 (100 nM) exhibit increased responsiveness to BMP-2, demonstrated by upregulation of *Bmpr2* expression, and enhanced E2-facilitated, BMP-2-directed osteogenic differentiation, evidenced by upregulation of osteogenic gene expression, increased ALPL specific activity and osteocalcin concentration.
c) The BAG-1 proteins interact with HSC70 in murine BMSCs.
d) Inhibition of binding of BAG-1 to HSC70 by Thioflavin-S results in downregulation of E2/ER-facilitated BMP-directed osteogenic responses of BMSCs of both *Bag-1*$^{+/+}$ and *Bag-1*$^{+/-}$ mice.
e) The short peptide derived from helix 2 of the BAG domain inhibits binding of BAG-1 to HSC70, thereby resulting in downregulation of E2/ER-facilitated BMP-directed osteogenic responses of BMSCs of both *Bag-1*$^{+/+}$ and *Bag-1*$^{+/-}$ mice.

6.6. Discussion

The present study has demonstrated, for the first time, the importance of the interaction between BAG-1 and HSC70 in mediating E2/ER-facilitated BMP-2-directed osteogenic differentiation of murine BMSCs.

Estrogen (E2) plays an important role in osteoblast function and exerts a protective effect on bone (Eriksen et al., 1988). The functions of estrogen are mediated by two isoforms of the estrogen receptor (ER), namely ERα and ERβ, members of the nuclear hormone receptor (NHR) family that act as ligand-dependent transcription factors (Mangelsdorf et al., 1995). Osteoblasts and bone marrow cells have been shown to express both ERα and ERβ (Arts et al., 1997, Lim et al., 1999). Gruber and co-workers have demonstrated the expression of *ERα* and *ERβ* in mouse primary bone marrow cells alongside osteoblastic MC3T3-E1 cells using conventional RT-PCR (Gruber et al., 1999). Similarly, the present study was able to demonstrate the expression of ERα and ERβ by primary murine BMSCs. Moreover, in the present study, in comparison to MC3T3-E1 cells, significantly lower levels of *ERα* expression were observed in mouse BMSCs cultured in basal medium, while the expression of *ERβ* was significantly higher in basal cultures of mouse BMSCs.

To investigate the role of BAG-1 in the transcriptional response of breast cancer cells to estrogen, concentrations of estrogen ranging from 1 pM to 1 nM were utilised (Cutress et al., 2003). In a separate study, MC3T3-E1 cells were treated with 100 nM estrogen to establish the effects of estrogen on BMP-induced osteoblastic differentiation (Matsumoto et al., 2013). Therefore, in the present study, a range of concentrations of estrogen from 10 pM to 100 nM were applied to the cultures of mouse BMSCs to determine the optimal concentration of estrogen capable of facilitating BMP-2-directed ostegenic differentiation. Significant upregulation of *Bmpr2* expression was observed in BMP-2-containing cultures of BMSCs (of both *Bag-1*$^{+/+}$ and *Bag-1*$^{+/-}$ female mice) supplemented with 100 nM estrogen. Thus, estrogen enhanced the responsiveness of BMSCs to BMP-2 by upregulating *Bmpr2* expression and facilitated robust BMP2-directed osteogenic differentiation of BMSCs, as previously demonstrated by Matsumoto and co-workers (Matsumoto et al., 2013).

Treatment of mouse BMSCs with BMP-2 has been shown to increase ALPL activity in conjunction with the number of adipocytes, indicating the ability of BMP-2 to stimulate both osteoblastic and adipogenic differentiation of the mouse BMSC population (Okazaki et al., 2002). The study also showed that co-treatment of mouse BMSCs with BMP-2 and estrogen enhanced ALP activity and suppressed adipogenic differentiation,

and the regulatory action of estrogen on BMSC differentiation occurred in an ER-specific manner, but without ER subtype specificity. Thus, estrogen is able to directly modulate BMP-2-directed differentiation of BMSCs into osteoblasts and adipocytes, specifically, by supporting a lineage shift toward the osteoblast phenotype.

BAG-1 potentiates the activity of some NHRs and inhibits the activity of others; moreover, the spectrum of BAG-1 isoforms that regulate NHR activity is distinct for different receptors (Townsend et al., 2003b). Therefore, there is probably no single mechanism of action that accounts for the effects of BAG-1 proteins on NHRs. However, it is important to recognise that the interaction of BAG-1 with NHRs requires the BAG-1 carboxy terminus and is mediated by HSC70/HSP70 chaperone proteins, which can interact with most NHRs in their non-native states and assist them to achieve functional active conformations (Gassler et al., 2001, Cato and Mink, 2001). BAG-1S (the predominant isoform in murine BMSCs) has been demonstrated to stimulate HSC70-mediated refolding of artificially denatured protein substrates *in vitro* (Luders et al., 2000). Although the protein folding activity of HSC70/HSP70 has been the focus of most studies, chaperones also play important roles in protein translocation, degradation and heterocomplex assembly, which are likely to be regulated by BAG-1 (Agarraberes and Dice, 2001). Since the various BAG-1 isoforms, in association with HSC70/HSP70, interact with NHRs, it is possible that BAG-1-dependent functional changes result indirectly from changes in the behaviour of HSC70/HSP70 towards the target proteins (Cheung and Smith, 2000, Cato and Mink, 2001).

The present study applied the co-immunoprecipitation technique to determine whether endogenous BAG-1 and HSC70 interact in mouse primary BMSCs and demonstrated the presence of BAG-1:HSC70 interaction in BMSCs. The interaction of the BAG-1 co-chaperone with HSC70/HSP70 regulates the chaperone activity of these proteins (Fig. 6-2, Townsend et al., 2003b). Briefly, in the ATP-bound form, the peptide-binding pocket of the chaperone molecule is open, permitting rapid binding and dissociation of the misfolded protein substrate. Hydrolysis of ATP causes the pocket to close, allowing the substrate to bind with high affinity to the ADP-bound form of the chaperone. Release of ADP and subsequent binding of ATP to the chaperone, referred to as nucleotide exchange, is stimulated by BAG-1 and enables release of the refolded protein substrate. Thus, by acting as a nucleotide exchange factor, BAG-1 plays an important role in the establishment of functional NHRs/ERs and modulates cellular responses to hormones, such as estrogen. Moreover, after hormone binding, BAG-1 has been shown to interact with ERs via HSC70 in a hormone-dependent manner and promote estrogen-dependent gene transcription (Cutress et al., 2003). Thus, before

hormone binding, BAG-1 can potentially alter the dynamics of complex assembly and the establishment of functional NHRs, and after hormone binding, BAG-1 can influence receptor-mediated transcription of hormone-responsive genes (Fig. 6-16, Cheung and Smith, 2000).

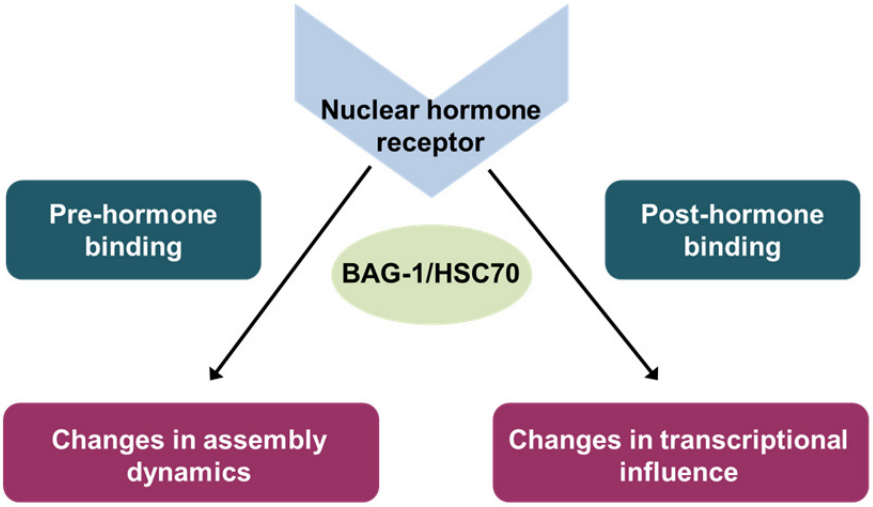

Figure 6-16. *Potential role of BAG-1 in nuclear hormone signalling (Adapted from Cheung and Smith, 2000)*

The BAG domain is composed of three alpha helices, which facilitate binding between BAG-1 and the ATPase domain of HSC70 (Takayama et al., 1999). Helices 2 and 3 are involved in electrostatic interactions with the ATPase domain of HSC70; helix 1 is not directly involved in binding, however, it contributes to intramolecular interactions that stabilise the overall structure of the BAG domain (Sondermann et al., 2001).

Compound collections obtained from the National Cancer Institute Developmental Therapeutics Programme (Rockville, MD) for detection of small molecule inhibitors of the BAG-1 – HSC70 interaction, resulted in the identification of NSC71948/Thioflavin-S - a mixture of components arising from the methylation and sulfonation of primulin base (Sharp et al., 2009a) (Fig. 6-17).

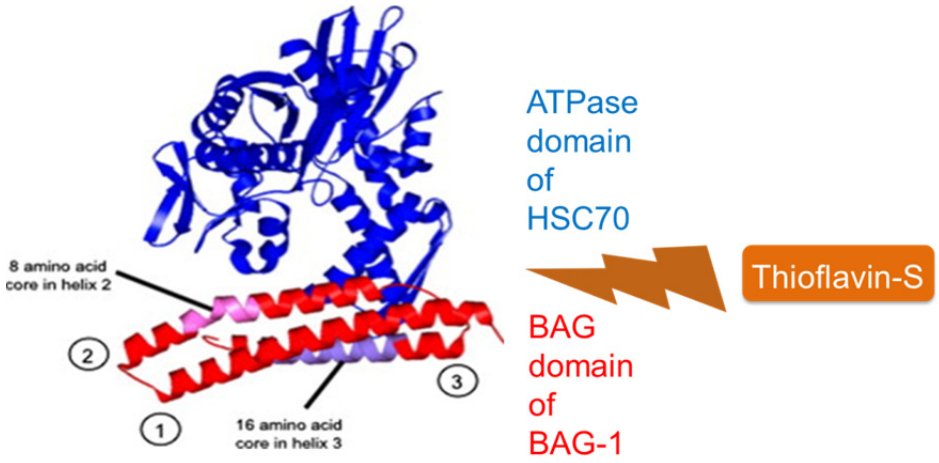

Figure 6-17. *Disruption of binding of BAG-1 to HSC70 by Thioflavin S; 1, 2 and 3 – helix1, helix 2 and helix 3 of BAG domain; adapted from Sharp et al., 2009b.*

Binding of BAG-1S to HSC70 and HSP70 in MCF7 breast cancer cells was observed to be decreased significantly following exposure to 100 μM Thioflavin S (Sharp et al., 2009a). Moreover, NSC71948/Thioflavin S was demonstrated to interfere with BAG-1-HSC/HSP70 binding and suppress BAG-1-mediated potentiation of VDR (vitamin D_3 receptor)-dependent transactivation of the vitamin D_3-responsive reporter construct (Sharp et al., 2009a). Furthermore, dose-dependent targeting of the BAG-1S:HSC70 interaction by Thioflavin S in human embryonic kidney (HEK293) cells demonstrated that Thioflavin S was capable of decreasing the binding between BAG-1S and HSC70 over the concentration range of 6.25 to 75 μM (Enthammer et al., 2013). In the present study, a low concentration (5 μM) of Thioflavin S was used to disrupt the interaction between BAG-1 and HSC70 in 28-day cultures of murine BMSCs. Since Thioflavin S was constituted in DMSO, it was critical that the cells were not exposed to potentially toxic levels of DMSO, especially in long-term cultures. By using a low concentration of Thioflavin S to disrupt the binding between BAG-1 and HSC70, it was possible to reduce the concentration of DMSO in the murine BMSC cultures to 0.05% and minimise cell toxicity.

Thioflavin S is able to disrupt the interaction between BAG-1 and HSC70 since the binding site for the compound lies within helix 2 of the BAG domain, which is required for the interaction with HSC70; alternatively, it is possible that Thioflavin S may bind elsewhere within BAG-1 and elicit a conformational change in the BAG domain leading to the loss of multiple interaction partners, including HSC70 (Sharp et al., 2009a). Although NSC71948/Thioflavin S serves as a useful tool to demonstrate the functional significance of BAG-1-mediated protein-protein interactions in estrogen-facilitated, BMP-2-directed osteogenic differentiation of BMSCs, the results should be interpreted

cautiously given NSC71948 is a mixture of compounds (Kelenyi, 1967, Enthammer et al., 2013) whose selectivity profile is not fully characterised and the likelihood of off-target effects cannot be ruled out.

A small region comprising of 8 amino acid residues of helix 2 of the BAG domain has been shown to be vital for binding of BAG-1 to HSC70 (Sharp et al., 2009b). Therefore, a short peptide, H2-Penetratin, containing the 8 amino acid binding core of helix 2, coupled via a peptide bond at its C-terminus to Penetratin, a cell permeable fragment of the Antennaepaedia protein that enhances cellular uptake, was used to inhibit the binding between BAG-1 and HSC70. A mutant peptide, H2mutant-Penetratin, with alanine (A) substitutions, particularly for arginine (R) residues at positions 205 and 206, representing the 'hot-spot' on the interaction surface between BAG-1 and HSC70, was used as a control peptide (Fig. 6-18).

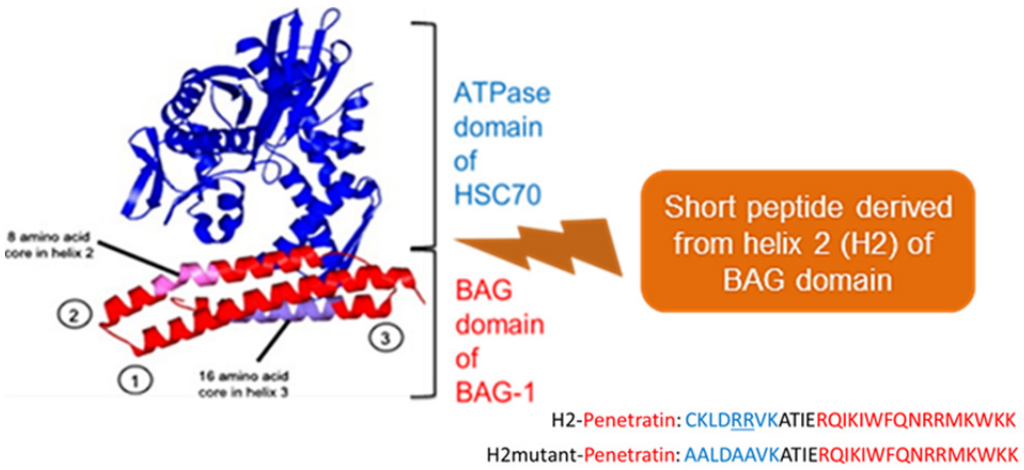

Figure 6-18. *Inhibition of binding of BAG-1 to HSC70 by the short peptide derived from helix 2 of the BAG domain; 1, 2 and 3 – helix1, helix 2 and helix 3 of BAG domain; adapted from Sharp et al., 2009b.*

Having tested the effects of varying concentrations (1 μM, 10 μM and 100 μM) of the BAG-1 peptide on inhibition of the BAG-1S:HSC70 interaction, significant inhibition of the binding between BAG-1S and HSC70 by the peptide was observed at concentrations of 10 μM and 100 μM (Sharp et al., 2009b). Thus, in the present study, the short peptides were applied to cultures of mouse BMSCs at a concentration of 10 μM.

The BAG-1 peptide has been demonstrated to bind the ATPase domain of HSC70 and exert its effects, such as growth inhibition in human breast cancer cells, by preventing the interaction between BAG-1 and HSC70 (Sharp et al., 2009b). Similarly, in our study, inhibition of binding of BAG-1 to HSC70 by the short peptide derived from helix 2 of the

BAG domain resulted in significant downregulation of estrogen-facilitated, BMP-2-directed osteogenic responses of BMSCs of both *Bag-1*$^{+/+}$ and *Bag-1*$^{+/-}$ mice. The mutant peptide with alanine substitutions for arginine residues at positions 205 and 206, representing the 'hot-spot' on the interaction surface between BAG-1 and HSC70, was significantly less active in downregulating the osteogenic responses, thereby confirming that the BAG-1 peptide was able to exert its effect by disrupting the BAG-1:HSC70 interaction.

The addition of Thioflavin S and short peptides derived from the BAG domain to cultures of BMSCs did not affect cell viability, as evidenced by negligible differences in cell number/DNA content between day-28 cultures of BMSCs in osteogenic medium containing E2 and osteogenic medium containing E2 and Thioflavin-S or the short peptides derived from the BAG domain. Thus, the downregulation of estrogen-facilitated, BMP-2-directed osteogenic responses of BMSCs by Thioflavin S and the short peptide derived from helix 2 of the BAG domain was due to inhibition of the BAG-1:HSC70 interaction and not as a result of compromised cell viability. However, it is important to note that, in addition to HSC70 binding, the BAG domain facilitates binding of BAG-1 to RAF-1 through helices 1and 2 (Song et al., 2001). As the binding sites for HSC70 and RAF-1 overlap, which can result in competitive binding, more specific mutations in the HSC70 binding region of the BAG domain would yield valuable information on the significance of the independent role of the HSC70 interaction in regulation of cellular functions by BAG-1.

In conclusion, this study has confirmed that murine BMSCs express estrogen receptors, namely *ER*α and *ER*β, and estrogen facilitates BMP-2 directed osteogenic differentiation of mouse BMSCs. BAG-1 and HSC70 interact in mouse BMSCs and disruption of this interaction leads to downregulation of E2/ER-facilitated, BMP-directed osteogenic responses of BMSCs of both *Bag-1*$^{+/+}$ and *Bag-1*$^{+/-}$ mice. This is the first study that has demonstrated the significance of BAG-1-regulated activation of ERs by HSC70 in E2/ER-facilitated, BMP-directed osteogenic differentiation of BMSCs.

Chapter 7

General discussion

7. General discussion

7.1. Summary of the role of *Bag-1* in skeletal development

Work described in this thesis has elucidated the important functions of *Bag-1* in skeletal development (Fig. 7-1). The current studies have demonstrated upregulation of chondrocyte hypertrophy and matrix mineralisation in the cartilage nodules generated by limb bud mesenchymal cells lacking both *Bag-1* alleles. This observation highlights the importance of *Bag-1* in the regulation of chondrocyte development and transition from chondrogenesis to osteogenesis at the vascular front during the process of endochondral ossification. Analyses of postnatal skeletal development demonstrated an important role for *Bag-1* in bone marrow stromal cell (BMSC) osteogenic differentiation, matrix biosynthesis and mineralisation. The present study established that loss of one functional *Bag-1* allele impaired the ability of BMSCs of skeletally mature *Bag-1*$^{+/-}$ female mice to differentiate into osteoblasts in response to BMP-2 *in vitro,* while robust osteogenic response to BMP-2 of BMSCs of age-matched *Bag-1*$^{+/-}$ male mice was not affected. This highlighted the need to understand the role of interacting factors capable of modulating gender differences in BMP-2-directed osteogenic differentiation of BMSCs of *Bag-1*$^{+/-}$ mice.

We therefore investigated the role of estrogen (E2) in the modulation of BMP-2-directed osteogenic differentiation of BMSCs of skeletally mature *Bag-1*$^{+/-}$ female mice. We have confirmed that murine BMSCs express estrogen receptors (ERs), both α and β, and E2 enhances the osteogenic response of BMSCs, including BMSCs of female *Bag-1*$^{+/-}$ mice, to BMP-2 by upregulating *Bmpr2* expression. Estrogen, therefore, facilitates robust BMP-2-directed osteoblast differentiation of BMSCs of wild-type and *Bag-1* heterozygous female mice. Moreover, BAG-1 interacts with HSC70 in BMSCs and disruption of this interaction by the small-molecule chemical inhibitor, Thioflavin-S, and a short peptide containing the 8 amino acid binding core of helix 2 of the BAG domain leads to downregulation of E2/ER-facilitated, BMP-directed osteogenic responses of BMSCs of both *Bag-1*$^{+/+}$ and *Bag-1*$^{+/-}$ mice. To the best of our knowledge, the present study is the first report highlighting the significance of BAG-1-regulated activation of ERs by HSC70 in E2/ER-facilitated, BMP-directed osteogenic differentiation of BMSCs.

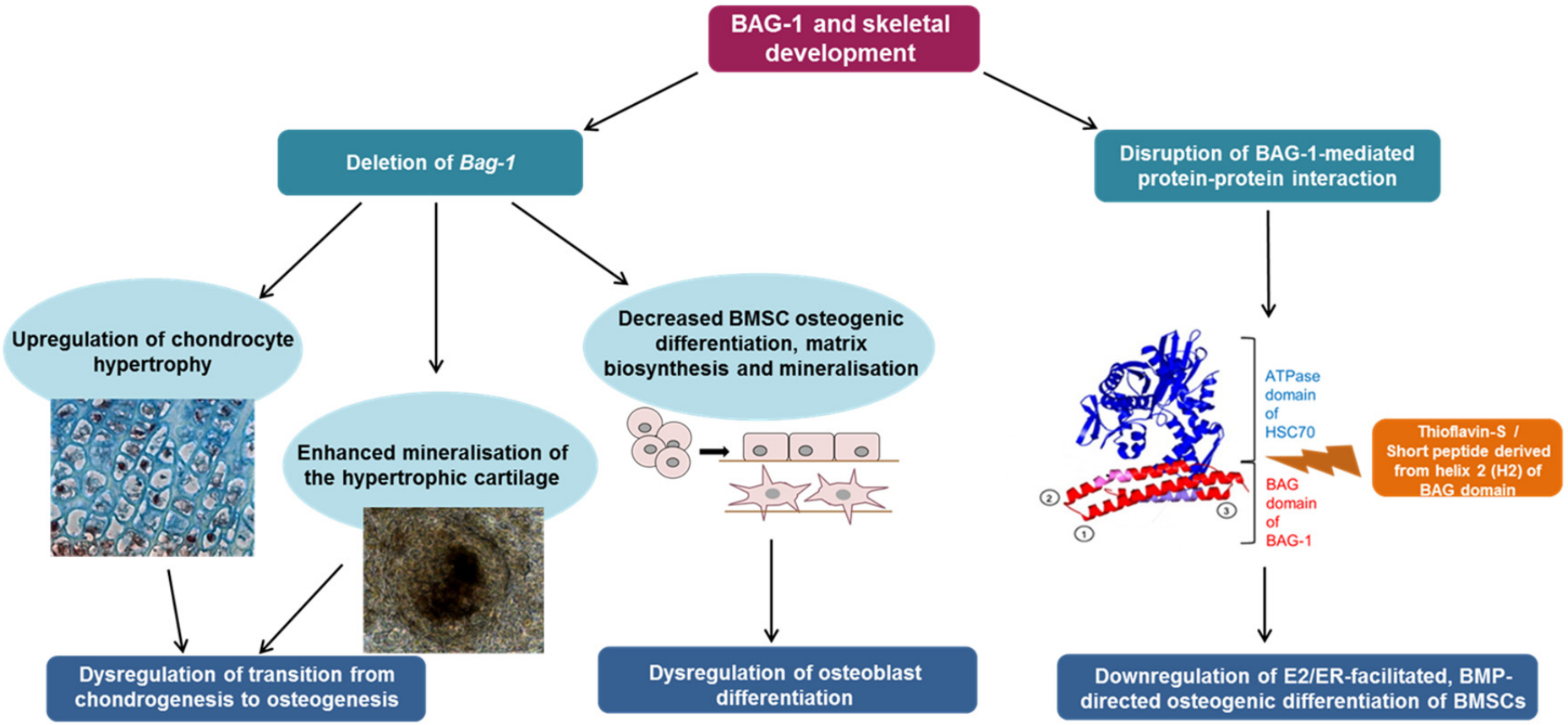

Figure 7-1. *Role of BAG-1 in skeletal development (image of hypertrophic chondrocytes adapted from Tare et al., 2008)*

Additionally, work described in this thesis has presented a number of observations that suggest a wide range of potential regulatory roles of BAG-1 in development and maintenance of skeletal system (Fig. 7-2).

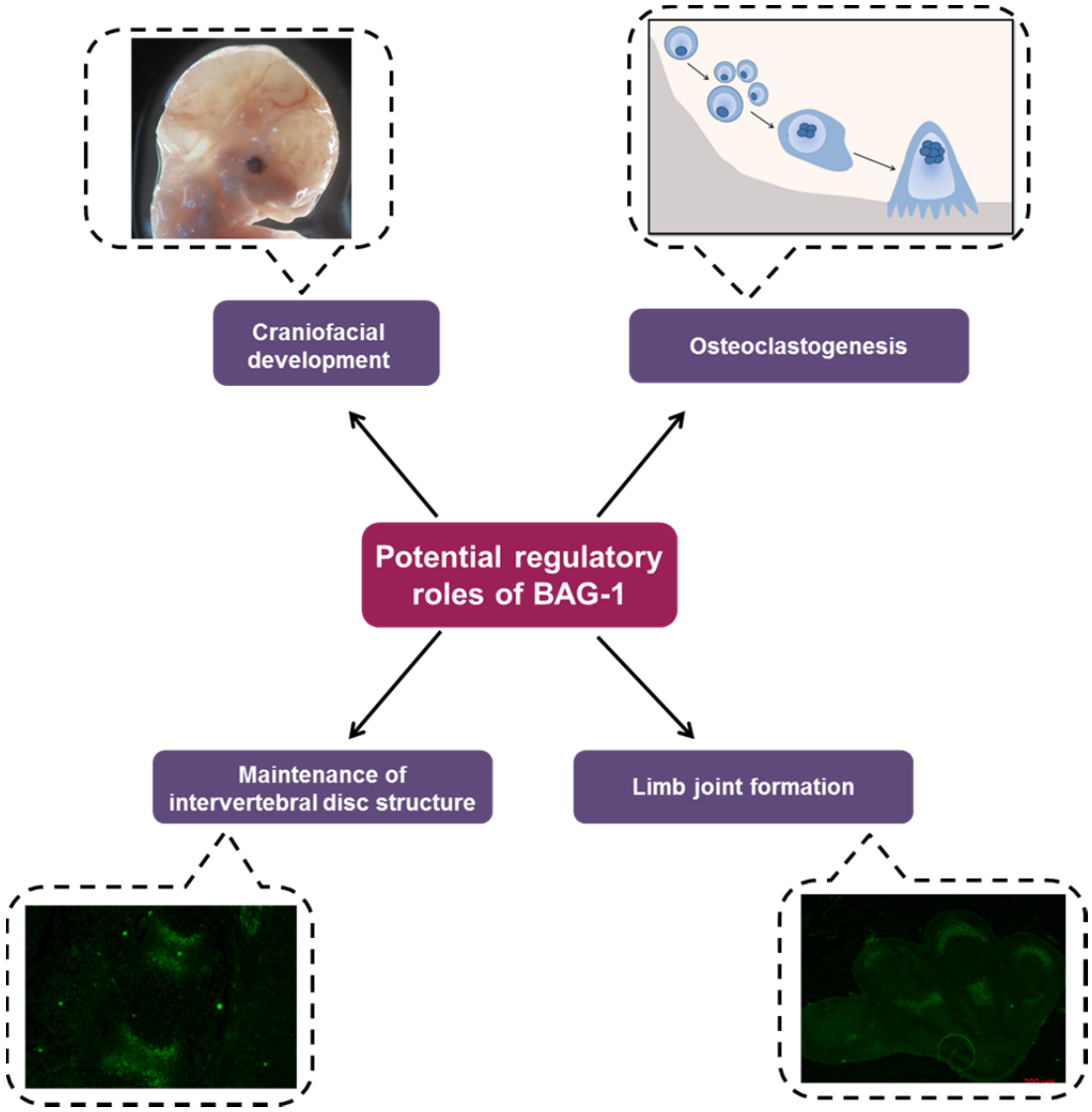

***Figure 7-2**. Potential regulatory roles of BAG-1 in development and maintenance of skeletal system.*

Underdeveloped lower jaws were consistently observed in *Bag-1*$^{-/-}$ fetuses, indicating a role for *Bag-1* in the regulation of craniofacial development. Epidermal growth factor receptor (EGFR) signalling is crucial for normal craniofacial development (Miettinen et al., 1999). It is possible that BAG-1 can regulate craniofacial development by interacting with EGF-like growth factor, namely heparin-binding EGF-like growth factor (HB-EGF), in a HSC70/HSP70-independent manner and participating in EGFR downstream signalling. Alongside previously characterised expression of *Bag-1* in cartilaginous tissues of the developing mouse embryo, the present work has

demonstrated expression of BAG-1 in cells of the future intervertebral discs and the mesenchymal tissue in the incipient joints of the developing limbs. As elucidated before, it is possible that BAG-1, in association with other factors with defined roles in joint formation, may have a regulatory role in the process of limb joint formation by the *Gdf5*-expressing progenitor cells or assist GDF-5 (growth/differentiation factor-5) in the maintenance of normal intervertebral disc structure (Koyama et al., 2008)

The development and maintenance of a healthy skeletal system relies on the perfectly balanced actions of osteoblasts and osteoclasts; any dysregulation in the homeostasis between bone formation and bone resorption can impact overall bone mass and lead to skeletal disorders, namely osteoporosis, Paget's disease and osteopetrosis (Raisz, 2005, Crockett et al., 2011). The present study has demonstrated that loss of one functional *Bag-1* allele impaired the ability of BMSCs of 14-week old female mice to differentiate into osteoblasts in response to BMP-2 *in vitro*. Comparison of the expression of an array of genes crucial for skeletal development between osteogenic cultures of BMSCs of *Bag-1*$^{+/-}$ and *Bag-1*$^{+/+}$ female mice indicated that 30 genes were differentially expressed between the two groups. Interestingly, expression of *Tnsf11* was upregulated almost 4-fold in BMSCs of *Bag-1*$^{+/-}$ female mice in comparison to BMSCs of *Bag-1*$^{+/+}$ female mice. The cytokine TNFSF11 (Tumor necrosis factor (ligand) superfamily, member 11 or RANKL: Receptor activator of nuclear factor kappa-B ligand), alongside macrophage colony stimulating factor (M-CSF), is essential for osteoclast formation. RANKL is expressed mostly on the surface of stromal cells, immune cells and osteoblasts in the bone marrow (Teitelbaum and Ross, 2003). Interaction of RANKL with RANK on the surface of osteoclast precursors stimulates osteoclastogenesis, while the action of RANKL on the surface of mature osteoclasts leads to continued bone resorption (Li et al., 2000). It is therefore likely that downregulation of osteogenic differentiation of BMSCs in *Bag-1*$^{+/-}$ female mice results in dysregulation of the balance between osteogenesis and osteoclastogenesis, and may even favour osteoclastogenesis by upregulating the expression of TNFSF11/ RANKL in BMSCs of *Bag-1*$^{+/-}$ female mice.

7.2. Improved understanding of skeletal diseases through appreciation of the role of BAG-1 in skeletal cells

The present study has provided evidence supporting the hypothesis that BAG-1 plays an important role in skeletal development. Based on our observations, continuation of the research into the role of BAG-1 in the skeletal system would contribute to improved understanding of skeletal development and facilitate the development of new

treatments for musculoskeletal diseases and skeletal tissue regeneration strategies. Two examples are discussed below:

1. Osteoarthritis (OA) is characterised by degeneration of the articular cartilage and the underlying subchondral bone that leads to progressive joint degradation. OA is the most common form of arthritis in the western world and affects approximately 8.75 million and 27 million individuals in the UK and USA, respectively. Moreover, it is estimated that around 630 million individuals suffer from OA worldwide. The disease causes pain and loss of function of joints that can lead to loss of mobility and independence, thereby compromising the quality of life(Arthritis Research UK, 2013). Expression of BAG-1 has been shown to be upregulated in human OA cartilage and the protein is distributed across the depth of the articular cartilage in advanced disease, compared to its restricted distribution in the surface zone in minimally involved OA cartilage (Nugent et al., 2009). The exact reason and mechanism underlying upregulation of BAG-1 expression in OA chondrocytes remain poorly defined.

It has been suggested that chondrocytes upregulate BAG-1 expression in an attempt to antagonise apoptotic signals characteristic for OA (Nugent et al., 2009). Upregulation of BAG-1 may therefore represent a survival mechanism adopted by chondrocytes for maintenance of the chondrogenic phenotype. Alternatively, upregulation of BAG-1 expression in chondrocytes is thought to stimulate the proliferative signal via activation of the Raf-1 MAP-kinase proliferation pathway (Wang et al., 1996). Thus, elucidation of the mechanism of upregulation of BAG-1 expression in OA chondrocytes may contribute to the understanding of the role of BAG-1 in the aetiology of OA.

The human *Bag-1* gene promoter is characterised by the presence of CpG-rich island (Yang et al., 1999), suggesting the potential role of epigenetic mechanisms such as DNA methylation in the control of *Bag-1* gene transcription/expression. Analysis of the methylation status of the *Bag-1* gene promoter in osteoarthritic and non-osteoarthritic chondrocytes would assist in establishing whether the *Bag-1* promoter is hypomethylated in osteoarthritic chondrocytes and contributes to increased BAG-1 expression in osteoarthritic cartilage.

2. It is widely acknowledged that $1,25(OH)_2D_3$ or calcitriol (the active form of vitamin D_3) is important for the development and maintenance of the healthy skeleton, since it promotes intestinal absorption of dietary calcium, osteoblast development and mineralisation of the osteoid (Norman, 1990, van Driel and van Leeuwen, 2014). At the cellular level, $1,25(OH)_2D_3$ stimulates osteogenic differentiation of human bone marrow-derived mesenchymal stem cells and the production of ALPL+ matrix vesicles

to promote matrix mineralisation (Woeckel et al., 2010, van de Peppel and van Leeuwen, 2014).Vitamin D_3 deficiency causes rickets in children and osteomalacia in adults, while the persistent state of secondary hyperparathyroidism due to vitamin D_3 deficiency can be an important risk factor in osteoporosis(Lips et al., 2006) and bone fracture (Välimäki et al.). Low levels of vitamin D_3 have been associated with progression/incident of OA (McAlindon et al., 1996, Lane et al., 1999).

The presence of the vitamin D receptor (VDR) in osteoblasts enables direct effects of calcitriol on osteoblasts, but the magnitude of the effects is subject to the presence of many other factors, such as HSC70/HSP70 and BAG-1. Binding of the BAG-1 co-chaperone to the HSC70/HSP70 chaperone proteins has now been recognised to be vital for most functions of BAG-1, including its effects on nuclear hormone receptors such as the vitamin D receptor (VDR). By binding to HSC70, BAG-1 interacts with the VDR in a hormone-dependent manner and significantly enhances the sensitivity of cells to vitamin D_3, resulting in increased transcription of vitamin D_3-responsive genes, namely *Osteocalcin*, a phenotypic marker of differentiated osteoblasts (Lee et al., 2007). The significance of the interaction between BAG-1 and HSC70 in the maintenance of a healthy skeleton via regulation of VDR/vitamin D_3-dependent differentiation of human skeletal stem cells into osteoblasts and mineralisation of the bone matrix, therefore, warrants investigation.

7.3. Future directions

1. To generate chondrocyte and osteoblast-specific conditional *Bag-1* knock-out mice

Expansion of our understanding of the intricacies of skeletal development could not have happened without the gene knock-out mouse models. As the targeted genes can be characterised by non-redundant systemic roles, gene knock-out strategies can lead to limited analyses of the role of the gene of interest in different stages of development when the knock-out strategy results in embryonic lethality. Early embryonic lethality of *Bag-1* null mice limited studies of the role of the gene in skeletal development *in vivo* beyond E12.5/E13.5 of gestation. In order to address these limitations, generation of tissue-specific conditional knock-out mouse model, where the target gene is specifically inactivated in the tissue of interest, can be utilised. The preferred method of achieving this genetic manipulation is the use of the Cre-Lox system (Rajewsky et al., 1996, Le and Sauer, 2000). When expressed in mice or cultured mammalian cells, the bacteriophage P1 Cre recombinase effectively excises DNA flanked by two repeated recognition sites (LoxP) (Sternberg and Hamilton, 1981). In order to produce

conditional knock-out mice, a transgenic mouse strain expressing Cre recombinase at high levels in the cell type of interest should be crossed with a mouse line that contains the target gene flanked by two LoxP sites. For the purposes of delineating the role of *Bag-1* in chondrocytes, a mouse strain carrying the *Bag-1* conditional allele (flanked with LoxP sites) should be crossed with transgenic mice expressing Cre recombinase specifically in chondrocytes under the control of the *Col2a1* promoter (Ovchinnikov et al., 2000). Similarly, a strain of mice carrying the *Bag-1* floxed allele, when mated with transgenic mice expressing osteoblast-specific Cre (*Col1a1* – Cre) would facilitate investigation of the role of *Bag-1* in osteoblasts (Dacquin et al., 2002). As the aim of studying the role of *Bag-1* in bone development is to better understand its function in the skeleton as a whole, a more desirable approach would be to use *Runx2*-Cre transgenic mice. *Runx2*-Cre transgenic mice are characterised by the *Cre* expression in the hypertrophic chondrocytes alongside periosteal cells, osteoblasts and osteocytes (Rauch et al., 2010). Generation of *Bag-1* conditional knock-out mice using the *Runx2*-Cre transgenic mice would facilitate elucidation of the role of *Bag-1* in regulation of chondrocyte hypertrophy and osteoblast development in a single animal model. Importantly, it would substantially decrease the number of animals required to demonstrate *Bag-1* function in skeletal development *in vivo*.

2. To elucidate the role of *Bag-1* in prenatal and postnatal skeletal development in the chondrocyte and osteoblast-specific conditional *Bag-1* knock-out mouse model using extensive histology, μCT, *in vitro* cell and organotypic culture techniques.

3. To determine whether loss of *Bag-1* function alters the balance between osteoblastogenesis and osteoclastogenesis in favour of the latter, in the conditional *Bag-1* knock-out mouse model. This will require comprehensive characterisation of osteoclast development and osteoblast development *in vitro*, in addition to characterisation of skeletal development detailed above.

4. To investigate the mechanism of upregulation of *Bag-1* expression in OA chondrocytes by analysis of the methylation status of the *Bag-1* gene promoter in human osteoarthritic chondrocytes. The methylation status of the CpG island in the promoter region of the human *Bag-1* gene will be investigated by methylation-specific polymerase chain reaction and bisulphite genomic sequencing (Ferreri et al., 2004).

5. To demonstrate the interaction between BAG-1 and HSC70 in human bone marrow-derived skeletal stem cells (SSCs) and to characterise the significance of this interaction in the regulation of VDR/vitamin D_3-dependent osteogenic differentiation of SSCs by examining whether disruption of the interaction using Thioflavin-S and the

highly specific BAG domain-derived short peptide downregulates vitamin D_3-dependent transcription of osteogenic genes and the differentiation of SSCs into osteoblasts.

7.4. Concluding remarks

Work described in this thesis has provided evidence for the importance of BAG-1 in the development and function of cartilage and bone tissue. Persistently, attempts to delineate biological systems and to elucidate answers to questions on natures principles, lead to the constant discovery of new unresolved issues. Similarly, in the case of the research into the role of BAG-1 in skeletal development, the present work successfully established that BAG-1 indeed is an important component of embryonic skeletal development and osteogenesis in adult bone. However, simultaneously, the current studies also suggest multiple avenues for further in depth characterisation of the functional role of BAG-1. These include conditional knock-out mouse model or the potential impact of BAG-1/NHRs interaction. Whichever direction of further investigation is undertaken in the future, evidence would suggest the research will be fruitful and exciting.

Appendices

Appendices

Appendix 1. Antibodies

Antibody		Working dilution
Rabbit α-BAG-1 (C-16), polyclonal	Santa Cruz Biotechnology, USA	1:200 (Western Blot)
Rabbit α-SOX-9 primary antibody	Millipore, UK	1:800 (Western Blot)
Rabbit α-Collagen Type II, polyclonal	Calbiochem, UK	1:1000 (Western Blot)
Rabbit α-β-Actin-Peroxidase, monoclonal	Sigma-Aldricht, UK	1:30000 (Western Blot)
Goat polyclonal Secondary Antibody to Rabbit IgG - H&L (HRP)	Abcam, UK	1:5000 (Western Blot)

Appendix 2. Buffers and electrophoresis gels

DNA isolation buffer	1M Tris (hydroxymethyl) methylamine, pH 8.9			25 ml
	500 mM $MgCl_2$			12.5 ml
	Tween 20			2.5 m
	up H_2O			460 ml
ALP Assay Substrate Buffer	Phosphate Substrate			0.04 g
	1.5 M Alkaline buffer			10 ml
	up H_2O			20 ml
PCR Master Mix	Amplification of Bag-1 region		Amplification of Neomycin region	
	5x PCR buffer	6 µl	5x PCR buffer	6 µl
	dNTP mix (2mM)	3 µl	dNTP mix (2mM)	3 µl
	F primer (20 µM)	0.3 µl	F primer (20 µM)	0.3 µl
	R primer (20 µM)	0.3 µl	R primer (20 µM)	0.3 µl
	GoTaq DNA Polymerase (5U/µl)	0.3 µl	GoTaq DNA Polymerase (5U/µl)	0.3 µl
	Betaine	6 µl	Betaine	6 µl
	DMSO	1.51 µl	up H_2O	12.1 µl
	up H_2O	10.59 µl		
Equilibration buffer	Potassium cacodylate (pH 6.6 at 25°C)			200 mM

	Tris-HCl (pH 6.6 at 25°C)			25 mM
	DTT			0.2 mM
	BSA			0.25mg/ml
	Cobalt chloride			2.5 mM
Nucleodide Mix	Fluorescein-12-dUTP			50 µM
	dATP			100 µM
	Tris-HCl (pH7.6)			10 mM
	EDTA			1mM
rTDT incubation buffer	Equilibration buffer			90 µl
	Nucleotide Mix			10 µl
	Terminal Deoxynucleotidyl Transferase, Recombinant (rTDT)			2 µl
20 x SSC	NaCl			87.7 g
	Sodium citrate			44.1 g
	Top up with di H_20, pH 7.0			to 500 ml
RIPA buffer	Tris base			0.079 g
	NaCl			0.09 g
	10% NP-40			1 ml
	10% Na-deoxy-cholate			500 µl
	100 mM EDTA			100 µl
	10% SDS			100 µl
	Top up with up H_2O			to 10 ml
	protease inhibitor cocktail tablet			1
Homogenisation buffer	10% SDS			20 ml
	DTT			0.0154 g
	Tris base			0.048 g
	protease inhibitor cocktail tablet			2
Electrophoresis gels	10% Resolvin gel		Stacking Gel	
	ProtoGel	1.65 ml	ProtoGel	0.65 ml
	Resolving Buffer	1.3 ml	Stacking Buffer	1.35 ml
	TEMED	5 µl	TEMED	5 µl
	10% APS	50 µl	10% APS	25 µl
	up H_2O	1.95 ml	up H_2O	3.05 ml
Western Blot buffers:				
Running Buffer 10x	Tris			30.39 g
	Glycine			144 g

	SDS	10 g
	Top up with di H_2O	to 1l
Transfer buffer	Running Buffer (10x)	80 ml
	Methanol	200 ml
	Top up with di H_2O	To 1l
Stripping Buffer	Glycine	3.75 g
	SDS	0.25 g
	Tween	2.5 ml
	pH=2.2	
HMKEN buffer	HEPES,	10 mM
	$MgCl_2$	5 mM
	KCl	142 mM
	EGTA	2 mM
	Igepal CA-630	0.2% (v/v)

Appendix 3. Reagents

Reagent	Manufacturer
Proteinase K	Promega, UK
DNase I	Promega, UK
WST-1 substrate	Roche Diagnostics, UK
PicoGreen® DNA quantification reagent	Invitrogen, UK
RLT Buffer	QIAGEN, UK
RNeasy Mini Kit	QIAGEN, UK
SuperScript VILO cDNA synthesis Kit	Invitrogen, UK
SYBRGreen Master Mix	Invitrogen, UK
BCA Protein Assay Kit	Thermo Scientific, UK
Blue Loading Buffer Pack	New England Biolabs, UK
GelRed™ Nucleic Acid Gel Stain	Biotium, UK
ColorPlus Prestained Protein Marker	New England Biolabs, UK
Spectra Multicolor Broad Range Protein Ladder	Thermo Scientific, UK
Immobilon Western Chemiluminescent HRP Substrate	Merck Millipore, UK
Mouse Osteocalcin EIA Kit	Bioquote, UK

α-MEM	Lonza, UK
D-MEM	Lonza, UK
Phenol red-free α-MEM	Gibco, UK
Fetal Calf Serum/Fetal Calf Serum (FSC)	Gibco, UK
Charcoal stripped FSC	Sigma-Aldrich, UK
Penicilin/Streptomycin	Lonza, UK
Estrogen (E2) (E2758-1G)	Sigma-Aldrich, UK
Tripsin/EDTA	Lonza, UK
Thioflavin S	Sigma-Aldrich, UK
BAG domain-derived short peptides	ProteoGenix SAS, Schiltigheim, France

Appendix 4. qPCR primers

Gene	Primer pairs	Product size (bp)
β-Actin NM_007393	F: 5' TTG CTG ACA GGA TGC AGA AG 3' R: 5' GTA CTT GCG CTC AGG AGG AG 3'	86
Scinderin (Adseverin) NM_009132 NM_001146196	F: 5' CAA AGG CGG TCT GAA GTA C 3' R: 5' CGC AGT CAG ATC ATT GGT G 3'	76
Col10a1 NM_009925	F: 5' ACG GCA CGC CTA CGA TGT 3' R: 5' CCA TGA TTG CAC TCC CTG AA 3'	78
Indian Hedgehog (Ihh) NM_010544	F: 5' CAC TTG TGG TGG AGG ATG TG 3' R: 5' AAC TGA GCC AGA TGG TGG TC 3'	67
Alkaline Phosphatase (Alpl) NM_007431	F: 5' CTG ACT GAC CCT TCG CTC TC 3' R: 5' CCA GCA AGA AGA AGC CTT TG 3'	82
Osteocalcin NM_007541	F: 5' CTG ACC TCA CAG ATG CCA AG 3' R: 5' ACC TTA TTG CCC TCC TGC TT 3'	76
Osterix NM_130458	F: 5' AGT TCA CCT GCC TGC TCT GT 3' R: 5' CTC AAG TGG TCG CTT CTG GT 3'	52
Estrogen Receptor α (ERα) NM_ 007956 NM_001302531 NM_001302532	F: 5' CCTTCTAGACCCTTCAGTGAAGCC 3' R: 5' CGAGACCAATCATCAGAATCTCC 3'	178

Estrogen Receptor β (ERβ) NM_ 207707 NM_010157 NR_104386	F: 5' CAGTAACAAGGGCATGGAAC 3' R: 5' GTACATGTCCCACTTCTGAC 3'	243
BMPR2 NM_ 007561	F: 5' GAAACGATAATCATTGCTTTGGC 3' R: 5' CCCTGTTTCCGGTCTCCTGT 3'	101

Appendix 5. Equipment

Equipment	Manufacturer
PowerShot G10 Camera	Canon
Veriti® Thermal Cycler	Applied Biosciences
DotSlide microscope	Olympus
Axiovert fluorescent microscope	Zeiss
Bio-Tek KC4 microplate fluorescent reader	BioTek
NanoDrop® ND-1000 spectrophotometer	Thermo Fisher Scientific
7500 Real Time PCR System	Applied Biosystems
VersaDoc Imaging System	BioRad
InGenius Gel Imaging System	SynGene

Appendix 6. PCR reaction performed using Veriti® Thermal Cycler (Applied Biosciences) for the genotyping of mouse samples

Stage 1 x1	**Stage 2** x35 (ear punctures), x38 (tail snips)			**Stage 3** x1	
95°C	95°C	55.2°C	72°C	72°C	4°C
2 min	30 sec	30 sec	2 min	10 min	~

Appendix 7. Cycling conditions of the PCR reaction performed using Veriti® Thermal Cycler (Applied Biosciences) for the preamplification of cDNA

Cycles	**Duration**	**Temperature**
1	10 minutes	95°C
8	15 seconds 2 minutes	95°C 60°C
Hold		4°C

Appendix 8. Genes analysed in Mouse osteogenesis RT² Profiler™ PCR arrays

Acvr1	*Cdh11*	*Fgf1*	*Itgb1*	*Sox9*
Ahsg	*Chrd*	*Fgf2*	*Mmp10*	*Sp7*
Alpl	*Col10a1*	*Fgfr1*	*Mmp2*	*Spp1*
Anxa5	*Col14a1*	*Fgfr2*	*Mmp8*	*Tgfb1*
Bglap	*Col1a1*	*Flt1*	*Mmp9*	*Tgfb2*
Bgn	*Col1a2*	*Fn1*	*Nfkb1*	*Tgfb3*
Bmp1	*Col2a1*	*Gdf10*	*Nog*	*Tgfbr1*
Bmp2	*Col3a1*	*Gli1*	*Pdgfa*	*Tgfbr2*
Bmp3	*Col4a1*	*Icam1*	*Phex*	*Tgfbr3*
Bmp4	*Col5a1*	*Igf1*	*Runx2*	*Tnf*
Bmp5	*Comp*	*Igf1r*	*Serphinh1*	*Tnfsf11*
Bmp6	*Csf1*	*Ihh*	*Smad1*	*Twist1*
Bmp7	*Csf2*	*Itga2*	*Smad2*	*Vcam1*
Bmpr1a	*Csf3*	*Itga2b*	*Smad3*	*Vdr*
Bmpr1b	*Ctsk*	*Itga3*	*Smad4*	*Vegfa*
Bmpr2	*Dlx5*	*Itgam*	*Smad5*	*Vegfb*
Cd36	*Egf*	*Itgav*	*Sost*	

References

9. References

Abad, V., Meyers, J. L., Weise, M., Gafni, R. I., Barnes, K. M., Nilsson, O., Bacher, J. D. & Baron, J. (2002). The role of the resting zone in growth plate chondrogenesis. *Endocrinology, 143*, 1851-1857.

Adams, C. S. & Shapiro, I. M. (2002). The fate of the terminally differentiated chondrocyte: evidence for microenvironmental regulation of chondrocyte apoptosis. *Crit Rev Oral Biol Med, 13*, 465-473.

Addison, W. N., Masica, D. L., Gray, J. J. & McKee, M. D. (2010). Phosphorylation-dependent inhibition of mineralization by osteopontin ASARM peptides is regulated by PHEX cleavage. *J Bone Miner Res, 25*, 695-705.

Agarraberes, F. A. & Dice, J. F. (2001). A molecular chaperone complex at the lysosomal membrane is required for protein translocation. *J Cell Sci, 114*, 2491-2499.

Ahmed, Y. A., Tatarczuch, L., Pagel, C. N., Davies, H. M., Mirams, M. & Mackie, E. J. (2007). Physiological death of hypertrophic chondrocytes. *Osteoarthritis Cartilage, 15*, 575-586.

Ahrens, P. B., Solursh, M. & Reiter, R. S. (1977). Stage-related capacity for limb chondrogenesis in cell culture. *Dev Biol, 60*, 69-82.

Akiyama, H., Hiraki, Y., Shigeno, C., Kohno, H., Shukunami, C., Tsuboyama, T., Kasai, R., Suzuki, F., Konishi, J. & Nakamura, T. (1996). 1 alpha,25-dihydroxyvitamin D3 inhibits cell growth and chondrogenesis of a clonal mouse EC cell line, ATDC5. *J Bone Miner Res, 11*, 22-28.

Alini, M., Matsui, Y., Dodge, G. R. & Poole, A. R. (1992). The extracellular matrix of cartilage in the growth plate before and during calcification: changes in composition and degradation of type II collagen. *Calcif Tissue Int, 50*, 327-335.

Amling, M., Neff, L., Tanaka, S., Inoue, D., Kuida, K., Weir, E., Philbrick, W. M., Broadus, A. E. & Baron, R. (1997). Bcl-2 lies downstream of parathyroid hormone-related peptide in a signaling pathway that regulates chondrocyte maturation during skeletal development. *J Cell Biol, 136*, 205-213.

Andrade, A. C., Nilsson, O., Barnes, K. M. & Baron, J. (2007). Wnt gene expression in the post-natal growth plate: regulation with chondrocyte differentiation. *Bone, 40*, 1361-1369.

Arthritis_Research_UK (2013). Osteoarthritis in general practice.

Arts, J., Kuiper, G. G., Janssen, J. M., Gustafsson, J. A., Lowik, C. W., Pols, H. A. & van Leeuwen, J. P. (1997). Differential expression of estrogen receptors alpha and beta mRNA during differentiation of human osteoblast SV-HFO cells. *Endocrinology, 138*, 5067-5070.

Asahina, I., Sampath, T. K. & Hauschka, P. V. (1996). Human osteogenic protein-1 induces chondroblastic, osteoblastic, and/or adipocytic differentiation of clonal murine target cells. *Exp Cell Res, 222*, 38-47.

Asou, Y., Rittling, S. R., Yoshitake, H., Tsuji, K., Shinomiya, K., Nifuji, A., Denhardt, D. T. & Noda, M. (2001). Osteopontin facilitates angiogenesis, accumulation of osteoclasts, and resorption in ectopic bone. *Endocrinology, 142*, 1325-1332.

Bagi, C. M., Berryman, E. & Moalli, M. R. (2011). Comparative bone anatomy of commonly used laboratory animals: implications for drug discovery. *Comp Med, 61*, 76-85.

Bagi, C. M., Wilkie, D., Georgelos, K., Williams, D. & Bertolini, D. (1997). Morphological and structural characteristics of the proximal femur in human and rat. *Bone, 21*, 261-267.

Balemans, W. & Van Hul, W. (2002). Extracellular regulation of BMP signaling in vertebrates: a cocktail of modulators. *Dev Biol, 250*, 231-250.

Bardelli, A., Longati, P., Albero, D., Goruppi, S., Schneider, C., Ponzetto, C. & Comoglio, P. M. (1996). HGF receptor associates with the anti-apoptotic protein BAG-1 and prevents cell death. *EMBO J, 15*, 6205-6212.

Baur, S. T., Mai, J. J. & Dymecki, S. M. (2000). Combinatorial signaling through BMP receptor IB and GDF5: shaping of the distal mouse limb and the genetics of distal limb diversity. *Development, 127*, 605-619.

Bellows, C. G., Ciaccia, A. & Heersche, J. N. (1998). Osteoprogenitor cells in cell populations derived from mouse and rat calvaria differ in their response to corticosterone, cortisol, and cortisone. *Bone, 23*, 119-125.

Bertazzo, S., Bertran, C. A. & Camilli, J. A. (2006). Morphological characterization of femur and parietal bone mineral of rats at different ages. *Bioceramics 18, Pts 1 and 2, 309-311*, 11-14.

Berthois, Y., Katzenellenbogen, J. A. & Katzenellenbogen, B. S. (1986). Phenol red in tissue culture media is a weak estrogen: implications concerning the study of estrogen-responsive cells in culture. *Proc Natl Acad Sci U S A, 83*, 2496-2500.

Bi, W. M., Deng, J. M., Zhang, Z. P., Behringer, R. R. & de Crombrugghe, B. (1999). Sox9 is required for cartilage formation. *Nature Genetics, 22*, 85-89.

Bianco, P. & Robey, P. G. (2004). Skeletal stem cells. In "Handbook of Adult and Fetal Stem Cells" (ed. Lanza, R.P.), pp 415–424, Academic Press, San Diego.

Biederman, J., Yee, J. & Cortes, P. (2004). Validation of internal control genes for gene expression analysis in diabetic glomerulosclerosis. *Kidney International, 66*, 2308-2314.

Binkert, C., Demetriou, M., Sukhu, B., Szweras, M., Tenenbaum, H. C. & Dennis, J. W. (1999). Regulation of osteogenesis by fetuin. *J Biol Chem, 274*, 28514-28520.

Bitgood, M. J. & McMahon, A. P. (1995). Hedgehog and Bmp genes are coexpressed at many diverse sites of cell-cell interaction in the mouse embryo. *Dev Biol, 172*, 126-138.

Boskey, A. L. (1989). Noncollagenous matrix proteins and their role in mineralization. *Bone Miner, 6*, 111-123.

Boskey, A. L., Gadaleta, S., Gundberg, C., Doty, S. B., Ducy, P. & Karsenty, G. (1998). Fourier transform infrared microspectroscopic analysis of bones of osteocalcin-deficient mice provides insight into the function of osteocalcin. *Bone, 23*, 187-196.

Bossard, M. J., Tomaszek, T. A., Levy, M. A., Ijames, C. F., Huddleston, M. J., Briand, J., Thompson, S., Halpert, S., Veber, D. F., Carr, S. A., Meek, T. D. & Tew, D. G. (1999). Mechanism of inhibition of cathepsin K by potent, selective 1, 5-diacylcarbohydrazides: a new class of mechanism-based inhibitors of thiol proteases. *Biochemistry, 38*, 15893-15902.

Boyle, W. J., Simonet, W. S. & Lacey, D. L. (2003). Osteoclast differentiation and activation. *Nature, 423*, 337-342.

Briknarova, K., Takayama, S., Brive, L., Havert, M. L., Knee, D. A., Velasco, J., Homma, S., Cabezas, E., Stuart, J., Hoyt, D. W., Satterthwait, A. C., Llinas, M., Reed, J. C. & Ely, K. R. (2001). Structural analysis of BAG1 cochaperone and its interactions with Hsc70 heat shock protein. *Nat Struct Biol, 8*, 349-352.

Brodsky, B. & Persikov, A. V. (2005). Molecular structure of the collagen triple helix. *Adv Protein Chem, 70*, 301-339.

Brunet, L. J., McMahon, J. A., McMahon, A. P. & Harland, R. M. (1998). Noggin, cartilage morphogenesis, and joint formation in the mammalian skeleton. *Science, 280*, 1455-1457.

Bukau, B. & Horwich, A. L. (1998). The Hsp70 and Hsp60 chaperone machines. *Cell, 92*, 351-366.

Byers, P. H. (1995). Disorders of collagen biosynthesis and structure. In: Metabolic Basis of Inherited Disease, 7th ed., C. R. Scriver, A. L. Beaudet, W. S. Sly, and D. Valle (Eds). McGraw-Hill, New York, p. 4029.

Capecchi, M. R. (1989). The new mouse genetics: altering the genome by gene targeting. *Trends Genet, 5*, 70-76.

Caplan, A. I. (1991). Mesenchymal stem cells. *J Orthop Res, 9*, 641-650.

Carpenter, G. & Cohen, S. (1990). Epidermal growth factor. *J Biol Chem, 265*, 7709-7712.

Castagnola, P., Dozin, B., Moro, G. & Cancedda, R. (1988). Changes in the expression of collagen genes show two stages in chondrocyte differentiation in vitro. *J Cell Biol, 106*, 461-467.

Cato, A. C. & Mink, S. (2001). BAG-1 family of cochaperones in the modulation of nuclear receptor action. *J Steroid Biochem Mol Biol, 78*, 379-388.

Chappell, T. G., Welch, W. J., Schlossman, D. M., Palter, K. B., Schlesinger, M. J. & Rothman, J. E. (1986). Uncoating ATPase is a member of the 70 kilodalton family of stress proteins. *Cell, 45*, 3-13.

Chaudhary, L. R., Hofmeister, A. M. & Hruska, K. A. (2004). Differential growth factor control of bone formation through osteoprogenitor differentiation. *Bone, 34*, 402-411.

Chenevix-Trench, G., Jones, K., Green, A. C., Duffy, D. L. & Martin, N. G. (1992). Cleft lip with or without cleft palate: associations with transforming growth factor alpha and retinoic acid receptor loci. *Am J Hum Genet, 51*, 1377-1385.

Cheung, J. & Smith, D. F. (2000). Molecular chaperone interactions with steroid receptors: an update. *Mol Endocrinol, 14*, 939-946.

Clarke, B. (2008). Normal bone anatomy and physiology. *Clin J Am Soc Nephrol, 3 Suppl 3*, S131-139.

Clemens, T. L., Tang, H., Maeda, S., Kesterson, R. A., Demayo, F., Pike, J. W. & Gundberg, C. M. (1997). Analysis of osteocalcin expression in transgenic mice reveals a species difference in vitamin D regulation of mouse and human osteocalcin genes. *J Bone Miner Res, 12*, 1570-1576.

Cohen, M. M., Jr. (2006). The new bone biology: pathologic, molecular, and clinical correlates. *Am J Med Genet A, 140*, 2646-2706.

Coldwell, M. J., deSchoolmeester, M. L., Fraser, G. A., Pickering, B. M., Packham, G. & Willis, A. E. (2001). The p36 isoform of BAG-1 is translated by internal ribosome entry following heat shock. *Oncogene, 20*, 4095-4100.

Cooper, R. R., Milgram, J. W. & Robinson, R. A. (1966). Morphology of the osteon. An electron microscopic study. *J Bone Joint Surg Am, 48*, 1239-1271.

Couchourel, D., Escoffier, C., Rohanizadeh, R., Bohic, S., Daculsi, G., Fortun, Y. & Padrines, M. (1999). Effects of fibronectin on hydroxyapatite formation. *J Inorg Biochem, 73*, 129-136.

Crockett, J. C., Mellis, D. J., Scott, D. I. & Helfrich, M. H. (2011). New knowledge on critical osteoclast formation and activation pathways from study of rare genetic diseases of osteoclasts: focus on the RANK/RANKL axis. *Osteoporos Int, 22*, 1-20.

Crocoll, A., Blum, M. & Cato, A. C. (2000). Isoform-specific expression of BAG-1 in mouse development. *Mech Dev, 91*, 355-359.

Crocoll, A., Herzer, U., Ghyselinck, N. B., Chambon, P. & Cato, A. C. (2002). Interdigital apoptosis and downregulation of BAG-1 expression in mouse autopods. *Mech Dev, 111*, 149-152.

Cutress, R. I., Townsend, P. A., Sharp, A., Maison, A., Wood, L., Lee, R., Brimmell, M., Mullee, M. A., Johnson, P. W., Royle, G. T., Bateman, A. C. & Packham, G. (2003). The nuclear BAG-1 isoform, BAG-1L, enhances oestrogen-dependent transcription. *Oncogene, 22*, 4973-4982.

Dacquin, R., Starbuck, M., Schinke, T. & Karsenty, G. (2002). Mouse alpha1(I)-collagen promoter is the best known promoter to drive efficient Cre recombinase expression in osteoblast. *Dev Dyn, 224*, 245-251.

Daculsi, G., Pilet, P., Cottrel, M. & Guicheux, G. (1999). Role of fibronectin during biological apatite crystal nucleation: ultrastructural characterization. *J Biomed Mater Res, 47*, 228-233.

Dafforn, T. R., Della, M. & Miller, A. D. (2001). The molecular interactions of heat shock protein 47 (Hsp47) and their implications for collagen biosynthesis. *J Biol Chem, 276*, 49310-49319.

Daluiski, A., Engstrand, T., Bahamonde, M. E., Gamer, L. W., Agius, E., Stevenson, S. L., Cox, K., Rosen, V. & Lyons, K. M. (2001). Bone morphogenetic protein-3 is a negative regulator of bone density. *Nature Genetics, 27*, 84-88.

Delany, A. M., Amling, M., Priemel, M., Howe, C., Baron, R. & Canalis, E. (2000). Osteopenia and decreased bone formation in osteonectin-deficient mice. *J Clin Invest, 105*, 1325.

Demay, M. B., Gerardi, J. M., DeLuca, H. F. & Kronenberg, H. M. (1990). DNA sequences in the rat osteocalcin gene that bind the 1,25-dihydroxyvitamin D3 receptor and confer responsiveness to 1,25-dihydroxyvitamin D3. *Proc Natl Acad Sci U S A, 87*, 369-373.

Dessau, W., von der Mark, H., von der Mark, K. & Fischer, S. (1980). Changes in the patterns of collagens and fibronectin during limb-bud chondrogenesis. *J Embryol Exp Morphol, 57*, 51-60.

Doege, K., Sasaki, M. & Yamada, Y. (1990). Rat and human cartilage proteoglycan (aggrecan) gene structure. *Biochem Soc Trans, 18*, 200-202.

Doi, Y., Horiguchi, T., Kim, S. H., Moriwaki, Y., Wakamatsu, N., Adachi, M., Ibaraki, K., Moriyama, K., Sasaki, S. & Shimokawa, H. (1992). Effects of non-collagenous proteins on the formation of apatite in calcium beta-glycerophosphate solutions. *Arch Oral Biol, 37*, 15-21.

Doty, S. B. (1981). Morphological evidence of gap junctions between bone cells. *Calcif Tissue Int, 33*, 509-512.

Ducy, P. & Karsenty, G. (2000). The family of bone morphogenetic proteins. *Kidney International, 57*, 2207-2214.

Ducy, P., Zhang, R., Geoffroy, V., Ridall, A. L. & Karsenty, G. (1997). Osf2/Cbfa1: a transcriptional activator of osteoblast differentiation. *Cell, 89*, 747-754.

Duprez, D., Bell, E. J., Richardson, M. K., Archer, C. W., Wolpert, L., Brickell, P. M. & Francis-West, P. H. (1996). Overexpression of BMP-2 and BMP-4 alters the size and shape of developing skeletal elements in the chick limb. *Mech Dev, 57*, 145-157.

Ek-Rylander, B., Flores, M., Wendel, M., Heinegard, D. & Andersson, G. (1994). Dephosphorylation of osteopontin and bone sialoprotein by osteoclastic tartrate-resistant acid phosphatase. Modulation of osteoclast adhesion in vitro. *J Biol Chem, 269*, 14853-14856.

Enomoto, H., Enomoto-Iwamoto, M., Iwamoto, M., Nomura, S., Himeno, M., Kitamura, Y., Kishimoto, T. & Komori, T. (2000). Cbfa1 is a positive regulatory factor in chondrocyte maturation. *J Biol Chem, 275*, 8695-8702.

Enthammer, M., Papadakis, E. S., Salome Gachet, M., Deutsch, M., Schwaiger, S., Koziel, K., Ashraf, M. I., Khalid, S., Wolber, G., Packham, G., Cutress, R. I., Stuppner, H. & Troppmair, J. (2013). Isolation of a novel thioflavin S-derived compound that inhibits BAG-1-mediated protein interactions and targets BRAF inhibitor-resistant cell lines. *Mol Cancer Ther, 12*, 2400-2414.

Eriksen, E. F., Colvard, D. S., Berg, N. J., Graham, M. L., Mann, K. G., Spelsberg, T. C. & Riggs, B. L. (1988). Evidence of estrogen receptors in normal human osteoblast-like cells. *Science, 241*, 84-86.

Farnum, C. E. & Wilsman, N. J. (1989). Cellular turnover at the chondro-osseous junction of growth plate cartilage: analysis by serial sections at the light microscopical level. *J Orthop Res, 7*, 654-666.

Fell, H. B. & Mellanby, E. (1955). The biological action of thyroxine on embryonic bones grown in tissue culture. *J Physiol, 127*, 427-447.

Feng, L., Balakir, R., Precht, P. & Horton, W. E., Jr. (1999). Bcl-2 regulates chondrocyte morphology and aggrecan gene expression independent of caspase activation and full apoptosis. *J Cell Biochem, 74*, 576-586.

Ferreri, A. J., Dell'Oro, S., Capello, D., Ponzoni, M., Iuzzolino, P., Rossi, D., Pasini, F., Ambrosetti, A., Orvieto, E., Ferrarese, F., Arrigoni, G., Foppoli, M., Reni, M. & Gaidano, G. (2004). Aberrant methylation in the promoter region of the reduced folate carrier gene is a

potential mechanism of resistance to methotrexate in primary central nervous system lymphomas. *Br J Haematol, 126*, 657-664.
Fisher, L. W. & Fedarko, N. S. (2003). Six genes expressed in bones and teeth encode the current members of the SIBLING family of proteins. *Connect Tissue Res, 44 Suppl 1*, 33-40.
Fisher, L. W., McBride, O. W., Termine, J. D. & Young, M. F. (1990). Human bone sialoprotein. Deduced protein sequence and chromosomal localization. *J Biol Chem, 265*, 2347-2351.
Froesch, B. A., Takayama, S. & Reed, J. C. (1998). BAG-1L protein enhances androgen receptor function. *J Biol Chem, 273*, 11660-11666.
Frost, H. M. (1990). Skeletal Structural Adaptations to Mechanical Usage (Satmu) .2. Redefining Wolff Law - the Remodeling Problem. *Anatomical Record, 226*, 414-422.
Gamer, L. W., Nove, J., Levin, M. & Rosen, V. (2005). BMP-3 is a novel inhibitor of both activin and BMP-4 signaling in Xenopus embryos. *Dev Biol, 285*, 156-168.
Gassler, C. S., Wiederkehr, T., Brehmer, D., Bukau, B. & Mayer, M. P. (2001). Bag-1M accelerates nucleotide release for human Hsc70 and Hsp70 and can act concentration-dependent as positive and negative cofactor. *J Biol Chem, 276*, 32538-32544.
Gehring, U. (2006). Activities of the cochaperones Hap46/BAG-1M and Hap50/BAG-1L and isoforms. *Cell Stress Chaperones, 11*, 295-303.
Gerstenfeld, L. C. & Landis, W. J. (1991). Gene expression and extracellular matrix ultrastructure of a mineralizing chondrocyte cell culture system. *J Cell Biol, 112*, 501-513.
Glimcher, M. J. (1989). Mechanism of calcification: role of collagen fibrils and collagen-phosphoprotein complexes in vitro and in vivo. *Anat Rec, 224*, 139-153.
Glimcher, M. J. (1992). The nature of the mineral component of bone and the mechanisms of calcification. In: Coe FL, Favus MJ (eds) Disorders of bone and mineral metabolism. Raven Press, New York, pp 265-286.
Globus, R. K., Doty, S. B., Lull, J. C., Holmuhamedov, E., Humphries, M. J. & Damsky, C. H. (1998). Fibronectin is a survival factor for differentiated osteoblasts. *J Cell Sci, 111 (Pt 10)*, 1385-1393.
Gotoh, T., Terada, K., Oyadomari, S. & Mori, M. (2004). hsp70-DnaJ chaperone pair prevents nitric oxide- and CHOP-induced apoptosis by inhibiting translocation of Bax to mitochondria. *Cell Death Differ, 11*, 390-402.
Gotz, R., Kramer, B. W., Camarero, G. & Rapp, U. R. (2004). BAG-1 haplo-insufficiency impairs lung tumorigenesis. *BMC Cancer, 4*, 85.
Gotz, R., Wiese, S., Takayama, S., Camarero, G. C., Rossoll, W., Schweizer, U., Troppmair, J., Jablonka, S., Holtmann, B., Reed, J. C., Rapp, U. R. & Sendtner, M. (2005). Bag1 is essential for differentiation and survival of hematopoietic and neuronal cells. *Nat Neurosci, 8*, 1169-1178.
Green, D. R. & Reed, J. C. (1998). Mitochondria and apoptosis. *Science, 281*, 1309-1312.
Gruber, R., Czerwenka, K., Wolf, F., Ho, G. M., Willheim, M. & Peterlik, M. (1999). Expression of the vitamin D receptor, of estrogen and thyroid hormone receptor alpha- and beta-isoforms, and of the androgen receptor in cultures of native mouse bone marrow and of stromal/osteoblastic cells. *Bone, 24*, 465-473.
Guo, J., Chung, U. I., Yang, D., Karsenty, G., Bringhurst, F. R. & Kronenberg, H. M. (2006). PTH/PTHrP receptor delays chondrocyte hypertrophy via both Runx2-dependent and -independent pathways. *Dev Biol, 292*, 116-128.
Guzey, M., Takayama, S. & Reed, J. C. (2000). BAG1L enhances trans-activation function of the vitamin D receptor. *J Biol Chem, 275*, 40749-40756.
Hall, B. K. & Miyake, T. (1992). The membranous skeleton: the role of cell condensations in vertebrate skeletogenesis. *Anat Embryol (Berl), 186*, 107-124.
Hamerman, D. (1989). The biology of osteoarthritis. *N Engl J Med, 320*, 1322-1330.

Hammond, C. & Helenius, A. (1995). Quality control in the secretory pathway. *Curr Opin Cell Biol, 7*, 523-529.
Hankenson, K. D., Bain, S. D., Kyriakides, T. R., Smith, E. A., Goldstein, S. A. & Bornstein, P. (2000). Increased marrow-derived osteoprogenitor cells and endosteal bone formation in mice lacking thrombospondin 2. *J Bone Miner Res, 15*, 851-862.
Hankenson, K. D. & Bornstein, P. (2002). The secreted protein thrombospondin 2 is an autocrine inhibitor of marrow stromal cell proliferation. *J Bone Miner Res, 17*, 415-425.
Harrison, G., Shapiro, I. M. & Golub, E. E. (1995). The phosphatidylinositol-glycolipid anchor on alkaline phosphatase facilitates mineralization initiation in vitro. *J Bone Miner Res, 10*, 568-573.
Hartl, F. U. (1996). Molecular chaperones in cellular protein folding. *Nature, 381*, 571-579.
Hartmann, C. (2002). Wnt-signaling and skeletogenesis. *J Musculoskelet Neuronal Interact, 2*, 274-276.
Hartmann, C. & Tabin, C. J. (2000). Dual roles of Wnt signaling during chondrogenesis in the chicken limb. *Development, 127*, 3141-3159.
Hatori, M., Klatte, K. J., Teixeira, C. C. & Shapiro, I. M. (1995). End labeling studies of fragmented DNA in the avian growth plate: evidence of apoptosis in terminally differentiated chondrocytes. *J Bone Miner Res, 10*, 1960-1968.
Hauschka, P. V., Lian, J. B., Cole, D. E. & Gundberg, C. M. (1989). Osteocalcin and matrix Gla protein: vitamin K-dependent proteins in bone. *Physiol Rev, 69*, 990-1047.
Haussler, M. R., Whitfield, G. K., Haussler, C. A., Hsieh, J.-C., Thompson, P. D., Selznick, S. H., Dominguez, C. E. & Jurutka, P. W. (1998). The Nuclear Vitamin D Receptor: Biological and Molecular Regulatory Properties Revealed. *Journal of Bone and Mineral Research, 13*, 325-349.
Haynesworth, S. E., Goshima, J., Goldberg, V. M. & Caplan, A. I. (1992). Characterization of cells with osteogenic potential from human marrow. *Bone, 13*, 81-88.
Herring, G. M. (1977). Methods for the study of the glycoproteins and proteoglycans of bone using bacterial collagenase. Determination of bone sialoprotein and chondroitin sulphate. *Calcif Tissue Res, 24*, 29-36.
Hershko, A. & Ciechanover, A. (1998). The ubiquitin system. *Annu Rev Biochem, 67*, 425-479.
Hill, T. P., Spater, D., Taketo, M. M., Birchmeier, W. & Hartmann, C. (2005). Canonical Wnt/beta-catenin signaling prevents osteoblasts from differentiating into chondrocytes. *Dev Cell, 8*, 727-738.
Hohfeld, J. (1998). Regulation of the heat shock conjugate Hsc70 in the mammalian cell: the characterization of the anti-apoptotic protein BAG-1 provides novel insights. *Biol Chem, 379*, 269-274.
Horton, J. A., Bariteau, J. T., Loomis, R. M., Strauss, J. A. & Damron, T. A. (2008). Ontogeny of skeletal maturation in the juvenile rat. *Anat Rec (Hoboken), 291*, 283-292.
Horton, W. A. (1993). Morphology of connective tissue: Cartilage.

In Connective tissue and its heritable disorders. *Wiley-Liss, New York, NY.*, 73-84.
Huang, Z., Ren, P. G., Ma, T., Smith, R. L. & Goodman, S. B. (2010). Modulating osteogenesis of mesenchymal stem cells by modifying growth factor availability. *Cytokine, 51*, 305-310.
Hung, W. J., Roberson, R. S., Taft, J. & Wu, D. Y. (2003). Human BAG-1 proteins bind to the cellular stress response protein GADD34 and interfere with GADD34 functions. *Mol Cell Biol, 23*, 3477-3486.
Hunziker, E. B., Wagner, J. & Zapf, J. (1994). Differential effects of insulin-like growth factor I and growth hormone on developmental stages of rat growth plate chondrocytes in vivo. *J Clin Invest, 93*, 1078-1086.
Hwang, W. S. (1978). Ultrastructure of human foetal and neonatal hyaline cartilage. *J Pathol, 126*, 209-214.

Ihara, H., Denhardt, D. T., Furuya, K., Yamashita, T., Muguruma, Y., Tsuji, K., Hruska, K. A., Higashio, K., Enomoto, S., Nifuji, A., Rittling, S. R. & Noda, M. (2001). Parathyroid hormone-induced bone resorption does not occur in the absence of osteopontin. *J Biol Chem, 276*, 13065-13071.

Inada, M., Yasui, T., Nomura, S., Miyake, S., Deguchi, K., Himeno, M., Sato, M., Yamagiwa, H., Kimura, T., Yasui, N., Ochi, T., Endo, N., Kitamura, Y., Kishimoto, T. & Komori, T. (1999). Maturational disturbance of chondrocytes in Cbfa1-deficient mice. *Dev Dyn, 214*, 279-290.

Ishijima, M., Rittling, S. R., Yamashita, T., Tsuji, K., Kurosawa, H., Nifuji, A., Denhardt, D. T. & Noda, M. (2001). Enhancement of osteoclastic bone resorption and suppression of osteoblastic bone formation in response to reduced mechanical stress do not occur in the absence of osteopontin. *J Exp Med, 193*, 399-404.

Iwamoto, M., Kitagaki, J., Tamamura, Y., Gentili, C., Koyama, E., Enomoto, H., Komori, T., Pacifici, M. & Enomoto-Iwamoto, M. (2003). Runx2 expression and action in chondrocytes are regulated by retinoid signaling and parathyroid hormone-related peptide (PTHrP). *Osteoarthritis Cartilage, 11*, 6-15.

Jia, L., Young, M. F., Powell, J., Yang, L., Ho, N. C., Hotchkiss, R., Robey, P. G. & Francomano, C. A. (2002). Gene expression profile of human bone marrow stromal cells: high-throughput expressed sequence tag sequencing analysis. *Genomics, 79*, 7-17.

Jiang, D., Franceschi, R. T., Boules, H. & Xiao, G. (2004). Parathyroid hormone induction of the osteocalcin gene. Requirement for an osteoblast-specific element 1 sequence in the promoter and involvement of multiple-signaling pathways. *J Biol Chem, 279*, 5329-5337.

Joeng, K. S. & Long, F. (2009). The Gli2 transcriptional activator is a crucial effector for Ihh signaling in osteoblast development and cartilage vascularization. *Development, 136*, 4177-4185.

Kalderon, D., Richardson, W. D., Markham, A. F. & Smith, A. E. (1984). Sequence requirements for nuclear location of simian virus 40 large-T antigen. *Nature, 311*, 33-38.

Karsenty, G. (1999). The genetic transformation of bone biology. *Genes Dev, 13*, 3037-3051.

Karsenty, G. (2003). The complexities of skeletal biology. *Nature, 423*, 316-318.

Katagiri, T., Yamaguchi, A., Ikeda, T., Yoshiki, S., Wozney, J. M., Rosen, V., Wang, E. A., Tanaka, H., Omura, S. & Suda, T. (1990). The non-osteogenic mouse pluripotent cell line, C3H10T1/2, is induced to differentiate into osteoblastic cells by recombinant human bone morphogenetic protein-2. *Biochem Biophys Res Commun, 172*, 295-299.

Kaufman, R. J. (1999). Stress signaling from the lumen of the endoplasmic reticulum: coordination of gene transcriptional and translational controls. *Genes Dev, 13*, 1211-1233.

Kelenyi, G. (1967). On the histochemistry of azo group-free thiazole dyes. *J Histochem Cytochem, 15*, 172-180.

Kerner, S. A., Scott, R. A. & Pike, J. W. (1989). Sequence elements in the human osteocalcin gene confer basal activation and inducible response to hormonal vitamin D3. *Proc Natl Acad Sci U S A, 86*, 4455-4459.

Kerr, J. F., Wyllie, A. H. & Currie, A. R. (1972). Apoptosis: a basic biological phenomenon with wide-ranging implications in tissue kinetics. *Br J Cancer, 26*, 239-257.

King, F. W., Wawrzynow, A., Hohfeld, J. & Zylicz, M. (2001). Co-chaperones Bag-1, Hop and Hsp40 regulate Hsc70 and Hsp90 interactions with wild-type or mutant p53. *EMBO J, 20*, 6297-6305.

Kinkel, M. D. & Horton, W. E., Jr. (2003). Coordinate down-regulation of cartilage matrix gene expression in Bcl-2 deficient chondrocytes is associated with decreased SOX9 expression and decreased mRNA stability. *J Cell Biochem, 88*, 941-953.

Kinkel, M. D., Yagi, R., McBurney, D., Nugent, A. & Horton, W. E., Jr. (2004). Age-related expression patterns of Bag-1 and Bcl-2 in growth plate and articular chondrocytes. *Anat Rec A Discov Mol Cell Evol Biol, 279*, 720-728.

Kirsch, T. & von der Mark, K. (1992). Remodelling of collagen types I, II and X and calcification of human fetal cartilage. *Bone Miner, 18*, 107-117.

Kliewer, S. A., Umesono, K., Mangelsdorf, D. J. & Evans, R. M. (1992). Retinoid X receptor interacts with nuclear receptors in retinoic acid, thyroid hormone and vitamin D3 signalling. *Nature, 355*, 446-449.

Kobayashi, T., Soegiarto, D. W., Yang, Y., Lanske, B., Schipani, E., McMahon, A. P. & Kronenberg, H. M. (2005). Indian hedgehog stimulates periarticular chondrocyte differentiation to regulate growth plate length independently of PTHrP. *J Clin Invest, 115*, 1734-1742.

Komori, T., Yagi, H., Nomura, S., Yamaguchi, A., Sasaki, K., Deguchi, K., Shimizu, Y., Bronson, R. T., Gao, Y. H., Inada, M., Sato, M., Okamoto, R., Kitamura, Y., Yoshiki, S. & Kishimoto, T. (1997). Targeted disruption of Cbfa1 results in a complete lack of bone formation owing to maturational arrest of osteoblasts. *Cell, 89*, 755-764.

Kosher, R. A., Kulyk, W. M. & Gay, S. W. (1986). Collagen gene expression during limb cartilage differentiation. *J Cell Biol, 102*, 1151-1156.

Koyama, E., Leatherman, J. L., Noji, S. & Pacifici, M. (1996). Early chick limb cartilaginous elements possess polarizing activity and express hedgehog-related morphogenetic factors. *Dev Dyn, 207*, 344-354.

Koyama, E., Shibukawa, Y., Nagayama, M., Sugito, H., Young, B., Yuasa, T., Okabe, T., Ochiai, T., Kamiya, N., Rountree, R. B., Kingsley, D. M., Iwamoto, M., Enomoto-Iwamoto, M. & Pacifici, M. (2008). A distinct cohort of progenitor cells participates in synovial joint and articular cartilage formation during mouse limb skeletogenesis. *Dev Biol, 316*, 62-73.

Kronenberg, H. M. (2003). Developmental regulation of the growth plate. *Nature, 423*, 332-336.

Kronenberg, H. M. (2006). PTHrP and skeletal development. *Ann N Y Acad Sci, 1068*, 1-13.

Kullmann, M., Schneikert, J., Moll, J., Heck, S., Zeiner, M., Gehring, U. & Cato, A. C. (1998). RAP46 is a negative regulator of glucocorticoid receptor action and hormone-induced apoptosis. *J Biol Chem, 273*, 14620-14625.

Lane, N. E., Gore, L. R., Cummings, S. R., Hochberg, M. C., Scott, J. C., Williams, E. N. & Nevitt, M. C. (1999). Serum vitamin D levels and incident changes of radiographic hip osteoarthritis: a longitudinal study. Study of Osteoporotic Fractures Research Group. *Arthritis Rheum, 42*, 854-860.

Lanham, S. A., Roberts, C., Perry, M. J., Cooper, C. & Oreffo, R. O. (2008). Intrauterine programming of bone. Part 2: alteration of skeletal structure. *Osteoporos Int, 19*, 157-167.

Lanyon, L. E. (1993). Osteocytes, strain detection, bone modeling and remodeling. *Calcif Tissue Int, 53 Suppl 1*, S102-106; discussion S106-107.

Le, Y. & Sauer, B. (2000). Conditional gene knockout using cre recombinase. *Methods Mol Biol, 136*, 477-485.

Lee, K., Deeds, J. D. & Segre, G. V. (1995). Expression of parathyroid hormone-related peptide and its receptor messenger ribonucleic acids during fetal development of rats. *Endocrinology, 136*, 453-463.

Lee, K., Lanske, B., Karaplis, A. C., Deeds, J. D., Kohno, H., Nissenson, R. A., Kronenberg, H. M. & Segre, G. V. (1996). Parathyroid hormone-related peptide delays terminal differentiation of chondrocytes during endochondral bone development. *Endocrinology, 137*, 5109-5118.

Lee, S. S., Crabb, S. J., Janghra, N., Carlberg, C., Williams, A. C., Cutress, R. I., Packham, G. & Hague, A. (2007). Subcellular localisation of BAG-1 and its regulation of vitamin D receptor-mediated transactivation and involucrin expression in oral keratinocytes: implications for oral carcinogenesis. *Exp Cell Res, 313*, 3222-3238.

Lefebvre, V., Huang, W., Harley, V. R., Goodfellow, P. N. & de Crombrugghe, B. (1997). SOX9 is a potent activator of the chondrocyte-specific enhancer of the pro alpha1(II) collagen gene. *Mol Cell Biol, 17*, 2336-2346.

Lefebvre, V. & Smits, P. (2005). Transcriptional control of chondrocyte fate and differentiation. *Birth Defects Res C Embryo Today, 75*, 200-212.

Legros, R., Balmain, N. & Bonel, G. (1987). Age-related changes in mineral of rat and bovine cortical bone. *Calcif Tissue Int, 41*, 137-144.

Lengner, C. J., Lepper, C., van Wijnen, A. J., Stein, J. L., Stein, G. S. & Lian, J. B. (2004). Primary mouse embryonic fibroblasts: a model of mesenchymal cartilage formation. *J Cell Physiol, 200*, 327-333.

Li, J., Sarosi, I., Yan, X. Q., Morony, S., Capparelli, C., Tan, H. L., McCabe, S., Elliott, R., Scully, S., Van, G., Kaufman, S., Juan, S. C., Sun, Y., Tarpley, J., Martin, L., Christensen, K., McCabe, J., Kostenuik, P., Hsu, H., Fletcher, F., Dunstan, C. R., Lacey, D. L. & Boyle, W. J. (2000). RANK is the intrinsic hematopoietic cell surface receptor that controls osteoclastogenesis and regulation of bone mass and calcium metabolism. *Proc Natl Acad Sci U S A, 97*, 1566-1571.

Li, X., Leo, B. M., Beck, G., Balian, G. & Anderson, G. D. (2004). Collagen and proteoglycan abnormalities in the GDF-5-deficient mice and molecular changes when treating disk cells with recombinant growth factor. *Spine (Phila Pa 1976), 29*, 2229-2234.

Lian, J. B., Shalhoub, V., Aslam, F., Frenkel, B., Green, J., Hamrah, M., Stein, G. S. & Stein, J. L. (1997). Species-specific glucocorticoid and 1,25-dihydroxyvitamin D responsiveness in mouse MC3T3-E1 osteoblasts: dexamethasone inhibits osteoblast differentiation and vitamin D down-regulates osteocalcin gene expression. *Endocrinology, 138*, 2117-2127.

Lian, J. B. & Stein, G. S. (1992). Concepts of osteoblast growth and differentiation: basis for modulation of bone cell development and tissue formation. *Crit Rev Oral Biol Med, 3*, 269-305.

Lim, S. K., Won, Y. J., Lee, H. C., Huh, K. B. & Park, Y. S. (1999). A PCR analysis of ERalpha and ERbeta mRNA abundance in rats and the effect of ovariectomy. *J Bone Miner Res, 14*, 1189-1196.

Lin, J., Hutchinson, L., Gaston, S. M., Raab, G. & Freeman, M. R. (2001). BAG-1 is a novel cytoplasmic binding partner of the membrane form of heparin-binding EGF-like growth factor: a unique role for proHB-EGF in cell survival regulation. *J Biol Chem, 276*, 30127-30132.

Lips, P., Hosking, D., Lippuner, K., Norquist, J. M., Wehren, L., Maalouf, G., Ragi-Eis, S. & Chandler, J. (2006). The prevalence of vitamin D inadequacy amongst women with osteoporosis: an international epidemiological investigation. *J Intern Med, 260*, 245-254.

Lison, L. (1954). Alcian blue 8 G with chlorantine fast red 5 B.A technic for selective staining of mycopolysaccharides. *Stain Technol, 29*, 131-138.

Liu, R., Takayama, S., Zheng, Y., Froesch, B., Chen, G. Q., Zhang, X., Reed, J. C. & Zhang, X. K. (1998). Interaction of BAG-1 with retinoic acid receptor and its inhibition of retinoic acid-induced apoptosis in cancer cells. *J Biol Chem, 273*, 16985-16992.

Lodish H, B. A., Zipursky SL, et al. (2000). Molecular Cell Biology. 4th edition.: New York: W. H. Freeman; 2000.

Long, F., Chung, U. I., Ohba, S., McMahon, J., Kronenberg, H. M. & McMahon, A. P. (2004). Ihh signaling is directly required for the osteoblast lineage in the endochondral skeleton. *Development, 131*, 1309-1318.

Long, F., Zhang, X. M., Karp, S., Yang, Y. & McMahon, A. P. (2001). Genetic manipulation of hedgehog signaling in the endochondral skeleton reveals a direct role in the regulation of chondrocyte proliferation. *Development, 128*, 5099-5108.

Luders, J., Demand, J., Papp, O. & Hohfeld, J. (2000). Distinct isoforms of the cofactor BAG-1 differentially affect Hsc70 chaperone function. *J Biol Chem, 275*, 14817-14823.

Luo, G., Ducy, P., McKee, M. D., Pinero, G. J., Loyer, E., Behringer, R. R. & Karsenty, G. (1997). Spontaneous calcification of arteries and cartilage in mice lacking matrix GLA protein. *Nature, 386*, 78-81.

Macias, D., Ganan, Y., Sampath, T. K., Piedra, M. E., Ros, M. A. & Hurle, J. M. (1997). Role of BMP-2 and OP-1 (BMP-7) in programmed cell death and skeletogenesis during chick limb development. *Development, 124*, 1109-1117.

Mackie, E. J., Tatarczuch, L. & Mirams, M. (2011). The skeleton: a multi-functional complex organ: the growth plate chondrocyte and endochondral ossification. *Journal of Endocrinology, 211*, 109-121.

Mangelsdorf, D. J., Thummel, C., Beato, M., Herrlich, P., Schutz, G., Umesono, K., Blumberg, B., Kastner, P., Mark, M., Chambon, P. & Evans, R. M. (1995). The nuclear receptor superfamily: the second decade. *Cell, 83*, 835-839.

Matsumoto, Y., Otsuka, F., Takano-Narazaki, M., Katsuyama, T., Nakamura, E., Tsukamoto, N., Inagaki, K., Sada, K.-e. & Makino, H. (2013). Estrogen facilitates osteoblast differentiation by upregulating bone morphogenetic protein-4 signaling. *Steroids, 78*, 513-520.

Mayer, M. P., Brehmer, D., Gassler, C. S. & Bukau, B. (2001). Hsp70 chaperone machines. *Adv Protein Chem, 59*, 1-44.

McAlindon, T. E., Felson, D. T., Zhang, Y., Hannan, M. T., Aliabadi, P., Weissman, B., Rush, D., Wilson, P. W. & Jacques, P. (1996). Relation of dietary intake and serum levels of vitamin D to progression of osteoarthritis of the knee among participants in the Framingham Study. *Ann Intern Med, 125*, 353-359.

McKee, M. D., Glimcher, M. J. & Nanci, A. (1992). High-resolution immunolocalization of osteopontin and osteocalcin in bone and cartilage during endochondral ossification in the chicken tibia. *Anat Rec, 234*, 479-492.

Merry, K., Dodds, R., Littlewood, A. & Gowen, M. (1993). Expression of osteopontin mRNA by osteoclasts and osteoblasts in modelling adult human bone. *J Cell Sci, 104 (Pt 4)*, 1013-1020.

Miettinen, P. J., Chin, J. R., Shum, L., Slavkin, H. C., Shuler, C. F., Derynck, R. & Werb, Z. (1999). Epidermal growth factor receptor function is necessary for normal craniofacial development and palate closure. *Nature Genetics, 22*, 69-73.

Minina, E., Kreschel, C., Naski, M. C., Ornitz, D. M. & Vortkamp, A. (2002). Interaction of FGF, Ihh/Pthlh, and BMP signaling integrates chondrocyte proliferation and hypertrophic differentiation. *Dev Cell, 3*, 439-449.

Minina, E., Wenzel, H. M., Kreschel, C., Karp, S., Gaffield, W., McMahon, A. P. & Vortkamp, A. (2001). BMP and Ihh/PTHrP signaling interact to coordinate chondrocyte proliferation and differentiation. *Development, 128*, 4523-4534.

Moursi, A. M., Damsky, C. H., Lull, J., Zimmerman, D., Doty, S. B., Aota, S. & Globus, R. K. (1996). Fibronectin regulates calvarial osteoblast differentiation. *J Cell Sci, 109 (Pt 6)*, 1369-1380.

Nakada, D., Oguro, H., Levi, B. P., Ryan, N., Kitano, A., Saitoh, Y., Takeichi, M., Wendt, G. R. & Morrison, S. J. (2014). Oestrogen increases haematopoietic stem-cell self-renewal in females and during pregnancy. *Nature, 505*, 555-558.

Nakashima, K., Zhou, X., Kunkel, G., Zhang, Z., Deng, J. M., Behringer, R. R. & de Crombrugghe, B. (2002). The novel zinc finger-containing transcription factor osterix is required for osteoblast differentiation and bone formation. *Cell, 108*, 17-29.

Narisawa, S., Yadav, M. C. & Millan, J. L. (2013). In vivo overexpression of tissue-nonspecific alkaline phosphatase increases skeletal mineralization and affects the phosphorylation status of osteopontin. *J Bone Miner Res, 28*, 1587-1598.

Ng, L. J., Wheatley, S., Muscat, G. E., Conway-Campbell, J., Bowles, J., Wright, E., Bell, D. M., Tam, P. P., Cheah, K. S. & Koopman, P. (1997). SOX9 binds DNA, activates transcription,

and coexpresses with type II collagen during chondrogenesis in the mouse. *Dev Biol, 183*, 108-121.
Nilsson, O., Marino, R., De Luca, F., Phillip, M. & Baron, J. (2005). Endocrine regulation of the growth plate. *Horm Res, 64*, 157-165.
Niyaz, Y., Zeiner, M. & Gehring, U. (2001). Transcriptional activation by the human Hsp70-associating protein Hap50. *J Cell Sci, 114*, 1839-1845.
Norman, A. W. (1990). Intestinal calcium absorption: a vitamin D-hormone-mediated adaptive response. *Am J Clin Nutr, 51*, 290-300.
Nugent, A. E., Speicher, D. M., Gradisar, I., McBurney, D. L., Baraga, A., Doane, K. J. & Horton, W. E., Jr. (2009). Advanced osteoarthritis in humans is associated with altered collagen VI expression and upregulation of ER-stress markers Grp78 and bag-1. *J Histochem Cytochem, 57*, 923-931.
Nurminsky, D., Magee, C., Faverman, L. & Nurminskaya, M. (2007). Regulation of chondrocyte differentiation by actin-severing protein adseverin. *Dev Biol, 302*, 427-437.
Ogawa, M., Porter, P. N. & Nakahata, T. (1983). Renewal and commitment to differentiation of hemopoietic stem cells (an interpretive review). *Blood, 61*, 823-829.
Okazaki, R., Inoue, D., Shibata, M., Saika, M., Kido, S., Ooka, H., Tomiyama, H., Sakamoto, Y. & Matsumoto, T. (2002). Estrogen promotes early osteoblast differentiation and inhibits adipocyte differentiation in mouse bone marrow stromal cell lines that express estrogen receptor (ER) alpha or beta. *Endocrinology, 143*, 2349-2356.
Ornitz, D. M. & Marie, P. J. (2002). FGF signaling pathways in endochondral and intramembranous bone development and human genetic disease. *Genes Dev, 16*, 1446-1465.
Otsuka, G., Kubo, T., Imanishi, J. & Hirasawa, Y. (1996). Expression of heat-shock-proteins in the differentiation process of chondrocytes. *Nihon Geka Hokan, 65*, 39-48.
Ovchinnikov, D. A., Deng, J. M., Ogunrinu, G. & Behringer, R. R. (2000). Col2a1-directed expression of Cre recombinase in differentiating chondrocytes in transgenic mice. *Genesis, 26*, 145-146.
Packham, G., Brimmell, M. & Cleveland, J. L. (1997). Mammalian cells express two differently localized Bag-1 isoforms generated by alternative translation initiation. *Biochem J, 328 (Pt 3)*, 807-813.
Pajevic, P. D. (2009). Regulation of Bone Resorption and Mineral Homeostasis by Osteocytes. *IBMS BoneKEy, 6(2):63-70*.
Parfitt, A. M. (1994). Osteonal and hemi-osteonal remodeling: the spatial and temporal framework for signal traffic in adult human bone. *J Cell Biochem, 55*, 273-286.
Parfitt, A. M. (2002). Misconceptions (2): turnover is always higher in cancellous than in cortical bone. *Bone, 30*, 807-809.
Parfitt, A. M., Han, Z. H., Palnitkar, S., Rao, D. S., Shih, M. S. & Nelson, D. (1997). Effects of ethnicity and age or menopause on osteoblast function, bone mineralization, and osteoid accumulation in iliac bone. *J Bone Miner Res, 12*, 1864-1873.
Phinney, D. G., Kopen, G., Isaacson, R. L. & Prockop, D. J. (1999). Plastic adherent stromal cells from the bone marrow of commonly used strains of inbred mice: variations in yield, growth, and differentiation. *J Cell Biochem, 72*, 570-585.
Pizette, S. & Niswander, L. (2000). BMPs are required at two steps of limb chondrogenesis: formation of prechondrogenic condensations and their differentiation into chondrocytes. *Dev Biol, 219*, 237-249.
Price, P. A. (1989). Gla-containing proteins of bone. *Connect Tissue Res, 21*, 51-57; discussion 57-60.
Price, P. A. & Williamson, M. K. (1981). Effects of warfarin on bone. Studies on the vitamin K-dependent protein of rat bone. *J Biol Chem, 256*, 12754-12759.
Raisz, L. G. (2005). Pathogenesis of osteoporosis: concepts, conflicts, and prospects. *J Clin Invest, 115*, 3318-3325.

Rajewsky, K., Gu, H., Kuhn, R., Betz, U. A., Muller, W., Roes, J. & Schwenk, F. (1996). Conditional gene targeting. *J Clin Invest, 98*, 600-603.

Rao, R. V., Ellerby, H. M. & Bredesen, D. E. (2004). Coupling endoplasmic reticulum stress to the cell death program. *Cell Death Differ, 11*, 372-380.

Rassow, J., von Ahsen, O., Bomer, U. & Pfanner, N. (1997). Molecular chaperones: towards a characterization of the heat-shock protein 70 family. *Trends in cell biology, 7*, 129-133.

Rauch, A., Seitz, S., Baschant, U., Schilling, A. F., Illing, A., Stride, B., Kirilov, M., Mandic, V., Takacz, A., Schmidt-Ullrich, R., Ostermay, S., Schinke, T., Spanbroek, R., Zaiss, M. M., Angel, P. E., Lerner, U. H., David, J. P., Reichardt, H. M., Amling, M., Schutz, G. & Tuckermann, J. P. (2010). Glucocorticoids suppress bone formation by attenuating osteoblast differentiation via the monomeric glucocorticoid receptor. *Cell Metab, 11*, 517-531.

Recker, R. R. (1992). Embryology, anatomy, and microstructure of bone. In: Coe FL, Favus MJ (eds) Disorders of bone and mineral metabolism. Raven Press, New York, pp 219-240.

Reed, J. C. (1998). Bcl-2 family proteins. *Oncogene, 17*, 3225-3236.

Reinholt, F. P., Hultenby, K., Oldberg, A. & Heinegard, D. (1990). Osteopontin--a possible anchor of osteoclasts to bone. *Proc Natl Acad Sci U S A, 87*, 4473-4475.

Roach, H. I. & Clarke, N. M. (1999). "Cell paralysis" as an intermediate stage in the programmed cell death of epiphyseal chondrocytes during development. *J Bone Miner Res, 14*, 1367-1378.

Roach, H. I. & Clarke, N. M. (2000). Physiological cell death of chondrocytes in vivo is not confined to apoptosis. New observations on the mammalian growth plate. *J Bone Joint Surg Br, 82*, 601-613.

Robertson, W. W., Jr. (1990). Newest knowledge of the growth plate. *Clin Orthop Relat Res*, 270-278.

Robey, P. G., Young, M. F., Fisher, L. W. & McClain, T. D. (1989). Thrombospondin is an osteoblast-derived component of mineralized extracellular matrix. *J Cell Biol, 108*, 719-727.

Romano, T., Wark, J. D., Owens, J. A. & Wlodek, M. E. (2009). Prenatal growth restriction and postnatal growth restriction followed by accelerated growth independently program reduced bone growth and strength. *Bone, 45*, 132-141.

Ross, S. & Hill, C. S. (2008). How the Smads regulate transcription. *Int J Biochem Cell Biol, 40*, 383-408.

Salmon, P. & Sasov, A. (2007). Application of Nano-CT and High-Resolution Micro-CT to Study Bone Quality and Ultrastructure, Scaffold Biomaterials and Vascular Networks. In L. Qin, H. Genant, J. Griffith & K. Leung (Eds.) *Advanced Bioimaging Technologies in Assessment of the Quality of Bone and Scaffold Materials.* pp. 323-331). Springer Berlin Heidelberg.

Schlesinger, M. J. (1990). Heat shock proteins. *J Biol Chem, 265*, 12111-12114.

Shao, Y. Y., Wang, L. & Ballock, R. T. (2006). Thyroid hormone and the growth plate. *Rev Endocr Metab Disord, 7*, 265-271.

Sharp, A., Crabb, S. J., Johnson, P. W., Hague, A., Cutress, R., Townsend, P. A., Ganesan, A. & Packham, G. (2009a). Thioflavin S (NSC71948) interferes with Bcl-2-associated athanogene (BAG-1)-mediated protein-protein interactions. *J Pharmacol Exp Ther, 331*, 680-689.

Sharp, A., Cutress, R. I., Johnson, P. W., Packham, G. & Townsend, P. A. (2009b). Short peptides derived from the BAG-1 C-terminus inhibit the interaction between BAG-1 and HSC70 and decrease breast cancer cell growth. *FEBS Lett, 583*, 3405-3411.

Shi, Y. & Massague, J. (2003). Mechanisms of TGF-beta signaling from cell membrane to the nucleus. *Cell, 113*, 685-700.

Sondermann, H., Scheufler, C., Schneider, C., Hohfeld, J., Hartl, F. U. & Moarefi, I. (2001). Structure of a Bag/Hsc70 complex: convergent functional evolution of Hsp70 nucleotide exchange factors. *Science, 291*, 1553-1557.

Song, J., Takeda, M. & Morimoto, R. I. (2001). Bag1-Hsp70 mediates a physiological stress signalling pathway that regulates Raf-1/ERK and cell growth. *Nat Cell Biol, 3*, 276-282.

St-Jacques, B., Hammerschmidt, M. & McMahon, A. P. (1999). Indian hedgehog signaling regulates proliferation and differentiation of chondrocytes and is essential for bone formation. *Genes Dev, 13*, 2072-2086.

Stanton, L. A., Sabari, S., Sampaio, A. V., Underhill, T. M. & Beier, F. (2004). p38 MAP kinase signalling is required for hypertrophic chondrocyte differentiation. *Biochem J, 378*, 53-62.

Stepien, E. (2011). Acceleration of New Biomarkers Development and Discovery in Synergistic Diagnostics of Coronary Artery Disease. In: Coronary Angiography - Advances in Noninvasive Imaging Approach for Evaluation of Coronary Artery Disease, Prof. Baskot Branislav (Ed.), ISBN: 978-953-307-675-1, InTech, DOI: 10.5772/18940.

Sternberg, N. & Hamilton, D. (1981). Bacteriophage P1 site-specific recombination. I. Recombination between loxP sites. *J Mol Biol, 150*, 467-486.

Stewart, A., Guan, H. & Yang, K. (2010). BMP-3 promotes mesenchymal stem cell proliferation through the TGF-beta/activin signaling pathway. *J Cell Physiol, 223*, 658-666.

Sturzenbaum, S. R. & Kille, P. (2001). Control genes in quantitative molecular biological techniques: the variability of invariance. *Comp Biochem Physiol B Biochem Mol Biol, 130*, 281-289.

Sysa-Shah, P., Xu, Y., Guo, X., Belmonte, F., Kang, B., Bedja, D., Pin, S., Tsuchiya, N. & Gabrielson, K. (2012). Cardiac-Specific Over-Expression of Epidermal Growth Factor Receptor 2 (ErbB2) Induces Pro-Survival Pathways and Hypertrophic Cardiomyopathy in Mice. *PLoS One, 7*.

Tachibana, M., Kasukabe, T., Kobayashi, Y., Suzuki, T., Kinoshita, S. & Matsushima, Y. (2000). Expression of estrogen receptor alpha and beta in the mouse cornea. *Invest Ophthalmol Vis Sci, 41*, 668-670.

Taher, L., Collette, N. M., Murugesh, D., Maxwell, E., Ovcharenko, I. & Loots, G. G. (2011). Global gene expression analysis of murine limb development. *PLoS One, 6*, e28358.

Takayama, S., Bimston, D. N., Matsuzawa, S., Freeman, B. C., Aime-Sempe, C., Xie, Z., Morimoto, R. I. & Reed, J. C. (1997). BAG-1 modulates the chaperone activity of Hsp70/Hsc70. *EMBO J, 16*, 4887-4896.

Takayama, S., Kochel, K., Irie, S., Inazawa, J., Abe, T., Sato, T., Druck, T., Huebner, K. & Reed, J. C. (1996). Cloning of cDNAs encoding the human BAG1 protein and localization of the human BAG1 gene to chromosome 9p12. *Genomics, 35*, 494-498.

Takayama, S., Krajewski, S., Krajewska, M., Kitada, S., Zapata, J. M., Kochel, K., Knee, D., Scudiero, D., Tudor, G., Miller, G. J., Miyashita, T., Yamada, M. & Reed, J. C. (1998). Expression and location of Hsp70/Hsc-binding anti-apoptotic protein BAG-1 and its variants in normal tissues and tumor cell lines. *Cancer Res, 58*, 3116-3131.

Takayama, S. & Reed, J. C. (2001). Molecular chaperone targeting and regulation by BAG family proteins. *Nat Cell Biol, 3*, E237-241.

Takayama, S., Sato, T., Krajewski, S., Kochel, K., Irie, S., Millan, J. A. & Reed, J. C. (1995). Cloning and functional analysis of BAG-1: a novel Bcl-2-binding protein with anti-cell death activity. *Cell, 80*, 279-284.

Takayama, S., Xie, Z. & Reed, J. C. (1999). An evolutionarily conserved family of Hsp70/Hsc70 molecular chaperone regulators. *J Biol Chem, 274*, 781-786.

Tare, R. S., Babister, J. C., Kanczler, J. & Oreffo, R. O. (2008a). Skeletal stem cells: phenotype, biology and environmental niches informing tissue regeneration. *Mol Cell Endocrinol, 288*, 11-21.

Tare, R. S., Townsend, P. A., Packham, G. K., Inglis, S. & Oreffo, R. O. (2008b). Bcl-2-associated athanogene-1 (BAG-1): a transcriptional regulator mediating chondrocyte survival and differentiation during endochondral ossification. *Bone, 42*, 113-128.

Tare, R. S., Townsend, P. A., Packham, G. K. & Oreffo, R. O. (2011). Bag-1 haploinsufficiency affects cartilage development and osteogenic differentiation. *Bone, 48*, S100-S101.

Teitelbaum, S. L. & Ross, F. P. (2003). Genetic regulation of osteoclast development and function. *Nat Rev Genet, 4*, 638-649.

Termine, J. D., Kleinman, H. K., Whitson, S. W., Conn, K. M., McGarvey, M. L. & Martin, G. R. (1981). Osteonectin, a bone-specific protein linking mineral to collagen. *Cell, 26*, 99-105.

Tew, S. R., Murdoch, A. D., Rauchenberg, R. P. & Hardingham, T. E. (2008). Cellular methods in cartilage research: primary human chondrocytes in culture and chondrogenesis in human bone marrow stem cells. *Methods, 45*, 2-9.

Topol, L., Jiang, X., Choi, H., Garrett-Beal, L., Carolan, P. J. & Yang, Y. (2003). Wnt-5a inhibits the canonical Wnt pathway by promoting GSK-3-independent beta-catenin degradation. *J Cell Biol, 162*, 899-908.

Townsend, P. A., Cutress, R. I., Sharp, A., Brimmell, M. & Packham, G. (2003a). BAG-1 prevents stress-induced long-term growth inhibition in breast cancer cells via a chaperone-dependent pathway. *Cancer Res, 63*, 4150-4157.

Townsend, P. A., Cutress, R. I., Sharp, A., Brimmell, M. & Packham, G. (2003b). BAG-1: a multifunctional regulator of cell growth and survival. *Biochim Biophys Acta, 1603*, 83-98.

Townsend, P. A., Stephanou, A., Packham, G. & Latchman, D. S. (2005). BAG-1: a multi-functional pro-survival molecule. *International Journal of Biochemistry & Cell Biology, 37*, 251-259.

Turner, C. H. & Pavalko, F. M. (1998). Mechanotransduction and functional response of the skeleton to physical stress: the mechanisms and mechanics of bone adaptation. *J Orthop Sci, 3*, 346-355.

Välimäki, V.-V., Alfthan, H., Lehmuskallio, E., Löyttyniemi, E., Sahi, T., Suominen, H. & Välimäki, M. J. Risk factors for clinical stress fractures in male military recruits: A prospective cohort study. *Bone, 37*, 267-273.

van de Peppel, J. & van Leeuwen, J. P. (2014). Vitamin D and gene networks in human osteoblasts. *Front Physiol, 5*, 137.

van Donkelaar, C. C. & Wilson, W. (2012). Mechanics of chondrocyte hypertrophy. *Biomech Model Mechanobiol, 11*, 655-664.

van Driel, M. & van Leeuwen, J. P. (2014). Vitamin D endocrine system and osteoblasts. *Bonekey Rep, 3*, 493.

Vortkamp, A., Lee, K., Lanske, B., Segre, G. V., Kronenberg, H. M. & Tabin, C. J. (1996). Regulation of rate of cartilage differentiation by Indian hedgehog and PTH-related protein. *Science, 273*, 613-622.

Wallis, G. A. (1996). Bone growth: coordinating chondrocyte differentiation. *Curr Biol, 6*, 1577-1580.

Wang, H. G. & Reed, J. C. (1998). Bc1-2, Raf-1 and mitochondrial regulation of apoptosis. *Biofactors, 8*, 13-16.

Wang, H. G., Takayama, S., Rapp, U. R. & Reed, J. C. (1996). Bcl-2 interacting protein, BAG-1, binds to and activates the kinase Raf-1. *Proc Natl Acad Sci U S A, 93*, 7063-7068.

Waterston, R. H., Lindblad-Toh, K., Birney, E., Rogers, J., Abril, J. F., Agarwal, P., Agarwala, R., Ainscough, R., Alexandersson, M., An, P., Antonarakis, S. E., Attwood, J., Baertsch, R., Bailey, J., Barlow, K., Beck, S., Berry, E., Birren, B., Bloom, T., Bork, P., Botcherby, M., Bray, N., Brent, M. R., Brown, D. G., Brown, S. D., Bult, C., Burton, J., Butler, J., Campbell, R. D., Carninci, P., Cawley, S., Chiaromonte, F., Chinwalla, A. T., Church, D. M., Clamp, M., Clee, C., Collins, F. S., Cook, L. L., Copley, R. R., Coulson, A., Couronne,

O., Cuff, J., Curwen, V., Cutts, T., Daly, M., David, R., Davies, J., Delehaunty, K. D., Deri, J., Dermitzakis, E. T., Dewey, C., Dickens, N. J., Diekhans, M., Dodge, S., Dubchak, I., Dunn, D. M., Eddy, S. R., Elnitski, L., Emes, R. D., Eswara, P., Eyras, E., Felsenfeld, A., Fewell, G. A., Flicek, P., Foley, K., Frankel, W. N., Fulton, L. A., Fulton, R. S., Furey, T. S., Gage, D., Gibbs, R. A., Glusman, G., Gnerre, S., Goldman, N., Goodstadt, L., Grafham, D., Graves, T. A., Green, E. D., Gregory, S., Guigo, R., Guyer, M., Hardison, R. C., Haussler, D., Hayashizaki, Y., Hillier, L. W., Hinrichs, A., Hlavina, W., Holzer, T., Hsu, F., Hua, A., Hubbard, T., Hunt, A., Jackson, I., Jaffe, D. B., Johnson, L. S., Jones, M., Jones, T. A., Joy, A., Kamal, M., Karlsson, E. K., et al. (2002). Initial sequencing and comparative analysis of the mouse genome. *Nature, 420***,** 520-562.

Watson J, M. J. (n/d). Distinguishing Human From Animal Bone. *http://www.statemuseum.arizona.edu/crservices/human_animal_bone.shtml*.

Weinstein, R. S., Jilka, R. L., Parfitt, A. M. & Manolagas, S. C. (1998). Inhibition of osteoblastogenesis and promotion of apoptosis of osteoblasts and osteocytes by glucocorticoids. Potential mechanisms of their deleterious effects on bone. *J Clin Invest, 102***,** 274-282.

Wenstrup, R. J., Florer, J. B., Brunskill, E. W., Bell, S. M., Chervoneva, I. & Birk, D. E. (2004). Type V collagen controls the initiation of collagen fibril assembly. *J Biol Chem, 279***,** 53331-53337.

Winnard, R. G., Gerstenfeld, L. C., Toma, C. D. & Franceschi, R. T. (1995). Fibronectin gene expression, synthesis and accumulation during in vitro differentiation of chicken osteoblasts. *J Bone Miner Res, 10***,** 1969-1977.

Woeckel, V. J., Alves, R. D., Swagemakers, S. M., Eijken, M., Chiba, H., van der Eerden, B. C. & van Leeuwen, J. P. (2010). 1Alpha,25-(OH)2D3 acts in the early phase of osteoblast differentiation to enhance mineralization via accelerated production of mature matrix vesicles. *J Cell Physiol, 225***,** 593-600.

Wozney, J. M., Rosen, V., Celeste, A. J., Mitsock, L. M., Whitters, M. J., Kriz, R. W., Hewick, R. M. & Wang, E. A. (1988). Novel regulators of bone formation: molecular clones and activities. *Science, 242***,** 1528-1534.

Wozney, J. M. R., V. (1993). Bone morphogenic proteins. In *Physiology and Pharmacology of Bone (eds. Martin, T.J. & Mundy, G.)*. *Springer-Verlag, Berlin***,** 725-748.

Wu, B., Hunt, C. & Morimoto, R. (1985). Structure and expression of the human gene encoding major heat shock protein HSP70. *Mol Cell Biol, 5***,** 330-341.

Xiao, G., Jiang, D., Gopalakrishnan, R. & Franceschi, R. T. (2002). Fibroblast growth factor 2 induction of the osteocalcin gene requires MAPK activity and phosphorylation of the osteoblast transcription factor, Cbfa1/Runx2. *J Biol Chem, 277***,** 36181-36187.

Yamaguchi, A., Ishizuya, T., Kintou, N., Wada, Y., Katagiri, T., Wozney, J. M., Rosen, V. & Yoshiki, S. (1996). Effects of BMP-2, BMP-4, and BMP-6 on osteoblastic differentiation of bone marrow-derived stromal cell lines, ST2 and MC3T3-G2/PA6. *Biochem Biophys Res Commun, 220***,** 366-371.

Yang, L., Carlson, S. G., McBurney, D. & Horton, W. E., Jr. (2005). Multiple signals induce endoplasmic reticulum stress in both primary and immortalized chondrocytes resulting in loss of differentiation, impaired cell growth, and apoptosis. *J Biol Chem, 280***,** 31156-31165.

Yang, L., McBurney, D., Tang, S. C., Carlson, S. G. & Horton, W. E., Jr. (2007). A novel role for Bcl-2 associated-athanogene-1 (Bag-1) in regulation of the endoplasmic reticulum stress response in mammalian chondrocytes. *J Cell Biochem, 102***,** 786-800.

Yang, X., Chernenko, G., Hao, Y., Ding, Z., Pater, M. M., Pater, A. & Tang, S. C. (1998). Human BAG-1/RAP46 protein is generated as four isoforms by alternative translation initiation and overexpressed in cancer cells. *Oncogene, 17***,** 981-989.

Yang, X., Hao, Y., Ding, Z. & Pater, A. (2000). BAG-1 promotes apoptosis induced by N-(4-hydroxyphenyl)retinamide in human cervical carcinoma cells. *Exp Cell Res, 256*, 491-499.

Yang, X., Pater, A. & Tang, S. C. (1999). Cloning and characterization of the human BAG-1 gene promoter: upregulation by tumor-derived p53 mutants. *Oncogene, 18*, 4546-4553.

Yang, Y., Topol, L., Lee, H. & Wu, J. (2003). Wnt5a and Wnt5b exhibit distinct activities in coordinating chondrocyte proliferation and differentiation. *Development, 130*, 1003-1015.

Yarden, Y. & Sliwkowski, M. X. (2001). Untangling the ErbB signalling network. *Nat Rev Mol Cell Biol, 2*, 127-137.

Yates, K. E., Shortkroff, S. & Reish, R. G. (2005). Wnt influence on chondrocyte differentiation and cartilage function. *DNA Cell Biol, 24*, 446-457.

Yin, H. L. (1987). Gelsolin: calcium- and polyphosphoinositide-regulated actin-modulating protein. *Bioessays, 7*, 176-179.

Yoshida, C. A., Yamamoto, H., Fujita, T., Furuichi, T., Ito, K., Inoue, K., Yamana, K., Zanma, A., Takada, K., Ito, Y. & Komori, T. (2004). Runx2 and Runx3 are essential for chondrocyte maturation, and Runx2 regulates limb growth through induction of Indian hedgehog. *Genes Dev, 18*, 952-963.

Yoshitake, H., Rittling, S. R., Denhardt, D. T. & Noda, M. (1999). Osteopontin-deficient mice are resistant to ovariectomy-induced bone resorption. *Proc Natl Acad Sci U S A, 96*, 8156-8160.

Yu, P. B., Deng, D. Y., Beppu, H., Hong, C. C., Lai, C., Hoyng, S. A., Kawai, N. & Bloch, K. D. (2008). Bone morphogenetic protein (BMP) type II receptor is required for BMP-mediated growth arrest and differentiation in pulmonary artery smooth muscle cells. *J Biol Chem, 283*, 3877-3888.

Zambonin Zallone, A., Teti, A. & Primavera, M. V. (1984). Resorption of vital or devitalized bone by isolated osteoclasts in vitro. The role of lining cells. *Cell Tissue Res, 235*, 561-564.

Zeiner, M., Gebauer, M. & Gehring, U. (1997). Mammalian protein RAP46: an interaction partner and modulator of 70 kDa heat shock proteins. *EMBO J, 16*, 5483-5490.

Zeiner, M. & Gehring, U. (1995). A protein that interacts with members of the nuclear hormone receptor family: identification and cDNA cloning. *Proc Natl Acad Sci U S A, 92*, 11465-11469.

Zeiner, M., Niyaz, Y. & Gehring, U. (1999). The hsp70-associating protein Hap46 binds to DNA and stimulates transcription. *Proc Natl Acad Sci U S A, 96*, 10194-10199.

Zhang, R., Ducy, P. & Karsenty, G. (1997). 1,25-dihydroxyvitamin D3 inhibits Osteocalcin expression in mouse through an indirect mechanism. *J Biol Chem, 272*, 110-116.

Zheng, Q., Zhou, G., Morello, R., Chen, Y., Garcia-Rojas, X. & Lee, B. (2003). Type X collagen gene regulation by Runx2 contributes directly to its hypertrophic chondrocyte-specific expression in vivo. *J Cell Biol, 162*, 833-842.

Zhou, G., Zheng, Q., Engin, F., Munivez, E., Chen, Y., Sebald, E., Krakow, D. & Lee, B. (2006). Dominance of SOX9 function over RUNX2 during skeletogenesis. *Proc Natl Acad Sci U S A, 103*, 19004-19009.